DENDROCHRONOLOGICAL RECONSTRUCTION OF THE VARIABILITY IN ATMOSPHERIC CIRCULATION AND FIRE WEATHER CONDITIONS FOR THE PAST THREE CENTURIES IN THE CANADIAN BOREAL FOREST

A thesis submitted to the faculty of
Graduate Studies of the University of Manitoba
by

Martin-Philippe Girardin

in partial fulfillment of the requirement
for the degree of Doctor of Philosophy

July 2005

DENDOCHRONOLOGICAL RECONSTRUCTION OF THE VARIABILITY IN ATMOSPHERIC CIRCULATION AND FIRE WEATHER CONDITIONS FOR THE PAST THREE CENTURIES IN THE CANADIAN BOREAL FOREST

BY

Martin-Philippe Girardin

A Thesis/Practicum submitted to the Faculty of Graduate Studies of The University of Manitoba in partial fulfillment of the requirement of the degree

Of

Doctor of Philosophy

PREFACE

The present thesis comprises three published manuscripts and one submitted:

Girardin, M.P., Tardif, J., Flannigan, M.D., and Bergeron, Y. (2004) Multicentury reconstruction of the Canadian Drought Code from eastern Canada and its relationship with paleoclimatic indices of atmospheric circulation. Climate Dynamics 23: 99-115.

Girardin, M.P., Tardif, J., Flannigan, M.D., Wotton, B.M., and Bergeron, Y. (2004) Trends and periodicities in the Canadian Drought Code and their relationships with atmospheric circulation for the southern Canadian boreal forest. Canadian Journal of Forest Research 34: 103-119.

Girardin, M.P., and Tardif, J. (2005) Sensitivity of tree growth to the atmospheric vertical profile in the Boreal Plains of Manitoba. Canadian Journal of Forest Research 35: 48-64.

Girardin, M.P., Tardif, J.C., Flannigan, M.D., and Bergeron, Y. (submitted) Synoptic scale atmospheric circulation and summer drought variability of the past three centuries, boreal Canada. Journal of Climate 00: 00-00.

The leading author developed the experimental designs, collected the data in the province of Ontario, conducted the statistical analyses, and wrote the four manuscripts. This thesis and the four related manuscripts are thus original contributions from Martin P. Girardin. The comments and suggestions from the coauthors were greatly appreciated and significantly improved the quality of the research.

ACKNOWLEDGMENTS

I want to thank Elizabeth Penner and Daniel Card for their incredible help with the development of the Ontario tree-ring chronologies. This work could not have been done without their contribution. Many thanks to the Ontario Ministry of Natural Resources and particularly the following people: Stan Vasiliauskas (South Porcupine district), Ed Iskra (Dryden district), Don Armit (Ignace district), Charlotte Bourdignon (Geraldton district), and Dave New (Red Lake district) for making my search for sites of old trees successful. I wish to thank the Ontario Provincial Park and particularly Tim Sullivan (Thunder Bay district) for granting us permission to conduct this research. Special thanks to Steven Gerrard for the boat ride on Lake Nipigon and the off road pick-up ride on Camp 75 road. I thank the people of Weyerhauser for the maps and tips. I thank the truck drivers who helped us out those many times our Econoline van got stuck in the sand. I thank Kim, Alanna, Derrick, Jennifer, Brock, Brin and other students that have crossed my path in Winnipeg and Montreal over the past years and by one way or another contributed to my research.

I thank the Sustainable Forest Management Network (SFM), the Fonds Québécois de la Recherche sur la Nature et les Technologies (FQRNT), the Groupe de recherche en écologies forestière interuniversitaire (GREFi), and the Prairies Adaptation Research Collaborative (PARC) for funding my research.

Mes sentiments les plus sincères vont à mes directeurs Jacques Tardif et Mike Flannigan pour leur soutien, confiance, et dévouement à l'égard de mon projet. Merci à France Conciatori pour sa généreuse aide au laboratoire de dendroécologie (University of Winnipeg). Merci également à Yves Bergeron pour m'avoir nourri de questions qui auront servi de support à ma recherche. Merci à Danielle Charron et Luc Lauzon (Université du Québec à Montréal) pour leur aide logistique et pour m'avoir donné un espace de travail à Montréal lorsque j'en avais besoin.

Merci Héloïse pour ton amour et encouragement! Merci Pauline, ma mère, pour m'avoir soutenu durant toutes ses années. Merci Claire, Gilles, Marcel, Mariette, Robert, Norbert, Huguette, Mark, Paul, Brunel, Rose-Marie, Gérald, Marielle, Jeff, Alain, Suzanne et tous les membres de la famille pour votre accueil et soutien.

ABSTRACT

Disturbance by forest fire is responsible for the spatial and temporal variations in the forest mosaic of the boreal forest. It has been an integral ecological process since the arrival of vegetation on the landscape. Because weather and climate are crucial to fire occurrence and growth, forest practices that attempt to emulate natural disturbance must take into account the role of weather/climate on forest fires. The relationship between climate and fire is however dynamic and will continue to change as the climate changes. Additionally, the impact of future warming on the fire regime could be significant and any insights gained from looking at the historical relationships between climate and fire can assist the forest sector in the development of adaptation plans for climate change. This thesis describes the progress so far in terms of characterizing the variability in fire weather conditions of the past three centuries in the central and eastern Canadian boreal forest. Meteorological data obtained simultaneously across the Northern Hemisphere were used for the purpose of presenting a comprehensive picture of the state of the atmosphere during years of anomalous drought severity and tree-ring width. The obtained relationships were extrapolated to the past using transfer function models applied on a dense network of tree-ring chronologies. The final results are *i*) a reconstruction of the evolution of the summertime eastern Canadian boreal climate from the early 18th century to present and *ii*) the development of a plausible climate scenario for observed changes in the fire frequency since approximately 1850 across the portion of the boreal forest covering the eastern Boreal Plains to the eastern Boreal Shield.

In the first article, inter-annual and -decadal scale variability in drought over the Abitibi Plains ecoregion (eastern Canada) was investigated using a 380-year dendroclimatic reconstruction of the Canadian Drought Code (CDC; July monthly average). The CDC is a daily drought severity index of deep organic layers used daily by the fire management agencies to monitor forest fire danger. The CDC is derived from a complex soil water balance model, which incorporates soil moisture capacity, evaporation, transpiration, canopy interception, moisture recharge, and runoff. Spectral analyses conducted on the reconstructed CDC indicated a shift in spectral power after 1850 toward less prolonged drought events. Investigation on the causes for this shift suggested a decrease in North Pacific forcing after the mid-nineteenth century. Cross-continuous wavelet transformation analyses indicated coherency in the 8–16 and 17–32-year per cycle oscillation bands between the CDC reconstruction and the Pacific Decadal Oscillation (PDO) prior to 1850. Following 1850, the coherency shifted toward the North Atlantic Oscillation (NAO). Principal component analysis conducted over varying time windows reaffirmed that the Pacific forcing was restricted to the period about 1750 to 1850. Prior to and after this period, the CDC was correlated with the NAO. It is speculated that the shift around 1850 reflected a northward displacement of the polar jet stream induced by a warming of the sea

surface temperature along the North Pacific coast. A northward displacement of the jet stream, which inhibits the outflow of dry Arctic air over eastern Canada, could have allowed the advection of air masses from the Atlantic subtropical regions.

In the second article, investigation of the relationship between regional drought severity and atmospheric circulation through the 20th century was conducted by calculating daily CDC for the period 1913-1998 across a network of 62 meteorological stations extending western Manitoba to central Quebec. The relationship and coherency between CDC indices and ocean–atmosphere circulation patterns were also examined. Trend analyses indicated that climate warming and the increases in the amount and frequency of precipitation in eastern Canada during the last century had no significant impact on summer drought severity. Composite analyses indicated that for most of the corridor, severe drought seasons occurred with a combination of positive 500-hPa geopotential height anomalies centred over the Gulf of Alaska and over Baffin Bay. Additional severe drought seasons developed across the corridor in the presence of positive height anomalies located over or upstream of the affected regions. According to spectral analyses, the North Atlantic and the North Pacific circulation patterns modulated the drought variability at the decadal scale.

In the third article, the relationships between surface climate, atmospheric circulation and radial growth of eight boreal tree species growing in the Duck Mountain Provincial Forest, Manitoba, Canada, was investigated. Tree-ring residual chronologies were built, transformed into principal components (PCs) and analyzed using correlation and response function to reveal their associations with climate (temperature, precipitation and drought data for the period 1912-1999 as well as local geopotential height data for the period 1948-1999). Geopotential height correlation and composite charts for the Northern Hemisphere were also constructed. Correlation and response function coefficients indicated that radial growth of all species was negatively affected by temperature induced drought stresses from the summers previous and current to ring formation. Warm spring temperature was also a positive factor for conifers but a negative one for hardwoods. Analyses performed on geopotential heights highlighted the importance of the Northern Hemispheric atmospheric circulation in the species' response to climate. The relationships were highly significant with the middle and high troposphere during spring and late summer (determinant factor for growing season length) and with the troposphere and stratosphere during summertime. The sensitivity of tree growth to atmospheric circulation exceeded the synoptic scale, with a response associated to yearly variations in the amplitude of the mid-troposphere longwaves.

In the fourth article, five independent multicentury reconstructions of the July Canadian Drought Code and one reconstruction of mean July to August temperature were developed using a network of 120 well-replicated tree-ring chronologies

covering the area of the eastern Boreal Plains to the eastern Boreal Shield of Canada. The reconstructions were performed using 54 time varying reconstruction sub-models that explained up to 50% of the regional drought variance during the period 1919-1984. Spatial correlation fields on the six reconstructions and on a rectangular matrix of 90-multicentury tree-ring chronologies revealed that the meridional component of the climate system from central to eastern Canada increased since the mid-19th century. The most obvious change was observed in the decadal scale of variability, with the amplification of a 9-32-years/cycle-oscillation mode. Using 500-hPa geopotential height and wind composites, we interpreted this zonal to meridional transition as a response to an amplification of planetary waves flowing over the eastern North Pacific onto boreal Canada, from approximately 1851 to 1940. Composites with NOAA extended reconstructed SST indicated a coupling between the meridional component and tropical and North Pacific SST for a period covering at least the past 150-years, supporting previous findings of a summertime global ocean-atmosphere-land surface coupling.

In conclusion, this thesis provides empirical evidences of a shift in summer drought variability over boreal Canada during the mid-19th century. The period 1851-1940 was marked by frequent northward displacements of the storm track over western boreal Canada and frequent advections of humid air masses from the subtropical Atlantic onto the eastern Boreal Shield. The net result was a decrease in the frequency of extreme fire prone weather conditions during that time interval over much of the boreal forest. These findings give credence to many fire history studies conducted across the Canadian boreal forest indicating a period of decreased fire frequency starting at ca. 1850. In addition, the synoptic analysis suggested that patterns of variability in ring-width and fire weather conditions were, in the past, significantly coupled with the global climate and this in several time scales. Changes in fire frequency could be expected under a changing global climate, as suggested by the climate simulation models.

TABLE OF CONTENT

LIST OF FIGURES

LIST OF TABLES

LIST OF APPENDIX

CHAPTER 1

INTRODUCTION

1.1 Fire disturbance and forest management

Wildfire has been a recurrent disturbance in the boreal forest and many tree-species show adaptation to fire (Clark and Richard 1996). The vegetation-type mosaic in fire dependent ecosystems such as the boreal forest is to a large extent an expression of its fire regime (Bergeron 2000; Bourgeau-Chavez et al. 2000; Bonan 2002). Forest communities are essentially a successional mosaic of broadleaf deciduous and needleleaf evergreen trees that reflects recovery from recurring fires (Bergeron 2000; Bonan 2002). For instance, in the mixedwood forest shade intolerant species like *Populus tremuloide* Michx. and *Betula papyrifera* Marsh. that reproduce vegetatively will be favoured by high fire recurrence. These species have shallow to deeply buried vegetative parts that often survive fire and are capable of sprouting (Burns and Honkala 1990; Bourgeau-Chavez et al. 2000). Intermediate fire recurrence favours species that can avoid crown fires and survive low-intensity ground fires (Bourgeau-Chavez et al. 2000). They also favour species that have long-lived seeds protected from fire (serotinous cones) (Bourgeau-Chavez et al. 2000). Such species are *Pinus banksiana* Lamb. and *Picea mariana* (Mill.) BSP. Very long fire recurrence favours species such as *Thuja occidentalis* L., *Abies balsamea* (L.) Mill. and *Picea glauca* (Moench) Voss, which are more shade tolerant species that invade forests later in the successional chronosequence.

There is an increasing interest for incorporating natural disturbance regimes such as fire into boreal forest management (e.g., sylviculture and conservation). The rationale is that management that favours the development of stand and landscape compositions and structures similar to those characterizing natural ecosystems should

favour the maintenance of biological diversity and essential ecological functions (Hunter 1999; Bergeron 2004). Significant work on how to incorporate disturbances into forest management has already been undertaken (Harvey et al. 2003). A sylviculture system inspired by natural dynamics, in which fire is emulated by clear-cutting and natural canopy succession is imitated by partial cutting, was developed by Bergeron and Harvey (1997). A portion of deciduous mixed and coniferous stands are clear-cut to recreate fire disturbance. At the landscape level, the proportion of stands belonging to deciduous, mixed and coniferous compositions are determined to represent the proportion that would be observed under a natural disturbance regime (Bergeron et al. 2002a; Harvey et al. 2002).

Management that attempts to emulate natural disturbance must take into account the role of climate on natural disturbance (Bergeron et al. 2001). This role can be viewed in term of impacts of climate on the fire regime, that is, on aspects related to the fire frequency (return interval), size, severity (degree to which a site has been altered or disrupted by fire), intensity (energy release per unit length of flame front), and type (crown versus surface fires) (Weber and Flannigan 1997). The relationship between climate and fire is however dynamic and will change as the climate changes. Inevitably, the impact of the anticipated global warming (Houghton et al. 2001) on disturbance regimes could be significant (Flannigan et al. 1998, Stocks et al. 1998) and any insights gained from looking at the historical relationships between climate and natural disturbance could assist in the development of forest sustainable management, conservation, and climate change adaptation plans.

The present work intends to increase our understanding of the historical relationship between the global climate and fire weather conditions across the portion of the boreal forest covering the eastern Boreal Plains (Manitoba) to the eastern Boreal Shield (Quebec). Empirical data and model simulations suggest important changes in the Canadian boreal forest natural disturbance regimes in a context of a

rapid change of the global climate (refer to Bergeron et al. 2004a for a review). Warming of the Northern Hemisphere, estimated at ~0.6°C in the past century (Houghton et al. 2001), has already had a detectable influence. In Canada, climate change of the last century has been associated with a decrease in the frequency of fire in many regions of the boreal forest (Johnson 1992; Bergeron et al. 2004a; 2004b; see next section). In addition, there are concerns with a recent increase in fire activity over Canada since the 1970s (Podur et al. 2002; Gillett et al. 2004), although it is possible that fire statistics were under-reported prior to 1960s (Amiro et al. 2004).

Changes in vegetation composition and structure have also been well documented (Morin and Payette 1984; Bégin and Payette 1988; Bégin et al. 1993; Lavoie and Sirois 1998; Tardif and Bergeron 1999). In the southeastern boreal forest, an increase of spring flood severity and frequency at ca. 1850 caused a movement of *Fraxinus nigra* March. populations from low floodplain sites to more elevated sites along the flooding gradient (Tardif and Bergeron 1999). Bergeron et al. (2001) were also concerned that late successional species (*Thuja occidentalis*, *Abies balsamea* and *Picea glauca*, Section 1.1) become more abundant in the landscape as a result of a decrease in fire frequency. Furthermore, with forests ageing, insect outbreaks and wind throw are now playing a greater role in the forest dynamics of the southwestern Quebec boreal forest, notably by creating gaps and maintaining heterogeneous stands of conifers (Bergeron et al. 2001).

It is predicted that changes in vegetation composition and structure may accentuate as the magnitude of global warming increases. Fire could even be viewed as a catalyst for vegetation change. According to Weber and Flannigan (1997), fire responds rapidly to changes in weather and climate in comparison to vegetation. Therefore, the rate and magnitude of fire-regime-induced changes to the boreal forest landscape could greatly exceed anything expected owing to the atmospheric warming

alone (Webber and Flannigan 1997). This accentuated shift in vegetation composition and structure could lead to several ecological, economical, and industrial concerns (Bergeron et al. 2001). Sylviculture systems that favour the development of stand and landscape compositions and structures similar to those characterizing natural ecosystems will have to be adapted to reflect potential changes, notably in the abundance of mature to overmature forests and in species composition (Bergeron et al. 2001).

1.2 Fire and climate

Fire characteristics are directly influenced by day-to-day weather because fire behaviour is linked to fuel moisture and the effects of precipitation (particularly its frequency), relative humidity, air temperature, wind speed, and lightning (Flannigan and Harrington 1988; Flannigan and Van Wagner 1991; Agee 1997; Harrington et al. 1991; Johnson 1992; Weber and Flannigan 1997; Bergeron et al. 2001). Most of the area burned in the boreal forest is attributed to large persistent blocking high-atmospheric pressure systems that cause dry fuel conditions and wind (Newark 1975; Johnson and Wowchuk 1993; Bessie and Johnson 1995; Skinner et al. 1999; Skinner et al. 2002). When high-pressure systems have significant moisture or begin to breakdown, convective activity leading to numerous lightning strikes occurs and these ignite forest fires (Nash and Johnson 1996). Though humans over the past decades or so have been an important source of fire ignition (Stock et al. 2003), dry forest fuels and wind are major contributors to large stand-renewing fires (e.g. Johnson et al. 1990; Masters 1990; Johnson 1992).

Climate is always changing due to a number of factors such as changes in the earth's orbital characteristics, the chemical composition of the atmosphere, and volcanic activities (Bonan 2002). Thus, with a dynamic climate and the strong

linkage between climate and forest fires, variations in historical observations of fire activity due to changes in the climate are expected (Flannigan and Harrington 1988, Johnson 1992, Swetnam 1993). Evidence of changing fire frequencies across the Canadian boreal forest are numerous (Table 1.1). While fire suppression during the past 50-80 years contributed to changes in the recurrence of fire in many regions of Canada (Bourgeau-Chavez et al. 2000), climate change is suspected to be the leading cause of changes in 1730s, 1780s, 1850s and 1920s (Table 1.1; Master 1990; Johnson and Larsen 1991; Larsen 1997; Bergeron et al. 2001; Bergeron et al. 2004b; Tardif 2004). In the Southern Rockies of British Columbia, Masters (1990) reported the onset of longer fire cycles around 1788 and 1928 (the fire cycle length constitutes the time required to burn an area equal to the area of interest; Van Wagner 1978; Rowe 1983; Johnson 1992). In Wood Buffalo National Park, Alberta, Larsen (1997) reported the existence of a longer fire cycle around 1860. In the Duck Mountain Provincial Forest, Manitoba, Tardif (2004) reported a shorter fire cycle during the pre-settlement period. In southwestern Quebec, Bergeron et al. (2001) reported that a lengthening of the fire cycle occurred in ca. 1850, and again in ca. 1920.

With the use of tree-rings as proxy records of regional climate, several hypotheses have been put forward to explain the observed changes in the fire regimes. According to Bergeron and Archambault (1993), the occurrence of longer fire cycles in eastern Canada since ca. 1850 was concordant with a long-term increase of mean ring width of *Thuja occidentalis* L. in the same area. The authors suggested that the decrease in fire frequency could reflect a decrease in the frequency of drought periods. The mechanism behind this climate change remains to be elucidated, though Hofgaard et al. (1999) provided evidences that it may have been triggered by an inhibition of dry arctic air outflows. Larsen (1997) suggested that the reduction in fire frequency in Northern Alberta was attributed to a decrease in the frequency of high-pressure systems over the southern Yukon, contributing to greater amounts of precipitation over his study area.

Simulations of future fire activity using $2\times CO_2$ and $3\times CO_2$ simulation scenarios showed that for many areas of the boreal forest, future burn rates would be lower than current ones (Bergeron 2004; Bergeron et al. 2004a). For these other areas (Prince Albert National Park, western Quebec, Algonquin National Park, and Abitibi Plains east), despite increases in burn rates for the $2\times CO_2$ and $3\times CO_2$ simulation scenarios, most sites show $2\times CO_2$ and $3\times CO_2$ burn rates lower than historical ones (period prior to ca. 1850; Bergeron et al. 2004a). How and to what degree the climate will be changing is debatable, because simulations based on different models lead to a wide range of results (Houghton et al. 2001). Fire statistics, however, do show an increase in fire activity over Canada in the last few years, an increase that is concordant with the warming of the Northern Hemisphere (Gillett et al. 2004) and an apparent shift of the mid-troposphere atmospheric circulation over Canada (Skinner et al. 2002). This apparent discord between model simulations and fire statistics highlights the complexity of estimating and predicting the effect of climate change on fire activity across Canada. Establishing the history of past fire weather conditions using other proxies could provide valuable inputs for establishing future fire regimes.

1.3 Defining "fire weather conditions"

Fire is a conjunction of day-to-day weather parameters and often the result of daily interactions among precipitation, temperature, humidity, solar radiation, ignition agents, and wind (Van Wagner 1987; Flannigan and Harrington 1988). In the 1920s J.G. Wright began the research on fire danger rating systems tracking day-to-day susceptibility of the forest to fire (Van Wagner 1987). In the following decades, four different fire danger systems were developed for various regions of Canada, each version based on field research in the fuel types of local importance. During the late 1960s there was an increasing demand by forest fire control agencies for the development of a new fire danger-rating index. The result was called the Canadian

Forest Fire Weather Index (FWI) System. This system retained a solid link with previous systems, by building on the best features and adding new components where necessary (Van Wagner 1987). Today, the FWI System is used daily across Canada by the Canadian fire management agencies to monitor forest fire danger. Expansion of the monitoring system has begun in foreign countries. Forest fire researchers from Canada, Russia, and Germany have recently developed methodologies for electronically gathering daily weather data and producing daily fire weather and fire behaviour potential maps for large portions of northern Europe and northern Asia (Fire Ecology Research Group 2005).

The FWI System consists of six components that account for the effects of fuel moisture and wind on fire behaviour. The first three components, the fuel moisture codes, are numeric ratings of the moisture content of litter and other fine fuels (Fine Fuel Moisture Code), the average moisture content of loosely compacted organic layers of moderate depth (Duff Moisture Code), and the average moisture content of deep, compact organic layers (Canadian Drought Code, CDC). The remaining three components are fire behaviour indices, which represent the rate of fire spread (Initial Spread Index), the fuel available for combustion (Buildup Index), and the frontal fire intensity (Fire Weather Index). Their values rise as the fire danger increases. The Initial Spread Index combines the effects of wind and the Fine Fuel Moisture Code. The Buildup Index combines the Duff Moisture Code and the CDC. The Fire Weather Index combines the Initial Spread Index and the Buildup Index.

The American Meteorological Society (2000) defined drought as "a period of abnormally dry weather sufficiently long enough to cause a serious hydrological imbalance". The CDC was developed to serve as an index of the water stored in the soil, on average about 18 cm deep, and to warn when lower layers of deep duff may be dryer than the upper. It represents the net effect of evapotranspiration and precipitation in producing daily cumulative moisture depletion. Real fire danger may

be affected by the state of these layers common in many parts of Canada (Turner 1972; Van Wagner 1987). At this soil depth, drought is a determinant factor for forest fire severity by allowing deep burn and smouldering. Therefore, via its influence on fire severity, it becomes an important controlling factor of postfire ecosystem structure and function through direct impacts on underground plant root, reproductive tissues, and soil seed bank (Weber and Flannigan 1997).

The CDC is used throughout this thesis because, as opposed to other drought indices used across North America, it was specifically developed to monitor fire weather conditions in the boreal forest. As stated by the American Meteorological Society (2000), "drought is a relative term; therefore any discussion in terms of precipitation deficit must refer to the particular precipitation-related activity that is under discussion". Many drought indices rely on the same principle and basic mathematical functions, but substantially vary in terms of water holding capacity, drying rates, and weather inputs. The CDC, for instance, differs from the Crop Moisture Index (CMI, Palmer 1968) used in agriculture to monitor short-term drought conditions that result in adverse crop responses (usually because plants cannot meet potential transpiration as a result of high atmospheric demand and/or limited soil moisture) (American Meteorological Society 2000). The CDC also differs from the Palmer Drought Severity Index (PDSI, Palmer 1965), also used in agriculture to monitor prolonged period of below-normal precipitation causing deficiencies in soil moisture. In addition to the different drying rates used, the CDC also takes into account the cumulative effect of day-to-day weather. In contrast, because it is calculated on monthly average data, the PDSI is based on periods no shorter than one month. This is objectionable in that no account is taken of the distribution of precipitation within the month (Palmer 1965). The CMI on the other hand, calculated using weekly average data, is based on periods no shorter than one week. The CDC is more realistic for determining the fire danger because it is the distribution of rainfall

events, rather than the total amount, that is important when monitoring fire weather conditions (Flannigan and Harrington 1988).

1.4 Climatology

1.4.1 Climate of the Northern Hemisphere

The warming trend over the Northern Hemisphere that started in 1850s and accelerated in 1970s has become a major issue worldwide (Jacoby and D'Arrigo 1989; Mann et al. 1998; Briffa 2000; Mann and Jones 2003). Many scientists are studying the causes and impacts of climate change, and many others are attempting to predict its future trend (e.g. Hurrell 1996; Flannigan et al. 1998; Mann et al. 1998; Benestad 1999). The enhanced greenhouse effect generated by a release of CO_2 and other greenhouse gases into the atmosphere is the most probable cause for this warming or at least a substantial amount of the warming (Mann et al. 1998; Houghton et al. 2001; Meehl et al. 2003). Changes in the atmosphere circulation patterns may also have contributed to the warming (Mann et al. 1998) but it has also been suggested that an increase in solar activity forced the increase in global temperature (Benestad 1999). The contribution of anthropogenic forcing to recent Northern Hemisphere temperature changes versus that of solar radiation, ozone depletion and volcanic aerosols is still being investigated (e.g. Shindell et al. 2001a; 2001b; Gillett et al. 2002).

The warmest temperatures of the 20th century were reached in the 1990s and the largest warming was observed over mid- and high-latitude Asia and parts of western Canada (Houghton et al. 2001). The only large areas of observed cooling are south and east of Greenland and in a few scattered continental regions in the tropics and sub-tropics (Hurrell 1996; Houghton et al. 2001). Before this warming, the cooler than average temperatures characterizing the period between the late-1930s to mid-

1960s are indications of the existence of decadal variability in the climate system. Global warming is not constant, but rather consists of warming and cooling cycles at intervals of several decades. Nonetheless, the long-term trend is one of net global warming. Climate reconstructions conducted for various parts of the Northern Hemisphere generally show four centuries of cooler temperature from ~1450 to 1850, and a net progressive warming after 1850s (Jacoby et al. 1988; Briffa et al. 1990; Briffa et al. 1994; Luckman et al. 1997; Esper et al. 2002; Mann and Jones 2003). The former period, often referred to as the 'Little Ice Age', was preceded by a warm epoch (the Medieval Warm Period) with maximum warmth attained around year 1000 (Esper et al. 2002; Mann and Jones 2003). The magnitude of the recent warming relative to the medieval warmth epoch is currently being debated (Cook et al. 2004; Esper et al. 2004; McIntyre and McKitrick 2005; Moberg et al. 2005).

The quasi-stationary upper-atmospheric circulation plays an essential role in the formation and change of the short-term surface climate worldwide. To better understand atmospheric circulation – its characteristic nature, temporal behaviour, and relationship to the surface climate – classifications of the persistent patterns and definition of their seasonality have been undertaken several times, starting in the late 1960. One can refer to Barnston and Livezey (1987) for a brief history and a reanalysis. Since the classification conducted by these authors, many studies have focused on identifying the drivers of these patterns (solar variability, oceans dynamics, volcanic eruptions, etc.) (e.g. Bonsal et al. 1993; Mehta et al. 2000; Robertson et al. 2000; Seager et al. 2000; Newman et al. 2003; Yang and Zhang 2003; Baldwin et al. 2003). Such works are done using both empirical data and Coupled General Circulation Models (CGCM).

Because of the limited lenght of modern meteorological data series, several authors have used tree-rings for the identification of the low frequency atmospheric

and oceanic circulation variations emerging from the Pacific and Atlantic climate systems (Cook et al. 1998; Stahle et al. 1998; D'Arrigo et al. 2001; Glueck and Stockton 2001; Cook and D'Arrigo 2002). However, as highlighted by both Cook and D'Arrigo (2002) and Timm et al. (2004), the regional response of surface climate and of these proxies to the upper atmospheric circulation is dynamic. The issue of the non-stationary atmospheric circulation may account for apparent discrepancies between studies in which major modes of atmospheric circulation were reconstructed (Stahle et al. 1998; Cook and D'Arrigo 2002; Timm et al. 2004).

1.4.2 Key elements of the Northern Hemisphere atmospheric circulation

With the classification of the Northern Hemisphere's climate came the identification of several atmospheric circulation patterns (Barnston and Livezey 1987). Three of these patterns are important to this thesis.

1.4.2.1 The North Atlantic Oscillation

One of the major sources of Northern Hemisphere seasonal climate variability is the North Atlantic Oscillation (NAO; Hurrell 1995), a large-scale alternation of atmospheric mass between the Icelandic Low and the Azores High (Van Loon and Rogers 1978). The seasonal alternation typically accounts for one third of the hemispheric temperature variability during winter, whereas the effect on the temperatures of other seasons is reported to be minor (Hurrell 1995). Thompson and Wallace (2001) recently referred the NAO as the Northern Hemisphere annular mode (NAM) since its impacts are not only restricted to the Atlantic sector but occur at virtually all longitudes (Thompson and Wallace 2001).

One of the most intriguing aspects of the NAO is the out of phase phenomena that simultaneously occurs on the Atlantic. When winter temperatures (December through March) are low over northern Canada and Greenland, they are mild over

Scandinavia and the eastern United States (Rogers 1984; Hurrell 1995). The inverse is also true. Furthermore, because the NAO is accompanied by shifts in the storms tracks, it intimately affects the transportation of atmospheric moisture over large land areas (Hurrell 1995).

As a measure of the temporal behaviour of the NAO, an index was created based on the normalized sea-level pressure difference between Stykkisholmur/ Reykjavik, Iceland, and Ponta Delgada, Azores (Rogers 1984) dating back to 1867. The index value is positive when pressure is above normal in Iceland, and negative when pressure is above normal in Azores. It is when pressure is above normal in Iceland that temperatures are low over Scandinavia and the eastern United States (Hurrell 1995). Roger (1984)'s analysis of the frequencies contained in the NAO index revealed the presence of oscillations of 7.3-8.0 and 24 years. According to Cook et al. (1998), these oscillations have been present since at least year 1700. Periods of low NAO index values occurred in the 1940s and 1950s. Starting in the 1970s, the index strengthened, reaching a record high in the early 1990s. According to Hurrell (2000), this trend is consistent with changes in precipitation over much of the Atlantic basin. The author reports that over the Alps, snow depth and duration in recent winters have been among the lowest recorded this century, and the retreat of alpine glaciers has been widespread. Severe droughts have persisted throughout parts of Spain and Portugal as well.

Often the NAO is referred to as a manifestation of the Arctic Oscillation (AO) in the Atlantic sector. Thompson and Wallace (1998) defined the AO as the leading mode of atmospheric circulation variability of the extratropical Northern Hemisphere. The AO is characterized by sea level pressure anomalies of one sign in the Arctic and anomalies of opposite sign centred at about 37-45°N (Thompson and Wallace 1998). An index of this oscillation covers the period 1899 to present. When winter pressure is below normal in the Arctic, the index value is positive. In this phase, the circulation

pattern brings wetter weather to Alaska, Scotland and Scandinavia, as well as drier conditions to the western United States and the Mediterranean. Much of the United States east of the Rocky Mountains is warmer than normal, but Greenland and Newfoundland are colder than usual. Weather patterns in the negative phase are in general opposite to those of the positive phase.

1.4.2.2 The Southern Oscillation

The Southern Oscillation (SO) has important influences on temperature and precipitation over Canada (Shabbar and Khandekar 1996; Shabbar et al. 1997a). Its effects on climate over vast geographical areas have been studied and, as opposed to other patterns, are judged significant year-round. The SO is often referred as El Niño (or ENSO, El Niño Southern Oscillation) during its warm episodes and La Niña during its cold episodes. In average winter conditions, the trade winds blow towards the west across the tropical Pacific. During El Niño events, lower than normal pressure occurs over the eastern tropical Pacific and higher than normal pressure occurs over Indonesia and northern Australia (Ropelewski and Jones 1987). The trade winds relax in the central and western Pacific leading to a depression of the thermocline in the eastern Pacific, and an elevation of the thermocline in the west. Warm waters exert enhanced cloudiness and rainfall in the central and eastern equatorial Pacific, especially during winter and spring. Extratropical storms and frontal systems follow paths that are significantly different from normal, resulting in persistent temperature and precipitation anomalies in many regions of the Northern Hemisphere. Positive surface temperature anomalies spread eastward from the west coast of Canada to the Labrador coast from the late fall to early spring following the onset of El Niño episodes (Shabbar and Khandekar 1996). During La Niña episodes, mid-latitude low-pressure systems tend to be weaker than normal in the region of the Gulf of Alaska. This favours the build-up of colder and wetter than normal air over Alaska and Western Canada, which often penetrates into the northern Great Plains

and extend into the upper Great Lakes region by the winter season (Shabbar and Khandekar 1996).

An index of the SO is available back to 1866 from the normalized Tahiti and Darwin mean monthly sea-level pressures (Ropelewski and Jones 1987). It is positive when pressure is higher than normal in the Southeast Pacific (La Niña years). Negative values are referred to as El Niño years, and are often called ENSO events. The index is characterized by oscillations of 1.7, 2.2 and 7.3-8.4 years (Schneider and Schönwiese 1989).

1.4.2.3 The Pacific Decadal Oscillation

The Pacific Decadal Oscillation (PDO) refers to the long-term fluctuation in sea surface temperature of the North Pacific Ocean, with oscillations of 15-25 and 50-70 years (Zhang et al. 1997). The North American climate anomalies associated with the PDO warm and cool extremes are broadly similar to those connected with El Niño and La Niña (Latif and Barnett 1994; Latif and Barnett 1996; Zhang et al. 1997; Mantua et al. 1997). Warm phases of the PDO are usually associated with above average winter and spring temperatures in northwestern North America, below average temperatures in the southeastern US, above average winter and spring rainfall in the southern US and northern Mexico, and below average precipitation in the interior Pacific Northwest and Great Lakes regions. Cool phases of the PDO are correlated with the reverse climate anomaly patterns over North America, broadly similar to the typical La Niña patterns. Other studies have identified PDO connections with summer rainfall and drought in the United States (Nigam et al. 1999).

The PDO index was constructed from the leading principal component of North Pacific monthly sea surface temperature variability (poleward of 20°N) (Trenberth 1990; Trenberth and Hurrell 1994; Zhang et al. 1997). When sea surface temperatures are anomalously cool in the central North Pacific and warm along the

Pacific Coast, and when sea level pressures are below average over the east North Pacific, the respective indices have positive values.

1.4.3 Climate change in Canada

The American Meteorological Society (2000) defined *climate change* as any systematic change in the long-term statistics [average or variability] of climate elements (such as temperature, pressure, and winds) sustained over several decades or longer. Climate change may be due to natural external forcing, such as changes in solar emission or slow changes in the earth's orbital elements, natural internal processes of the climate system, or anthropogenic forcing (American Meteorological Society 2000).

Many aspects of Canadian weather, such as wind patterns, the amount and type of precipitation, and the types and frequency of severe weather events have changed significantly in the past century, but with large variations from one region to another. Although annual precipitation over Canada has increased by an average 11 mm per decade since 1948 (for a total increase of 8.2% for 1948-1995, Mekis and Hogg 1999), this increase was not distributed evenly. All regions showed an increase in precipitation, but it is in the Arctic Tundra zone and the Yukon/North British Columbia zone that the largest increases were observed (Mekis and Hogg 1999). The increases were largest in spring and autumn. Winter precipitation has also increased in these two regions, and also in the boreal forest regions of Ontario and Quebec. If summer precipitation is considered, it is in eastern and western Canadian boreal forest regions that the increase was the highest (Mekis and Hogg 1999).

Temperature has also significantly increased since 1950. It is in the Yukon, Northeast British-Columbia, Northern Alberta and the Southern edge of Saskatchewan and Alberta that the increase was the greatest (over 1.5°C) (Vincent

and Gullett 1999; Zhang et al. 2000). The warming trend has occurred mostly in winter and spring. In regions west of Ontario, the increase was about 0.5°C to 1.5°C, whereas in the east (Maritimes, Appalachians and Northern Quebec), a decrease of 0.5°C was reported (Vincent and Gullett 1999).

1.5 Objectives

The present work intends to increase our understanding of the historical relationship between the global climate and fire weather conditions across the portion of the boreal forest covering the eastern Boreal Plains to the eastern Boreal Shield. An understanding of the influence of climate change on fire weather conditions and therefore on the fire regime is crucial to understand the impacts of climate change on the Canadian forest. This may be extremely important to the forest sector and to the general public from a timber loss and community protection standpoint (Spittlehouse and Stewart 2003). Much of this thesis focuses on one aspect of the FWI System: the moisture content of deep soil layers as estimated by the CDC.

The main objective of this thesis is the development of an empirical model that can provide an explanation for the observed changes in the Canadian boreal forest fire regimes since ca. 1850. Meteorological data obtained simultaneously across the Northern Hemisphere are used for the purpose of presenting a comprehensive picture of the state of the atmosphere during years of anomalous drought and tree-ring width. The obtained relationships are extrapolated to the past using transfer function models applied on a dense network of tree-ring chronologies distributed in an area covering the eastern Boreal Plains to the eastern Boreal Shield, on the 49°–51°N parallels. The final result is a reconstruction of the evolution of the summertime climate from the early 18th century to present.

The main hypothesis was that reported changes in the boreal forest fire regime (refer to Table 1.1) were concordant with changes in drought, either in the frequency or magnitude of extreme events, in trends or in spatiotemporal variability. By demonstrating that regional climate and the fire regimes are driven by global patterns of atmospheric circulation, it can then be postulated that changes in climate and in the fire regimes imply dynamical changes in the global climate, that is, in the circulation of global air masses.

A network of tree-ring chronologies collected from several tree species is developed for the purpose of reconstructing past drought variability. The species' response to drought is tested as well as the hypothesis stating that species are sharing strong common signals related to climate. The validation of this hypothesis has strong implication since the ultimate objective is to reconstruct the evolution of spatial drought variability using the tree-ring chronologies. This necessitates that nearly all chronologies share the same drought signal. Previous works in the boreal coniferous, the mixedwood and the deciduous forests indicated that tree species generally do share very similar relationship with climate (Graumlich 1993; Hofgaard et al. 1999; Tardif et al. 2001; Tardif et al. 2002). For instance, *Acer saccharum* Marsh., *Fagus grandifolia* Ehrh., *Picea mariana* (Mill.) BSP, *Pinus banksiana* Lamb., and *Tsuga Canadensis* (L.) Carrière growing in the Quebec southwestern boreal and mixedwood forests all show a negative correlation with temperature from the late summer months of the year prior to ring formation (Hofgaard et al. 1999; Tardif et al. 2001). Significant dissimilarities however do exist between conifers and hardwood (Graumlich 1993; Tardif et al. 2002).

1.6 Study area

The study area encompasses the Boreal Plains and Boreal Shield ecozones that covers most of the boreal forest from western Manitoba to eastern Quebec (Fig. 1.1). The

study area covers six climate regions, with boundaries approximating actual ecoregions defined by the Ecological Stratification Working Group (1996). These climatic regions are the Boreal Plains (BP), Lake Seul Upland and Lake of the Woods (LS), Lake Nipigon (LN), the Abitibi Plains (*east* and *west*, APe and APw) and the Southern Laurentians (SL).

All six regions under study have a sub humid to humid mid-boreal ecoclimate (west to east gradient), marked by warm summers and cold, snowy winters according to the Ecological Stratification Working Group's (1996) regional classification. In regions BP and LS, average annual temperature ranges between −1.0°C and 1.0°C, whereas it ranges between 1.0°C to 1.5°C in eastern regions LN to SL. The average summer temperature is essentially constant across the six regions, at approximately 14.0°C. The average winter temperatures are more variable, ranging from −16.0°C in region BP to −11.0°C in region SL. The average annual precipitation ranges from 450 mm in the west to 1 600 mm in the east. In the study area most of the annual precipitation falls between the months of June to October (Environment Canada 2002).

1.7 Structure of the thesis

The thesis is mainly composed of four research articles (chapters 2, 3, 4 and 5). A general discussion is found in Chapter 6. A glossary of specific terms is provided at the end of the thesis. The first article (Chapter 2) examines the relationship among tree radial growth, climate, fire, and atmospheric circulation in the eastern Abitibi Plains region. The first objective was to identify a climate variable among others that shared significant variance with an existing set of tree-ring chronologies and that was representative of seasonal fire weather conditions. The second objective was to develop a statistical radial growth-climate relationship to reconstruct past variations in drought from past variation in tree radial growth. The third objective was to

analyse long-term variability in drought against that of the Northern Hemisphere's climate. The hypothesis postulated was that changes in the western Quebec boreal forest fire regimes corresponded to changes in *i*) drought and *ii*) in the circulation of global air masses.

In parallel with the first article, preliminary analyses conducted on tree-ring chronologies from the Duck Mountain Provincial Forest, Manitoba, also identified the CDC as a predictand for reconstruction of past drought conditions in the Boreal Plains region. This work led to the development of a network of instrumental CDC indices across the area covering the eastern Boreal Plains to the eastern Boreal Shield. The network, which is presented in Chapter 3, was developed from 62 meteorological stations and was created in preparation of the reconstruction of past drought variability in the six regions shown in Fig. 1.1. Statistical properties of the CDC indices, such as the presence of red noise, of serial and monthly correlation and of linear trends were investigated. The relationship between the indices and atmospheric circulation, fire frequency, and area burnt was also studied. The initial hypothesis was that changes in Canadian precipitation and temperatures (Chapter 1.3.3) have had a detectable influence on drought variability.

In the third article (Chapter 4) the relationship between atmospheric circulation and tree-ring chronologies originating from the Duck Mountain Provincial Forest, Manitoba Boreal Plains, is investigated. The aim was to test the hypothesis that radial growth in tree was not only an indicator of surface climate variability but also of underlying processes in the upper atmosphere (position of the storm tracks for instance). Tree radial growth responses to surface climate and with the vertical profile of the atmosphere were analysed on eight species using a bootstrap procedure and a mechanistic interpretation of the relationship between tree growth and atmospheric circulation was developed. In addition to the classical approach of inferring the

relation between tree growth and the horizontal structure of the troposphere, analyses were extended vertically to the mid-stratospheric level.

The fourth article (Chapter 5) presents a large spatial scale study in which statistical procedures and concepts elaborated and developed in the earlier articles were applied to the area covering the eastern Boreal Plains to the eastern Boreal Shield. First, a network of 120 tree-ring chronologies from 13 species was built and the relationship with the surface climate was analysed. Second, five independent multicentury reconstructions of the July CDC and one reconstruction of mean July to August temperature going back to the early 1700s were developed. Third, the spatiotemporal variability between the reconstructions was analysed and the average surface atmospheric circulation back to 1781 was reconstructed. Finally, the relationship between atmospheric circulation and global sea surface temperatures over the period 1854 to present was explored. Finally, a synoptic interpretation of the summertime climate change that occurred ca. 1850 was elaborated.

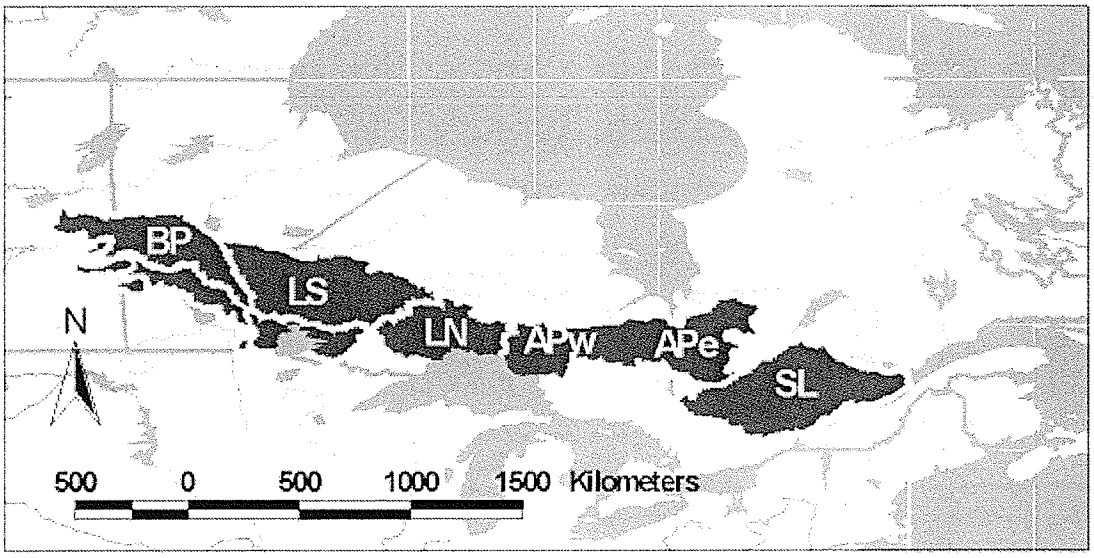

Figure 1.1 Domain of the area under study. Regions enclosed by the shaded areas were selected for the climate reconstruction (see text for details): Boreal Plains (BP), Lac Seul Upland and Lake of the Woods (LS), Lake Nipigon (LN), Abitibi Plains *west* (APw), Abitibi Plains *east* (APe), and Southern Laurentian (SL).

Table 1.1 Geographic locations and annual burn rates for various locations in Canada (from Bergeron 2004; Bergeron et al. 2004a). All areas show current burn rates significantly lower than their associated historical burn rates.

Study area	Study area (km^2)	Time period	Past burn rate (%) (<1959)	Current burn rate (%) (1959–1999)
Wood Buffalo Park	44807	1750–1989	1.410	0.660
Prince Albert	3461	<1890	1.030	0.470
Northern Ontario	24000	~1870–1974	1.920	0.462
Lake Abitibi Model Forest	8245	1740–1998	0.580	0.046
Western Quebec	15793	~1750–1998	0.720	0.032
Central Quebec	3844	1720–1998	0.790	0.111
Southeastern Labrador	48500	1870–1975	0.200	0.038

CHAPTER 2

MULTICENTURY RECONSTRUCTION OF THE CANADIAN DROUGHT CODE FROM EASTERN CANADA AND ITS RELATIONSHIP WITH PALEOCLIMATIC INDICES OF ATMOSPHERIC CIRCULATION

2.1 Abstract

Inter-annual and -decadal scale variability in drought over the Abitibi Plains ecoregion (eastern Canada) was investigated using a 380-year dendroclimatic reconstruction of the Canadian Drought Code (CDC; July monthly average), i.e., a daily numerical rating of the average moisture content of deep organic layers. Spectral analyses conducted on the reconstructed CDC indicated a shift in spectral power after 1850 leading to a reduction in interdecadal variability and an increase in interannual variability. Investigation of the causes for this shift suggested a decrease in North Pacific forcing after the mid-nineteenth century. Cross-continuous wavelet transformation analyses indicated coherency in the 8–16 and 17–32-year, cycle oscillation bands between the CDC reconstruction and the Pacific Decadal Oscillation (PDO) prior to 1850. Following 1850, the coherency shifted toward the North Atlantic Oscillation (NAO). Principal component analysis conducted over varying time windows reaffirmed that the Pacific forcing was restricted to the period about 1750–1850. Prior to and after this period, the CDC was correlated with the NAO. The shift around 1850 could reflect a northward displacement of the polar jet stream induced by a warming of the sea surface temperature along the North Pacific coast. A northward displacement of the jet stream, which inhibits the outflow of dry Arctic air, could have allowed the incursion of air masses from the Atlantic subtropical regions.

2.2 Introduction

Interactions between the oceans and the atmosphere can affect air mass circulation and climate over vast geographical areas (Minobe 1997; Nigam et al. 1999; Latif et al. 2000; Barlow et al. 2001; Bonsal et al. 2001). In North America, several investigations reported extreme weather events associated with anomalous sea surface temperatures (SST) or sea level pressures (SLP) across the Arctic, the Pacific, and the Atlantic sectors (Shabbar and Khandekar 1996; Hurrell and Van Loon 1997; Shabbar et al. 1997a, b; Thompson and Wallace 1998; Nigam et al. 1999; Barlow et al. 2001). These anomalies act by altering the atmospheric circulation patterns across the oceans, which subsequently influence temperature, precipitation and storm tracks over large land areas. These anomalies can typically last for weeks to several months, and in some cases they can persist for several years and decades (Rogers 1984; Ropelewski and Jones 1987; Bonsal et al. 1993; Hurrell 1995, 1996; Zhang et al. 1997).

There is substantial evidence of long-term changes in atmospheric circulation patterns across the Arctic, the Pacific, and the Atlantic sectors (Cook et al. 1998; Luterbacher et al. 1999, 2002; D'Arrigo et al. 2001; Glueck and Stockton 2001; Thompson and Wallace 2001). The contribution of anthropogenic forcing to recent Northern Hemisphere changes versus that of solar radiation, ozone depletion and volcanic aerosols is still being investigated (e.g. Gillett et al. 2002; Shindell et al. 2001a, b). Nevertheless, changes in atmospheric circulation may have affected the climate in eastern Canada (Bergeron and Archambault 1993). Eastern Canada's climate is notably becoming moister (Bergeron and Archambault 1993; Tardif and Bergeron 1997a), in spite of global warming (Houghton et al. 2001). Instrumental climate records in eastern Canada effectively show an increase of annual mean temperature by 0.5 to 1.5 °C in the last 100 years, with a greater warming in minimum than maximum temperature (Vincent and Gullett 1999; Zhang et al. 2000).

However, mean precipitation has also significantly increased and particularly the amount of snowfall received in spring (Mekis and Hogg 1999; Zhang et al. 2000). Climate simulations using general circulation models (GCMs) supported an increase in the frequency of precipitation under a $2 \times CO_2$ scenario (Bergeron and Flannigan 1995; Flannigan et al. 1998, 2001; Flannigan and Wotton 2001).

Paleo-climatological and -ecological investigations suggested that climate in eastern Canada started to change with the end of the Little Ice Age (1850). In the southeastern boreal forest, analysis of ice scars on flooded *Thuja occidentalis* L. trees indicated an increase in height and frequency of spring water levels at ice break-up since 1850 (Tardif and Bergeron 1997a). This increase in flood severity occurred in conjunction with a movement of *Fraxinus nigra* March. populations from low floodplain sites to more elevated sites along the flooding gradient (Tardif and Bergeron 1999). In addition, dendroecological reconstructions of stand dynamics revealed that *Thuja occidentalis* (a late successional species) became more abundant in the landscape after 1850 as a result of a decrease in fire frequency (Bergeron 1998, 2000, Bergeron et al. 2001). Many other studies reported changes in forest dynamics associated with climatic change across the boreal and the subarctic areas of eastern Canada (Morin and Payette 1984; Bégin and Payette 1988; Bégin et al. 1993; Hofgaard et al. 1999; Bégin 2000).

It was speculated that the poleward retreat of the Arctic air mass starting at the end of the Little Ice Age contributed to the incursion of moister air masses into eastern Canada (Bergeron and Archambault 1993; Hofgaard et al. 1999). However, numerous indications suggest that a more complex change in climate dynamics occurred around 1850. In many tree-ring chronologies of eastern Canada, Hofgaard et al. (1999) observed an increase in mean sensitivity around 1850. This coincides with the shift in the power spectrum of paleoclimatic records from the Pacific (Stahle et al. 1998; D'Arrigo et al. 2001). Such a shift was not reported in paleoclimatic records of

the North Atlantic (Cook et al. 1998; Glueck and Stockton 2001; Wanner et al. 2001; D'Arrigo et al. 2002).

The objective of this study was to (1) reconstruct past summer drought over the Abitibi Plains ecoregion, eastern Canada, and (2) analyze its relationships with climate variability of the North Pacific, tropical Pacific and North Atlantic between 1700 to present-day. First, a 380-year reconstruction of the July monthly average of the Canadian Drought Code (CDC; Van Wagner 1987) was developed from sixteen well-replicated residual tree-ring chronologies. Past studies have shown a good correlation between the CDC and ring width (Archambault and Bergeron 1992; Tardif and Bergeron 1997b; Girardin et al. 2001). The coherency between the reconstructed CDC and other climate reconstructions from the North Pacific (D'Arrigo et al. 2001), the tropical Pacific (Stahle et al. 1998) and the North Atlantic (Luterbacher et al. 1999) was analyzed. In addition, the CDC reconstruction was compared with records of fire history to test its ability to estimate past fire seasons. Since our record is an estimate of the average moisture content of the deep organic layers, it was expected that most periods of extensive burned area coincided with severe drought estimates.

2.3 Materials and methods

2.3.1 Description of the area

The study area (49°N, 79°W; approximately 125,664 km^2) is located about 530 km north of Montréal and is part of the Northern Clay Belt of Quebec and Ontario (Fig. 2.1). The geomorphology of the region is characterized by the influence of a post-glacial lacustrine phase that formed the Clay Belt (Vincent and Hardy 1977). The region is classified as having a humid mid-boreal ecoclimate (Ecological Stratification Working Group 1996). Mean annual temperature (1971–2000) at La

Sarre is 0.7°C, and total annual precipitation is 889.8 mm (Environment Canada 2002). The mean number of days with minimum temperature above 0°C is 148. Snow represents 27.7% of the yearly total precipitation whereas most of the liquid precipitation falls during May to September (Environment Canada 2002). Human settlement mainly started in 1910s,and fire suppression started around 1970s (Bergeron et al. 2001).

2.3.2 The Canadian Drought Code

The CDC is a numerical daily rating of the average moisture content of deep, compact, organic layers (Turner 1972). The CDC is a component of the Fire Weather Index System (Van Wagner 1987) that is used daily across Canada by the Canadian Forest Service (Natural Resources Canada) to monitor forest fire danger. In an ecological perspective, the CDC has many notable features: (1) the effect of snowmelt is accounted for in its calculation; (2) it is an adequate indicator of moisture conditions of deep organic layers in boreal conifer stands (Van Wagner 1970), (3) it correlates well with tree radial growth (Bergeron and Archambault 1993; Tardif and Bergeron 1997b; Girardin et al. 2001), (4) it is an indicator of water table depth, and (5) it represents conditions conducive to fire involving deep soil layers (Turner 1972). In addition, monthly CDC averages possess these statistical features: (a) the absence of serial autocorrelation in the monthly indices, (b) strong monthly persistence (high correlation between CDC indices from one month to the next), and (c) the presence of white noise in the CDC indices spectra (decreasing power with increasing period) (Girardin et al. 2004b).

The CDC maintains a daily budget of stored moisture, accounting for daily losses and gains (McAlpine 1990). The CDC is calculated each year independently of the previous one and the amount of winter precipitation. Each year a snowmelt time is simulated (usually around May 1st in the eastern boreal forest). At that moment it is

assumed that deep organic layers are fully recharged with water (as a consequence of melting snow). Thereafter, moisture losses are the result of daily evaporation and transpiration, while daily precipitation accounts for moisture gains. Evaporation and transpiration losses are first estimated as a maximum potential evapotranspiration based on temperature and date. Second, this maximum potential evapotranspiration value is scaled by the available soil moisture to reflect the fact that as soil moisture content is reduced, evaporation is increasingly difficult (Turner 1972; McAlpine 1990). In the moisture recharge procedure total precipitation is reduced by 2.8 mm per 24 h period to allow for canopy and surface fuel interception. The maximum water holding capacity of the CDC is 100 mm for a layer with a bulk density of about 25 kg/m^2, which amounts to approximately 400% of water per unit of mass. Excess water is considered as runoff and not accounted for in the CDC.

The minimum CDC value of zero represents 20.32 cm of available water held in the soil. The scale of the CDC is cumulative, with each unit change representing a decrease of 0.254 mm of available water in the soil. Van Wagner (1970) estimated the CDC exponential drying rate time constant at 52 days. A CDC rating of 200 is an indication of high drought severity, and 300 or more is extreme drought severity. The CDC generally peaks in mid- to late August, beyond which it either declines or maintains the same value (McAlpine 1990; Girardin et al. 2004b). The reversal in August is only attributed to a change in day length, and is not a function of seasonal precipitation.

Daily CDC indices were computed using daily maximum temperature and daily precipitation data for each of the following stations: Amos, Abitibi Post, Cochrane, Duparquet, Haileybury, Kirkland, Iroquois Falls, La Sarre, and Val St-Gilles (data from Environment Canada 2000). Monthly average CDC indices of all stations were tested for homogeneity (Vincent 1998; program HOM, Holmes 1999) and a regional monthly CDC value was calculated using program MET (Holmes

1999). In this procedure, the mean and standard deviation was calculated for each month at each station. The departure for each month and year was then calculated and averaged across stations to produce regional average departures for each month and year.

2.3.3 Dendrochronological data

Sixteen well replicated tree-ring chronologies (a total of 1,191 measurement series) all greater than 170 years were obtained for reconstruction of the July CDC. These site chronologies are briefly described in Table 2.1. Most of these chronologies originated from the Lake Duparquet and surrounding areas (Fig. 2.1).

The site residual chronologies were created as follows. During sampling years, cores and cross sections were taken from trees. Cross sections were also taken from dead trees. The collected samples were sanded, crossdated, and each annual ring was measured at 0.001 mm accuracy (Stokes and Smiley 1996). For each measurement series, the crossdating was verified statistically using the program COFECHA (Holmes et al. 1986) and graphically using program ITRVIEW 2.0 (Varem-Sanders 2000). The age/size-related trend was removed from the tree-ring measurement series using a spline function giving a 50% oscillation response of 60 years (Cook and Peters 1981). Although this resulted in the loss of information relative to long-term climatic changes, 99% of the variance contained in oscillations less than 19 years was preserved. This flexible smoothing was necessary because many of the tree-ring series were less than a 100-year length, presenting important growth trends that needed to be removed. The biological persistence (autocorrelation) contained in the standardized measurement series was removed (autoregressive modeling) to eliminate variation not due to climate (Cook and Holmes 1986; Holmes et al. 1986). Biweight means of these residual series were computed for each data set

to create the site residual chronologies. All chronologies were constructed using ARSTAN (1999).

2.3.4 Subset models

The July CDC reconstruction was made from varying site residual chronologies and residual series. In this procedure, four sub-reconstruction models were created: model I (1820–1984), model II (1768–1984), model III (1714–1984), and model IV (1605–1984). The difference between models I, II, and III relates to the number of site residual chronologies included (16, 8, and 5, respectively; Table 2.1). Model IV was made from 39 long residual series greater than 380 years extracted from the two *T. occidentalis* data sets (Table 2.1). Segments of models I (1820–1989), II (1768–1819), III (1714–1767), and IV (1605–1713) were joined into one single 380-year time series. Because of the flexible smoothing performed on the measurement series, a fifth reconstruction model (model V) was made for assessment of long-term variability. In this model, the 39 *T. occidentalis* residual series were detrended using a spline function giving a 50% oscillation response of 300 years (preserving 99% of the variance contained in oscillations less than 99 years).

2.3.5 Tree growth and climate relationships

Development of each July CDC sub-reconstruction models was conducted as described by Cook and Kairiukstis (1990), Fritts (1991), and Cook et al. (1994). The first step involved in the development of the models was to determine which monthly CDC value to reconstruct. Both redundancy analysis (RDA) and principal component analysis (PCA) (Tardif et al. 2003) were used for this purpose. For these analyses, the chronology data set included the 16 site residual chronologies and the climate data set included monthly CDC (from Girardin et al. 2004a) and monthly regional temperature and precipitation series (from Tardif and Bergeron 1997b) (period 1895-

1985). Both RDA and PCA were performed on correlation matrices and program CANOCO 4.0 was used (Ter Braak and Smilauer 1998).

Redundancy analysis is the canonical extension of PCA and intends to display the main trends in variation of a multidimensional data set in a reduced space of a few linearly independent dimensions (Legendre and Legendre 1998). In RDA, however, the canonical axes differ from the principal components (PCs) in that they are constrained to be linear combination of supplied environmental variables (Ter Braak and Prentice 1988; Ter Braak 1994). RDA may be understood as a two-step process: (1) each site residual chronology is regressed on the climate variables and the predicted values are computed; (2) a PCA is then carried out on the matrix of predicted values to obtain the eigenvalues and eigenvectors (Legendre and Legendre 1998). The climate variables were selected using a forward selection on the basis of the goodness-of-fit and tested for significance using a randomization test (9999 Monte Carlo unrestricted permutations). This procedure was repeated until a variable was tested non-significant at the 5% level. RDA was also performed on subsets of site residual chronologies (models II and III) and residual series (models IV and V). For cross verification, a PCA was conducted on the 16 site residual chronologies and the first and second principal components were correlated with the climate variables using the Pearson correlation coefficient.

2.3.6 July CDC reconstruction

In each July CDC sub-reconstruction model, the site residual chronologies were transformed into orthogonal eigenvectors to remove multicollinearity between the predictors (Cook and Kairiukstis 1990; Legendre and Legendre 1998). In models I, II, and III the 16 residual site chronologies were entered in a PCA and the first and second principal components (which contains over 53% of the total variance) were used in subsequent procedures (Table 2.1). For models IV and V, the 39 residual

measurement series were entered in a PCA. PCI, PCII, PCIII and PCIV (49.5% and 48% of the total variance, respectively for model IV and V) were used later as July CDC predictors.

Because tree growth in the year of ring formation is influenced by weather conditions in both the current and prior growing season (Cook and Kairiukstis 1990; Archambault and Bergeron 1992; Hofgaard et al. 1999; Fritts 2001), the PCs were forwarded by one year and included in the models. A total of four July CDC predictor time series were included in models I-II and III, and eight in models IV and V.

Calibration models were computed using multiple linear regression analyses between the instrumental drought indices (CDC July monthly averages) and the PCs (present and forward lags) (Cook and Kairiukstis 1990). The yearly July CDC for the early period covered by the site residual chronologies was estimated from the calibration model equations (transfer function). The stability of each model was tested (verification procedure) after conducting two sub-calibrations of the periods 1895–1939 and 1940–1984. The rReduction of error (RE), product means test (PM), Spearman rank correlation coefficient and sign test values were calculated on the independent periods (period not included in the calibration) according to standard procedures (Cook and Kairiukstis 1990; Fritts 2001).

2.3.7 Validation with fire history

As a mean of validation, a fire history reconstruction conducted by Bergeron (1991) in the Lake Duparquet area (Fig. 2.1) was used to validate the ability of the reconstructed July CDC to capture the years of severe drought events that often lead to forest fires. This data set consists of years (±1-year accuracy) of large areas burned (>1 km^2) near Lake Duparquet derived from fire-scarred trees. These fire years were 1760, 1797, 1816, 1823, 1847, 1870, 1907, 1919, 1923, and 1944.

2.3.8 Ocean-atmosphere circulation patterns

One objective of this study is the comparison of the variability in the CDC with that of paleoclimatic indices of atmospheric circulation. Numerous proxy records of interannual and interdecadal scale climate variability for the Pacific and Atlantic sectors exist (Stahle et al. 1998; Cook et al. 1998; Luterbacher et al. 1999; Biondi et al. 2001; D'Arrigo et al. 2001; Glueck and Stockton 2001). Because the reconstructed July CDC is an estimate of spring and early summer climate variability (May–July), paleoclimatic indices spanning this season were prioritized over others for the analysis.

D'Arrigo et al. (2001) presented two annual Pacific Decadal Oscillation (PDO; Mantua et al. 1997) reconstructions, a decadal scale oscillatory mode of North Pacific SST. The two reconstructions (differing in the number of chronologies incorporated in the models) are based on summer temperature sensitive tree-ring chronologies from the Gulf of Alaska and winter sensitive tree-ring chronologies from the southwestern United States (USA) and Mexico. Their 1790–1979 reconstruction accounts for 53% of the instrumental variance while the second reconstruction accounts for 44% of the variance and extends as far back as 1700. The 1790–1979 reconstruction demonstrated better predictive skills, and therefore it was selected and extended to 1700 by using the segment 1700–1789 from the later reconstruction.

Reconstructed monthly North Atlantic Oscillation (NAO; Rogers 1984; Hurrell 1995, 1996) indices by Luterbacher et al. (1999) were used in this study. Because this data set provides us with the possibility of using NAO seasonal averages of May to July, their record was chosen over Cook et al. (1998) and Glueck and Stockton (2001). The use of a seasonal NAO pattern is particularly appealing since

the NAO exerts strong seasonal variations over the Northern Hemisphere (Barnston and Livezey 1987) and at virtually all longitudes (Thompson and Wallace 2001). The NAO can also be viewed as the manifestation of the Arctic Oscillation in the North Atlantic sector (AO; Thompson and Wallace 1998). The NAO reconstruction of Luterbacher et al. (1999) is derived from varying time series of instrumental pressures, temperature, precipitation, and paleoenvironmental records. The period for which excellent results ($R^2 > 30\%$) were obtained by the authors spans 1770–1990. Prior to 1770, the predictive skills are poor.

Finally, the Southern Oscillation (SO) index (Ropelewski and Jones 1987), an important indicator of interannual climate variation that influence weather and climate all over the world, was reconstructed by Stahle et al. (1998). Even though the SO reconstruction (which covers the period 1706 to 1977) is restricted to the winter period of December to February, SO anomalies are persistent enough to affect climate many seasons after the onset (Kiladis and Diaz 1989; Bonsal and Lawford 1999).

2.3.9 Spatiotemporal analyses

Common variance at multiple-scales between the July CDC reconstruction and the reconstructed atmospheric circulation pattern indices (NAO, PDO, and SO) was analyzed using PCA conducted on correlation matrices. Five 100-year intervals, held in common by all reconstructed variables, from 1706 to 1979 were used (note that the period chosen was constrained by the length of the SO reconstruction). The first PCA was conducted on the period 1706–1805 whereas the last was conducted on the period 1880–1979. A PCA was also conducted on instrumental circulation pattern indices (monthly average of May to July) for the period 1900–1998. For this analysis only, instrumental AO indices as well as instrumental CDC indices were added as supplementary (passive) variables. Passive variables do not influence the formation of the PCs. They are added after the analysis so that their relation to the other variables

can still be judged from the reduced space. (The reduced space is a representation of a large fraction of the variability of a multidimensional data matrix, in a space with reduced dimensionality relative to the original data set (Legendre and Legendre 1998)).

2.3.10 Spectral analyses

Fourier multitaper spectra analyses (Lees and Park 1995; program AutoSignal version 1.5; AISN Software 1999) were conducted on the reconstructed July CDC for identification of stationary signals. Analyses of peak-based critical limit significance levels were performed to ascertain the significance of the largest spectral component. An unbiased average spectrum is produced and an F-ratio test is offered to determine the significance of any given peak in the spectrum. In this type of test, one seeks to disprove the null hypothesis where one postulates either a white noise signal (AR(1) = 0.0), or a red noise signal (AR(1) > 0.0) (Lees and Park 1995). Red noise is present when the background power decreases with increasing frequency.

In the Fourier method, the component sine and cosine waves are localized in frequency but not in time (Torrence and Compo 1998). This is problematic when analyzing time series with non-stationary signals. Alternatively, continuous wavelet transform (CWT) analyses were used to decompose signals into wavelets, small oscillations that are highly localized in time (Torrence and Compo 1998). Whereas the Fourier transform decomposes a signal into infinite length sines and cosines, effectively losing all time-localization information, the CWTs basis functions are scaled and shifted versions of the time-localized mother wavelet. The CWT is used to construct a time-frequency representation (spectrum) of a signal that offers very good time and frequency localization. Coherency between two time series (CDC against the NAO, the PDO, and the SO) at various time and period scales were identified by the cross products of the CWTs from the two time series (Torrence and Compo 1998;

Torrence and Webster 1999). Periodicities showing coherency were reconstructed with the use of spectral components isolated in the time-frequency domain (wavelet filtering and reconstruction; Torrence and Compo 1998). Pearson correlation coefficients were calculated between pairs of periodicities (waveforms) with 95% confidence intervals using a nonparametric stationary bootstrap. This technique resamples blocks of data pairs to account for the presence of serial correlation in the time series. The confidence intervals allow to test whether the correlation between two serially dependent time series is significant. When the confidence interval contains zero, the hypothesis of 'no correlation' cannot be rejected at the 95% level. The software used for the correlation analyses was PearsonT (Mudelsee 2003).

In this study, CWT analyses were performed using a nonorthogonal Morlet wavelet basis (wave number of 6), a Gaussian-windowed complex sinusoid (Torrence and Compo 1998). The wavelet basis was selected so that the time-space domain is maximized in length over the spectral-space domain (Torrence and Compo 1998). Other wavelet basis procedures (the Paul basis, for instance) with various adjustable parameters were also tested and results tended to be consistent (within the uncertainty of the wavelet basis definition). For the spectrum analyses, all reconstructions were updated to 1998 by using instrumental meteorological data (calculated as per the original method). Also, the SO data set (1706–1977) was padded with additional zeros for the years 1700–1705 for consistency with the PDO data set length. All reconstructed indices (CDC, NAO, PDO, and SO) were normalized before processing the CWT. CWT analyses were performed using the program AutoSignal version 1.5 (AISN Software 1999) and using IDL (Interactive Data Language, Research Systems) wavelet programs written by Torrence and Compo (1998).

2.3.11 Geopotential height maps

For assessment of the relationship between the CDC and atmospheric circulation during the instrumental climate period, May-July 500-hPa geopotential height composite and correlation maps were created with the aid of the NOAA-CIRES Climate Diagnostics Center, Boulder, Colorado (Kalnay et al. 1996; www.cdc.noaa.gov). The 500-hPa grid has a global spatial coverage of 2.5° latitude by 2.5° longitude with 144 × 73 points and a temporal coverage of 1948 to present, with output every 6 hours. Daily 500-hPa heights (expressed in m) were averaged by months for each grid point. For the composite maps, 500-hPa anomalies were determined relative to the mean value of the 1968–1996 reference period.

2.4 Results

The climate variable showing the strongest relationship with the sixteen site residual chronologies was the July monthly average CDC (Fig. 2.2, Table 2.2). Both RDA canonical axes were well correlated with this variable (Fig. 2.2). Temperature and June precipitation also accounted for an important part of the variability, particularly the temperatures prevailing in August the year prior to ring formation and in early spring of the year of ring formation (Fig. 2.2). With respect to seasonal variables, the correlation coefficients obtained from the July CDC indices exceeded those obtained from seasonal average temperature and total precipitation (Table 2.2). Correlation analyses (Table 2.1) indicated that the most drought sensitive site residual chronologies were *B. papyrifera*, and *P. banksiana* of Lake Hébécourt and Lake Duparquet. Chronologies of *T. occidentalis* from dry sites of Lake Duparquet, and of *P. mariana* from Hedge Hills and Lake Hébécourt also correlated well with the July CDC (Table 2.1). Redundancy analysis conducted on subsets of site residual chronologies (models II and III) and on *T. occidentalis* residual series (models IV and V) also identified the July CDC value as a significant climate variable (results not shown).

2.4.1 Reconstructed July CDC

Correlation analyses and visual assessment indicated that the interannual and interdecadal variability contained in the instrumental July CDC value was adequately reproduced in model I ($p < 0.001$; Fig. 2.3a). The Spearman rank correlation, sign tests, reduction of error (RE), and product means test (PM) statistics of the verification (Table 2.3) supported this statement by indicating significant predictive skills of the calibration model (Cook and Kairiukstis 1990; Cook et al. 1994; Fritts 2001). Whenever RE is greater than zero the reconstruction is considered as being a better estimation of climate than the calibration period mean. A significant sign test indicates good fidelity in the direction of year-to-year drought change in the real and estimated data, while the PM test result indicates that the magnitudes as well as the direction of these changes are statistically significant. Based on results of Table 2.3, we considered the reconstruction to be reliable from 1768 to present as an estimate of interannual and interdecadal climate variability. Prior to 1768, partially positive RE statistics indicated that the regression models on the average had some skill and that the reconstructions were of some value. A partitioning (Cook and Kairiukstis 1990) of the negative RE value from models III and IV indicated that the RE were effectively greater than the RISK factor (–0.63 and –0.44, respectively). It is recognized that values of RE that are negative but greater than the measure of the variability of both estimates and instrumental observation (RISK) may still contain some meaningful climate information. Loss in variability is however observed from model I to model IV (Fig. 2.3a–3d, respectively) judging by the intermodel Spearman rank correlation coefficients (r) (period 1895–1984: $r_{\text{I-II}} = 0.98$, $r_{\text{I-III}} = 0.63$, and $r_{\text{I-IV}} = 0.55$). As for model V (Fig. 2.3e) in which intercentennial variability was preserved, statistics ($R^2 = 0.46$; RE = 0.08 and –0.14) were very similar to model IV (Fig. 2.3d; Table 2.3).

A multitaper spectra analysis of the reconstructed July CDC 1700–1998 period showed no significant stationary signals (Fig. 2.4a). Analyses of two independent periods, pre-1850 and post-1850, however indicated that signals at around 14–36 years/cycle, although not significant, were considerably more pronounced during the interval 1700–1849 relative to 1850–1998 (Fig. 2.4b, 2.4c). These signals contributed to the small amount of red noise observed in the spectra (AR(1) > 0; refer to Sect. 2.10). Interannual signals (2.05–2.69 and 3.58–3.77 years/cycle) were considerably more pronounced after 1850.

2.4.2 Validation with fire history

To test the ability of the final CDC reconstruction to estimate past seasons of drought, yearly historical records of extensive burned area were compared with the reconstruction. Observation showed concordance between large areas burned in the vicinity of Lake Duparquet and years of drought. Out of the ten fires reported, six (1760, 1847, 1870, 1919, 1923, and 1944) accurately corresponded to drought estimates higher than 190. Fires in 1823 and 1907 corresponded with dry years estimated in 1822 and 1906, respectively. Fires in 1797 and 1816 did not corresponded to severe drought indices.

2.4.3 PCA and atmospheric circulation

PCA was used to investigate the common variability structure between the reconstructed July CDC and patterns of atmospheric circulation (PDO, SO and NAO). As a result of the varying site chronologies in the climate reconstruction process, caution must be taken when interpreting the correlations with atmospheric circulation patterns before 1770.

Reduced spaces in Fig. 2.5 all demonstrated that PCI was negatively correlated with the PDO and positively with the SO. The angle approximating 180° between the two vectors further highlighted the negative correlation between the two circulation patterns. As for PCII, it was positively and highly correlated with the NAO. Angles approximating 90° between the NAO and the SO and PDO suggested the absence of a correlation between the North Atlantic and the Pacific sectors. In every reduced space, the contribution of the NAO, PDO, and SO to the formation of PCI and PCII exceeded the expected one under the hypothesis of an equal contribution to all principal components (by comparing the length of the descriptors projection to the equilibrium circle). Percentages of explained variance by PCI and PCII remained relatively constant from one period of analysis to another (Fig. 2.5).

Reduced spaces demonstrated a positive correlation between the CDC and the NAO (sharp angle) along PCII at the beginning and end of the period of analysis (Fig. 2.5a, d, e). No correlation with the SO and PDO (angles close to 90°) was observed. This configuration shifted in the middle of the eighteenth century (1750–1849) as the correlation between the NAO and the CDC decreased (Fig. 2.5b,c), suggesting that the CDC may have been subject to another external forcing. The position of the CDC vector in relation to those of the PDO and SO suggested that the 1750–1849 forcing could have originated from the Pacific sector. Analysis conducted on instrumental circulation pattern and CDC indices indicated a correlation structure similar to the one observed using paleoclimatic indices (Fig. 2.5f, l). Also, the analysis indicated that variability in the CDC was better explained by the use of the NAO index rather than the AO index.

2.4.4 CWT and atmospheric circulation

The coherencies between the CDC reconstruction and the NAO, the PDO, and the SO reconstructions were evaluated using CWT analyses (Figs. 2.6, 2.7, and 2.8). As the

Fourier multitaper spectra analyses highlighted the problem of non-stationary signals in the CDC reconstruction (Fig. 2.4), CWT analysis was performed on each individual series for means of comparison of the stationary sections. The analyses (Fig. 2.6a) indicated that strong 17–32-years oscillations in the CDC characterized the first half of the nineteenth century. Similar analyses performed on the PDO, NAO and SO reconstructions revealed that the PDO (Fig. 2.6c) also showed high power in that range of frequencies from the middle eighteenth century to early nineteenth century. The NAO demonstrated a similar signal, but post 1840 (Fig. 2.6b). The coherency between the PDO and the CDC prior to 1850 was further highlighted by the cross-CWT analyses (Fig. 2.7b) and the reconstructed spectral components isolated in the time-frequency domain (Fig. 2.8b). It was found that the Pearson correlation between the CDC reconstruction and the PDO 17–32-year waveform was 0.32 ($P < 0.05$) for the period 1750–1840. The correlation increased to 0.74 with a 95% confidence interval [0.64; 0.82] when the PDO and CDC waveforms were correlated together (the hypothesis of a correlation between the two waveforms is rejected when the confidence interval contains zero; Mudelsee 2003). For the period post 1850, the CDC synchronized intermittently with the NAO waveform, with maximum synchronization occurring in the first half of the twentieth century (Fig. 2.7a). The two waveforms (CDC versus NAO, Fig. 2.8a) shared 50.4% of common variance during the period 1880–1940 ($r = 0.71$ with a 95% confidence interval [0.55; 0.82]). Prior to 1750, some coherency with the SO was observed (Figs. 2.7c, 2.8c).

Coherency between the PDO and the CDC prior to 1850 was further highlighted in the 9–16-year oscillation band (Fig. 2.7b). Additionally, some coherency with the SO was observed around 1750 (Fig. 2.7c) and with the NAO and SO in the first half of the twentieth century (Fig. 2.7a,c). Finally, dispersed 2–8-year oscillations in the CDC (Fig. 2.6a), though more prominent in the last century, were shown to be coherent with all three patterns (Fig. 2.7). However, greater coherency with the SO was observed from 1850 to 1950, and more specifically from 1910s to

1940s (Fig. 2.7c). Observed coherency in the late twentieth century may be affected by the edge effect (results from a discontinuity at the end of the data stream). Cross-CWT analyses conducted on instrumental pattern indices and instrumental CDC indices (analyses not shown) show patterns of coherency similar to that observed using reconstructed indices.

2.4.5 The 500-hPa geopotential height maps

Sections 2.3 and 2.4 suggest that July drought during the instrumental period was mainly driven by the North-Atlantic circulation mode. This is confirmed for the latter part of the twentieth century with the creation of the 500-hPa geopotential height composite and correlation maps (Fig. 2.9). The dipolar pattern that characterizes the NAO (inverse anomalies above Iceland and the Azores) was well reproduced, particularly in the composite map. In association with severe drought seasons, both maps were coherent by showing anomalous ridging (centred above Baffin Bay) over the Abitibi Plains. The ridge was accompanied by a northward deflection of the moisture carrying system. During low drought seasons, the ridge was displaced northward allowing the moisture carrying systems to penetrate north of the area of study. In addition to the North Atlantic circulation mode, a centre of positive correlation was observed in the North Pacific.

2.5 Discussion

2.5.1 July CDC reconstruction

In the Abitibi Plains ecoregion the results show that drought is among the most significant variables affecting ring-width when all site residual chronologies are combined. However, because the July CDC reconstruction was developed from varying site residual chronologies, the climate variability captured by the PCs is

lacking in stability with removal of site residual chronologies. While the drought signal captured by model I was perfectly reproduced in model II after the removal of eight site residual chronologies, removal of three additional chronologies prior 1768 (model III) contributed to a substantial decrease in the confidence of the sub-reconstruction models. Visual assessment and additional CWT analyses (not presented) conducted on sub-reconstruction models however demonstrated that non-stationary signals prior to 1850 on which this work focuses are well reproduced from one model to another.

The multitaper spectra and CWT analyses of drought variability in the Abitibi Plains ecoregion highlighted a shift in time scale variability around 1850 from an interdecadal toward a more pronounced interannual forcing. In addition, while the Little Ice Age climate was dryer (as revealed by the CDC-low frequency reconstruction, model V), the early twentieth century was an unprecedented period characterized by a high frequency of severe drought seasons. Interestingly, the largest forest fires of the last 150 years in eastern Canada were encountered during 1910s and 1920s (Bergeron et al. 2001). Prior to 1850, large forest fires occurred during 1760s–80s and 1810s–1840s (Bergeron et al. 2001).

2.5.2 Atmospheric circulation patterns

Analyses linking drought variability to major features of Northern Hemisphere circulation have identified a changing relationship over the past 300 years. Our results lead us to suggest that the end of Little Ice Age (1850–1870) over the Abitibi Plains sector corresponded to a decrease in the North Pacific decadal forcing around 1850s. This event could have been followed by an amplification and eastward displacement of the western Canadian ridge, an inhibition of the Arctic air outflow over eastern Canada and advection of more humid air masses from the subtropical Atlantic climate sector.

The mechanisms linking warm season regional climate variability with ocean-atmospheric circulation patterns are not firmly established. For that reason it is difficult to provide a precise explanation of the cause of the 1850s atmospheric circulation shift over the Abitibi Plains ecoregion. However, description of the PDO/SO winter modulations by Bonsal et al. (2001; investigation based on analyses of the instrumental data) may provide some insights. Bonsal et al. (2001) showed that in the winter season a +PDO/–SO phase is associated with a deeper than normal Aleutian low, an amplification and eastward displacement of the western Canadian ridge, and negative height anomalies over the southeastern USA. This combination reflects a northward-displaced polar jet stream, which inhibits the outflow of Arctic air over most of Canada. The reverse is true for the –PDO/+SO phase but with weaker effects. The evidence of a –PDO phase (warmer water in the interior Pacific and cooler water along the North Pacific coast; Mantua et al. 1997) from approximately 1750–1850 has been demonstrated with the investigation of prominent aquatic population declines in the Gulf of Alaska (Finney et al. 2000). A North Pacific forcing from 1750–1850 may thus have resulted in a modification of the circulation flow over the Abitibi Plains ecoregion.

There are several types of evidence suggesting the implication of ocean-atmospheric circulation patterns anomalies in extreme climate conditions of the last century. Nigam et al. (1999) and Barlow et al. (2001) demonstrated that Pacific decadal SST variability was strongly linked to large-scale patterns of warm-season drought and stream flow in the USA. Bonsal et al. (1993) and Bonsal and Lawford (1999) reported similar findings after documenting and analyzing teleconnections between the SO, North Pacific SSTs, and summer extended dry spells over the Canadian Prairies. Nigam et al. (1999) also hypothesized that SST anomalies in the North Atlantic Ocean, by creating positive feedback with circulation anomalies from

the Pacific, could contribute to enhanced drought seasons in the northeast USA. Moreover, implication of North Pacific SSTs in the regulation of Canadian boreal forest climatically induced disturbances has been postulated. Skinner et al. (1999) demonstrated a linkage between wildland areas burned and the presence of anomalous ridging at 500-hPa immediately over western and west-central Canada. In another study, Flannigan and Wotton (2001) demonstrated a linkage between Pacific SST and seasonal forest area burned in eastern Ontario. While ocean-atmosphere circulation patterns are reported to be most effective during winter, this study and those enumerated suggests that their regional impacts during the summer period could be underestimated.

Concerns are presently being directed toward recent changes in the North Pacific where a reversal of the PDO toward more pronounced decadal variability is suspected to be occurring (Hare and Mantua 2000; D'Arrigo et al. 2001). In our study, recent decadal signals (period post-1946) associated with the PDO were not clearly apparent. Preliminary analyses in the central Canadian boreal forest (western Manitoba), however, tend to suggest that climate in central Canada may be responding to a reversal of the circulation pattern (Girardin et al. 2002b, 2004a). Strong decadal signals starting in 1940s and coherent with the PDO are dominating the central Canada CDC spectra. As information gained from a dendroclimatological study conducted along a southern Canadian boreal forest transect will provide some insight on the speculated displacement of the jet stream around 1850, forecasting of future changes will require more extensive study. There is a need to develop an extensive network of dendrochronological data and climate reconstructions in Canada. This would enable the identification of sensitive regions. A network could also provide an additional time window for simulations of climate with general circulation models (Bradley 1999; Flannigan et al. 2001) and regional circulation models (Laprise et al. 2003). Further analyses will help forecast the potential effect of

anthropogenic climatic change, which could alter variations in low-frequency oscillations.

Our comprehension of the impacts of climate dynamics is not complete without considering the relationship between ocean-atmosphere circulation shifts and population dynamics over multicentury intervals (Finney et al. 2000; D'Arrigo et al. 2002). Biological functions might be more closely tied to atmospheric circulation than expected and this may affect projections of future changes in population dynamics (biodiversity, richness, and abundance). Natural resources management (water, fisheries, agriculture, forestry, and fauna) could greatly benefit from such understanding.

2.6 Acknowledgements

We thank S. Archambault, F. Biondi, D. Charron, E.R. Cook, R. D'Arrigo, M.F. Glueck, A. Hofgaard, R. Holmes, B. Lewis, J. Luterbacher, N. Mantua, D.W. Stahle, the International Tree-Ring Data Bank, and the National Oceanic & Atmospheric Administration who contributed to this research by providing us with their data and/or software. CWT and cross-CWT power spectrum analyses were performed using the wavelet software provided by C. Torrence and G. Compo. We also thank B.M. Wotton for his guidance throughout the computation of the daily Canadian Drought Code. This manuscript was improved through the comments of W. Lawrence Gates (editor), M. Cleaveland, three anonymous reviewers, and B. Laishley. Finally we acknowledge the Sustainable Forest Management Network of the Centre of Excellence for providing the funding for this research. During this study, M.P. Girardin received a scholarship from the Fonds québécois de la recherche sur la nature et les technologies (FQRNT) and the Groupe de recherche en écologie forestière inter universitaire (GREFi).

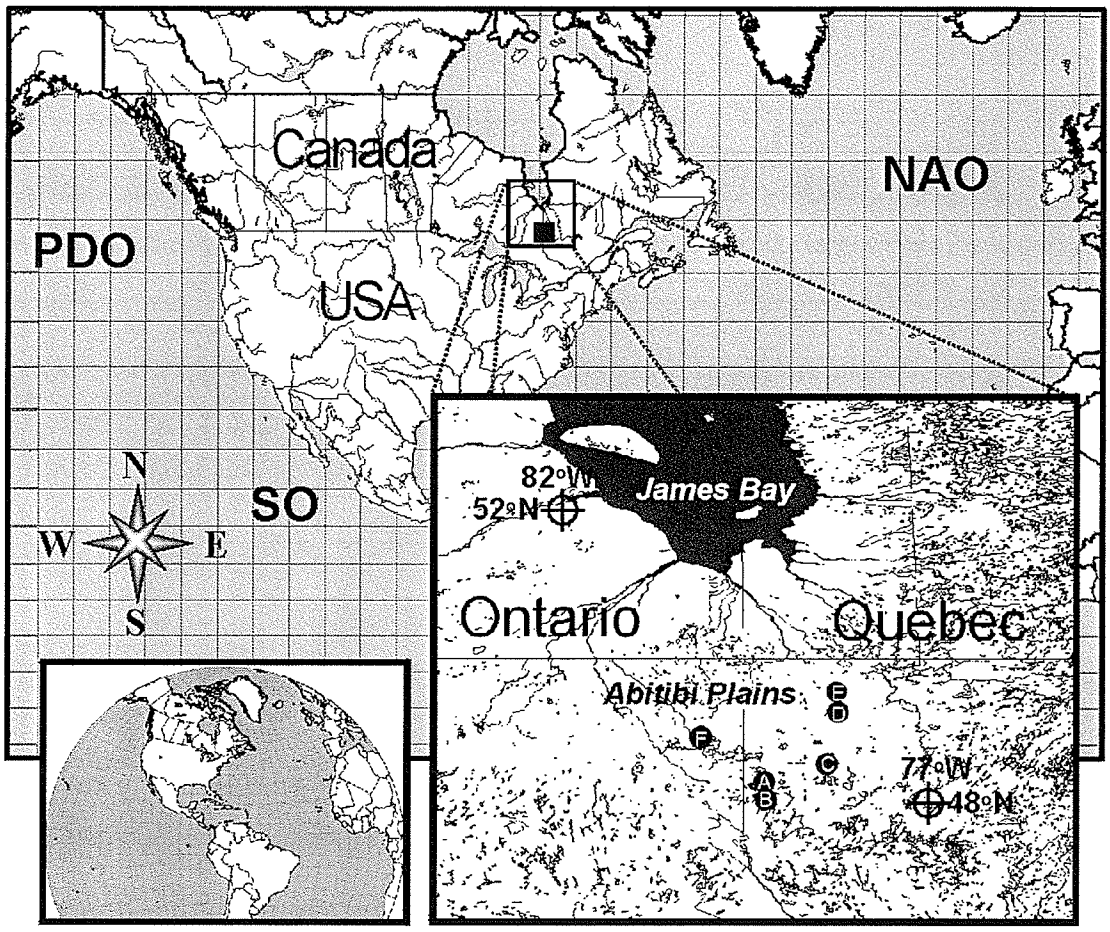

Figure 2.1 Map showing the location of the study area. Geographical locations of the indices of climate variability over the Atlantic and Pacific sectors are shown, as well as the location of the tree-ring data sets (*A* 1, 5, 7, 12–16; *B* 8; *C* 3, 10; *D* 4, 11; *E* 2, 9; *F* 6, refer numbers to Table 2.1 for identification of chronologies).

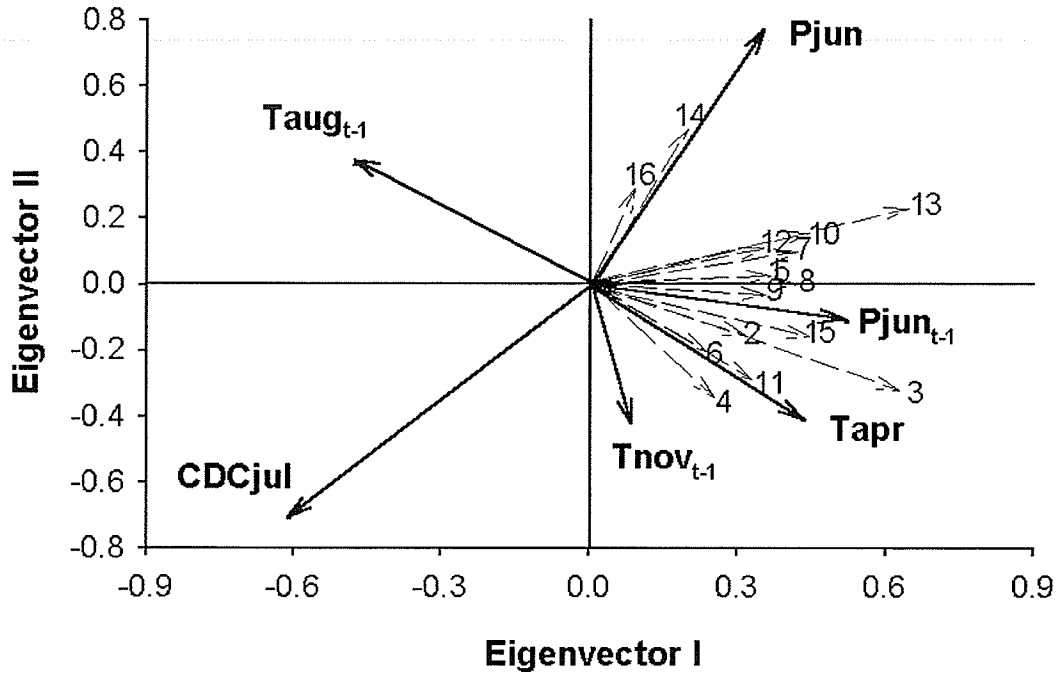

Figure 2.2 Eigenvectors of the redundancy analysis (RDA) conducted on the site residual chronologies from the Abitibi Plains ecoregion. The descriptors (arrows) are positioned in the biplot based on their correlations with the canonical axes. For instance, the variable CDCjul has a correlation of –0.61 with the first canonical axis and of –0.71 with the second one. In addition, the biplot also approximates the correlation coefficient among descriptors and climatic variables (Legendre and Legendre 1998). Climate variables and site residual chronologies with arrows at sharp angles are positively correlated (cos 0° = 1.0, i.e. perfect correlation). Conversely, obtuse angles indicate negative correlation (cos 180° = –1.0, i.e. perfect correlation). Variable abbreviations are June precipitation ($Pjun_{t-1}$) and November ($Tnov_{t-1}$) and August ($Taug_{t-1}$) temperatures of the year prior to ring formation, and June precipitation (Pjun), April temperature (Tapr) and July drought (CDCjul) of the year of ring formation. Refer numbers to Table 2.1 for identification of site residual chronologies. Eigenvalues (E) and descriptors - climate correlation coefficients are $E_1 = 0.129$, $E_2 = 0.075$, $r_1 = 0.598$, and $r_2 = 0.655$; percentage of explained variance of descriptors - climate relation are canonical axis I = 0.54 and canonical axis II = 0.31. The significance of all canonical axes is $P < 0.001$.

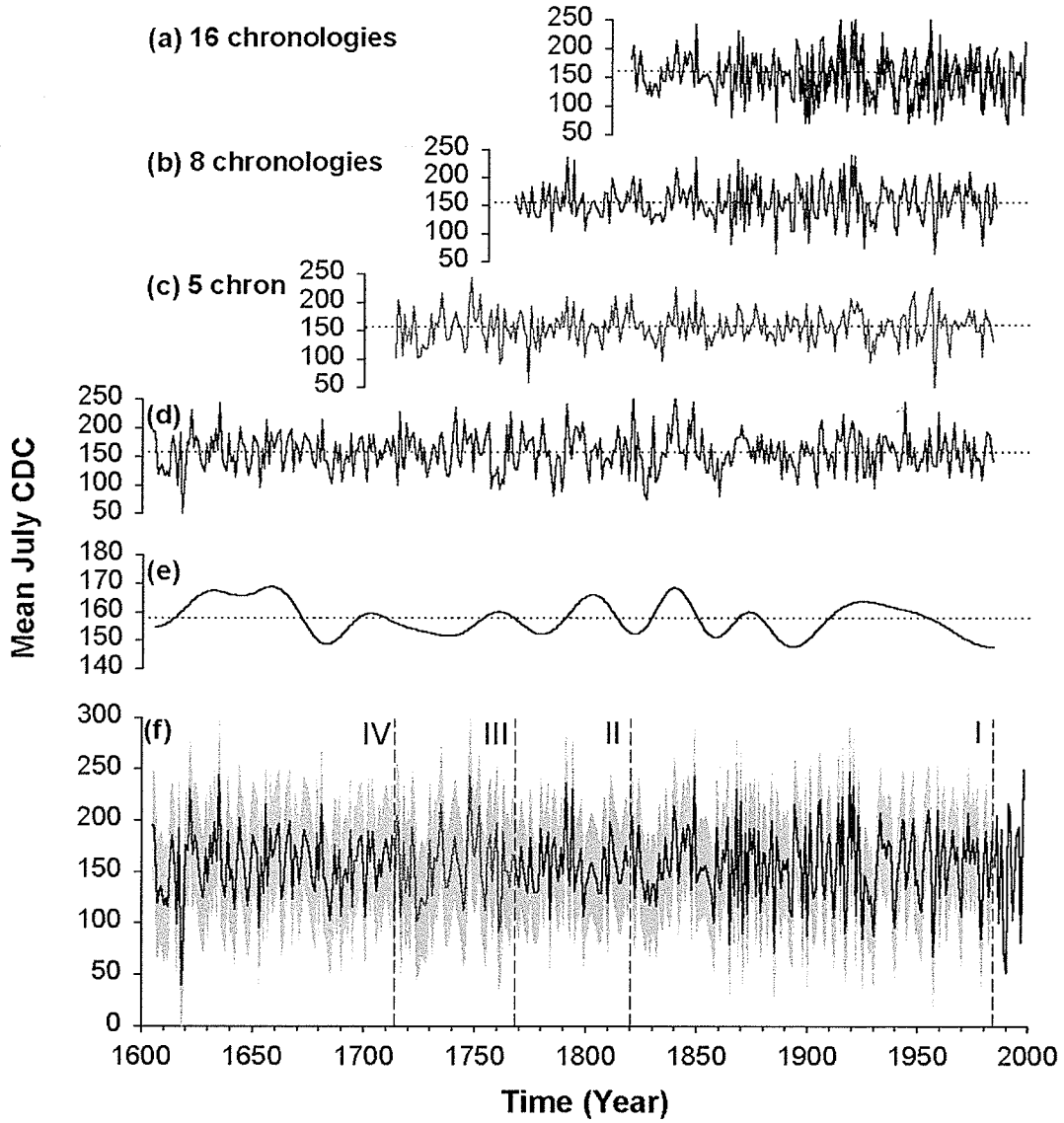

Figure 2.3a–d) Sub-reconstructed July CDC models I to IV. e) Smoothed July CDC model V. The smoothing was done using a second degree least squares polynomial fitting across a moving 20-year window. f) Final July-CDC reconstruction made from segments (delineated by dashed lines) of models I, II, III and IV and updated using instrumental CDC indices (period 1985–1998). Error bars are shown in f) (shaded area). In a) is also shown the instrumental CDC indices (black line).

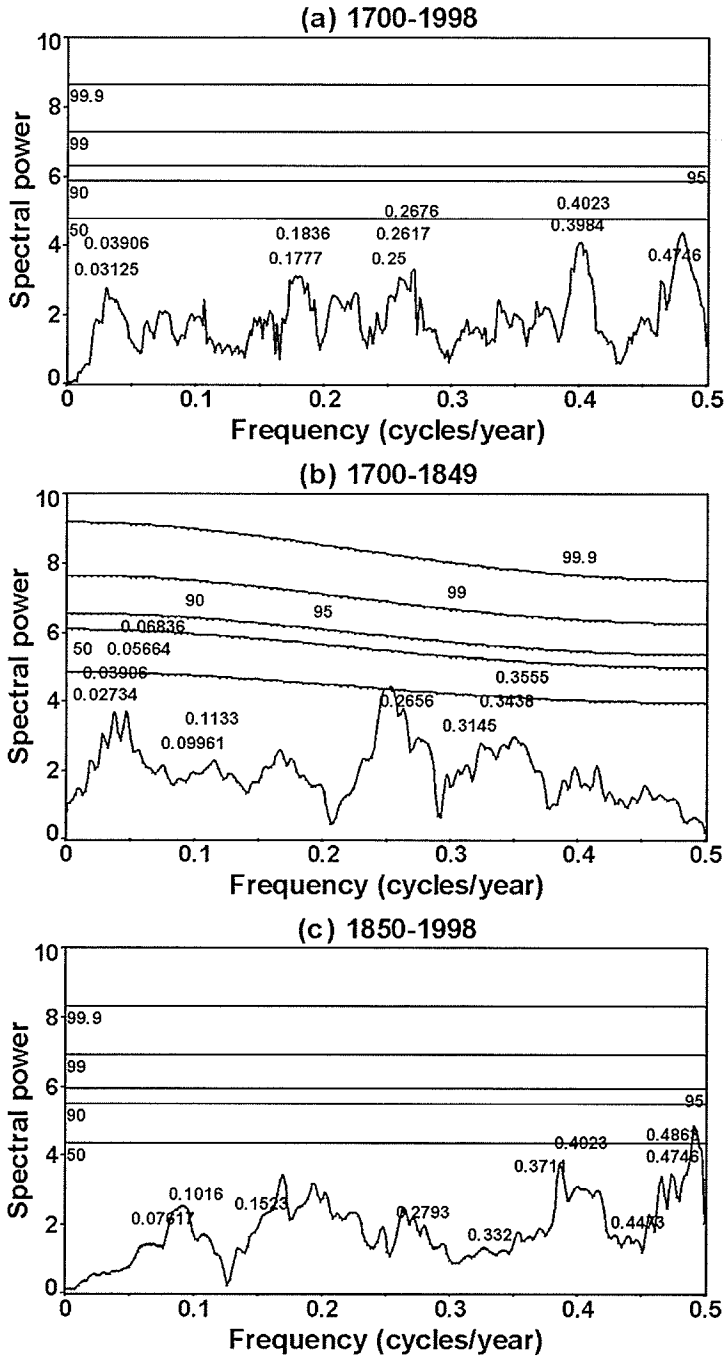

Figure 2.4 Fourier multitaper spectra of the CDC reconstruction for a) 1700–1998, b) 1700–1849, and c) 1850–1998. The 50, 90, 95, 99, 99.9% significance levels are indicated (lag-1 autoregressive spectrum AR(1) = 0.00 in a and c, and = 0.05 in b. The frequency locations of the detected peaks were drawn from the F-ratio maxima, and only those with F-ratio values exceeding 2.0 were processed as spectral peaks (displayed on plots). Target peaks to detect was set at 10. For each peak, the period (years/cycle) is given by the conversion 1/frequency.

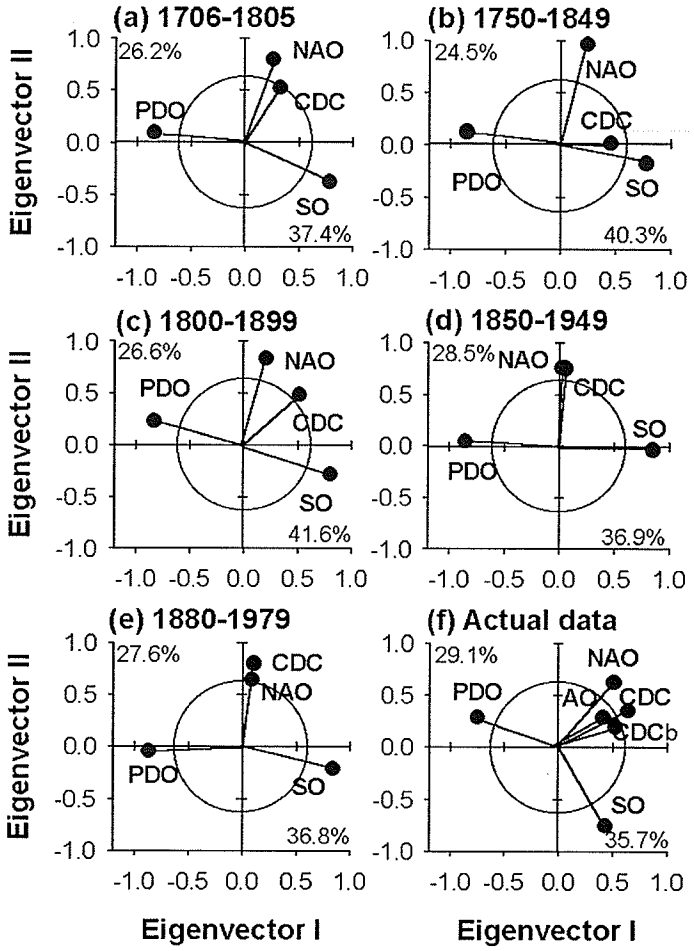

Figure 2.5a–e) Eigenvectors of the principal component analyses (PCA) illustrating the relationships among the reconstructed July CDC, the NAO, the PDO, and the SO through time. Five 100-year intervals a–e) are shown and each demonstrates the correlation coefficient between the reconstructions and PCI and PCII (the descriptors are positioned based on their correlations with the PCs). The correlation among descriptors is also approximated and those with arrows at sharp or obtuse angles are positively or negatively correlated, respectively (either cos 0° = 1.0 or cos 180° = –1.0, i.e. perfect correlation). The circle of equilibrium enables us to judge whether the contribution of each index to the reduced space is greater or smaller than expected under the hypothesis of an equal contribution to all principal components (Legendre and Legendre 1998). Indices that are clearly shorter than the value of their respective equilibrium contributions contribute little to the formation of the reduced space. A sixth plot f shows results of a PCA conducted on instrumental circulation pattern and drought indices for the period 1900–1998. For this last analysis, the AO index as well as the reconstructed CDC (CDCb) were added as supplementary descriptors for comparison with their analogue. Percentages of variance captured by PCI and PCII in the principal component analyses are also shown.

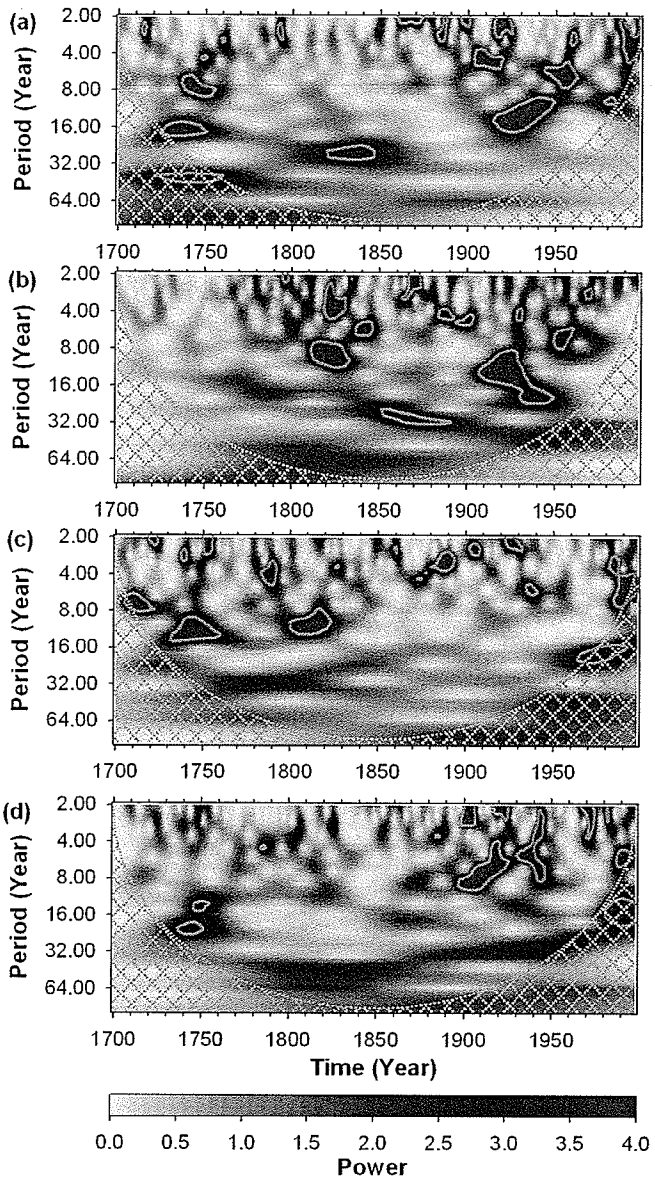

Figure 2.6 a) The CDC, b) the NAO, c) the PDO and d) the SO continuous wavelet transformation (CWT) power spectrums. The wavelet power at each period is normalized by the global wavelet spectra (GWS; Torrence and Webster 1999). The dark blue color indicates areas of large power equal three times the GWS. Red contour is the 5% significance level above the GWS. The crosshatched regions on either end indicate the cone of influence (edge effect; Torrence and Compo 1998; Zheng et al. 2000), where zero padding has reduced the variance.

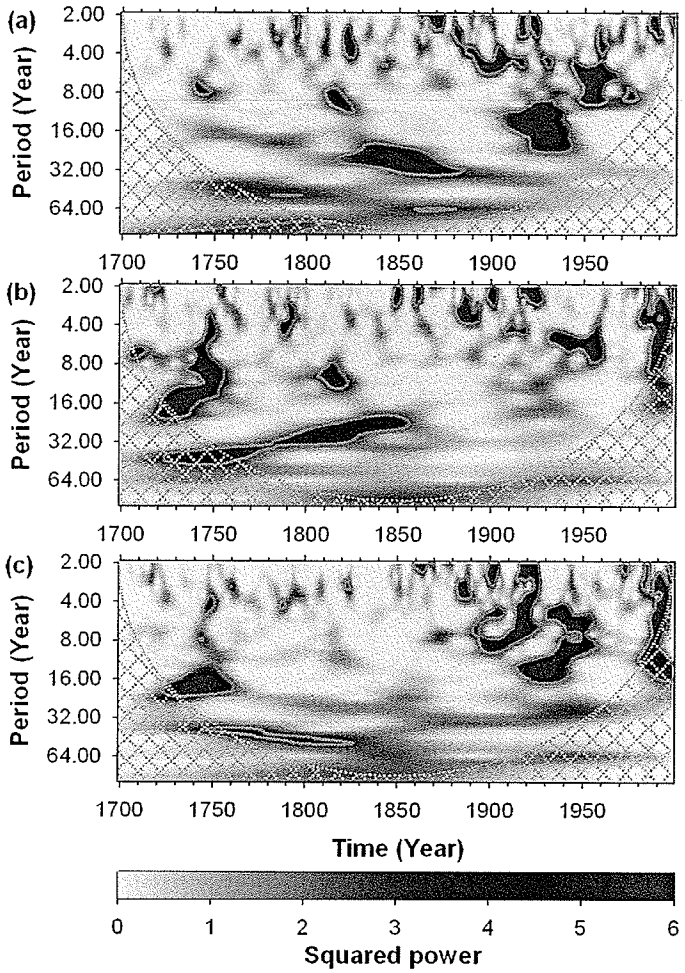

Figure 2.7 Cross-CWT power spectrums of a) the CDC and the NAO, b) the CDC and the PDO, and c) the CDC and the SO. The dark blue color indicates coherency in time and period scales. Red contour is the 1% significance level. The crosshatched regions on either end indicate the cone of influence, where zero padding has reduced the variance.

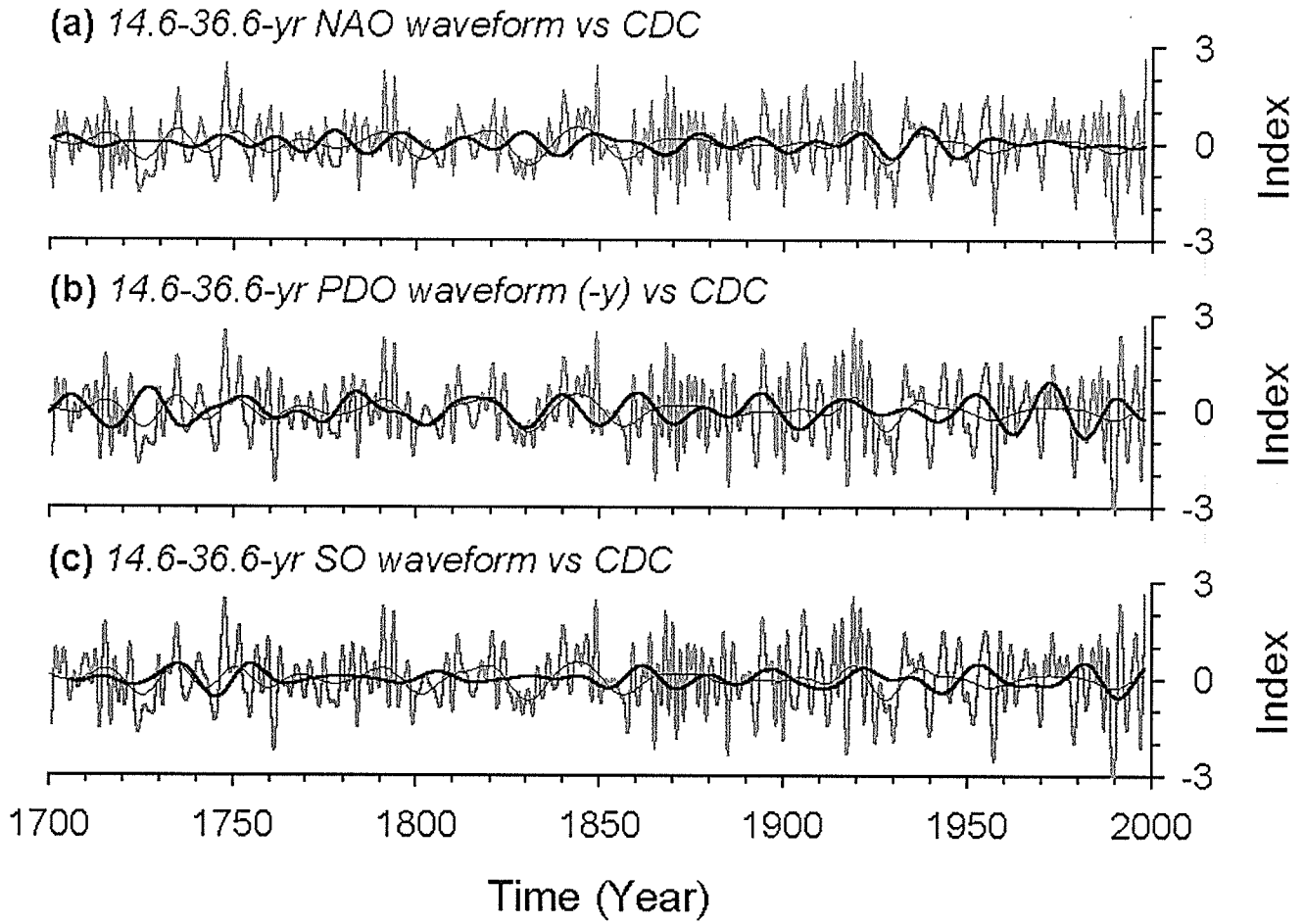

Figure 2.8 The 14.6–36.6-year/cycle waveforms of the a) NAO, b) PDO and c) SO (all thick lines). The normalized CDC (grey line) as well as its 14.6–36.6-year/cycle waveform (thin smooth line) are shown. Signs of the PDO were inverted (-*y*) for a better fit.

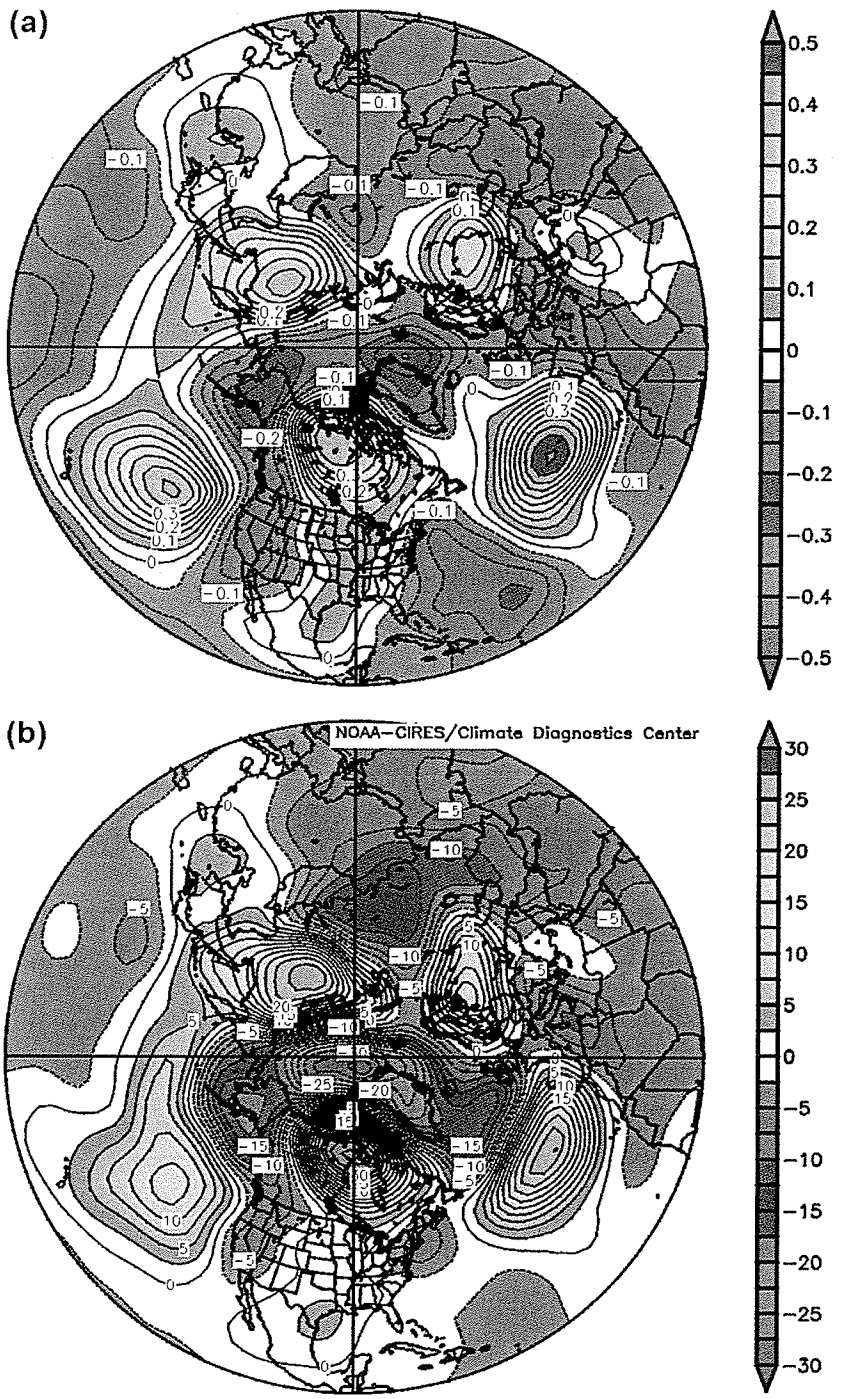

Figure 2.9 The 500-hPa geopotential height a) correlation and b) composite maps (period 1948–1998). The May to July season was used in the calculation of the height data (in m). In a), correlation coefficients are significant at $P < 0.05$ when $r>0.27$. In b), the anomalies were calculated by subtracting the height anomaly values from the ten driest years minus the ten years of lowest drought severity.

Table 2.1 Residual tree-ring chronologies sources and main characteristics of each reconstruction model.

Species	Source	Location	Length	N series total	$r(t)$	$r(t\text{-}1)$	Models I	II	III	IV	V
01- *Pinus banksiana*	Hofgaard et al. (1999)	Hébécourt Lake	219	49	-0.38	-0.12	†				
02- *Pinus banksiana*	Hofgaard et al. (1999)	Chicobi Hills	182	57	-0.13	-0.28	†				
03- *Pinus banksiana*	Hofgaard et al. (1999)	Hedge Hills	185	67	-0.08	-0.01	†				
04- *Pinus banksiana*	Hofgaard et al. (1999)	Joutel	282	51	0.11	-0.27	†	†	†		
05- *Pinus banksiana*	Bergeron et al. (2001)	Duparquet Lake	260	94	-0.38	-0.09	†	†			
06- *Pinus banksiana*	Bergeron et al. (2001)	Abitibi Lake	275	75	-0.02	-0.29	†	†			
07- *Picea mariana*	Hofgaard et al. (1999)	Hébécourt Lake	206	59	-0.33	-0.18	†				
08- *Picea mariana*	Hofgaard et al. (1999)	Opasatica Lake	298	61	-0.25	-0.23	†	†	†		
09- *Picea mariana*	Hofgaard et al. (1999)	Chicobi Hills	177	61	-0.28	-0.24	†				
10- *Picea mariana*	Hofgaard et al. (1999)	Hedge Hills	181	67	-0.32	-0.04	†				
11- *Picea mariana*	Hofgaard et al. (1999)	Joutel	218	57	0.03	-0.23	†				
12- *Thuja occidentalis*	Archambault & Bergeron (1992)	Duparquet Lake	802	55	-0.32	-0.16	†	†	†	‡	‡
13- *Thuja occidentalis*	Tardif and Bergeron (1997b)	Duparquet Lake (wet sites)	571	43	-0.13	-0.12	†	†	†	‡	‡
14- *Fraxinus nigra*	Tardif and Bergeron (1997b)	Duparquet Lake (mesic sites)	308	253	-0.27	0.14	†	†	†		
15- *Picea mariana*	Girardin et al. (2001; 2002a)	Duparquet Lake (wet sites)	166	68	-0.15	-0.16	†				
16- *Betula papyrifera*	Charron and Bergeron (2000)	Duparquet Lake	233	74	-0.46	0.13	†	†			
Characteristics											
Length of the spline curves							60	60	60	60	300
Number of PCs used in the calibrations							2	2	2	4	4

Legend:
Models: I) 1820-1984; II) 1768-1984; III) 1714-1984; IV-V) 1605-1984.
† Residual chronologies used in the models.
‡ Residual series used in the models.
r Pearson's correlation coefficients between the chronologies and the July instrumental CDC index (period 1895-1985) of the current year (t) of ring formation and the year prior (t-1) to ring formation. A correlation is significant at $p<0.05$ when $r>|0.21|$.

Table 2.2 Pearson correlation coefficients between monthly average CDC indices and PCI and PCII of the sixteen site residual chronologies (period 1895-1985)

	PCI	PCII
Monthly average CDC		
Year prior to ring formation		
April	-0.04	-0.05
May	-0.02	0.04
June	-0.16	0.05
July	-0.20	0.24
August	-0.18	0.12
September	-0.09	0.07
October	-0.03	0.00
Year of ring formation		
April	0.21	-0.20
May	0.08	-0.18
June	-0.17	-0.28
July	-0.36	-0.42
August	-0.15	-0.35
September	-0.05	-0.23
October	-0.10	-0.05
May-July average temperature		
Year prior to ring formation	0.14	-0.05
Year of ring formation	-0.18	-0.31
May-July total precipitation		
Year prior to ring formation	0.22	-0.15
Year of ring formation	0.25	0.42

Table 2.3 Calibration and verification statistics of all four sub-reconstruction models (Cook and Kairiukstis 1990; Fritts 2001).

	MODEL I (1820)			MODEL II (1768)		
Calibration periods	1895-1939	1940-1984	1895-1984	1895-1939	1940-1984	1895-1984
Verification periods	1940-1984	1895-1939	-	1940-1984	1895-1939	-
Calibrations						
Multiple *r*	0.69	0.58	0.63	0.70	0.52	0.61
r-square	0.48	0.34	0.40	0.49	0.27	0.38
Adjusted *r*-square	0.43	0.27	0.37	0.44	0.20	0.35
Std. error of the estimate	48.52	49.20	48.46	48.04	51.55	49.23
Analyses of variance						
p-value	0.000	0.002	0.000	0.000	0.011	0.000
Verifications						
Reduction of Error ++	0.29	0.47	-	0.23	0.41	-
Product Means test +++	2.67	3.62	-	2.66	3.62	-
Spearman rank correlation	0.51	0.65	0.60†	0.47	0.64	0.58†
Sign tests ++++						
Agreements	33	33	-	30	30	-
Disagreements	12	11	-	15	15	-
p-value	0.005	0.005	-	0.050	0.050	-

	MODEL III (1714)			MODEL IV (1605)		
Calibration periods	1895-1939	1940-1984	1895-1984	1895-1939	1940-1984	1895-1984
Verification periods	1940-1984	1895-1939	-	1940-1984	1895-1939	-
Calibrations						
Multiple *r*	0.54	0.45	0.43	0.52	0.67	0.54
r-square	0.29	0.21	0.18	0.27	0.45	0.29
Adjusted *r*-square	0.22	0.13	0.15	0.11	0.33	0.22
Std. error of the estimate	56.56	53.77	56.12	60.45	47.22	53.90
Analyses of variance						
p-value	0.007	0.052	0.002	0.148	0.003	0.000
Verifications						
Reduction of Error ++	-0.21	0.02	-	0.20	-0.05	-
Product Means test +++	‡	‡	-	2.79	‡	-
Spearman rank correlation	0.32	0.27	0.43†	0.41	0.27	0.52†
Sign tests ++++						
Agreements	25	29	-	31	27	-
Disagreements	20	16	-	14	18	-
p-value	‡	‡	-	0.020	‡	-

Legend:
‡ Non-significant.
† Correlations between estimated and instrumental data ($p<0.001$ if $r>0.35$).
++ Positive values signify predictive skills.
+++ Significant tests indicate that large departures from the mean are reconstructed any more reliably than smaller ones.
++++ Agreements indicate correct sign of tree-ring estimates.

CHAPTER 3

TRENDS AND PERIODICITIES IN THE CANADIAN DROUGHT CODE AND THEIR RELATIONSHIPS WITH ATMOSPHERIC CIRCULATION FOR THE SOUTHERN CANADIAN BOREAL FOREST

3.1 Abstract

Trends and periodicities in summer drought severity are investigated on a network of Canadian Drought Code (CDC) monthly average indices extending from central Quebec to western Manitoba and covering the instrumental period 1913–1998. The relationship and coherency between CDC indices and ocean–atmosphere circulation patterns are also examined. Trend analyses indicate that drought severity is unchanged in eastern and central Canada. Composite analyses indicate that for most of the corridor severe drought seasons occur with a combination of positive 500-hPa geopotential height anomalies centred over the Gulf of Alaska and over the Baffin Bay. Additional severe drought seasons develop across the corridor in the presence of positive height anomalies located over or upstream of the affected regions. According to spectral analyses, the North Atlantic and the North Pacific circulation patterns modulate the drought variability at the decadal scale. Our results lead us to conclude that climate warming and the increases in the amount and frequency of precipitation in eastern Canada during the last century had no significant impact on summer drought severity. It is unlikely that linear climate change contributed to the change in the boreal forest dynamics observed over the past 150 years.

3.2 Introduction

Fire frequency and area burned in the southeastern Canadian boreal forest have significantly diminished since the end of the "Little Ice Age" (~1850) (Bergeron et al. 2001). Consequently, even-aged stands composed of postfire species are decreasing in proportion and this to the benefit of uneven-aged and older stands composed of shade-tolerant species (Bergeron and Dubuc 1989). Secondary disturbances (insect outbreaks and windthrows) are also playing a greater role in the establishment of the forest mosaic at the landscape level. While the forest successional pathway itself is fairly well understood (Bergeron 2000), the functions regulating succession are not well elucidated. However, paleoecological evidence suggests that climate, by affecting the fire regime, determines the boreal forest species' composition (Carcaillet et al. 2001; Bergeron et al. 2002b).

Bergeron and Archambault (1993) and Bergeron et al. (2001) suggested that the reduction of area burnt in eastern Canada since 1850s reflects a change from extreme fire condition to a moister climate (i.e., fewer extreme seasons of drought). Recent analyses of instrumental meteorological records across Canada suggested significant trends in climate (both precipitation and temperature) over the 20th century for several regions of Canada (Houghton et al. 2001). From 1950 to 1998, temperature in northeastern Canada decreased while it increased in the south and west (Zhang et al. 2000). As well, summer precipitation increased significantly in the northeast (Mekis and Hogg 1999). Most of this increase is attributed to an increase in the frequency of small precipitation events (Zhang et al. 2001). General circulation models' output (Flannigan et al. 2001) also suggested that the increase in precipitation observed in the eastern boreal forest is sufficient to overcome the effect of climate warming with respect to fire weather severity. Contrasting results were found for central Canada, suggesting an increase in dry conditions as a response to climate change (Flannigan et al. 2001).

Ocean circulation patterns can alter regional climate and disturbance regimes over North America. Nigam et al. (1999) and Barlow et al. (2001) demonstrated that North Pacific sea surface temperature (SST) variability was strongly linked to large-scale patterns of drought and stream flow in the U.S.A. Bonsal et al. (1993) and Bonsal and Lawford (1999) also reported similar findings after analysing the teleconnections between Tropical and North Pacific SSTs and summer-extended dry spells in the Canadian Prairies. While the modulation between these patterns and regional climate is not well understood, there is great interest directed towards the use of circulation patterns' information for fire–climate modelling (Flannigan and Wotton 2001).

Understanding temporal changes in fire regimes cannot be entirely based on temperature and precipitation parameters. Fire is a conjunction of various weather parameters and often the result of interactions among precipitation, temperature, humidity, solar radiation, ignition agents, and wind (Van Wagner 1987; Flannigan and Harrington 1988). The daily drought indicators accounting for precipitation, evapotranspiration, and soil moisture capacity developed as components of the Canadian Fire Weather Index system (FWI; Van Wagner 1987) offer an alternative in fire–climate analyses. These indicators, which are the Fine Fuel Moisture Code, the Duff Moisture Code, and the Drought Code (Canadian Drought Code; CDC), differ in their water-holding capacity and their drying rate. The CDC has been used infrequently for climatic studies. In Quebec, CDC indices were used as estimates of soil moisture content to explain yearly variations within tree-ring width (Archambault and Bergeron 1992; Bergeron and Archambault 1993; Tardif and Bergeron 1997b; Girardin et al. 2001). Multicentury CDC reconstructions derived from tree-ring chronologies have also been successfully used to explain multicentury shifts in atmospheric circulation (Girardin et al. 2002b; Girardin et al. 2004a). The CDC has five aspects that are important for this study: (1) the effect of snowmelt is accounted

for in its calculation, (2) it is an adequate indicator of moisture conditions of deep organic layers in boreal conifer stands (Van Wagner 1974), (3) it correlates well with radial growth in boreal trees (Bergeron and Archambault 1993; Tardif and Bergeron 1997b; Girardin et al. 2001), (4) it is an indicator of water table depth, and (5) it represents conditions conducive to fire involving deep soil layers (Turner 1972).

In this study, we construct a network of mean monthly average instrumental CDC indices distributed along the southern Canadian boreal forest. The spatiotemporal variability within the network is analysed and linked with atmospheric circulation using 500-hPa geopotential height composite analyses. Periodicities within the network are also investigated and compared with those characterizing Northern Hemisphere ocean–atmosphere circulation indices. Finally, correlation structures between CDC indices and fire frequency and area burned are analysed to assess the potential use of the CDC indices as estimates of past fire seasons. As fire history data sets are limited in time and accuracy (Murphy et al. 2000), the development of other records that reflect past fire seasons could greatly benefit the understanding of temporal changes in the boreal forest dynamics.

3.3 Materials and methods

3.3.1 Study area

The corridor is located on the Boreal Shield and Boreal Plains ecozones that cover most of the boreal forest from eastern Quebec to northwestern Manitoba (Fig. 3.1). The corridor was divided into six climatic regions (A–F; Fig. 3.1), with boundaries approximating actual ecoregions defined by the Ecological Stratification Working Group (1996). These climatic regions are (A) the Southern Laurentian, (B) and (C) the Abitibi Plains east and west, respectively, (D) the Lake Nipigon, (E) the Lac Seul Upland and Lake of the Woods, and (F) the Boreal Plains (Fig. 3.1). Merging of

ecoregions in climatic regions E and F was necessary because of the lack of meteorological data required for homogenization of the CDC indices. In the Ecological Stratification Working Group's (1996) classification, the Lac Seul Upland (north) and the Lake of the Woods (south) occurs as two separate ecoregions (refer to Fig. 3.1). The Boreal Plains ecozone encompasses 10 separate, mostly upland, ecoregions south of the Canadian Shield, stretching from north-central Alberta to southwestern Manitoba. Eastern ecoregions of the Boreal Plains ecozone were merged to build the climatic region data set: the Mid-Boreal Lowland, the Interlake Plains, the Boreal Transition, and the Mid-Boreal Uplands (Manitoba area). In contrast, the Abitibi Plains ecoregion was divided into two climatic regions (regions B and C) because of its extensive area and availability of meteorological data.

All ecoregions under study have a humid to subhumid midboreal ecoclimate (east to west corridor) marked by warm summers and cold, snowy winters according to the Ecological Stratification Working Group's (1996) regional classification. In eastern climatic regions (A–D), average annual temperature ranges between 1.0 and 1.5 °C, whereas it ranges between –1.0 and 1.0 °C in regions E–F. The average summer temperature is essentially constant across the corridor, approximately 14.0 °C. The average winter temperatures are more variable, ranging from –11.0 °C in region A to –16.0 °C in region F. The average annual precipitation ranges from 1600 mm in the east to 450 mm in the west. In this corridor, most of the annual precipitation falls between June and October (Environment Canada 2002).

3.3.2 Canadian Drought Code calculation

The meteorological data used in this study were daily instrumental data of Environment Canada (2000). Meteorological stations showing the longest records (over 60 year) in the six climatic regions were selected as main stations. Other stations in a 200-km radius and with relatively long records were also selected for the

calculation of homogenized monthly regional CDC indices. In some climatic regions, the number of meteorological stations and extent of the data were insufficient for the construction of homogenized data sets. In this situation, stations outside the radius were used for estimation of remaining missing values. A total of 62 meteorological stations were gathered to construct regional monthly average CDC indices. These stations are summarized in Table 3.1 and plotted per climatic region in Fig. 3.1. Maximum daily temperature data sets were screened for the presence of missing daily values. Months (April–October) with more than 3 days of missing values were eliminated from the CDC calculation. For the remaining months, missing daily values were estimated by calculating the average of the previous and following days. For the precipitation data sets, months with at least one missing daily value were automatically eliminated from the calculation. The CDC is sensitive to daily precipitation, such that one rainfall can significantly affect the value of the index for many days after precipitation. In contrast, a temperature estimation error of a few degrees has little impact on the calculation for the days following. Note that because the CDC calculation is on a day-to-day cumulative basis, the occurrence of a missing daily value at a station in a given year disables the CDC calculation for the rest of the year at that station.

The CDC is a slow-drying index with a time lag estimated at 52 days (Turner 1972). Its calculation was processed as proposed by Turner (1972) and Van Wagner (1987). The calculation begins with a rainfall phase (RP) value of 771 on April 1 (771 being the value normally set by fire agencies when organic layer is fully recharged). The RP, which represents the moisture equivalent after rain (expressed in percentage of dry soil), is otherwise calculated from

[1] $RP = [800/\exp(CDC_{d-1}/400)] + 3.937ER$

where CDC_{d-1} represents the drought value of the previous day. RP can range from 0 to 800, with 800 being saturation in water and 0 being the driest condition normally encountered. RP never exceeds 800. ER (effective rainfall) is equivalent to the amount of rainfall available for storage after interception by the canopy (the constant 3.937 was introduced by Van Wagner 1987 to adapt ER to the metric system). The constant 400 represents the maximum water holding capacity of the soil, which amounts to approximately 400% of water per units of mass. The water-holding capacity of the CDC layer is 100 mm (or 4.0 in.) for a layer with a bulk density of about 25 kg/m^2. Excess water is considered as residual rainfall and is not accounted for by the CDC (see Appendix 3.1).

ER is calculated from

[2] $ER = 0.83P - 1.27$

where P represents the daily value of precipitation over 2.80 mm (intercepted rainfall). ER is not calculated unless precipitation exceeds 2.80 mm. The values of 0.83 and 1.27 mm are empirical constants representing canopy interception. Current drought (D) is calculated using the RP value of Eq. [1] and the following equation:

[3] $D = 400 \ln(800/RP)$

The calculation of the potential evapotranspiration (PET) (the daily dry-weather additive) is given by

[4] $PET = 0.36T + L$

T represents the maximum daily temperature value (°C), and L represents a seasonal day length adjustment. From April to October, the values of L are 0.9, 3.8, 5.8, 6.4,

5.0, 2.4, and 0.4, respectively (Van Wagner 1987). The PET calculation follows Thornthwaite and Mather (1955). The maximum daily temperature was not adjusted to the noon local standard time, as it is normally done in the FWI system (Turner 1972; Van Wagner 1987). The value of 0.36 is the average relationship between maximum temperature and PET (Turner 1972).

The CDC is calculated from

[5] $CDC = D + 0.5PET$

Because the scale length of the CDC is one-half that of the original scale used by Turner (1972), the value of PET is halved (see Van Wagner 1987). A CDC rating of 200 is high, and 300 or more is extreme, indicating that fire will involve deep subsurface and heavy fuels (Van Wagner 1987). Calculation of the RP (Eq. [1]) for April 2 is realised using the CDC value (Eq. [5]) and the ER (Eq. [2]) of April 1. Using the RP result from April 2, Eqs. 3 and 4 are processed for calculation of the April 2 CDC value. This procedure is repeated until October 31. Calculation of next year's CDC is started at April 1 with an RP value of 771. In our corridor, the probability that a current drought persists the following year as a result of insufficient winter precipitation is minimal (overwintering effect, Van Wagner 1987). Thus, no adjustment was made to the CDC calculation.

The effect of snowmelt on the starting value of the CDC was simulated with Turner's (1972) criteria. The snowmelt date is assumed to be the time at which the forest floor is saturated with water (usually occurs in May) and closely corresponds with a decreasing RP of five units a day for 3 days. The procedure that accounts for snowmelt was made as follows. For a given year, the CDC was calculated using eqs. 1–5 with an RP starting value of 771 set at April 1 (refer to Eq. [1]). Then, the output of the RP calculation was monitored, beginning in April. The initial value of 771 set

at April 1 was delayed to the third consecutive day of decreasing RP of five units. The CDC was recalculated for the whole year based on that new starting date.

Monthly average CDC data files were created for each station. Because of changes in measuring instruments and of station relocations through time, nonhomogeneity in the monthly indices may be observed among nearby meteorological stations (Mekis and Hogg 1999; Vincent and Gullet 1999). A test of homogeneity for identification of nonhomogeneous stations was performed between each pair of climate data sets according to the Holmes' (1999) procedure. The Mann–Kendall statistical test for randomness was performed on each paired data set. A pass–fail test was made at the 95% critical limit. All stations failing the test were rejected, unless the anomalies could be corrected.

The regional monthly averages of CDC indices were calculated using program MET (Holmes 1999). In this procedure, the average and standard deviation were calculated for each month at each station. The departure for each month and year was then calculated and averaged across stations to produce mean regional average departures for each month and year. Files of regional mean monthly average CDC indices per climatic region were then produced and used in further analyses. Gaps in CDC indices within single meteorological stations (Table 3.1) were also filled using Holmes' (1999) procedure. Missing monthly values were estimated by calculating the value with a departure from the mean for the month at that station equal to the average departure of the other stations for that month and year. The standard deviation for the month at that station was multiplied by the regional average departure for the month and year, and the mean value for the month at the station was added. New files with estimated data were produced. These data sets were developed for distribution in the scientific community and are not used throughout this paper.

3.3.3 Trends, periodicities, and spatial correlation

The presence of a linear trend in the regional mean monthly average CDC was determined using linear regression analyses for the period 1913–1998. This period was chosen so that all analyses could be performed on the same sample size. Autocorrelation analyses, monthly lagged correlation analyses, and Durbin–Watson tests were also performed on the indices. The presence of autocorrelation was tested, as autocorrelation reduces the effective number of independent observations and thus reduces the degrees of freedom used to determine the confidence in estimates of correlation coefficients (Legendre and Legendre 1998). Continuous wavelet transform (CWT) spectrums were created for identification of nonstationary periodicities within CDC indices (Lau and Weng 1995). CWTs were processed from a nonorthogonal Morlet 6 wavelet basis, a Gaussian windowed complex sinusoid (Torrence and Compo 1998; Program AutoSignal (version 1.5), AISN Software 1999). The wavelet basis was selected so that the time–space domain is maximized in length over the spectral–space domain (Torrence and Compo 1998). All time series were normalized before processing the CWT spectrums. Zero padding was used to eliminate the wraparound effect (see Torrence and Compo 1998).

Spatial patterns among the monthly average CDC indices were examined using S-mode principal component (PC) analyses performed on correlation matrices (Yarnal 1993; Legendre and Legendre 1998; ter Braak and Smilauer 1998; Barry and Carleton 2001). In this procedure, the monthly CDC data sets were transformed into new sets of monthly composite variables. The amount of variability is described using the same number of variables, but with the first principal component (PCI) accounting for the maximum possible proportion of the variance. Succeeding PCs, in turn, account for as much of the residual variance as possible. Eigenvectors, or the loading of each CDC index on each component, gives the spatial representation of the PCs.

Atmospheric circulation composite maps performed on 500-hPa geopotential heights, which approximate the actual height above sea level of the 500-hPa pressure surface, were created with the aid of the National Oceanic and Atmospheric Administration – Cooperative Institute for Research in Environmental Sciences (NOAA–CIRES) Climate Diagnostics Center, Boulder, Colo. (Kalnay et al. 1996; www.cdc.noaa.gov). The 500-hPa grid has a global spatial coverage of 2.5° latitude × 2.5° longitude with 144 × 73 points and a temporal coverage of 1948 to present, with output every 6 h. Daily 500-hPa heights were averaged by months for each grid point. 500-hPa anomalies (expressed in m) were calculated for each calendar month and at each grid point based on the period 1968 – 1996. Composites were created for seasons of 10 severe (10 highest CDC values) and 10 low (10 lowest CDC values) drought conditions. These seasons represent the upper and lower 20% of the sample population.

Coherency between CDC indices and atmospheric and oceanic circulation indices at various time and period scales were identified using the cross product of the CWTs (Torrence and Compo 1998; Torrence and Webster 1999). For comparison, periodicities showing coherency were reconstructed with the use of spectral components isolated in the time–frequency domain. Pearson correlation coefficients were calculated between pairs of periodicities (waveforms) and 95% confidence intervals were constructed using program PEASONT (Mudelsee 2003). The PEASONT procedure employes a nonparametric stationary bootstrap with an average block length proportional to the maximum estimated persistence time of the data (Mudelsee 2003). The hypothesis of a correlation between two serially dependent time series is rejected when the confidence interval contains zero.

The atmospheric and oceanic circulation patterns under study are the North Atlantic Oscillation (NAO; Hurrell 1995), the Pacific Decadal Oscillation (PDO;

Mantua et al. 1997), and the Southern Oscillation (SO; Ropelewski and Jones 1987). The NAO is defined as the north–south sea level pressure dipolar pattern, with one of the centres located over Ponta Delgada, Azores, and the other approximately over Iceland. A positive NAO value indicates strong midlatitude westerlies and is characterized by an intense Iceland Low with a strong Azores Ridge to its south. A negative NAO value indicates that the signs of these anomaly cells are reversed. Over the subtropical Pacific, the SO reflects a difference in sea level pressures between Tahiti and Darwin. A positive SO is an indication that sea level pressure is higher than normal in the Southeast Pacific. Finally, the PDO consists of the leading PC of the North Pacific monthly SSTs poleward of 20°N. A negative PDO value is an indication that SSTs are anomalously warm in the interior North Pacific and cool along the Pacific coast.

3.3.4 Drought and fire history

The CDC indices were correlated with forest area burned (surface burned per year per climatic region) and forest fire frequency (number of fires per year per climatic region) using PC analyses. Fire statistics were introduced as supplementary variables and do not affect the formation of the PCs; the PCs are the linear combinations of the mean monthly average CDC indices. Forest fire statistics were compiled for each climatic region using the forest fire data set of Stocks et al. (2003; period 1959–1998). The forest fire data set only includes fires greater than 200 ha in final size. This represents only a few percent of all fires, but accounts for most of the area burned (more than 97%, Stocks et al. 2003). The forest fire – CDC comparison is made without consideration for the time (i.e., month) and cause of fire ignition. According to Skinner et al. (1999), 84% of all total area burned in Canada occurs during June, July, and August.

3.4 Results

3.4.1 Monthly trends

Across the corridor under study, the month during which maximum drought severity is attained is August (Fig. 3.2). Drought severity decreases in September in climatic regions A, B, C, D, and E. In region F, it remains stable from August to October. Monthly lagged correlation analyses (Fig. 3.3) further suggest significant persistence in the monthly CDC indices (e.g., droughts that occur in June also occur in July ($p < 0.001$), August ($p < 0.05$), and September ($p < 0.05$)).

The CDC indices shown in Figure 3.2 indicate that episodes of extreme drought conditions (values greater than 300) are very common within region F. This contrasts with the eastern regions, which seem to have experienced a marked decrease in the frequency of extreme drought conditions in the early 1900s. Linear regression analyses performed on the monthly average CDC indices (Table 3.2), however, indicate no general trend toward a decrease or increase in drought severity across the corridor (only 1 significant result out of 42 tests). None of the CDC indices contain autocorrelation (Table 3.2).

3.4.2 Analyses of periodicities

For simplification, nonstationary periodic signals were examined within the July mean monthly average CDC indices only. The high month-to-month persistence (see Fig. 3.3) justified the assumption that the variance within the month of July is also representative of June and August. Figure 3.4 indicates that all climatic regions display high power in the frequency band 0.20–0.50 cycles/year (2–5 years/cycle). Power is higher in climatic regions D, E, and F around 1915, 1935, 1945, and 1955. A periodicity of 0.10–0.20 cycles/year (5–10 years/cycle) is observed in climatic regions D and E. Maximum magnitude was attained during 1915–1940 and 1945–

1965 in region D and during 1975–1990 in region E. The strongest periodicity, in the range of 0.05–0.10 cycles/year (10–20 years/cycle), is observed in climatic regions B and C. The lowest periodicity, in the frequency band 0.02–0.05 cycles/year (20–50 years/cycle), is observed in region F. Caution should be taken in the interpretation of this signal, as it is located within the cone of influence.

3.4.3 Spatial distribution of the variance

The identification of basic climatological patterns within the corridor was performed by decomposing the indices into six uncorrelated PCs. Scree plots (Yarnal 1993; results not shown) indicated that PCs I, II, and III were to be used in the interpretation. An exception is found for April, as only two PCs were necessary to describe most of the variation. Correlation structures (eigenvectors) are shown as correlation maps in Fig. 3.5. There is a distinct reduction in the amount of explained variance by the first eigenvector from April to July (first column). The percentage of explained variance decreases by 24.1% to the benefit of eigenvector II, for which the explained variance increases by more than 10% (second column). The correlation maps suggest that prior to July, only one pattern (PCI) dominates the corridor. By July, the partitioning of the variance along higher eigenvectors (Figs. 3.5j and 3.5k) is suggestive of additional patterns. One pattern (explained variance by eigenvector II) appears over the western climatic regions (Fig. 3.5, second column), with a variance negatively correlated with the eastern sector. This pattern slowly retreats from the western sector around August. Another pattern, for which the variance is explained by eigenvector III, is seen in central Quebec (Fig. 3.5, third column). This pattern remains present for most of the drought season, with some monthly variations (Figs. 3.5k and 3.5n).

3.4.4 500 geopotential height anomalies

Upper atmospheric circulation anomalies associated with low and severe drought seasons for the July PCI, PCII, and PCIII were investigated using composite analyses (refers to Fig. 3.5 for partitioning of the variance). Figure 3.6a indicates that on average, severe drought seasons in Ontario occurred with the development of positive geopotential height anomalies (ridges), with centres over the Baffin Bay (average height anomaly of 24 m) and the Gulf of Alaska (20 m). Negative height anomalies (troughs) accompany this over the east and west coasts of the U.S.A. During low severity drought seasons, the positive height anomaly over Baffin Bay is split and displaced over Greenland, allowing a strong zonal flow (–24 m) to penetrate from northern Manitoba toward central Quebec (Fig. 3.6b). This flow further penetrates into the North Atlantic basin between 30°N and 50°N (–16 m). The positive height anomaly over the Gulf of Alaska is displaced above the Bering Sea.

Drought seasons in southwestern Manitoba can also develop with the occurrence of positive height anomalies, with centres over the northwestern U.S.A. (10 m), the Norwegian Sea (16 m), and the Arctic (16 m) (Fig. 3.6c). The flow is displaced northward over northern Manitoba and Ontario (–10 m), well penetrating in Quebec. During low drought seasons (Fig. 3.6d), the northwestern U.S.A. positive height anomaly is replaced by a negative anomaly (–12 m), which penetrates inward Manitoba, while a positive anomaly (14 m) develops in the eastern U.S.A. In addition, the Norwegian Sea positive height anomaly is displaced over the Baffin Bay, while the positive anomaly over the Arctic weakens. This configuration of positive and negative height anomalies that reverses from severe drought to low drought seasons would explain much of the negative correlation observed in PCII between eastern and central Canada (refer to Fig. 3.5j).

Drought seasons in central Quebec can also coincide with the occurrence of a positive height anomaly (10 m) centred over the Great Lakes (Fig. 3.6e). This anomaly displaces the flow over northeastern Quebec. This is also accompanied by positive height anomalies over the northeast of Gulf of Alaska (20 m), the Arctic (25 m), and Iceland (20 m). During low drought seasons (Fig. 3.6f), a negative height anomaly replaces the positive anomaly located over the Great Lakes. This negative height anomaly is surrounded by a positive anomaly with split centres over the Baffin Bay and over the western coast.

3.4.5 Atmosphere–ocean circulation indices

The origin of the variance within the July PCI, PCII, and PCIII was also examined using atmospheric circulation indices (NAO, PDO, and SO). First, the Mann–Whitney statistical test was performed to test for differences in means among samples of NAO, PDO, and SO indices at the time of the 10 highest (severe droughts) and the 10 lowest CDC values (period 1913–1998). For the analyses of PCI, the test indicated statistically significant differences at $p < 0.01$ between the means of NAO during severe and low drought seasons. On average, severe drought seasons correspond with positive NAO values (mean of 0.67), while low drought seasons correspond with negative NAO values (mean of –0.75). A similar relationship at $p < 0.05$ was seen in PCIII. Severe drought seasons occur in conjunction with decreased NAO values (mean of –1.12 for severe vs. 0.03 for low). Tests performed on PCII and on SO and PDO indices were nonsignificant.

Coherencies between CDC indices and atmospheric circulation pattern indices in time and period scales were investigated by crossing CWTs of July PCI, PCII, and PCIII with CWTs of the atmospheric circulation indices (May–July seasonal average). The NAO demonstrates the strongest coherency with PCI (with peaks similar to Figs. 3.4b, 3.4c) and to some extent with PCII and PCIII (Figs. 3.7a–3.7c).

The coherency shifts from one band to another, being at 0.05–0.20 cycles/year in the first half of the century and around 0.50–0.10 cycles/year in the middle (Fig. 3.7a). Reconstruction of the 0.05–0.20 cycles/year (5–20 years/cycle) waveform (Fig. 3.8a) shows that this NAO modulation would explain 17.3% of the variance within PCI from 1913 to 1962. The relationship is no longer significant for the period post-1962 (decoupling between the NAO waveform and PCI beginning in 1970s). The PDO is demonstrating coherency with the PCs, mainly in the low frequency band (0.02–0.05 cycles/year) (Figs. 3.7d–3.7f). Reconstruction of the 20–25 years/cycle waveforms, however, demonstrates that this coherency contrasts among climatic regions. In PCII, this coherency is in phase and positive (Fig. 3.8b). In PCIII, the coherency is in phase, but negative (Fig. 3.8c). The PDO modulation would explain much of the low frequencies seen in Figs. 3.4e and 3.4f. As for the SO, peaks unique to the pattern are present ca. 1910–1920 (Fig. 3.7i) and ca. 1970–1990 (Fig. 3.7h) in the band 0.13–0.30 cycles/year. Other peaks in the band 0.20–0.50 cycles/year are seen in 1910s, 1940s–1950s, and 1990s.

3.4.6 Drought severity and fire history

Correlation maps presented in Fig. 3.9 indicate good agreement between area burned and drought severity. The drought severity variance associated with the first eigenvector (Fig. 3.9a) is significantly correlated with the seasonal area burned in climatic region D. The drought severity variance associated with the second eigenvector (Fig. 3.9b) is significantly correlated with area burned in climatic region F. The drought severity variance associated with the third eigenvector (Fig. 3.9c) correlates significantly with area burned in regions A and B (both correlations are 0.31). The analysis performed on fire frequency indicates very similar tendencies (except for the second eigenvector for which results were nonsignificant). July CDC indices are roughly representative of the overall variance in seasonal area burned and

fire frequency (based on analyses of fires with final area greater than 200 ha; period 1959–1998).

3.5 Discussion

3.5.1 Trends, periodicities, and variance

Linear regression analyses performed on CDC indices indicate that 20th century linear increases in summer temperature and in the amount and frequency of precipitation (Mekis and Hogg 1999; Zhang et al. 2000, 2001) have no significant impact on the moisture balance of the deep organic layer. However, other components of the boreal forest's water balance may be affected by climate change (e.g., more or less rainfall could be intercepted by the canopy, the fine fuels, and the duff layer). Critical investigation of the Fire Weather Index (FWI) and each of its compartments should thus be performed. Studies should focus on average, minimum, and maximum daily, monthly, and seasonal values, and on length of the seasons.

The absence of trends within the CDC indices suggests that factors other than a linear change in climate contributed to the shift in the eastern Canada's boreal forest dynamics over the past 150 years (Bergeron 2000; Bergeron et al. 2001). This interpretation assumes that the functions regulating the fire regime are stationary in time (i.e., they remain unchanged from one period to another). Our results thus give credence to Bergeron and Archambault (1993) and Lefort et al. (2003), who suggested that an increase in the fire cycle length (i.e., length of time required to burn an area equal in size to a specified area) since 1850s in the eastern Canadian boreal forest is a response to a decrease in the frequency of events conducive to extreme fire conditions. These extreme drought events would be similar to those experienced during 1910s and 1920s (Figs. 3.2a–3.2c), the period of largest area burned over the past 150 years in the Abitibi Plains (Bergeron et al. 2001). The 1850s phenomena

could be attributed to a shift in atmospheric circulation and its drivers (PDO and NAO variability; Girardin et al. 2002b; Girardin et al. 2004a).

3.5.2 Synoptic climatology

Our eigenvector analyses suggest that the dominant mode of atmospheric circulation over the corridor resembles a strong zonal flow accompanied by a weak meridional component that develops in July. The persistence of the high-pressure anomalies either over or upstream of the affected sector contributes to the development of the meridional flow. Bonsal et al. (1999) and Skinner et al. (1999) suggested that under these conditions a northward and southward deflection of the moisture carrying systems occurs. The greater probability of subsidence of air (warming and drying) associated with the positive anomalies contributes to the development of a water deficit, given the absence of precipitation and increase in surface evaporation (Skinner et al. 1999). This mechanism is conducive to the occurrence of severe drought seasons and large seasonal area burned (Skinner et al. 1999).

Causes for interannual and interdecadal variations in drought severity have been briefly investigated, with the composites and the coherency analyses conducted on dominant atmospheric circulation patterns. Although it is recognized that these are mostly winter circulation patterns, several investigations have concluded that they are strong enough during summer to affect regional climate (Bonsal et al. 1993; Bonsal and Lawford 1999; Skinner et al. 1999). Based on the cross-CWT analyses, the NAO has been active in the summer period, particularly in the centre of the corridor. The coherency was stronger in the frequency band of 5– 20 years/cycle, with a shift around the mid-century toward an increase in interannual forcing. The relationship appears to be decoupled since 1970s. A response in lower frequencies (20–25 years/cycle) also appears to be emerging from the North Pacific. However, given the

length of the data array and the limited number of wavelengths in the low frequency band, it is difficult to fully quantify the PDO response.

As pointed out by Yarnal et al. (2001), several studies have documented the instability of the atmosphere–surface relationships and further raised serious questions about the long-term reliability of climate prediction models (such as general circulation models). Circulation patterns are dynamic, and wide variations in their amplitude and periodicities occurred over the last three centuries (Stahle et al. 1998; Luterbacher et al. 2002; D'Arrigo et al. 2001; Girardin et al. 2002b). Trying to determine the true relationships between the oceans and the atmosphere is also a great challenge (Mehta et al. 2000; Robertson et al. 2000; Seager et al. 2000). This may be complicated by the nonstationarity and nonlinearity of the ocean atmosphere couplings, but also by the length of the instrumental time series, which seriously limits the interpretation of the low frequency signals. A comprehensive study of multicentury climate change based on proxy data may be a prerequisite for understanding of present and prediction of future climates.

3.5.3 Limitation of the CDC

The CDC is a meteorological estimate, not an absolute drought index (Turner 1972). By using the Thornthwaite and Mather (1955) potential evapotranspiration models, the CDC calculation makes no allowance for seasonal changes in vegetation but only in daylight length (see Turner 1972). Temporal vegetation changes affect the water balance, as the development of herbs and shrubs tends to preserve ground moisture (Hély et al. 2000). This effect may, however, be counteracted by the development of the foliage, which contributes to increasing plant transpiration. In addition, the amount of precipitation (Eq. 2) allocated for canopy interception in the CDC calculation procedure is arbitrary and may vary from one stand type to another, reflecting changes in vegetation. Other potential evapotranspiration estimation

problems may be encountered because soil type, drainage, slope, watershed, atmospheric turbidity, cloudiness, changes in atmospheric CO_2, as well as many other meteorological, geological, and ecological parameters that can affect soil moisture content are not accounted for.

Other uncertainties within the CDC indices arise from exceptionally dry springs caused by an insufficient amount of snow. It is recognised that forest floors in Canada generally receive enough winter precipitation to saturate the CDC layer at spring (Turner and Lawson 1978; Alexander 1982). Exceptional years may, however, occur in regions west of Lake Nipigon and in the Great Plains. As the monthly lagged correlation between CDC indices decreases importantly from May to July (drought variability in May noncorrelated with that of July), this limitation may be of minor importance in the investigation of summer drought variability within our corridor. Studies to be conducted elsewhere could necessitate adaptations to the CDC calculation.

3.6 Summary

This paper summarizes the construction of a network of monthly average CDC indices using 62 meteorological stations distributed across the corridor extending from central Quebec to western Manitoba, in the range of the southern Canadian boreal forest. These records were used for the construction of regional CDC indices in six climatic regions. Linear trends fitted on the regional mean monthly averages revealed no major changes in summer drought severity from 1913 to 1998.

This paper also demonstrates the potential use of CDC indices in synoptic climatology. Composites and coherency analyses indicated that the North Atlantic and the North Pacific circulation patterns demonstrate the strongest relationship with drought variance. The coherencies, however, occur in a decadal scale, and the CDC

data length seriously limits our interpretation of the responses. Validation of these relationships may require the use of long paleoclimatic records. Combined with regional fire history studies developed from forest stand age distributions, paleoclimatic analyses may provide useful insights on the causes of the changes in eastern Canada's forest fire regime. Such understanding would benefit the prediction of the response of the boreal forest to anticipated climate change.

3.7 Acknowledgements

We acknowledge the Sustainable Forest Management Network (SFM) for funding this research and supporting M.P. Girardin. This author was also supported by the Fonds Québécois de la Recherche sur la Nature et les Technologies and by Groupe de recherche en écologie forestière interuniversitaire (GREFI), Université du Québec à Montréal. We thank Dr. Christopher Torrence, Dr. Richard Holmes, the National Oceanic and Atmospheric Administration (NOAA), the Cooperative Institute for Research in Environmental Sciences (CIRES), the Climate Diagnostics Center (CDC), the National Centers for Environmental Prediction (NCEP), the National Center for Atmospheric Research, and the Meteorological Service of Canada for their aid and contribution of data and (or) software. This manuscript was improved through the comments of Héloïse Le Goff, Dr. D. Maynard, and two anonymous reviewers.

3.8 Appendix

3.8.1 Calculation of the CDC residual rainfall

The amount of moisture from any specific rainfall that is absorbed in the CDC layer is given by the difference in moisture equivalent (RP) after (*d*; current day) and before ($_{d-1}$; previous day) rain.

[A1] $\Delta RP = RP_d - RP_{d-1} = [400 \exp(-CDC_d/400)] - [400 \exp(-CDC_{d-1}/400)]$

where the constant 400 represents the maximum theoretical moisture content of the soil. Once the effect of the rainfall phase is known, water absorbed (Wa; in mm) equals

[A2] $W_a = (\Delta RP25)/1000$

where 25 and 1000 (both in kg/m^3) represents the standard load and the weight of water per volume. The amount of residual rainfall (Drought Code Residual, DCR) is calculated from the total amount of rainfall (in mm, R_a) minus the intercepted rainfall ($R_i = 0.17P + 1.27$) and the absorbed water (W_a). Thus

[A3] $DCR = R_a - R_i - W_a$

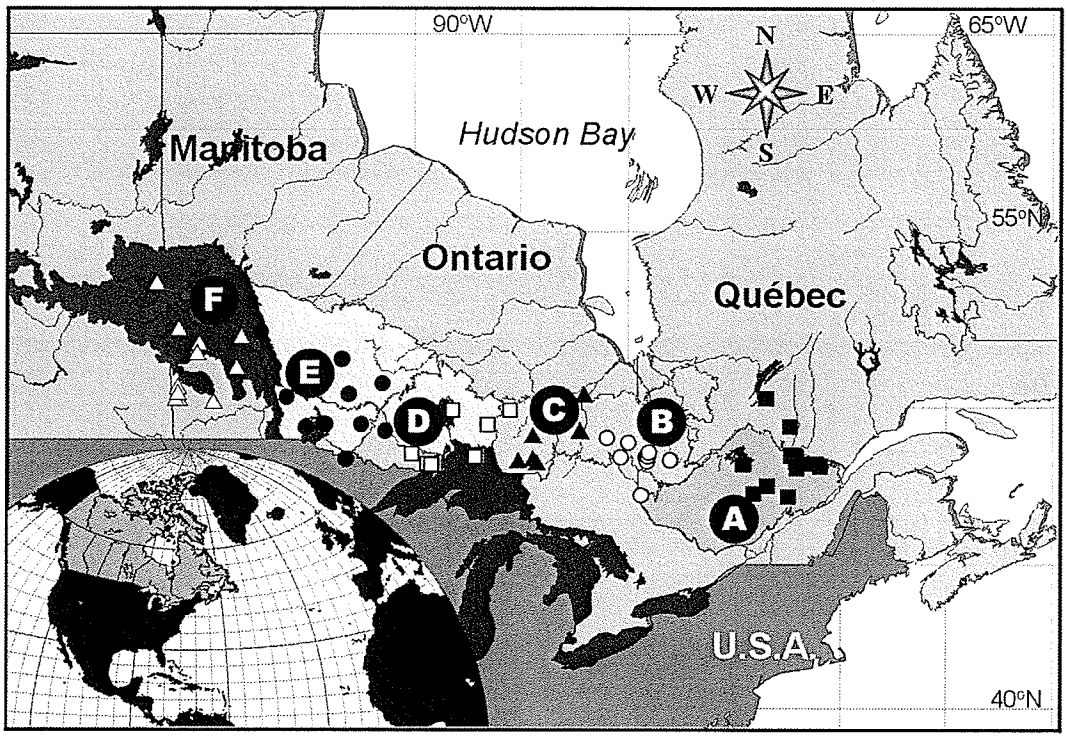

Figure 3.1 Geographical locations of the 62 meteorological stations per climatic regions: A, Southern Laurentians; B, Abitibi Plains east; C, Abitibi Plains west; D, Lake Nipigon; E, Lac Seul Upland and Lake of the Woods; and F, Boreal Plains. Symbols identify the stations used in each of the climatic regions. Ecoregions, as defined by the Ecological Stratification Working Group (1996), are also drawn.

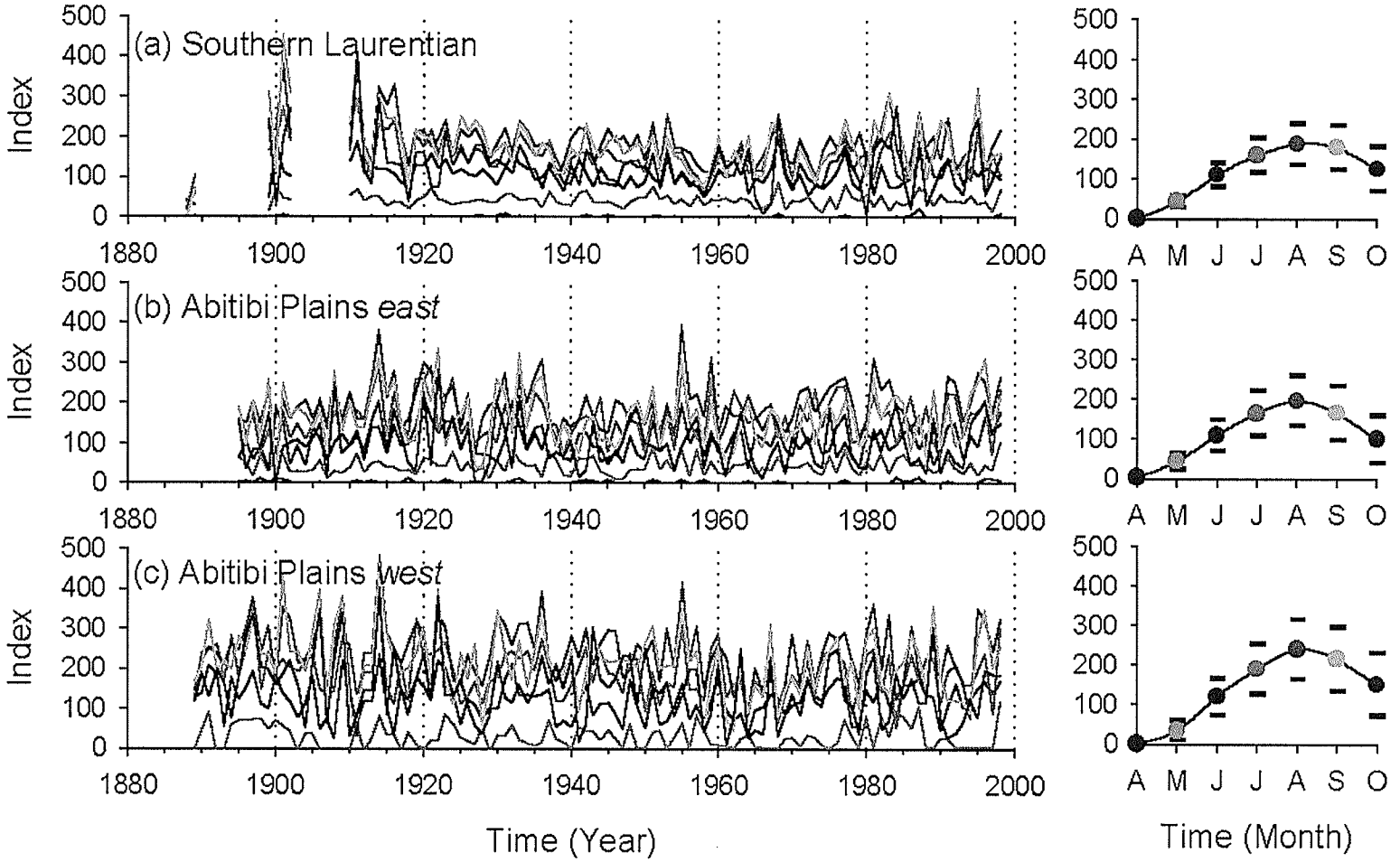

Figure 3.2 Regional mean monthly average Canadian Drought Code (CDC) indices (left column). The period prior 1913 in (a) and (e) contains uncertainties and missing values attributed to the number of station replicates for mean of comparison. The right column shows the average (with error bars) of the mean monthly values (April–October) for the period 1913–1998. A different shade is given for each month (refer to right column for month identification). Note the different y axis scale for (e) and (f).

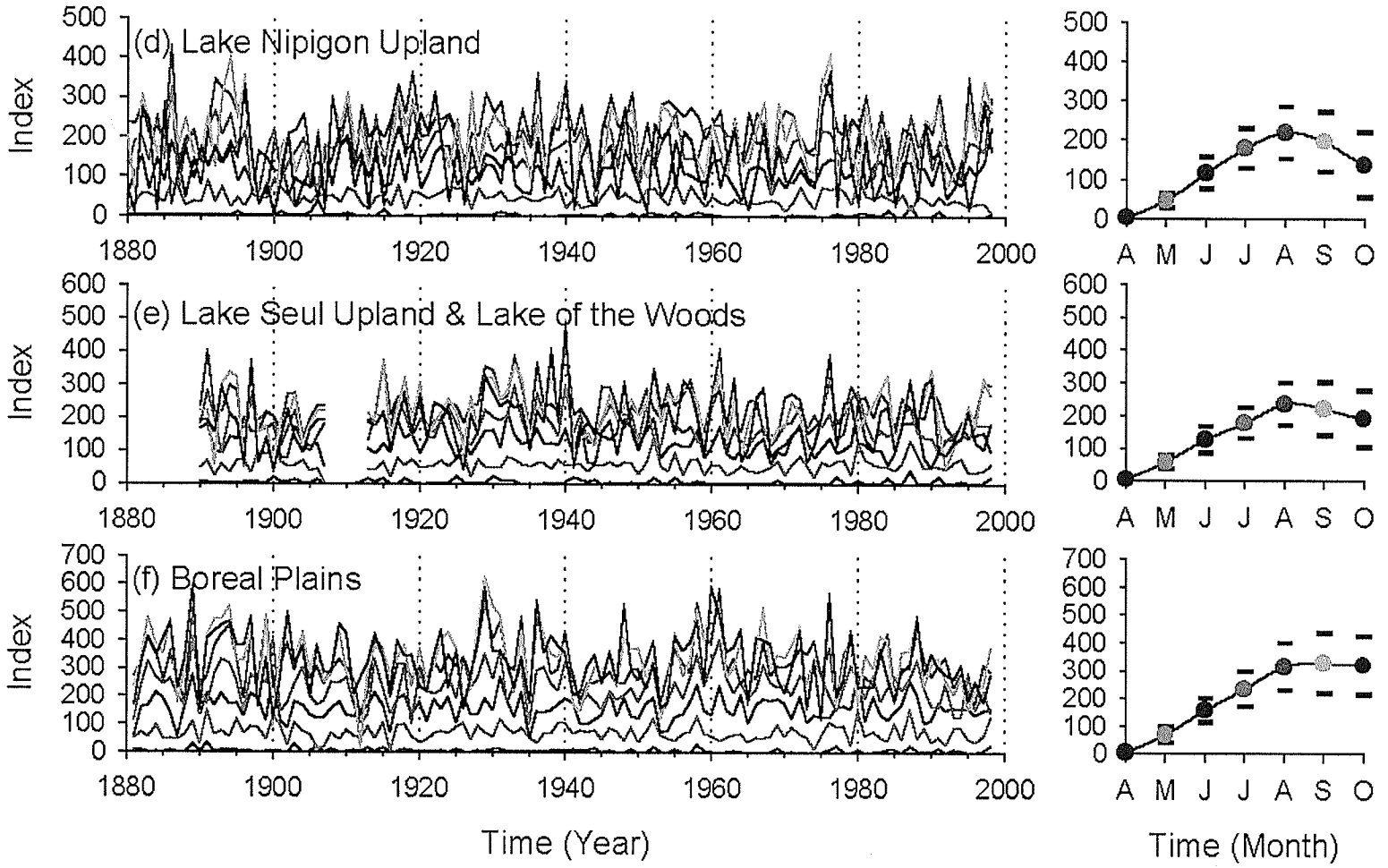

Figure 3.2 *Continues.*

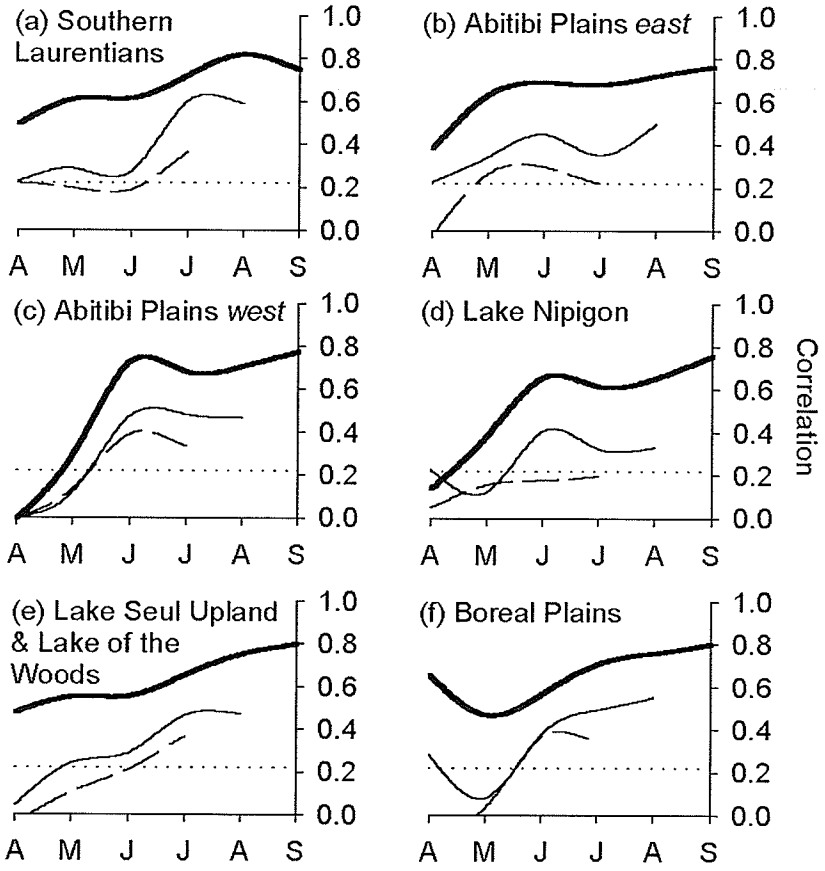

Figure 3.3 Monthly lagged Pearson's correlation coefficients. Analyses were conducted for the period 1913–1998. The thick line shows the correlation coefficient between a month and the following one (e.g., April vs. May). The thin line shows the correlation coefficient with the second following month (e.g., April vs. June). The dashed line shows the correlation coefficient with the third following month. The significance level at $p < 0.05$ is given by the dotted line.

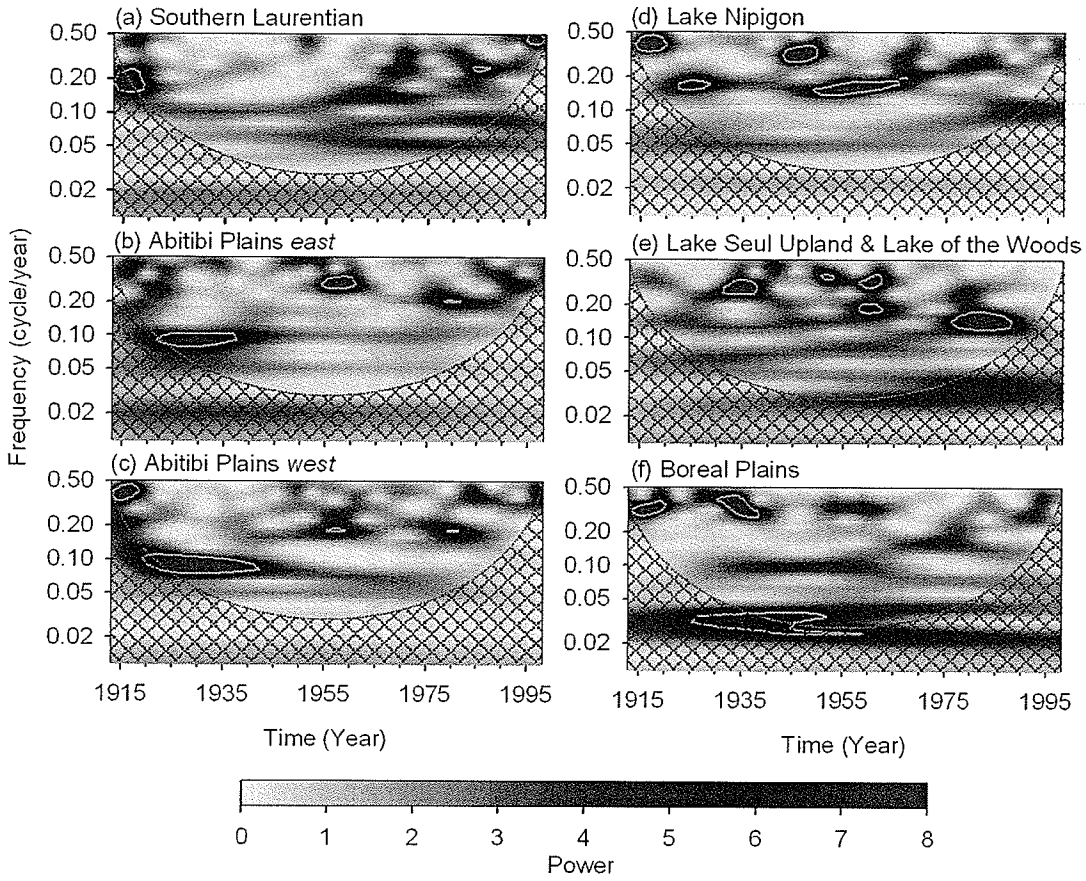

Figure 3.4 Continuous wavelet transform (CWT) spectrums of Canadian Drought Code (CDC) indices for July per climatic region. Analyses were conducted for the period 1913–1998. The period (years/cycle) of each peak is given by the conversion 1/frequency. The variance (in normalized units) is scaled from 0 to 10, where dark-blue area indicates large power. The red contour line delineates the 5% significance level for white noise. The crosshatched region delineates the cone of influence (area of decreased variance resulting from a discontinuity introduced at the end of the data stream; Torrence and Compo 1998).

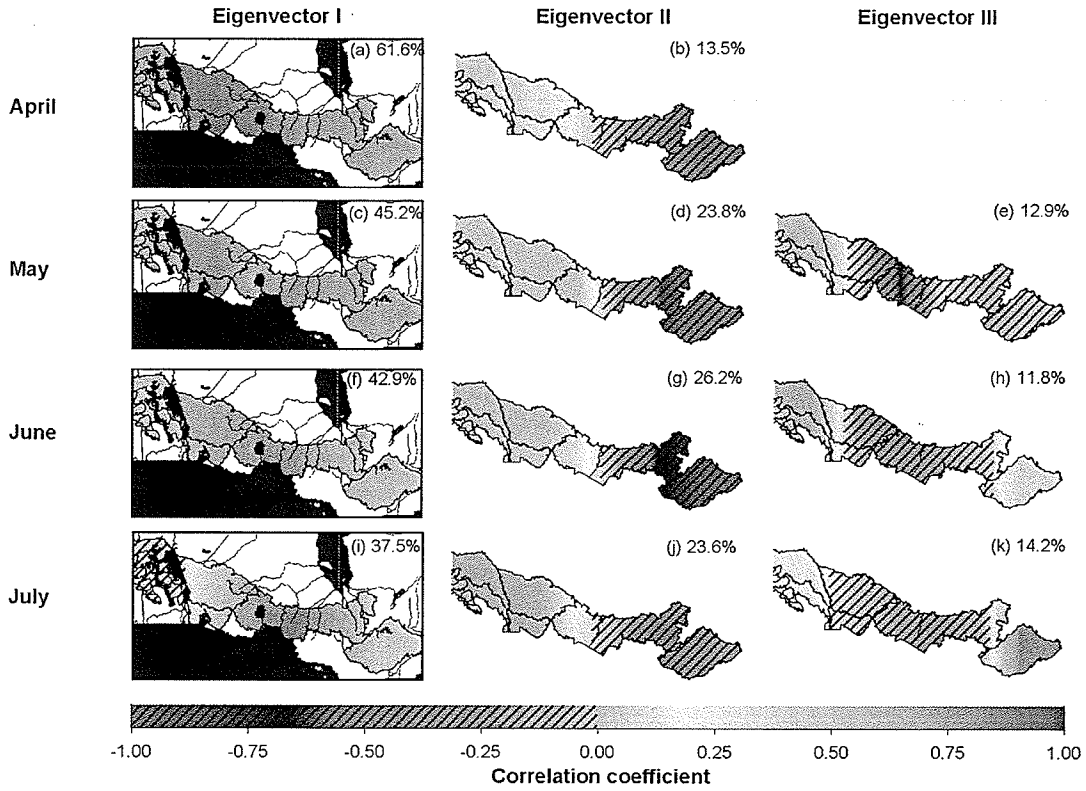

Figure 3.5 First, second, and third eigenvectors of the regional monthly average Canadian Drought Code (CDC) indices for April–October. The shadings indicate the correlation coefficients between the regional indices and the corresponding principal component. Correlation are significant at $p < 0.01$ when $-0.28 > r > 0.28$. For each map, the percentage of explained variance is indicated.

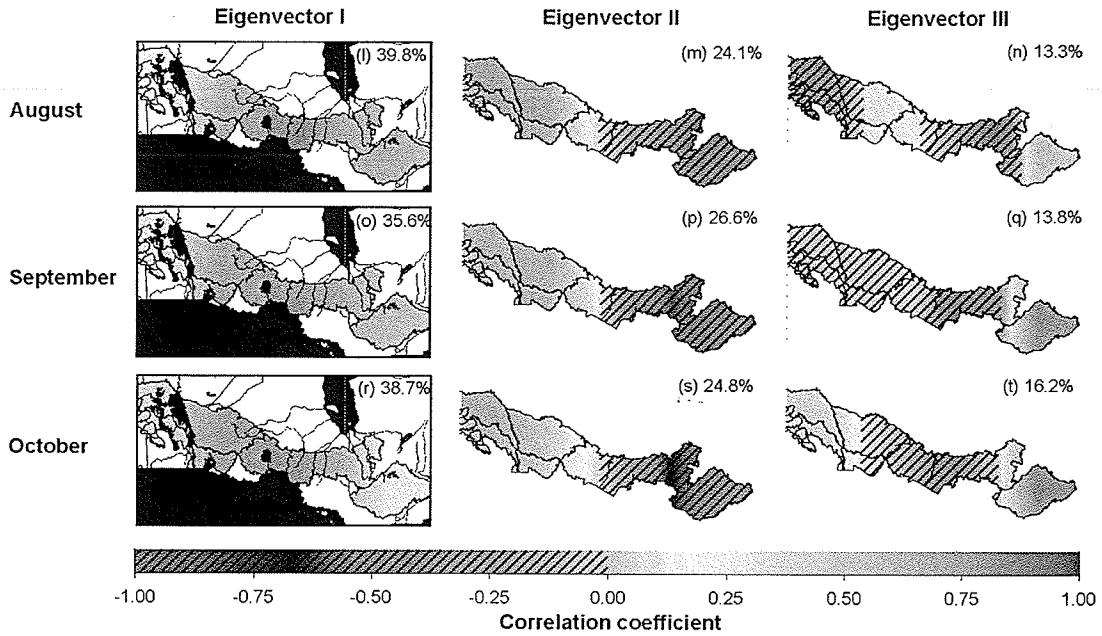

Figure 3.5 *Continues.*

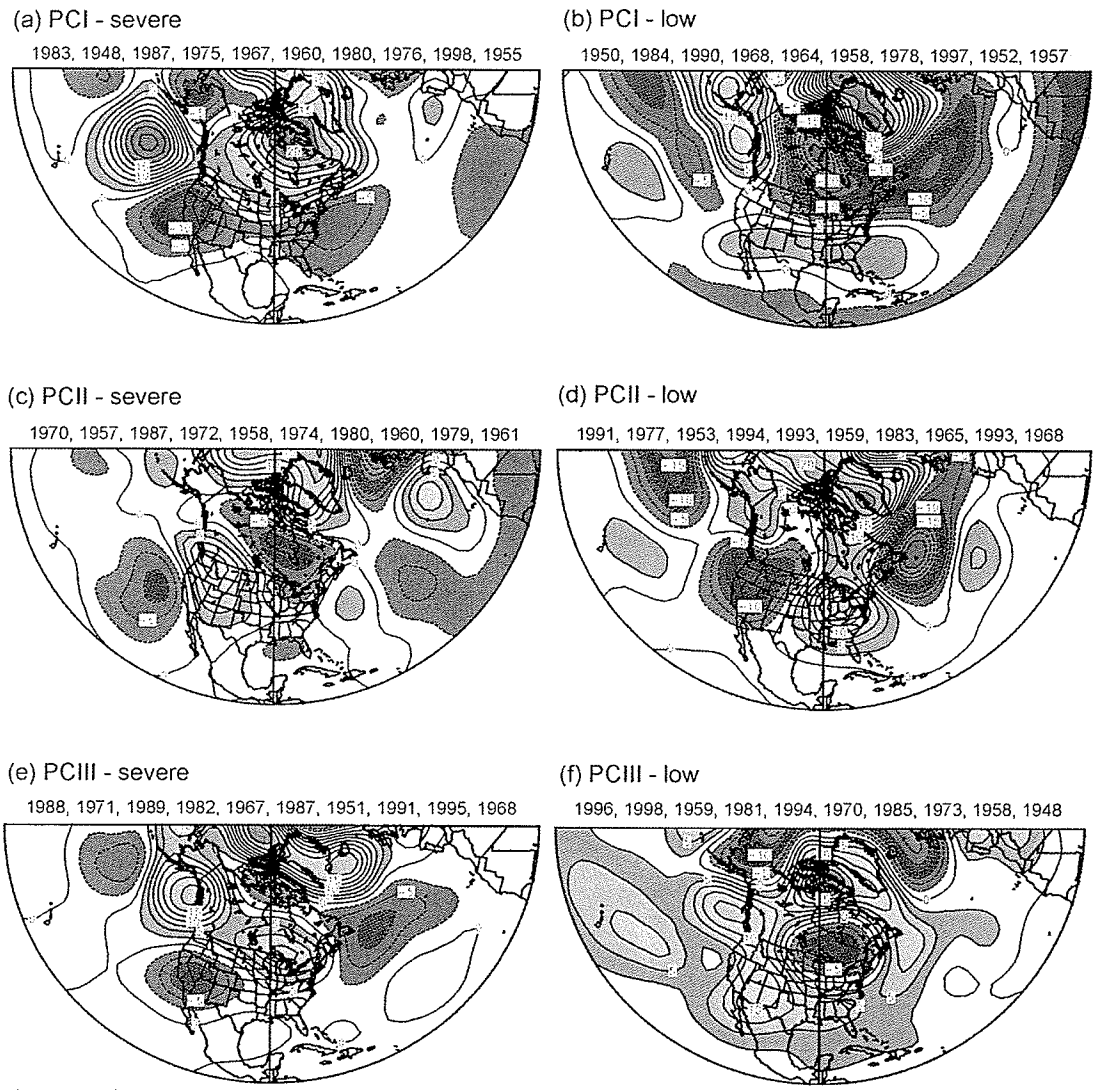

Figure 3.6 The 500-hPa geopotential height anomaly composites (in metres) for 10 seasons of severe and 10 seasons of low drought conditions for July: (a, b) principal component (PC) I, (c, d) PCII, and (e, f) PCIII (period 1948–1998). The May–July season was used in the calculation of the height data. Years used in the composites are listed above each map (in order of increasing drought severity).

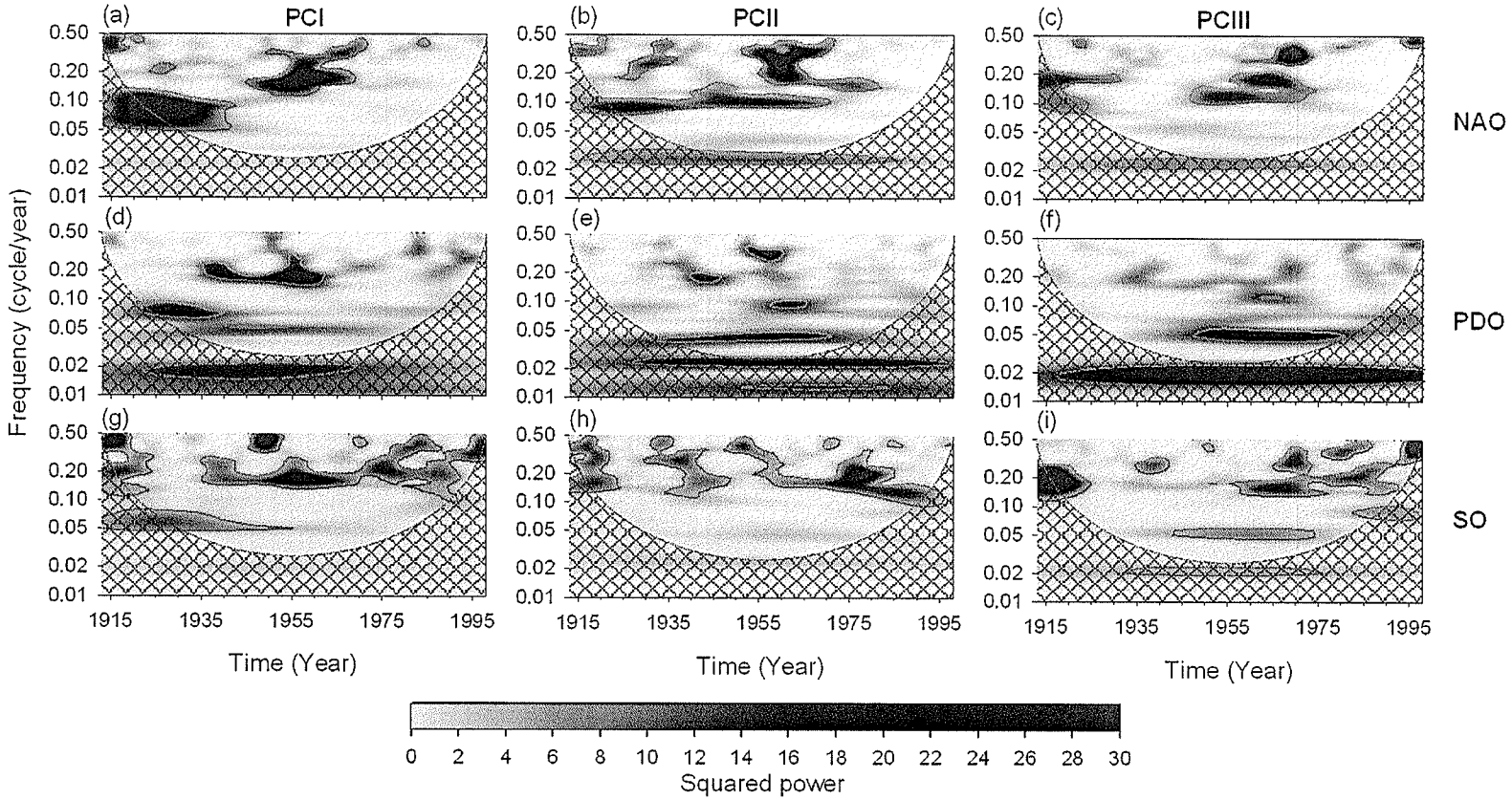

Figure 3.7 Cross-continuous wavelet transform (CWT) power spectrums of principal component (PC) I, PCII, and PCIII against the North Atlantic Oscillation (NAO), the Pacific Decadal Oscillation (PDO), and the Southern Oscillation (SO). The variance (in normalized units) is scaled from 0 to 20, where a dark-blue area indicates coherency between two time series in time and period scales. The red contour line delineates the 5% significance level.

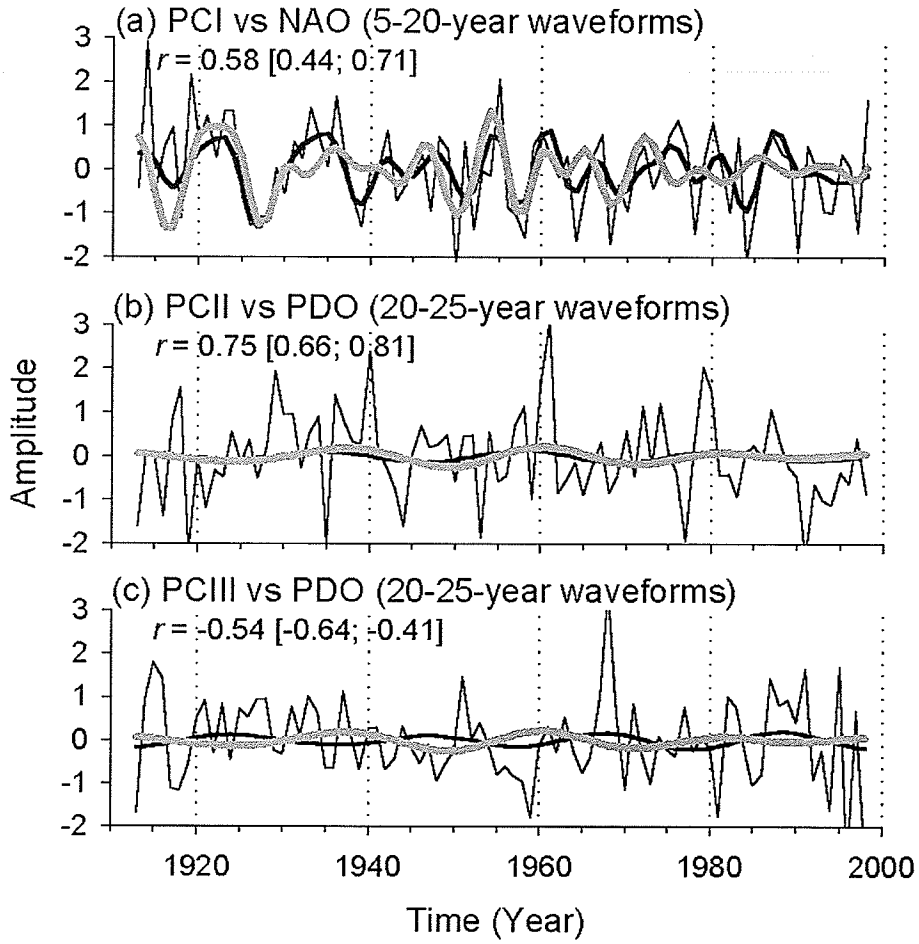

Figure 3.8 Examples of coherencies among principal component (PC) analysis loadings (thin lines) and atmospheric circulation pattern indices. In (a) are shown 5- to 20-year waveforms. In (b) and (c) are shown 20- to 25-year waveforms. Waveforms associated with the PCs are shown as thick, black, smoothed lines. Waveforms associated with the circulation indices appear as thick, grey lines. The Pearson's correlation coefficient *r* and the 95% confidence interval (in brackets) are given for each pair of waveforms. The hypothesis of a correlation between two waveforms is rejected when the interval contains zero (Mudelsee 2003). NAO, North Atlantic Oscillation; PDO, Pacific Decadal Oscillation.

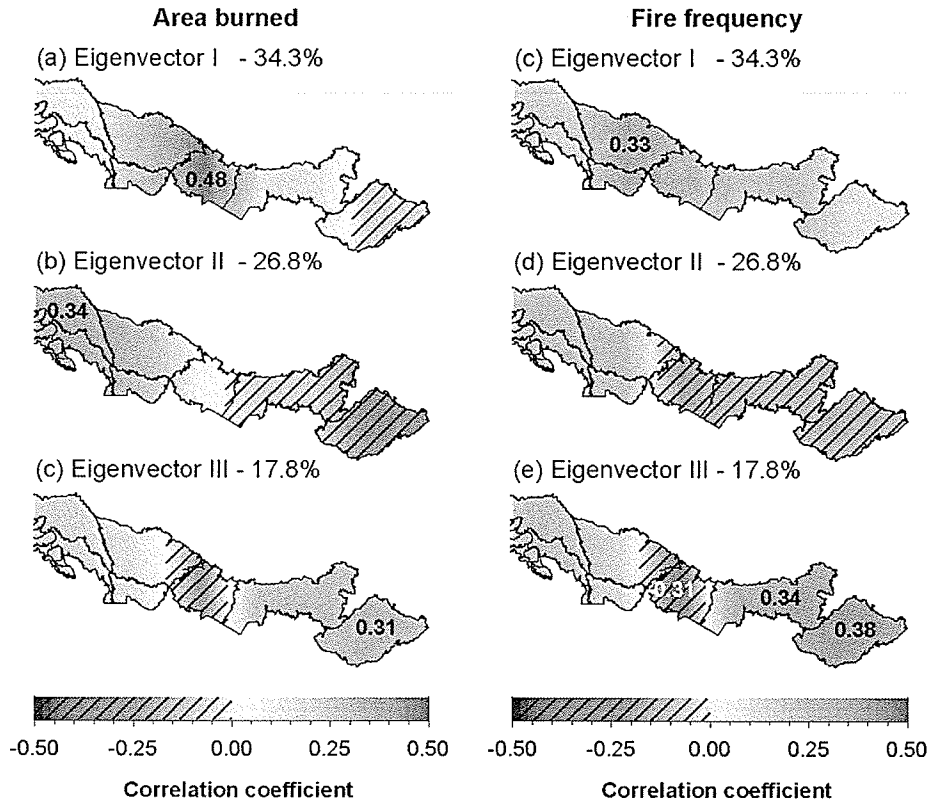

Figure 3.9 Correlations maps demonstrating the relationship between drought severity and area burned (a, b, c) and fire frequency (d, e, f) (period 1959–1998). The eigenvectors I, II, and III denote the correlation between the principal components (computed from the July mean monthly average Canadian Drought Code (CDC) indices) and the fire statistics. Correlations are significant at $p < 0.05$ when $-0.31 > r > 0.31$ (significant correlation coefficients are shown on maps). For each map, the percentage of explained variance is indicated.

Table 3.1 Meteorological stations used in the calculation of the mean monthly average Canadian Drought Code (CDC) indices.

Stations per ecoregions	Code	Longitude	Latitude	Elevation	Period
A-Southern Laurentian					
Normandin	7065640	72°32W	48°51N	137	1937-1992
Roberval airport	7066685	72°16W	48°31N	179	1958-1998
Roberval	7066688	72°14W	48°32N	102	1888-1966
Mistassini	7064998	72°12W	48°51N	122	1964-1994
Albanel	7060080	72°27W	48°53N	152	1923-1990
Bagotville	7060400	71°00W	48°20N	159	1943-1998
Lac Bouchette	7063560	72°10W	48°13N	358	1951-1998
Chicoutimi	7061441	71°50W	48°25N	175	1881-1979
Hemon	7063090	72°36W	49°40N	183	1966-1998
Kenogamie	7063400	71°15W	48°25N	116	1924-1964
Barrage à Lac Kempt	7070448	74°11W	47°33N	421	1913-1963
Barrage Gouin	7070454	74°60W	48°21N	404	1914-1979
La Tuque	7074240	72°47W	47°24N	152	1915-1998
Manouan Sanmaur	7074600	73°48W	47°54N	357	1919-1972
Mistassini Post	7095000	73°53W	50°25N	380	1899-1980
B-Abitibi Plains east					
Abitibi Post	7090050	79°22W	48°43N	259	1898-1935
Amos	7090120	78°07W	48°34N	259	1915-1997
Duparquet	709BBDH	79°16W	48°31N	290	1983-1993
La Sarre	7094120	79°12W	48°48N	244	1952-1998
Val St-Gilles	70986RN	79°07W	48°59N	290	1973-1998
Cochrane	6071712	81°02W	49°04N	275	1912-1991
Iroquois Falls	6073810	80°40W	48°45N	259	1913-1997
Kirkland Lake	6074209	80°00W	48°90N	324	1951-1996
Haileysbury	6073138	79°38W	47°27N	189	1895-1922
C-Abitibi Plains west					
Franz	6052563	84°25W	48°28N	373	1918-1949
Hornepayne	6053570	84°46W	49°12N	329	1920-1989
Steep Hill Falls	6058010	84°48W	48°40N	335	1920-1938
White River	6059475	85°17W	48°36N	379	1889-1975
Kapuskasing A	6073960	82°28W	49°25N	227	1919-1998
Kapuskasing	6073975	82°26W	49°27N	218	1937-1998
Smokey Falls	6077845	82°10W	50°40N	183	1934-1996
D-Lake Nipigon					
Cameron Falls	6041109	88°21W	49°90N	229	1925-1997
Geraldton A	6042716	86°56W	49°47N	349	1981-1998
Kakabeka Falls	6043930	89°37W	48°24N	278	1910-1976
Port Arthur	6046588	89°13W	48°26N	195	1878-1941
Schreiber	6047624	87°16W	48°49N	302	1910-1975

Stations per ecoregions	Code	Longitude	Latitude	Elevation	Period
Thunder Bay A	6048261	89°20W	48°22N	199	1942-1993
Manitouwadge	6044903	85°48W	49°90N	332	1956-1994
Savanne	6047615	90°12W	48°58N	459	1892-1946
E-Lac Seul Upland and Lake of the Woods					
Dryden	6032117	92°50W	49°47N	372	1914-1997
Ignace	6033690	91°39W	49°25N	447	1914-1970
Kenora	6034070	94°32W	49°48N	336	1900-1938
Kenora A	6034075	94°22W	49°47N	410	1939-1998
Sioux Lookout	6037775	91°54W	50°70N	390	1939-1998
Fort France	6022475	93°25W	48°37N	343	1892-1995
Earl Falls	6012198	93°13W	50°38N	361	1930-1996
Red Lake A	6016975	93°48W	51°40N	386	1939-1998
Channel Island	5030556	97°23W	52°18N	216	1890-1904
Great Falls	5031200	96°00W	50°28N	249	1923-1996
Indian Bay	5031320	95°12W	49°37N	327	1915-1998
F-Boreal Plains†					
Dauphin*	5040675	100°20W	51°90N	292	1890-1941
Swan River*	5042800	101°13W	52°30N	347	1910-1998
Dauphin A*	5040680	100°30W	51°60N	305	1943-1998
Gilbert Plains*	5040985	100°28W	51°60N	404	1959-1998
Moosehorn*	5041800	98°37W	51°18N	250	1910-1963
Russell Barnardo*	5042522	101°20W	50°59N	558	1896-1906
Ashern*	5040120	98°22W	52°08N	263	1967-1989
Russell*	5012520	101°17W	50°46N	567	1884-1990
Cumberland House*	4071960	102°18W	53°58N	271	1937-1964
Minnedosa	5011760	99°50W	50°16N	521	1881-1998
Fort Ellice	5010977	101°14W	50°25N	NA	1890-1894
Birtle	5010240	101°30W	50°26N	522	1917-1995

Legend:
NA: non-available.
†: The Boreal Plains regional data set was created using weather stations marked by an *. Remaining missing values within the regional data set were estimated using three other stations located southward (non-marked by *).
Elevation (meters) is above sea level.

Table 3.2 Analyses of Canadian Drought Code (CDC) monthly trends, period 1913–1998.

	R	Slope	*p*	D-W	Auto-*R*
A-Southern Laurentian					
April	0.07	0.01	0.51	1.88	0.02
May	0.01	0.00	0.95	2.17	-0.10
June	0.06	-0.07	0.58	2.06	-0.03
July	0.16	-0.28	0.13	2.00	-0.02
August	0.18	-0.37	0.09	1.83	0.07
September	0.12	-0.25	0.29	1.79	0.10
October	0.00	-0.23	0.35	1.91	0.04
B-Abitibi Plains east					
April	0.15	0.03	0.17	1.86	0.07
May	0.05	0.04	0.62	2.33	-0.21
June	0.05	-0.08	0.64	1.90	0.03
July	0.10	-0.22	0.37	2.17	-0.10
August	0.09	-0.22	0.43	1.77	0.10
September	0.07	-0.18	0.54	1.79	0.10
October	0.00	-0.25	0.34	1.93	0.03
C-Abitibi Plains west					
April	0.03	0.00	0.78	1.84	-0.01
May	0.07	0.07	0.51	2.06	-0.08
June	0.02	0.03	0.87	1.67	0.16
July	0.12	-0.31	0.26	2.08	-0.06
August	0.19	-0.59	0.07	2.02	-0.02
September	0.17	-0.55	0.12	2.00	0.01
October	0.21	-0.67	0.05	2.14	-0.07
D-Lake Nipigon Upland					
April	0.04	0.01	0.71	2.24	-0.12
May	0.16	-0.12	0.15	2.20	-0.05
June	0.02	0.03	0.86	1.93	-0.01
July	0.09	-0.17	0.44	2.06	-0.07
August	0.12	-0.32	0.27	2.09	-0.05
September	0.01	-0.04	0.91	2.11	-0.07
October	0.08	-0.28	0.44	2.15	-0.09
E-Lac Seul Upland & Lake of the Woods					
April	0.02	0.01	0.83	2.13	-0.10
May	0.01	0.01	0.92	2.13	-0.07
June	0.05	-0.09	0.63	1.83	0.08
July	0.19	-0.36	0.08	1.80	0.09
August	0.01	-0.37	0.20	1.90	0.04
September	0.12	-0.38	0.29	2.09	-0.05
October	0.13	-0.44	0.24	2.05	-0.03

	R	Slope	*p*	D-W	Auto-*R*
F-Boreal Plains					
April	0.07	0.02	0.52	2.05	-0.08
May	0.03	-0.03	0.80	2.30	-0.18
June	0.00	-0.01	0.98	2.18	-0.09
July	0.08	-0.21	0.46	1.97	-0.01
August	0.10	-0.33	0.38	1.85	0.06
September	0.15	-0.66	0.16	1.81	0.09
October	0.15	-0.62	0.17	2.15	-0.08

Legend:
R: multiple correlation of the linear trend model
p: analyses of variance significance level. Hypothesis stating that the slope of the regression line is zero is rejected when $p < 0.05$.
D-W: Dublin-Watson statistic; significant at $p < 0.05$ if $1.67 > d > 2.33$.
Auto-*R*: 1st order autocorrelation; significant at $p < 0.05$ if $-0.22 > r > 0.22$.
Underlined results are significant at $p < 0.05$.

CHAPTER 4

SENSITIVITY OF TREE GROWTH TO THE ATMOSPHERIC VERTICAL PROFILE IN THE BOREAL PLAINS OF MANITOBA, CANADA

4.1 Abstract

This paper investigates the influence of surface climate and atmospheric circulation on radial growth of eight boreal tree species growing in the Duck Mountain Provincial Forest, Manitoba, Canada. Tree-ring residual chronologies were built, transformed into principal components (PCs) and analyzed through correlation and response function to reveal their associations to climate (temperature, precipitation and drought data for the period 1912-1999 as well as local geopotential height data for the period 1948-1999). Geopotential height correlation and composite charts for the Northern Hemisphere were also constructed. Correlation and response function coefficients indicated that radial growth of all species was negatively affected by temperature–induced drought stresses from the summers previous and current to ring formation. The summer drought stress alone explained nearly 28% of the variance in PC1. Warm spring temperature was also a positive factor for *Pinus banksiana* Lamb. and *Picea glauca* (moench) Voss, but a negative one for all hardwoods. Analyses performed on geopotential height highlighted the importance of the Northern Hemispheric atmospheric circulation in the species' response to climate. The variability within the 500-hPa level over southern Manitoba explained 39% and 58% of the variability in PC1 and PC2, respectively. The relationships were highly significant with the middle and high troposphere during spring and late summer (determinant factor for growing season length) and with the troposphere and stratosphere during summer. The sensitivity of tree growth to atmospheric circulation

exceeded the synoptic scale, with a response associated with yearly variations in the amplitude of the mid-tropospheric longwaves.

4.2 Introduction

Terrestrial vegetation responds to weather and climate through a variety of physiological, demographic, and ecosystem functions (Bonan 2002). Together, these functions determine where plant species grow, how well they grow, and how their arrangement within the communities changes over time (Bonan 2002). In this context, any changes in the state of weather and climate will affect terrestrial vegetation. The impact may be direct via interference with the plants' physiology (e.g., growth, bud formation, flowering) or indirect via changes in the stand dynamics (e.g., regime of disturbances) (Loehle and Leblanc 1996; Weber and Flannigan 1997).

In Canada, northeastern Manitoba will likely be one of the regions most affected by a climate change caused by the doubling of CO_2 ($2\times CO_2$) (Boer et al. 2000). Simulations for years 2040-2049 indicated a summer warming of 4°C to 5°C and a winter warming of 5°C to 8°C as a consequence of this forcing (Laprise et al. 2003). In southwestern Manitoba, the warming is expected to be less severe, with a trend toward a decrease in precipitation by approximately 10 to 20% (Laprise et al. 2003). In terms of fire severity ratings, Flannigan et al. (2001) predicted large increases in area burned by wildfire with the upcoming $2\times CO_2$ scenario. Forest simulations further indicated that the southern limit of boreal Manitoba might be the area most affected by vegetation change (Hogg 1994). Notwithstanding the uncertainties associated with the circulation models (Laprise et al. 2003), the development of adaptation management strategies in the forest sector is a necessity (Spittlehouse and Stewart 2003).

Before applying forest adaptation management strategies, a vegetation and climate issue needs to be clarified, namely the development of a confidant forecast of species' response to climate change. In a review of the simulation models used to predict the effect of climate change on forests, Loehle and Leblanc (1996) warned that the climate-response functions implemented in many vegetation scenarios had no basis in plant physiology. The authors argued that because models assumed that climate was the only factor controlling species range limits, they overemphasized the role of climate in controlling tree growth and mortality and likely exaggerated the direct impact of climate change. The authors proposed a reconsideration of the direct relationship between tree growth and climate stressors, notably with the contribution of dendroclimatic analyses. In addition to the validation of the climate response functions, dendroclimatic analyses could lead to the identification of growth-climate relationships not included in the simulation models (Loehle and Leblanc 1996). Dendroclimatic studies are currently under-represented in boreal Canada.

In addition to proximate climate factors such as temperature, precipitation, and drought, a few studies have examined the relationship between tree growth and the ultimate delivery system for these factors: atmospheric circulation (see Hirschboeck et al. 1996 for a review; Garfin 1998). Trees do not respond directly to variations in upper atmospheric circulation, but such variations are linked to several climate parameters (namely cloud formation, radiation, wind, temperature, precipitation, humidity, etc.) that affect tree growth (Garfin 1998). This sub-discipline of synoptic climatology, referred to as synoptic dendroclimatology (Hirschboeck et al. 1996), has recently gained interest for use in time series reconstruction of large-scale atmospheric - oceanic teleconnection indices (e.g. Stahle et al. 1998; D'Arrigo et al. 2001; Cook et al. 2002; D'Arrigo et al. 2003). In boreal Canada, synoptic climatology has also been used to link large forest fires with upper atmospheric circulation (e.g. Skinner et al. 1999; 2002).

In this study we use geopotential height data to evaluate the radial growth response of eight boreal tree species growing in the Duck Mountain Provincial Forest of Manitoba to variations in the atmospheric vertical pressure profile at the synoptic scale (~2000 km) and the global scale (~5000 km). In addition to the classical approach of inferring the relation between tree growth and the horizontal structure of the troposphere, analyses were extended vertically to the mid-stratospheric level. There is increasing evidence that stratospheric processes influence the tropospheric circulation and several authors have reported stratospheric signatures in surface climate data (see, for example, Baldwin et al. 2003). By understanding the associations between tree growth and the vertical profile of the atmosphere, we may be able to determine the climate delivery systems to which species from a given site are most sensitive and, at most, estimate their vulnerability to a change in the state of these systems. Radial growth response to temperature, precipitation, and drought are examined to provide a mechanistic interpretation of the relationship between tree growth and atmospheric circulation.

4.3 Materials and methods

4.3.1 Study area

The Duck Mountain Provincial Forest (51°40'N, 100°55'W) is part of the Boreal Plains ecozone, a transition zone between the boreal forest to the north and the aspen parkland and prairie to the south (Fig. 4.1). The Duck Mountain Provincial Forest has an area of approximately 376,000 ha and a wide range of altitudes, with the eastern escarpment rising 300-400 m in elevation. Baldy Mountain is the highest elevation point at 825 m above sea level.

The history of the Duck Mountain is not well documented (Manitoba Conservation 2004). Fort Dauphin, established in 1741 by the French explorer La Vérendrye, is one of many forts built in sight of the Duck Mountain (Manitoba Provincial Park Branch 1973). Selective logging of white spruce in the area started in the late 1800s following the completion of the Canadian Northern Railway to Swan River in 1899. Homes and barns were built of local logs. At the turn of the century Duck Mountain became an important source of timber, with portable mills and fixed mills in Grandview and Swan River (Manitoba Conservation 2004). In the early 19th century, fires occurring in the Duck Mountain area were fought by local people to protect the stands being logged (Stilwell 1988). Some of the most notable fires occurred during 1885-1895 and burned more than half of the forested area of the uplands region (Gill 1930; Tardif 2004). In 1934, most of the timber licence lay within what is now the boundary of the provincial forest (Harrison 1934). At that time, Duck Mountain was surrounded by settlement on all sides, and its accessibility was considered unusually good (Harrison 1934).

Today, Duck Mountain Provincial Forest is composed predominantly of deciduous forest especially in the lowlands, with coniferous boreal forest in the upland areas and mixedwood deciduous/coniferous forest in the midlands (Ecological Stratification Working Group 1996; Kenkel and Hamel 2000). Most abundant are medium to tall closed stands of *Betula papyrifera* Marsh., *Populus tremuloides* Michx. and *Populus balsamifera* L. with *Picea mariana* (Mill.) BSP and *Picea glauca* (Moench) Voss, and *Abies balsamea* (L.) Mill. occurring in late successional stages. Open stands of *Pinus banksiana* Lamb. occur on dry, sandy sites. Deciduous stands have a diverse understory of shrubs and herbs; coniferous stands tend to promote feathermoss. Cold and poorly drained fens and bogs are covered with *Larix laricina* (Du Roi) K. Koch and *Picea mariana* (Ecological Stratification Working Group 1996).

The provincial forest lies within a mid-boreal climate that has predominantly short, cool summers and cold winters. At Swan River (52°30'N, 101°13', elevation 346.6 m), for the period 1971-2000, mean monthly temperatures ranged from –18.2°C in January to 18.1°C in July. Average total annual precipitation was 530.3 mm with most precipitation falling as rain between May and September (Ecological Stratification Working Group 1996; Environment Canada 2002). Compared with the surrounding lowlands, however, the Duck Mountain plateau has cooler summers and winters and also receives about 50% more precipitation (Manitoba Provincial Parks Branch 1973).

4.3.2 Development of tree-ring residual chronologies

Sampling for this study was conducted in the summers of 2000 and 2001 (Tardif 2004). A systematic grid of UTM squares (10 km by 10 km) was overlaid on the Duck Mountain. Though site (forest polygon) selection was constrained by accessibility, a total of 263 sites were located, georeferenced, and sampled. At each site, 8-10 trees were sampled and two cores were extracted from opposite directions and close to the ground level using an increment borer. In young sites (less than 80 years) only one core per tree was extracted. Four cores were systematically extracted from *B. papyrifera*, a species characterized by numerous missing rings. Each site was searched for fire-scarred trees, snags, and down woody debris that was charred or not. Many cross-sections were collected. Snags are often the result of past fire and they can be used to extend the tree-ring chronologies.

Nine tree-ring residual chronologies of *B papyrifera*, *Populus tremuloides*, *Populus balsamifera*, *Picea glauca*, *Pinus banksiana*, *A. balsamea*, *Picea mariana* (one chronology for dry sites and one for wet sites) and *L. laricina* were created as follows (refer to Table 4.1 for the number of samples used to build these

chronologies). The collected samples were sanded and crossdated (Yamaguchi 1991), and each annual ring was measured to 0.01mm accuracy using a VELMEX measuring system interfaced with a computer. For each measurement series, crossdating and measurement were statistically validated using program COFECHA (Holmes 1983), which calculates cross-correlation to a lag of 10 years between each individual standardized measurement series and a reference chronology. The age and size-related trend was removed from the tree-ring measurement series using a spline function, giving a 50% frequency response of 60 years (Cook and Peters 1981). Although this resulted in the loss of information relative to long-term climate changes, 99% of the variance contained in frequencies less than 19 years was preserved. This "flexible" smoothing was necessary because many of the tree-ring series were less than 100 years in length, presenting important growth trends that needed to be removed. The autocorrelation (the result of biological persistence) contained in the standardized measurement series was removed using autoregressive modelling (Cook and Holmes 1986). Autocorrelation reduces the effective number of independent observations and thus reduces the degrees of freedom used to determine the confidence in estimates of correlation coefficients (Legendre and Legendre 1998). Biweight robust means of the residual series were computed for each data set to create the site residual tree-ring chronologies. The nine site residual tree-ring chronologies were constructed using ARSTAN (Holmes 1999).

4.3.3 Analyses of tree growth and climate relationships

The variance within the site residual tree-ring chronologies was analysed using a non-rotated Principal Component Analysis (PCA) performed on a covariance matrix (Legendre and Legendre 1998; Barry and Carleton 2001). In this procedure, the nine site residual tree-ring chronologies were transformed into new sets of orthogonal variables. The amount of variability was described using the same number of

variables, but with the first principal component (PC) accounting for the maximum possible proportion of the variance in tree growth. Succeeding PCs, in turn, accounted for as much of the residual variance as possible. Eigenvectors, or the loading of each residual tree-ring chronology on each component, gave the spatial representation of the PCs. A common problem emerging from PCA is that the orthogonality constraint in space forces the second PC to be a domain-wide dipole (e.g., about half the data set being negatively correlated with the other half), although the two centres of the dipole may not necessarily be anticorrelated.

An approach often used as a means of interpretation consists of optimizing localized patterns by minimising the number of variables that have high loadings on each component (VARIMAX criterion). However, though the VARIMAX representation is often a very instructive representation of the data, it may often fail to find global patterns because of simplicity optimization (Dommenget and Latif 2002). Those authors warned that both rotated and non-rotated PCA might mislead the interpretation of dominant patterns of a multivariate data set. In the present study, we aimed for the maximization of the climate signals on the PC loadings and thus the non-rotated PCA solution was used as a means of data reduction. The results presented here were nonetheless cross-verified with the use of a rotated PCA using the VARIMAX criterion (Systat 1998), and the general conclusions were in agreement. Only those PCs with an eigenvalue ≥ 1.0 were kept for the analyses and the program CANOCO 4.0 (ter Braak and Smilauer 1998) was used.

The effects of climate fluctuations (temperature, precipitation, and drought severity) on radial growth were analysed using correlation and bootstrap response function analyses (Briffa and Cook 1990; Guiot 1991) for the period 1912-1999. The bootstrap response function analysis provides a test of significance of the stability of the regression coefficients within a specific time period by repeated, random

sampling of the data. A weight was associated with each monthly variable, expressing the separate relative effects of several climate factors on ring width. This method offers the advantage of avoiding errors caused by collinearity among variables and providing a more realistic estimate of tree response to climate. Bootstrap response function (processed through 999 iterations) and correlation analyses were performed using PRECON (Version 5.16) (Fritts 1998). Mean monthly temperature (from the Birtle (1905-1998) and Dauphin (1904-1999) meteorological stations) and total monthly precipitation data (from the Birtle (1918-1999), Dauphin (1912-1999), and Russell (1916-1990) meteorological stations) from Vincent and Gullett (1999) and Mekis and Hogg (1999), respectively, were used for the dendroclimate analyses. Regional data files were created following the procedure described in Holmes (1999; homogeneity testing, station adjustments for mean and standard deviation, and station averaging). For the response function analyses of temperature and precipitation, the period of analysis included June of the year previous to ring formation to September of the year of ring formation.

The monthly regional average Canadian Drought Code (CDC; 1912-1999) calculated by Girardin et al. (2004b) for the eastern Boreal Plains was used for the response function analysis of drought. The period of analysis covered June to October of the year previous to ring formation and April to September of the year of ring formation. The CDC (a numerical daily rating of the average moisture content of deep, compact, organic layers) is a component of the Fire Weather Index System (Van Wagner 1987) that is used daily across Canada by the Canadian Forest Service (Natural Resources Canada) to monitor forest fire danger. The CDC maintains a daily budget of stored moisture, accounting for daily losses and gains as a result of evapotranspiration and precipitation. The minimum CDC value of zero indicates that the maximum holding capacity of soil water is reached. A CDC rating of 200 is an indication of high drought severity, and 300 or more is extreme drought severity. For further details on the CDC, refer to Girardin et al. (2004b).

Bootstrap response functions and correlation analyses were also performed on monthly mean geopotential height of atmospheric pressure levels (1000, 925, 850, 700, 600, 500, 400, 300, 200, 100, 70, 50, 30, 20, and 10 hPa, for the period 1948-1999. Geopotential height approximates the actual height (in metres) of a pressure surface (hectopascals) above mean sea level. Positive height anomalies are generally associated with increased upper atmospheric pressure and temperature, and decreased storminess (Bonan 2002). Negative height anomalies are associated with decreased upper atmospheric pressure and temperature, and increased convection and precipitation (Bonan 2002; Ahrens 2003). Geopotential height data were obtained for the 50°N, 100°W geographical location from the NCEP/NCAR Reanalysis project (Kalnay et al. 1996). The NCEP/NCAR Reanalysis surface air temperature from the same location was also used in a response function analysis for comparison with our regional temperatures.

Geopotential height correlation and composite charts were also created with the aid of the NOAA-CIRES Climate Diagnostics Center, Boulder Colorado (Kalnay et al. 1996; http://www.cdc.noaa.gov). These charts are valuable tools for the analysis of wind-flow patterns and the movement of weather systems. Composite charts are often used in synoptic climatology to reveal the circulation patterns during signature years, while the single correlation field is produced to represent the circulation - tree growth relationship for the entire period as a whole (Hirschboeck et al. 1996). The NCEP/NCAR Reanalysis grid has a global spatial coverage of 2.5° latitude by 2.5° longitude with 144x73 points and a temporal coverage of 1948 to present, with output every 6 hours. Daily heights were averaged by month for each grid point.

This paper discusses anomalies in the 500-hPa circulation with respect to the mean climatology (after Skinner et al. 2002). As shown in Figure 4.1, the mean features of the upper atmospheric circulation are the presence of troughs located over

the North Pacific (WCT) and northeastern Canada (CPT) and a ridge across the northeastern Pacific onto the West Coast (CR). The circulation and amplitudes over Canada are generally similar from month to month, but the summer gradients are much weaker than those of the winter. Also, the CR and CPT set migrates toward the east in the summer. Winds at the 500-hPa level tend to flow parallel to the isohypses (height contours) (Ahrens 2003). The winds are called meridional when the isohypses form a strong wave-like pattern, and zonal when the isohypses are nearly parallel to the lines of latitude. Within these longwaves, an elongated area of high heights is known as a ridge (e.g. the CR) and an elongated area of low heights is a trough (e.g. the CPT). Correlation charts and composite anomalies in this paper should be compared with this climatology.

4.4 Results

4.4.1 Descriptive statistics and distribution of the variance

Standardised chronology statistics (Table 4.1) indicated that hardwood species (*B. papyrifera*, *Populus tremuloides*, and *Populus balsamifera*) had greater mean sensitivity than coniferous species. Standard deviations were also much greater within these species (with the exception of *L. laricina*, for which the standard deviation was greatest). Hardwood species also presented lower autocorrelation. These distinctions suggested that hardwood species were more sensitive to interannual variations in climate than coniferous species. Observation of the residual tree-ring chronologies (Fig. 4.2) further suggested that all species, with the exception of *L. laricina* had common yearly growth reductions, such as in 1961 (largest growth reduction in the 20th century) and 1915. Figure 4.2 also highlighted a distinct pattern of growth for *L. laricina* that appeared to be the result of prolonged growth suppressions beginning in the late 1910s and in 1940s.

The pattern of growth between species was differentiated using a PCA (Fig. 4.3). Loading for PC1 (Fig. 4.3a) indicated that all species except *L. laricina* were sharing common variance (46% of all variance). This interpretation was further supported by the high correlation between the species' residual chronologies and the first PC (correlation coefficients other than for *L. laricina* all greater than 0.59, $p<0.001$ with N=88; correlation coefficients are slightly lower for *B. papyrifera*, *A. balsamea*, and *Picea mariana* from wet sites). It is across the second PC (Fig. 4.3a) that the distinction between hardwood and coniferous species was observed (dipolar distribution). The PCA suggested that all species were responding to common signals, but that some signals had positive effects on one group and negative ones on the other. The third loading (Fig. 4.3b) indicated that *L. laricina* responded to a signal not common to any other species.

4.4.2 Surface climate response function

The relationship between tree radial growth and surface climate was investigated using the first, second, and third PCs. The analysis of PC1 indicated that all species but *L. laricina* were mainly responding to summertime temperature (Fig. 4.4a) and precipitation (Fig. 4.4b) from the year previous to ring formation. The summer drought stress response was also highlighted by the high correlation coefficients between PC1 and the CDC (Fig. 4.4c). In the year of ring formation, tree growth was negatively correlated with late winter temperature (February) and positively with June precipitation. The CDC also correlated well during the summer months.

Response function on PC2 indicated a positive response from warmer spring temperature (March and April) and negative response from warmer June temperature (Fig. 4.4d). Since positive PC2 implied positive conifer growth and negative

hardwood growth (refer to Fig. 4.3a), the climate-PC2 association suggested that conifer growth was positively correlated to temperature in March and April, and negatively to June temperature. In contrast, hardwoods would be negatively correlated to temperature from March and April, and positively to June temperature. This conifer-hardwood inverse correlation may be real, or it may be an artefact from the PCA approach. As outlined in the materials and methods section, the second PC will normally be characterized by a dipole with approximately half of the input data loading positively and half loading negatively. For cross-verification purposes, response function analyses were rerun on each site residual tree-ring chronology to ascribe physical significance of the temperature and precipitation relations.

First, results presented in Table 4.2 were found to be in agreement with the response function analyses conducted on PC1. All species demonstrated a drought stress signal from the July to September period the year prior to ring formation. The June precipitation response was also consistent in both approaches, with eight species being correlated with the variable at the 10% significance level (Table 4.2; Fig. 4.4b). The February temperature signal, on the other hand, appeared to be strictly associated with hardwood species. Second, results in Table 4.2 had some physical consistency with the response function analyses conducted on PC2. Both *Picea glauca* and *Pinus banksiana* were positively correlated to higher April temperatures (Table 4.2), while hardwoods were negatively correlated to higher March and April temperatures (particularly *B. papyrifera*). The June temperature response further indicated that *B. papyrifera* was less negatively affected by summer warmth than *Picea glauca*. As for *L. laricina*, the low model R^2 derived from the response function analyses conducted on the site residual chronology (Table 4.2) and on PC3 (Fig. 4.4g-4.4i) suggested that its radial growth does not respond strongly to climate. A significant response function coefficient was nonetheless obtained for August precipitation of the year previous to ring formation.

4.4.3 Geopotential height response functions

Response functions and correlation analyses performed on geopotential height (GpH) indicated that atmospheric pressure heights, particularly between 2.9 km and 11.7 km above sea level, were associated with a significant amount of variance in tree growth (Fig. 4.5). For the same reference interval (1948-1999), a single level of GpH explained more or less the same amount of variance in radial growth than any surface climate variables. For instance, the height of the 300-hPa level explained 42.2% and 55.3% of the variance within PC1 and PC2, respectively (Fig. 4.5a and 5b, left side of chart). In comparison, NCEP/NCAR Reanalysis surface temperatures for 1948-1999 (not shown) explained no more than 42.1% and 49.6% of the variance in PC1 and PC2, respectively. Similarly, response function analyses reconducted on our regional temperature, precipitation and drought monthly times series using the interval 1948-1999 also indicated an R^2 lower than those obtained from the NCEP height data (PC1 and PC2 R^2 for temperature were 37.0% and 48.7%, respectively; PC1 and PC2 R^2 for precipitation were 41.0% and 37.1% respectively; PC1 and PC2 R^2 for drought were 31.7% and 25.2%, respectively). Note that analyses of PC3 were not conducted because of a weak relationship with the surface climate data (Fig. 4.4g-i).

Response function analyses conducted on PC1 using height data were highly coherent with analyses conducted on temperature data (i.e., in the identification of a July to September signal the year prior to ring formation and of a February signal the year current to ring formation) (Fig. 4.5a). These signals were associated with nearly all levels of the troposphere and stratosphere, a picture that portrays well the strong vertical autocorrelation in the height data. According to Figure 4.5a, higher 700- to 10-hPa heights during July to September the year previous to ring formation were negatively associated with tree radial growth and vice versa. By definition, for a given pressure level of the upper atmosphere, a positive height anomaly is an indication of higher temperature as warm air is less dense. Also, a warm layer of air is

thicker than a cool layer of air. Higher 600- to 10-hPa heights during February of the year of ring formation also had the same association (Fig. 4.5a). At the 30- to 10hPa levels, the correlation coefficients were also significant for early and late summer of the year of ring formation (for a total of eight months negatively correlating with the stratospheric height levels). In addition, analyses at the 500-hPa level on site residual tree-ring chronologies (Table 4.2) indicated that the February signal was strictly associated with hardwood species while the summer signal was stronger within the conifers.

In contrast to PC1, PC2 was more closely associated with variability within the troposphere (Fig. 4.5b). Response function analyses between PC2 and the 850- to 200-hPa surface pressure levels also identified a situation similar to that obtained from temperature, that is, the most important responses were emerging from the beginning and end of the warm season. Since positive PC2 implies positive conifer growth and negative hardwood growth (refer to Fig. 4.3a), the climate – PC2 association suggested that conifer growth was positively associated with higher 850- to 200-hPa surface pressure levels in April and August, and negatively in June. This association suggested the reverse situation for hardwoods. Cross verification with the analyses on site residual chronologies at the 500-hPa level (Table 4.2) validated the April, June, and August responses of conifers. These responses, however, were not observed in hardwoods (only the April signal was observed at the 10% level).

4.4.4 Geopotential height correlation and composite charts

Dominant atmospheric pressure response functions described in the previous subsection were projected using 500-hPa correlation fields (Fig. 4.6). For instance, PC1 was correlated with each grid point of the NCEP/NCAR Reanalysis grid using the July to September height monthly time series of the year prior to ring formation.

Contour lines were then drawn from the correlation coefficients to obtain Figure 4.6a. In addition, the magnitude of changes within the atmospheric circulation patterns during extreme growth years was given by composite analyses. In Figure 4.7a, the mean heights corresponding to years of lowest PC1 values were subtracted from the mean heights corresponding to years of highest PC1 values to obtain mean height differences at each grid point. (Refer to the materials and methods section for a description of the main features affecting climate in North America.)

Figures 4.6a and 4.7a indicated that the amplitude of the longwaves in the summertime was associated with altering cells of anomalous heights above the Great Plains (negative correlation), the North Pacific (dipolar correlation between the northeast Pacific and the southeast subtropical region), and Northern Asia (positive correlation). Within each cell, the magnitude of changes between years of highest ring width (highest values of PC1) and lowest ring width (lowest values of PC1) was, on average, approximately 30 to 40 m in height (Fig. 4.7a). In terms of circulation, this suggested that during years of highest ring width, the West Coast Trough (WCT) and the Continental Ridge (CR) were on average weaker. From this configuration emerged a stronger zonal flow over the western North Pacific onto the West Coast and the study area. The Canadian Polar Trough (CPT) remained, on average, nearly unchanged between the two PC1 phases. By contrast, a stronger WCT and CR dominated the years of lowest ring width. This configuration is known for inducing stagnant circulation, low precipitation, and a warming caused by subsidence of air.

A similar correlation field was observed in February (Fig. 4.6b) but with a much weaker correlation over the North Pacific. A discernible difference between the July to September pattern and the February pattern was also the magnitude of the average change over Greenland. The 500-hPa level height difference between the two PC1 phases reached over 160 m (Fig. 4.7b). Years of highest ring width in the Duck Mountain Provincial Forest were on average associated with a westward

displacement of the CPT, a weaker Icelandic low, and a stronger Bermuda high. This configuration gave rise to stronger ridging over the Azores (east North Atlantic) and largely contrasted with the zonal flow characterizing the years of lowest ring width.

For the analysis of PC2, because the relationship with site residual chronologies at the 500-hPa was not highly significant with hardwood species, we refer to the positive correlation between conifer growth and PC2. By contrast with the situations observed in PC1, the correlation fields and composites with PC2 were reversed (Figs. 4.6c-4.6d), indicating that during April and August, stronger WCT-CR and CR-CPT favoured conifer growth. The highest mean height differences were observed in April, with values exceeding 70 m over Baffin Bay and Northern Europe (Figs. 4.7c-4.7d). The two phases of PC2 were mainly associated with the positions of the ridges and troughs, with the WCT and CR being placed eastward during years of high ring width and vice versa. This configuration agrees with the expectation that conifers were favoured by warmer conditions during these two months (Fig. 4.4d; Table 4.2). Intensified ridging favours stagnant circulation and a warming resulting from the subsidence of air.

A similar approach was used to study the association between tree growth and atmospheric circulation at the 50-hPa surface pressure level. The geopotential height in July to September (the year previous to ring formation) correlation chart indicated that the negative correlation observed in Figure 4.5a between PC1 and the stratospheric level was associated with a Northern Hemisphere global scale circulation, with a region of high significance located above western Canada (r=0.43, $p<0.001$; Fig. 4.8a). In February of the year of ring formation, a correlation field, extending across a mid-latitudinal band from the interior of the North Pacific to Africa and Eurasia, was observed (Fig. 4.8b). Composite analyses (Fig. 4.9a) revealed that the years of lowest ring width were effectively associated with a warmer July to September stratosphere (compared with low ring width years), with average height

differences of 20 to 60 m distributed over most of the Northern Hemisphere. However, the polar region depicted a different pattern, with positive height differences being associated with years of improved growth conditions, particularly in February (Fig. 4.9b). These correlation charts, supported by the response function analyses, indicated that a cooling of the Northern Hemisphere stratosphere in subtropical and subpolar regions (and a warming of the stratosphere in the polar region) had a positive effect on tree growth in the Duck Mountain Provincial Forest and vice versa.

4.5 Discussion

4.5.1 Common signals in species' growth

The partitioning of the variance in the PCA indicated that all species (with the exception of *L. laricina*) responded to common environmental signals. These results were consistent with those of Tardif et al. (2002), who observed few differences among the response to climate of seven boreal tree species in eastern Canada. Response function and correlation analyses indicated that the strongest factor influencing tree growth was the summer temperature-moisture budget. A proper moisture budget allows optimal tree growth and assimilation of carbohydrates for the next year's growth if soil moisture is sufficient to maintain foliage water potential and minimise vapour pressure deficits (Dang et al. 1998; Bonan 2002). This is consistent with other studies conducted at the southern limit of the evergreen conifers' distribution (Hogg 1994; Chhin et al. 2004). Our results further indicated that the impact of a moisture deficiency was crucial in the year previous to ring formation and that it was less important in hardwood species.

The analysis of the climate responses also indicated that hardwoods were negatively affected by warmer late winter and spring temperature, and that conifers were favoured by earlier springs. Presumably warm winters and springs interfere with the hardwoods' chilling requirements for bud break phenology. Exposure over several weeks or months to temperatures below a threshold is needed to break bud dormancy (Myking and Heide 1995; Linkosalo 2000; Bonan 2002). Otherwise, early releases expose trees to risk of frost damage and, in the next summer, to a decrease in total foliage area, in assimilated carbohydrates, and in growth. The conifers' response was consistent with findings of Graumlich (1993) and Tardif et al. (2002). By preserving their needles throughout the year, conifers can apparently take advantage of warmer April temperatures. Evergreen foliage also prevents large seasonal fluctuations in carbon reserves (Bonan 2002). Earlier spring thus favours conifer radial growth, but warm temperatures persisting through June in conjunction with low precipitation could counteract the earlier effect.

In comparison with other species, *L. laricina* was less sensitive to climate. A number of studies have found that *L. laricina* was subject to severe outbreaks of the larch sawfly (*Pristiphora erichsonii* [Hartig]) (Jardon et al. 1994; Girardin et al. 2001; Case and MacDonald 2003). According to historical records of sawfly infestations, several outbreak episodes have occurred in Manitoba in the course of the 20th century, namely from 1911 (or earlier) to 1920, from 1924 to 1927, and from the late 1930s to 1960s (or later) (Nairn et al. 1962; Turnock 1972). These episodes, which may be related to growth suppressions observed in Fig. 4.2i, could have contributed to the addition of noise in the tree-ring chronologies and to a reduction of the ring width variance explained by climate. As for other defoliators, such as the spruce budworm (*Choristoneura fumiferana* (Clemens)) and the forest tent caterpillar (*Malacosoma disstria* (Hubner)), there is no evidence that they have significantly altered their host's ring-width responses to climate.

4.5.2 Tree growth and atmospheric circulation

Variations in geopotential height during the period 1948-1999 accounted for more variance in tree growth than did surface climate variables such as temperature, precipitation, and drought. The relationship was greatest with the middle and high troposphere, at 700-hPa to 300-hPa (or 3 km to 9 km above sea level). In addition, results also indicated that the Northern Hemisphere stratospheric height (e.g., 200-hPa to 10-hPa or 12 km to 31 km above sea level) had a significant correlation with tree growth for 8 of the 16 months under study.

The radial growth responses to the 500-hPa level summer height variations were in agreement with the expectation that optimal growing conditions occur under the presence of a trough centred in the Great Plains. This synoptic scale system favours the development of baroclinic instabilities responsible for the formation and intensification of storm systems, which are necessary for optimal tree growth conditions (i.e., sufficient precipitation with lower evapotranspiration). Girardin et al. (2004b) and Skinner et al. (1999) also reported reduced seasonal soil drought severity and forest fire hazard under the presence of this trough.

The observed correlation fields and composites suggested that the relationship with upper atmospheric heights in all months analysed extended beyond the synoptic scale. Three altering cells of anomalous heights were the main contributors to the magnitude of the longwaves: one centred over the Gulf of Alaska, another over the Great Plains, and one over Greenland. The contribution of North Pacific sea surface temperature (SST) variability to the amplitude of the longwaves has been extensively studied (mostly for the wintertime) and is still under debate. For instance, Bonsal et al. (1993) hypothesized that warmer SSTs along the coast of British Columbia and cooler water near 150°W and 50°N affects the upper atmospheric longwaves pattern, causing 500-hPa ridging to dominate for extended periods over the Great Plains.

Others, however, affirmed that SST anomalies in the North Pacific are the result of atmospheric circulation that is tropically driven (e.g., Newman et al. 2003) and thus may not play an active role in the modulation of the longwaves. The conflict between these two classes of opinion is well summarized by Yang and Zhang (2003).

Downward propagation of stratospheric variations into the troposphere and onto the magnitude of the longwaves has been observed and simulated in general circulation models (Baldwin and Dunkerton 1999). This mechanism could explain the July-September and February vertical correlation (from 10- to 600-hPa) expressed in Figure 4.5a. The observed correlation fields with the stratosphere (presented in Figure 4.8) were not dissimilar to the stratospheric expression of the Northern Hemisphere annular mode (NAM), a recurrent pattern of surface climate. Recent studies reported the long-lived influence (beyond 30 days) of the stratosphere on the dynamical properties of the troposphere and on the NAM behaviour (Baldwin and Dunkerton 1999; 2001; Thompson et al. 2002; Baldwin et al. 2003). The relationship most likely reflects the impact of anomalies in the lower Northern Hemisphere stratospheric polar vortex (Thompson et al. 2002). These anomalies affect the momentum of the upper troposphere's polar longitudinal winds and induce a mean meridional circulation that extends to the earth's surface, causing amplification of the longwaves. The observed ring width response function models' R^2 and the ring-width correlation and anomaly fields at the stratospheric height levels are intriguing and should be subject to further study. Studies could be placed in the context of a stratospheric cooling that started approximately 30 years ago (Hartmann et al. 2000), a phenomenon reported to be caused by ozone depletion and increased greenhouse gases in the stratosphere (Forsters and Shine 1999).

The relationships observed between tree radial growth, surface climate, and the atmospheric pressure level heights and correlation fields may be of significance for the development of a scenario of impacts of climate change on the Duck

Mountain Provincial Forest. Surface responses could be implemented in deterministic regression models to forecast radial growth behaviours under current and $2\times CO_2$ level simulations, as done by Laroque and Smith (2003) for Vancouver Island. However, these growth simulations could be limited because of precipitation uncertainty characterizing circulation models. This precipitation uncertainty (refer to Laprise et al. 2003) may be non-trivial when it comes to determining future moisture budgets, which is often the leading variable for species' growth in the boreal forest and at its southern limit (e.g., Graumlich 1993; Hogg 1994; Tardif et al. 2002; Chhin et al. 2004). In contrast, scenarios of geopotential heights are comparable to the temperature output in terms of confidence (Dr. Daniel Caya, Climate Simulations Group - Ouranos Consortium, personal communication). Because geopotential heights contain information on temperature and often on precipitation, their implementation in vegetation simulation models could reduce the precipitation uncertainty and/or provide a means for cross verification. The troughing and ridging could also be taken into account in these models with the use of the indexing approach, commonly used to characterize the type of circulation over a geographic region (Yarnal 1993; Skinner et al. 2002).

4.6 Acknowledgment

We acknowledge the Sustainable Forest Management Network (SFMN) for funding this research and supporting M.-P. Girardin. The first author was also supported by the Fonds Québécois de la Recherche sur la Nature et les Technologies (FQRNT) and by the Prairie Adaptation Research Collaborative (PARC). We thank France Conciatori for developing the tree-ring chronologies and Norm Aime, Alanna Sutton, Cara Gill, and Derrick Ko Heinrichs for field assistance. We thank the National Oceanic and Atmospheric Administration (NOAA; NCEP/NCAR Reanalysis project) and the Meteorological Service of Canada for their aid and contribution of climate

data. This manuscript was much improved through the thoughtful comments of Dr. Mike D. Flannigan (Canadian Forest Service, Sault Ste. Marie), Dr. Ze'ev Gedalof, and an anonymous reviewer. We thank Dr. Danny Blair for commenting and editing the final version of the manuscript.

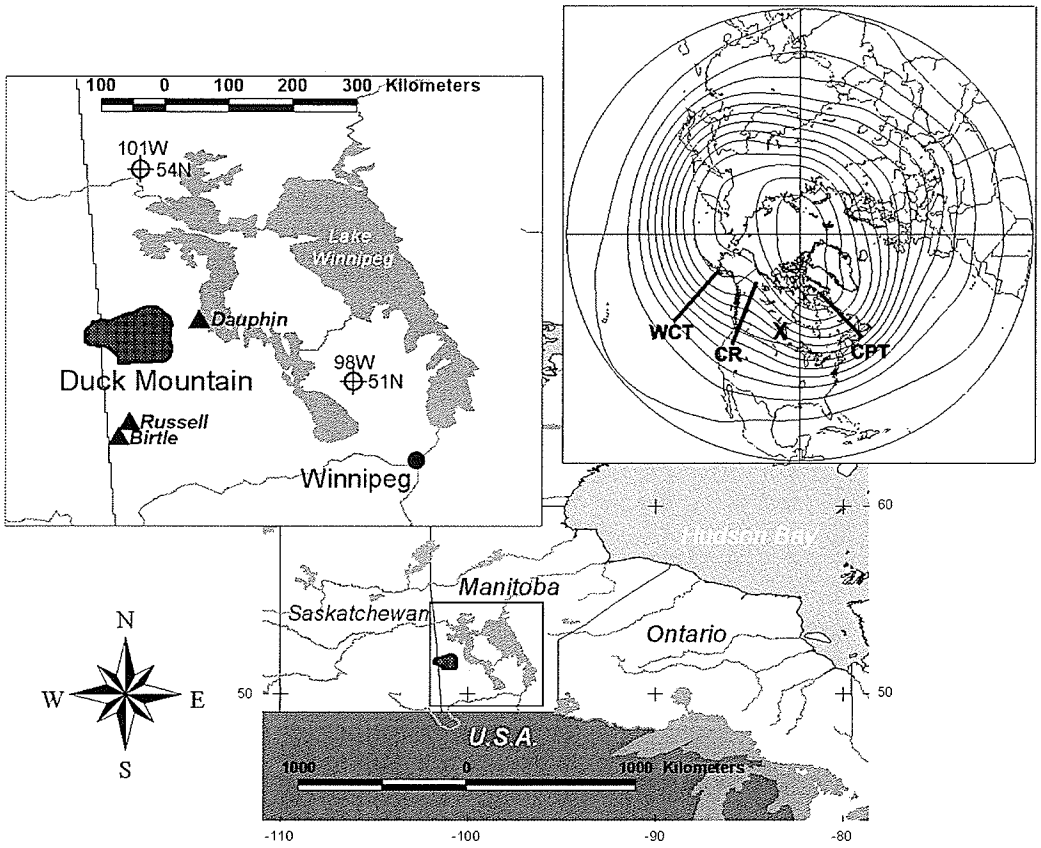

Figure 4.1 Map showing the geographical location of Duck Mountain Provincial Forest in Manitoba. Meteorological stations indicated by filled triangles. The Northern Hemisphere map shows the mean annual 500-hPa circulation for the reference period 1968-1996. Thick vertical lines indicate the location of the main features affecting the North American climate. From west to east these are the West Coast Trough (WCT), the Continental Ridge (CR), and the Canadian Polar Trough (CPT). Correlation charts and composite anomalies in this paper should be compared with this climatology. The × marks the location of the Duck Mountain Provincial Forest.

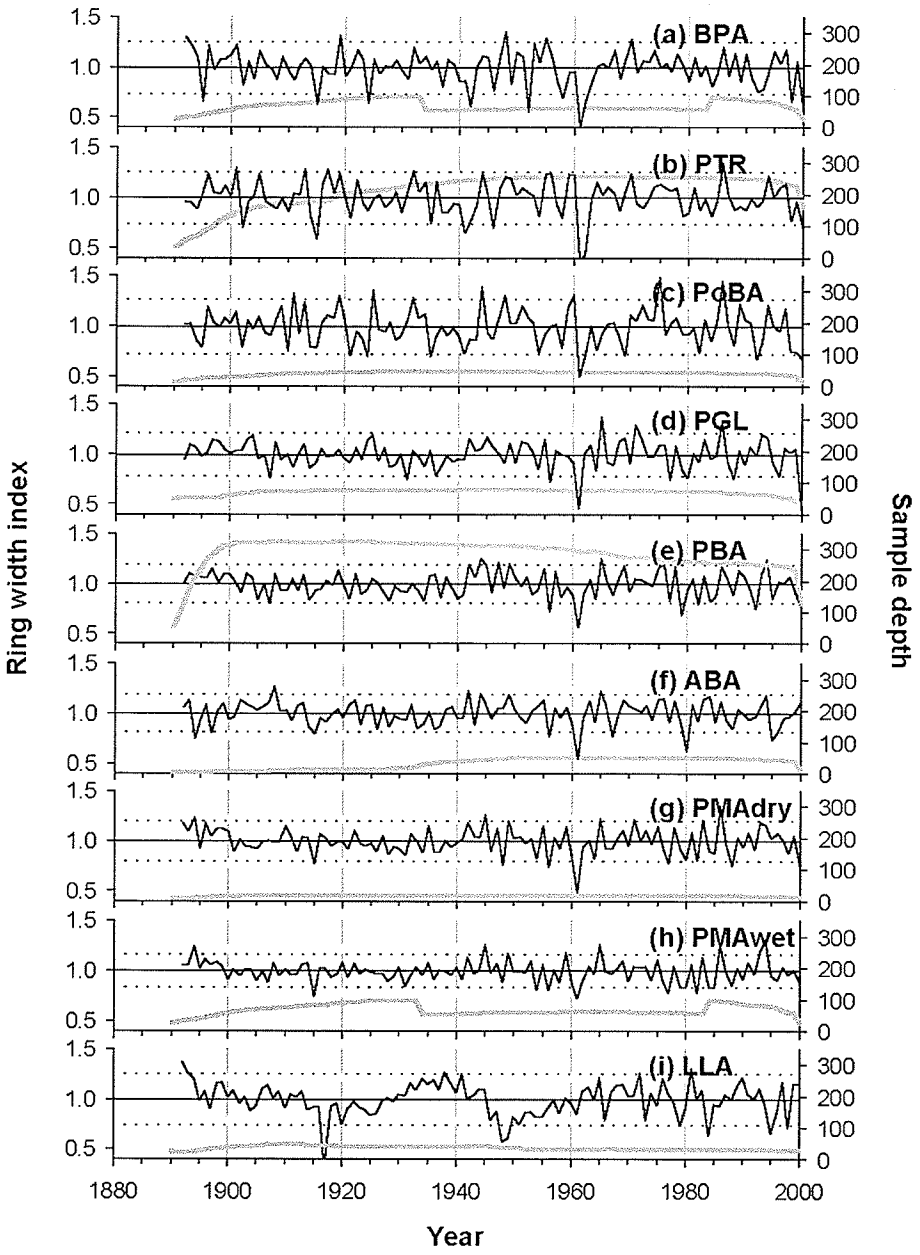

Figure 4.2 Residual chronologies of a) *Betula papyrifera* (BPA), b) *Populus tremuloides* (PTR), c) *Populus balsamifera* (PoBA), d) *Picea glauca* (PGL), e) *Pinus banksiana* (PBA), f) *Abies balsamea* (ABA), g) *Picea mariana* from dry sites (PMAdry), h) *Picea mariana* from wet sites (PMAwet), and i) *Larix laricina* (LLA). For each year, the thick grey line shows the sample depth. Dotted lines are set at 1.5 standard deviation.

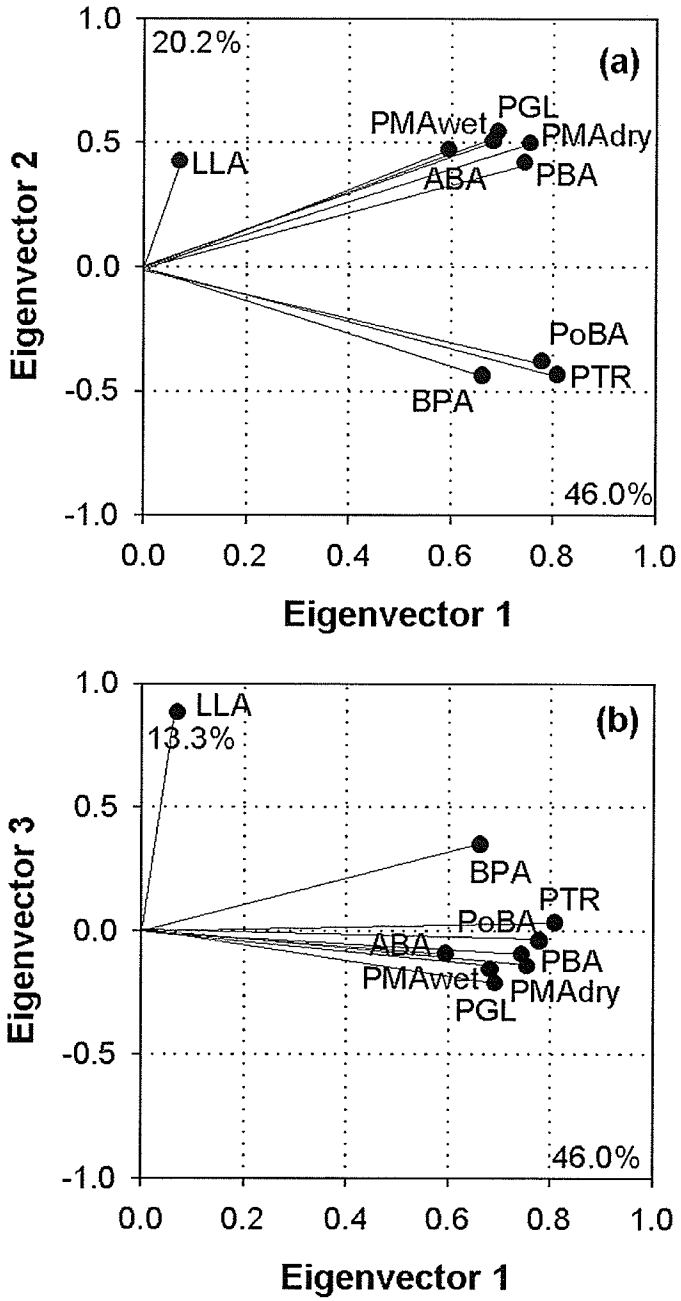

Figure 4.3 a) First against second and b) second against third eigenvector loadings of the principal component analysis conducted on the nine tree-ring residual chronologies for the period 1912-2000. The plots demonstrate the correlation coefficients between the residual tree-ring chronologies (the descriptors) and the principal components. As well, the plots approximate the correlation coefficient among the descriptors themselves. Descriptors with vectors at sharp angles are positively correlated. By contrast, an obtuse angle between descriptors indicates a negative correlation.

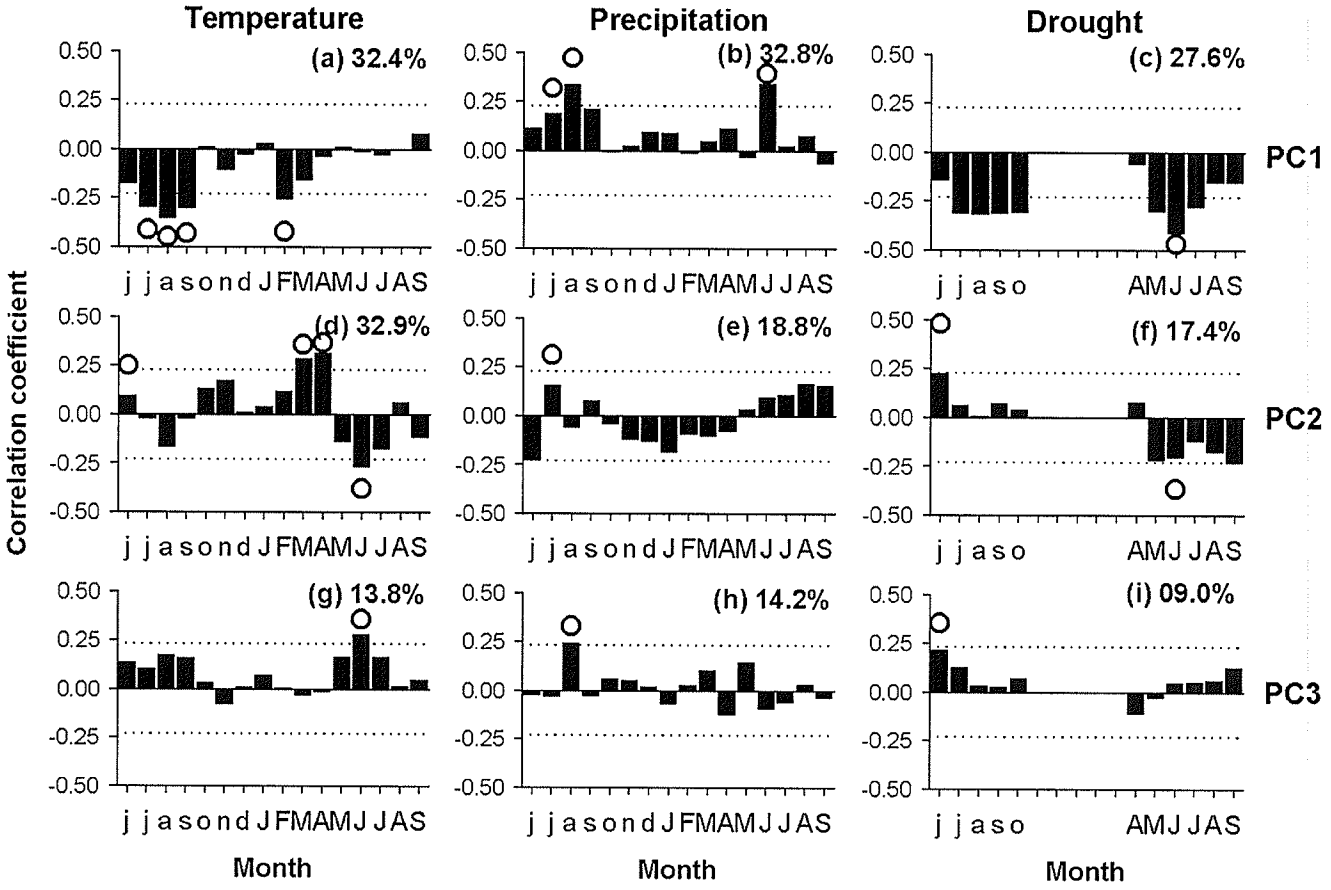

Figure 4.4 Correlation (vertical bars) and significant bootstrap response function coefficients (empty circles) computed between a-c) PC1, d-f) PC2, and g-i) PC3 and each monthly climatic variables (mean temperature, total precipitation, and monthly mean Canadian Drought Code). Correlation coefficients exceeding the dotted lines are significant at $p<0.05$. For the response function analyses, only those variables significant at $p<0.05$ are shown. Months previous to the year of ring formation (July-December) are labelled with small caps and those of current year to ring formation (January-October) are labelled with capital letters. The R^2 of the response models is shown. All analyses were performed for the 1912-1999 period.

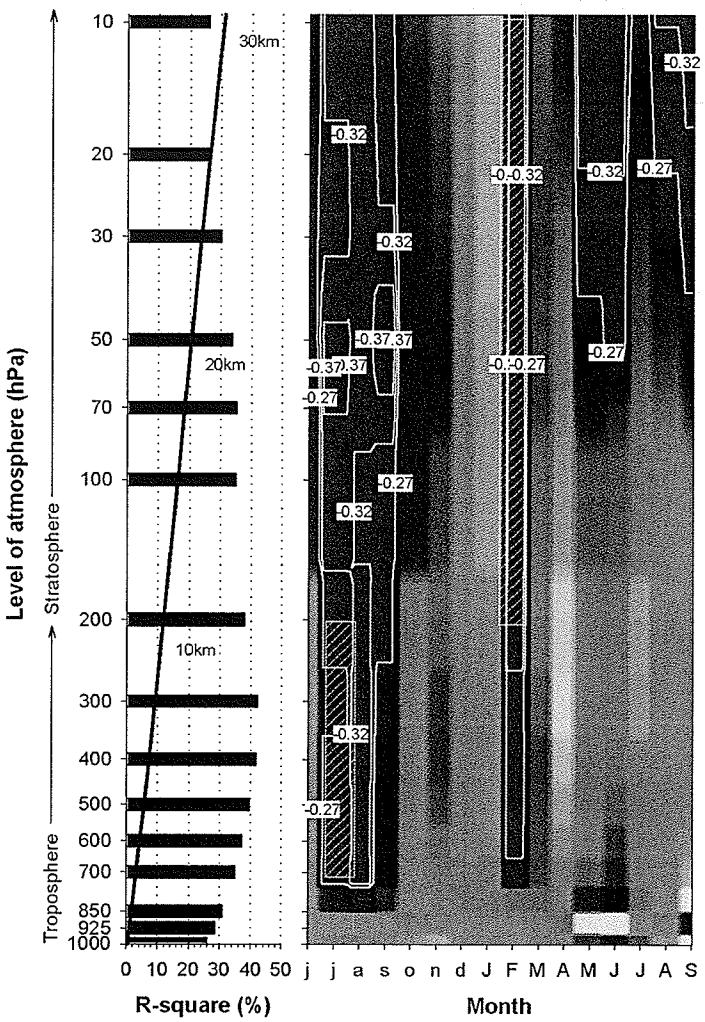

Figure 4.5a Correlation and bootstrap response function coefficients computed between PC1 and the estimated height (in metres) of various atmospheric pressure levels (hPa), from near the Earth's surface (1000-hPa) to the mid-stratosphere (10-hPa) (read from bottom to top). On the left side of the panels is a horizontal bar chart showing the response model R^2 for all levels. The thick grey line shows the average annual logarithmic relationship between air pressure (log*y* scale; in hPa) and height above sea level (*x* scale; converted into km). The right sides show the correlation schemes. Months of the year previous to ring formation are labelled with small caps and those of the year current to ring formation with capital letters. Dark grey areas indicate regions of negative correlation (a white contour line denotes areas significant at $p<0.05$). Light areas indicate regions of positive correlation (a black contour line denotes areas significant at $p<0.05$). Areas of significant correlation ($r>|0.27|$) are labelled at every 0.05 coefficient level. Areas for which significant response functions were obtained are crosshatched in black for positive coefficients and in white for negative coefficients. PC, principal component.

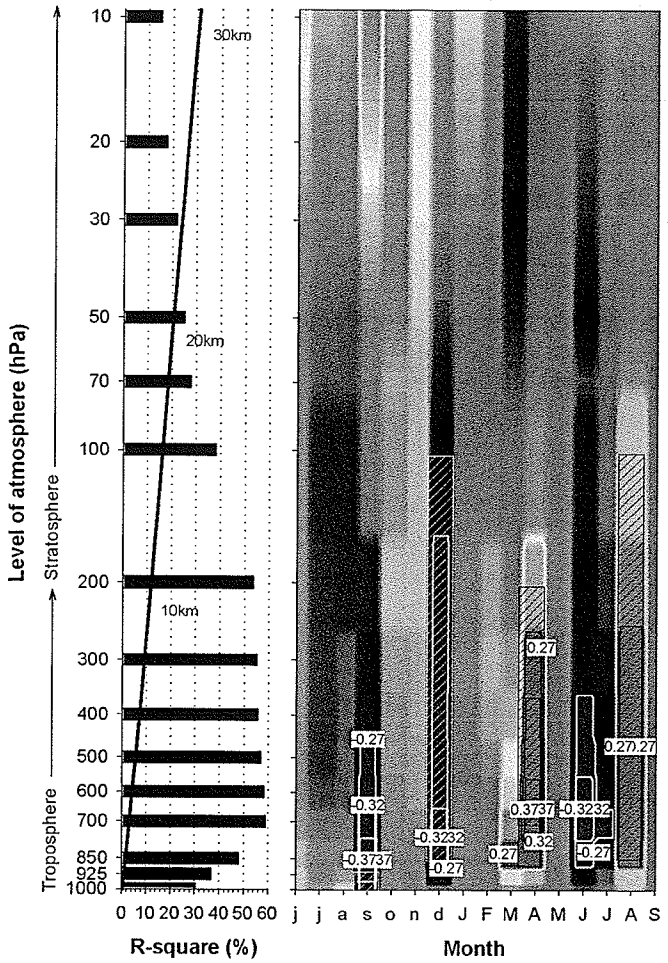

Figure 4.5b Correlation and bootstrap response function coefficients computed between PC2 and the estimated height (in metres) of various atmospheric pressure levels (hPa), from near the Earth's surface (1000-hPa) to the mid-stratosphere (10-hPa) (read from bottom to top).

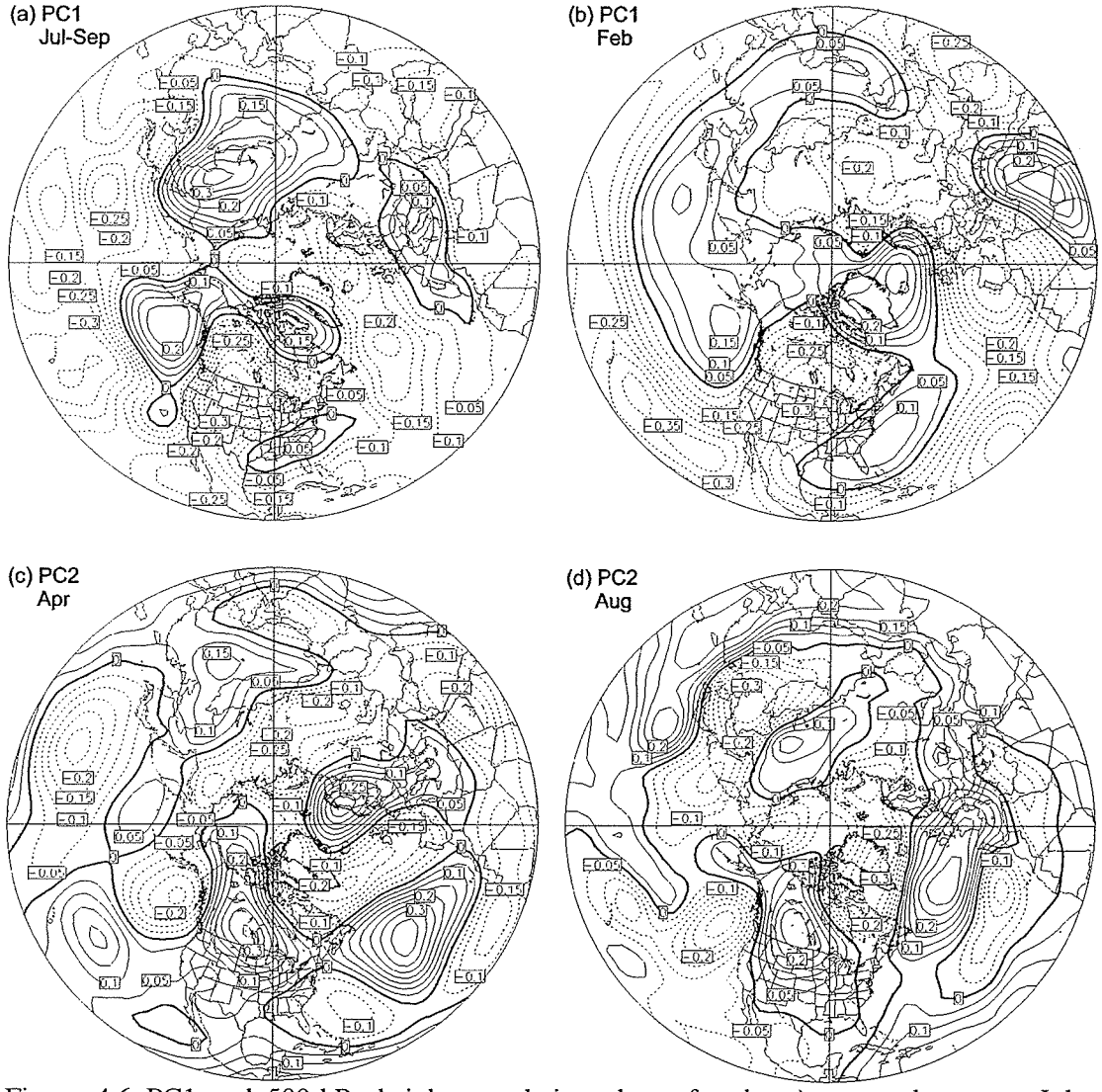

Figure 4.6 PC1 and 500-hPa height correlation charts for the a) seasonal average July-September of the year previous to ring formation and b) February of the year current to ring formation. PC2 and 500-hPa height correlation charts for c) April and d) August of the year current to ring formation. Contour lines are drawn at every 0.05 coefficient level (zero interval is bold). Solid contours indicate positive correlation; dashed contours indicate negative correlation. Correlation coefficients are significant at $p<0.05$ when $r>|0.27|$.

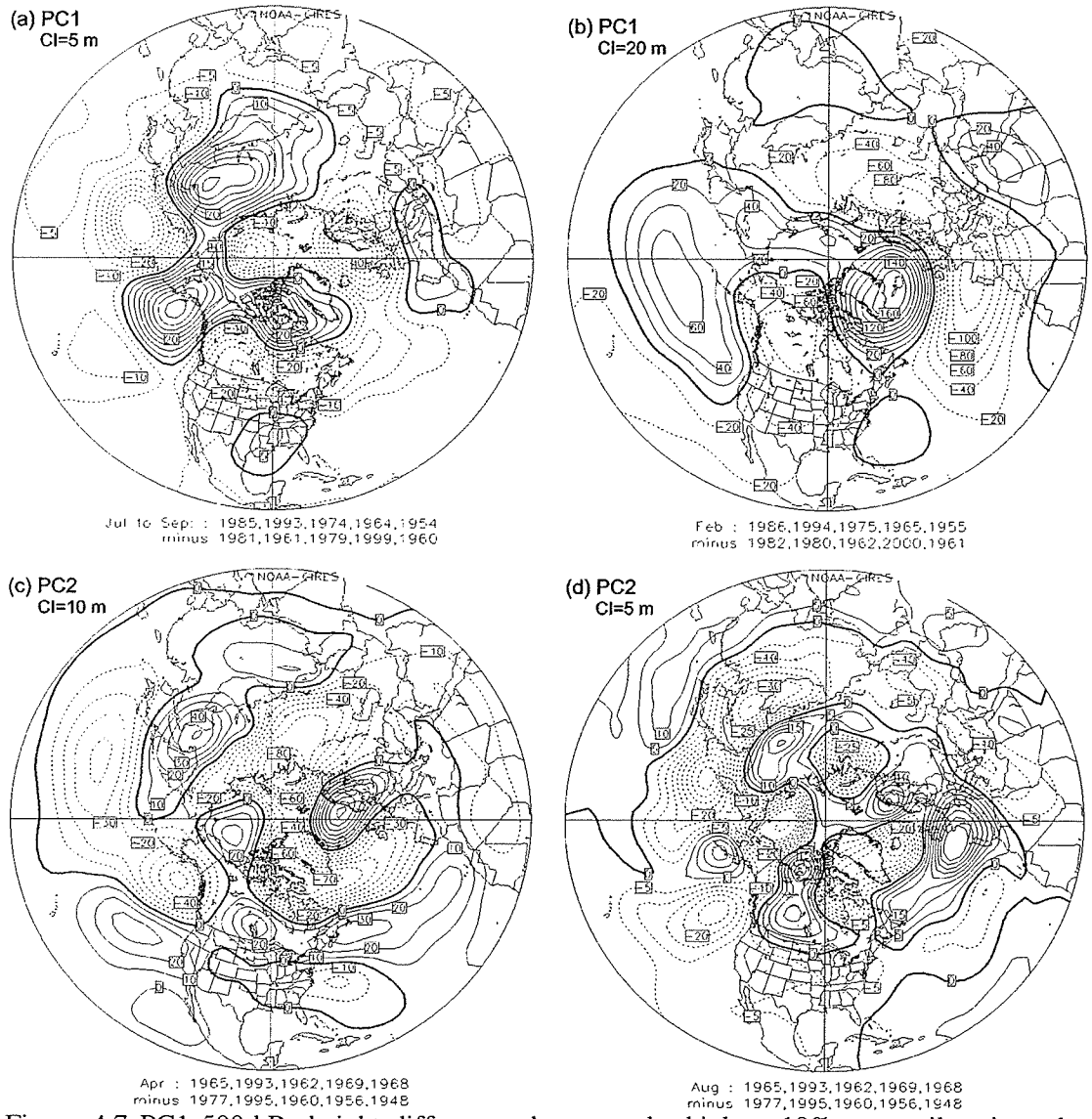

Figure 4.7 PC1 500-hPa height differences between the highest 10% percentile minus the lowest 10% percentile for a) the seasonal average July-September of the year previous to ring formation and b) February of the year current to ring formation. PC2 500-hPa height differences between the highest 10% percentile minus the lowest 10% percentile for c) April and d) August of the year current to ring formation. Solid contours indicate positive height differences; broken contours indicate negative differences.

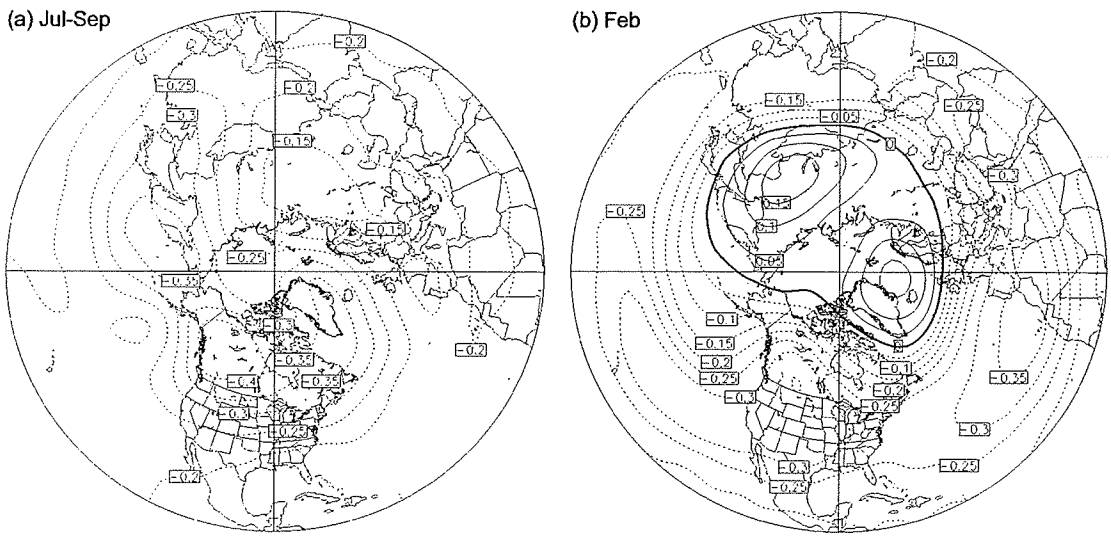

Figure 4.8 PC1 and 50-hPa height correlation charts for a) the seasonal average July-September of the year previous to ring formation and b) February of the year current to ring formation. Refer to Figure 4.6 for other definitions.

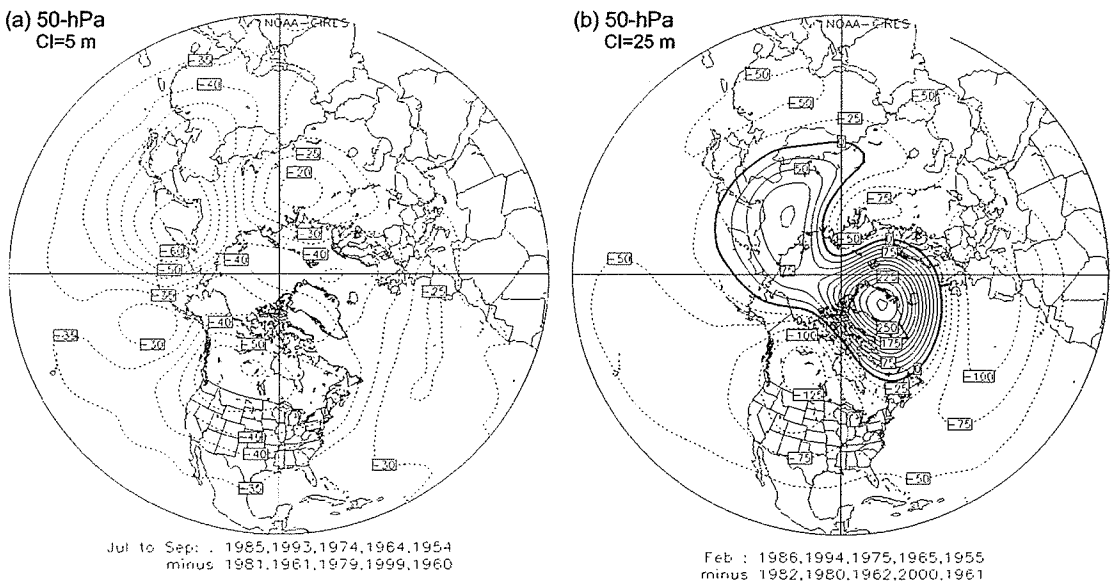

Figure 4.9 PC1 50-hPa height differences between the highest 10% percentile minus the lowest 10% percentile for a) the seasonal average July-September of the year previous to ring formation and b) February of the year current to ring formation.

Table 4.1 Standardized tree-ring chronology statistics for eight tree species from the Duck Mountain Provincial Forest

	Betula papyrifera	*Populus tremuloides*	*Populus balsamifera*	*Picea glauca*	*Pinus banksiana*	*Abies balsamea*	*Picea mariana dry*	*Picea mariana wet*	*Larix laricina*
Chronology length	1785-2001	1806-2001	1808-2001	1776-2001	1717-2001	1890-2001	1724-2000	1758-2001	1676-2002
No. of trees	64	194	29	44	291	35	11	33	54
No. of radii	114	264	47	81	521	58	19	64	89
Percentage of absent rings	0.77	0.27	0.04	0.05	0.12	0.00	0.07	0.12	0.89
Mean sensitivity	0.22	0.23	0.24	0.15	0.13	0.16	0.13	0.11	0.19
Standard deviation	0.24	0.29	0.27	0.20	0.17	0.17	0.17	0.16	0.30
First-order autorrelation	0.42	0.56	0.32	0.56	0.58	0.23	0.55	0.63	0.70
				Common interval analysis (1945-1998)					
No. of trees	21	36	23	31	25	25	10	26	24
No. of radii	33	46	37	54	43	40	16	45	27
Variance in first PCA vector (%)	36.95	35.31	35.28	37.70	30.52	35.81	36.94	29.49	55.62
Expressed population signal	0.91	0.95	0.91	0.94	0.90	0.92	0.77	0.89	0.96
Intercore correlation	0.32	0.32	0.32	0.34	0.27	0.33	0.28	0.25	0.53
Intertree correlation	0.32	0.32	0.31	0.34	0.26	0.32	0.26	0.24	0.53
Intratree correlation	0.62	0.67	0.60	0.59	0.59	0.64	0.67	0.52	0.89

Table 4.2 Monthly signs of the temperature, precipitation, and 500-hPa pressure level correlation coefficients (- for negative and + for positive) (p<0.10), by species, for each site residual chronology for (j) June of the year previous to ring formation to (S) September of the year current to ring formation. Significant response function variables are in parentheses. For each species the model response R^2 is shown. Analyses on temperature and precipitation were conducted on the period 1912-1999; analyses on the 500-hPa height were conducted on the period 1948-1999.

		previous year							current year								
Species	R^2	*j*	*j*	*a*	*s*	*o*	*n*	*d*	*J*	*F*	*M*	*A*	*M*	*J*	*J*	*A*	*S*
Temperature																	
Betula papyrifera	0.30		(-)							-	(-)	-		(+)			
Populus tremuloides	0.27		-	-	-					-	(-)						
Populus balsamea	0.35		-	-	(-)		-			(-)	(-)						
Picea glauca	0.34		-	(-)	-							(+)		-	(-)		
Pinus banksiana	0.35			(-)	(-)							(+)					
Abies balsamea	0.25			-	(-)	(+)	(+)										
Picea mariana dry	0.25		(-)	(-)	-												
Picea mariana wet	0.29		(-)	(-)	-											(+)	
Larix laricina	0.08																
Precipitation																	
Betula papyrifera	0.29	+		(+)					(+)		+			+			
Populus tremuloides	0.30	(+)		(+)										+			
Populus balsamea	0.21			(+)										+			
Picea glauca	0.24		+		(+)									(+)			
Pinus banksiana	0.34		(+)	(+)										(+)		(+)	
Abies balsamea	0.34		(+)		(+)									(+)			
Picea mariana dry	0.26		(+)	+	+									(+)			
Picea mariana wet	0.19		(+)	+		-								+			
Larix laricina	0.18			(+)					-								
500-hPa height																	
Betula papyrifera	0.26							+		-		-			+		
Populus tremuloides	0.38			-			-			-	-						
Populus balsamea	0.47			-	-		(-)			(-)					(+)		
Picea glauca	0.52		(-)		-							(+)		(-)		(+)	
Pinus banksiana	0.56		(-)	(-)	(-)							(+)		-		(+)	
Abies balsamea	0.49		(-)		(-)			-						-		(+)	
Picea mariana dry	0.46		(-)	-	-											(+)	
Picea mariana wet	0.49		(-)	(-)												(+)	
Larix laricina	0.12																

CHAPTER 5

SYNOPTIC SCALE ATMOSPHERIC CIRCULATION AND SUMMER DROUGHT VARIABILITY OF THE PAST THREE CENTURIES, BOREAL CANADA

5.1 Abstract

Five independent multicentury reconstructions of the July Canadian Drought Code and one reconstruction of mean July to August temperature were developed using a network of 120 well-replicated tree-ring chronologies covering the area of the eastern Boreal Plains to the eastern Boreal Shield of Canada. The reconstructions were performed using 54 time varying reconstruction sub–models that explained up to 50% of the regional drought variance during the period 1919-1984. Spatial correlation fields on the six reconstructions and on a rectangular matrix of 90-multicentury tree-ring chronologies revealed that the meridional component of the climate system from central to eastern Canada increased since the mid-19th century. The most obvious change was observed in the decadal scale of variability, with the amplification of a 9-32-years/cycle-oscillation mode. Using 500-hPa geopotential height and wind composites, we interpreted this zonal to meridional transition as a response to an amplification of longwaves flowing over the eastern North Pacific into boreal Canada, from approximately 1851 to 1940. Composites with NOAA Extended Reconstructed SSTs indicated a coupling between the meridional component and tropical and North Pacific SST for a period covering at least the past 150 years, supporting previous findings of a summertime global ocean-atmosphere-land surface coupling. This change in the global atmospheric circulation could be a key element

toward understanding the observed temporal changes in the Canadian boreal forest fire regimes over the past 150 years.

5.2 Introduction

Forest fires are responsible for the spatial and temporal variations in the forest mosaic of the boreal forest (Bourgeau-Chavez et al. 2000). Fire has been an integral ecological process since the arrival of vegetation on the landscape. Weather and climate are important determinants of fire activity (Flannigan and Harrington 1988; Johnson 1992; Flannigan and Wotton 2001). In particular, the frequency of precipitation through the fire season rather than the amount of precipitation is a critical aspect of the weather in terms of fire activity. A low frequency of precipitation is associated with a high probability of large area burnt and vice versa (Flannigan and Harrington 1988; Flannigan and Van Wagner 1991). Another key weather aspect related to a low frequency of precipitation is blocking ridges in the upper atmosphere. Most of the area burned in the boreal forest of Canada is attributed to large blocking high-pressure systems at the 500-hPa atmospheric pressure level that cause dry fuel conditions (Skinner et al. 1999; 2002; Flannigan and Wotton 2001). When high-pressure systems have significant moisture or begin to break down, convective activity leading to numerous lightning strikes occurs and these ignite forest fires (Nash and Johnson 1996). Lightning is the key ignition agent for naturally caused forest fires, but dry forest fuels are also required for large stand-renewing fires (Johnson 1992; Flannigan and Wotton 2001). Climate and the associated weather are always changing due to a number of factors such as changes in the earth's orbital characteristics, the chemical composition of the atmosphere, volcanoes etc. Thus, with a dynamic climate and the strong linkage between climate and forest fires, variations in historical observations of fire activity due to changes in the climate and weather are expected.

Studies have suggested that the fire regime in the Canadian boreal forest changed after the end of the Little Ice Age (~1850). The age distributions of forest stands across large areas of the Canadian boreal forest reconstructed from living trees, snags, and downed woody material, suggest that fire frequency and area burned have significantly diminished since 1850 (Larsen 1996; Weir et al. 2000; Bergeron et al. 2001; Bergeron et al. 2004a; 2004b). The existence of a trend toward a moister climate in eastern boreal Canada was further documented in studies of forest communities located in flood prone environments (Tardif and Bergeron 1997a; Tardif and Bergeron 1999), which revealed an increase in frequency and magnitude of spring water levels at ice break-up. This trend agrees with studies made in the Canadian Plains. Salinity reconstructions in Alberta revealed that past aridity severity (period 1300-1750) was generally greater than recorded during the instrumental period (Sauchyn et al. 2002). The eighteenth and nineteenth centuries were characterized by sustained periods of progressively wetter and drier conditions, including prolonged drought. While drought was frequent in the twentieth century, it tended to be of short duration separated by periods of relatively high precipitation (Sauchyn et al. 2003). With respect to fire weather severity under a $2\times CO_2$ scenario, General Circulation Model (GCM) simulations predict a trend toward a moister climate in the Boreal Shield, and a dryer climate in the Great Plains (Flannigan and Wotton 2001). This agrees with other simulations suggesting more intense, more frequent, and longer lasting 500-hPa blocking high-pressure systems over western-central North America, due to ongoing increases in greenhouse gases (Meehl and Tebaldi 2004).

Owing to the relationship between atmospheric circulation and area burned, it was hypothesized that historical changes in the boreal forest fire regime were attributed to changes in the circulation of air masses (Bergeron and Archambault 1993; Hofgaard et al. 1999) and of sea surface temperatures (Girardin et al. 2004a).

Ocean and atmosphere summertime couplings over Canada have been addressed and recognized by many authors (Bonsal et al. 1993; Bonsal and Lawford 1999; Nigam et al. 1999; Barlow et al. 2001; Girardin et al. 2004a; 2004b; Shabbar and Skinner 2004). Nevertheless, most climate studies are based on short-term data and can provide little or no information on past climate history and its influence on vegetation dynamics. Therefore, this paper investigates the spatial and temporal variations observed in summer drought severity during the last three centuries in the eastern Boreal Plains to the eastern Boreal Shield of Canada. The extent to which the variability in the proxy records reflects changes in atmospheric and oceanic circulation is also explored.

5.3 Data and Methods

Six independent annually resolved climate reconstructions going back to the early 1700s and representative of climate variability from the eastern Boreal Plains to the eastern Boreal Shield were developed from a dense network of 120 tree-ring chronologies. Five of these were reconstructions of the July Canadian Drought Code (CDC: Turner 1972; Girardin et al. 2004a). The sixth was a reconstruction of mean July-August temperature. In addition, the average surface atmospheric circulation back to 1781 was reconstructed by decomposing into principal components a network of 90 multi-century tree-ring chronologies from the eastern half of Canada and from the northern United States. The dynamics between drought variability and atmospheric and oceanic drivers was analyzed using NCEP Reanalysis gridded instrumental 500-hPa geopotential heights and vector winds (1948-1984; Kalnay et al. 1996), and NOAA Extended Reconstructed Sea Surface Temperatures (ERSST, period 1854-1984; Smith and Reynolds 2003).

5.3.1 Study area

The study area covers the eastern Boreal Plains to the eastern Boreal Shield ecozones, and covers most of the boreal forest from western Manitoba to eastern Quebec (Fig. 5.1). The study area covers six climate regions (Fig. 5.1) with boundaries approximating actual ecoregions defined by the Ecological Stratification Working Group (1996). These climate regions are the Boreal Plains (BP), the Lac Seul Upland and Lake of the Woods (LS), the Lake Nipigon (LN), the Abitibi Plains west and east (APw and APe), and Southern Laurentian (SL) (Fig. 5.1).

All six regions under study have a subhumid to humid mid-boreal ecoclimate (west to east gradient), marked by warm summers and cold, snowy winters according to the Ecological Stratification Working Group's (1996) regional classification. In regions BP and LS, average annual temperature ranges between −1.0°C and 1.0°C, whereas eastern regions LN to SL range between 1.0°C to 1.5°C. The average summer temperature is similar across the six regions, approximately 14.0°C. The average winter temperatures are more variable, ranging from −16.0°C in region BP to −11.0°C in region SL. The average annual precipitation ranges from 450 mm in the west to 1,600 mm in the east. In the study area most of the annual precipitation falls between the months of June to October (Environment Canada 2002).

5.3.2 Development of the tree-ring residual chronologies

In winter 2001, a survey of available ring width measurement series was made for the construction of a tree-ring chronology network covering the eastern portion of the Boreal Plains to the eastern portion of the Boreal Shield. A total of 63 data sets of ring width measurement series were gathered from the ITRDB data library, from Archambault and Bergeron (1992), Hofgaard et al. (1999), Tardif and Bergeron (1997b), Jardon et al. (2003), Girardin et al. (2004a), and Girardin and Tardif (2005)

(Table 5.2). In 2002 and 2003, sampling was conducted in Ontario to fill gaps within the network. Sites were systematically visited after gathering information from forest users (forest industries, Ontario Provincial Parks, Ontario Ministry of Natural Resources, Canadian Forest Service, etc.) on potential locations of old growth stands. In each site, dominant trees were sampled and two cores were extracted from each tree using a Pressler increment borer. When possible, more than one tree age/size class was sampled. Disks were taken from the basal most portions of snags and downed woody material to increase the length of the chronologies being constructed. All samples were dried, sanded, and crossdated (Yamaguchi 1991), and each annual ring was measured to 0.001mm accuracy using a VELMEX measuring system interfaced with a computer. For each measurement series, crossdating and measurement were statistically validated using program COFECHA (Holmes 1983). This sampling campaign led to the development of 57 ring width measurement series data sets distributed across Ontario (Table 5.2, Fig. 1).

In total, 120 data sets of ring width measurement series from 13 species and extending back to at least 1866 AD were gathered for the present dendroclimatic reconstruction (Table 5.2). The major species were conifers of the genus *Pinus* (45% of all data sets), with the exception of the Quebec area in which the genus *Picea* represented 51% of all data sets. The species *Thuja occidentalis* L. also represented an important fraction of the data sets (15%). In general, the data sets were well replicated with only 13% of them being composed of less than 30 measurement series (Table 5.2).

The age/size-related trend was removed from the tree-ring measurement series using a spline function giving a 50% frequency response of 60 years (Cook and Peters 1981). Although this detrending procedure resulted in the loss of information relative to long-term climate changes, 99% of the variance contained in frequencies lower than 19 years was preserved. This "flexible" smoothing was necessary because

many of the tree-ring series were less than 100 years in length (see Table 5.2), presenting important growth trends that needed to be removed. The biological persistence (autocorrelation) contained in the standardized measurement series was removed (autoregressive modeling) to eliminate variation not due to climate (Cook and Holmes 1986). Autocorrelation reduces the effective number of independent observations and thus reduces the degrees of freedom used to determine the confidence in statistical tests (Legendre and Legendre 1998). Biweight robust means of the residual measurement series were computed to create a total of 120 tree-ring residual chronologies. All residual tree-ring chronologies were constructed using ARSTAN (Holmes 1999).

5.3.3 Development of the climate data

Analyses of the tree growth-climate relationships were conducted using regional mean monthly average CDC (a description follows) from Girardin et al. (2004b), mean monthly temperature from Vincent and Gullett (1999), and total monthly precipitation from Mekis and Hogg (1999). The program MET from the Dendrochronology Program Library (Holmes 1999) was used to estimate the missing data for each station and to combine the stations into regional variables (refer to Table 5.1 for a list of stations per region and to Fig. 5.1b for the distribution of stations). Monthly variables for each station were normalized to give each station the same weight in calculating the mean values for each month and year.

The CDC is a daily component of the Fire Weather Index System (Van Wagner 1987) that is used across Canada by the Canadian Forest Service (Natural Resources Canada) to monitor forest fire danger. It is an indicator of summertime moisture in deep organic layers in boreal conifer stands (Van Wagner 1970) and correlates well with radial growth of numerous boreal tree species (Bergeron and

Archambault 1993; Tardif and Bergeron 1997b; Girardin et al. 2004a; Girardin and Tardif 2005).

The CDC maintains a daily budget of stored moisture, accounting for daily losses and gains. Each year a snowmelt time is simulated and it is assumed that deep organic layers are fully recharged as a consequence of snowmelt. Moisture losses in the CDC are the result of daily evaporation and transpiration, while daily precipitation accounts for moisture gains. Evaporation and transpiration losses are first estimated as a maximum potential evapotranspiration based on temperature and seasonal day length. Second, this maximum potential evapotranspiration value is scaled by the available soil moisture to reflect the fact that as soil moisture content is reduced, evaporation is increasingly difficult (Turner 1972). In the moisture recharge procedure, total precipitation is reduced by 2.80 mm per 24h period to allow for canopy and surface fuel interception. The scale of the CDC is cumulative, with each unit change representing a decrease of 0.254 mm of available water in the soil. The maximum water holding capacity of the CDC is 100 mm for a layer with a bulk density of about 25kg/m^2, which amounts to approximately 400% of water per unit of mass. The minimum CDC value of zero represents 20.32 cm of available water held in the soil. A CDC rating of 200 indicates high drought and a rating above 300 indicates extreme drought severity. Excess water is considered as residual rainfall and is not accounted for in the CDC. More details on the CDC calculation can be found in Van Wagner (1987) and Girardin et al. (2004b).

5.3.4 Tree growth and climate relationships

Redundancy Analysis (RDA) (Legendre and Legendre 1998; Tardif et al. 2003; Girardin et al. 2004a) was used to investigate the species' response to climate. RDA is the canonical extension of PCA and intends to display the main trends in variation

of a multidimensional data set in a reduced space of a few linearly independent dimensions. In RDA, the canonical axes differ from the principal components (PCs) in that they are constrained to be linear combinations of supplied environmental variables (ter Braak and Prentice 1988; ter Braak 1994). The RDA output not only displays the relationship between tree-ring chronologies, years, and supplied climate variables, but also displays the relationships observed within each data set, i.e., among climate variables and among chronologies. RDA may be understood as a two-step process: (i) each residual chronology is regressed on the selected climate variables and the predicted values are computed; (ii) a PCA is then carried out on the matrix of predicted values to obtain the eigenvalues and eigenvectors (Legendre and Legendre 1998). The climate variables were selected using a forward selection on the basis of the goodness-of-fit and tested for significance using 999 Monte Carlo unrestricted permutations. This procedure was repeated until a variable was tested non-significant at the 5% level.

One RDA was computed from each of the six regions. The dependant variables data set included all residual chronologies for a given climate region and the independent variables data set included the corresponding regional mean monthly CDC, mean monthly temperature and total monthly precipitation. All analyses were constrained to the common interval 1919-1984, due to the availability of meteorological data in the earliest years and of chronologies in the latest years. The period of analysis included June of the year previous to ring formation to September of the year of ring formation. All RDA were conducted on covariance matrices since the descriptors (the tree-ring chronologies) were of the same kind, shared the same order of magnitude, and were measured in the same units (Legendre and Legendre 1998). RDA were computed using program CANOCO 4.0 (ter Braak and Smilauer 1998) and scaling of ordination scores were done using correlation biplots.

5.3.5 Reconstruction of drought severity

The climate reconstructions were performed using the varying time series technique described by Cook and D'Arrigo (2002), Luterbacher et al. (2002), and Girardin et al. (2004a). Due to large time varying chronologies, 54 sub-models were developed for the reconstructions. The number of sub-models constructed for each region varied between six and eleven, starting with a minimum of five chronologies and adding chronologies in subsequent sub–models.

In each reconstruction sub–model, the available residual chronologies were transformed into non-rotated PCs to remove multicollinearity (Cook and Kairiukstis 1990; Legendre and Legendre 1998). The PCs are orthogonal linear combinations of the original data, each representing decreasing amounts of the original total variance. PC1, PC2, PC3 and PC4, which accounted for 64% to 97% of the total variance, were kept for the construction of the sub–models. Because tree growth in the year of ring formation is influenced by weather conditions in both the current and the prior growing seasons (e.g. Archambault and Bergeron 1992; Hofgaard et al. 1999; Fritts 2001; Girardin and Tardif 2005), the four PCs were also forwarded by one year and included in the calibrations. PCA were conducted on covariance matrices and program CANOCO 4.0 was used (ter Braak and Smilauer 1998).

Calibrations for the period 1919-1984 were conducted on the predictors using forward stepwise multiple linear regression analyses between the instrumental climate indices (predictands) and the PCs (predictors; present and forward lags) (Cook and Kairiukstis 1990). The yearly climate indices for the early period covered by the site residual chronologies were estimated from the calibration equations (transfer function). The stability of each sub-model was tested (verification procedure) after conducting a sub-calibration of the period 1941-1984. The strength of the relationship between reconstruction and observation over the verification period 1919-1940 was

measured by the Reduction of Error (RE) discussed in Cook et al. (1994). Whenever RE is greater than zero the reconstruction is considered as being a better estimation of climate than the calibration period mean. The final reconstructions were built after merging segments of the sub-models.

5.3.6 Atmospheric circulation

The long-term history of atmospheric circulation was analyzed using the non-rotated PCA approach (Yarnal 1993) on correlation matrices. The non-rotated PCA solution was preferred over the rotated PCA because of a focus on global patterns and not localized ones (see Dommenget and Latif 2003). A correlation matrix was used so that all descriptors could contribute equally to the clustering of objects, independent of the variance (and units) exhibited by each one (Legendre and Legendre 1998). First, a PCA was conducted on the six reconstructions on their common time interval 1768-1984. Second, the temporal stability of the shared variance among tree-ring chronologies was evaluated by conducting a PCA on a rectangular matrix of 90 tree-ring residual chronologies sharing the common period 1781-1980 (e.g., Fritts et al. 1991; Bradley 1999; Gajewski and Atkinson 2003; Tardif et al. 2003). The rectangular matrix was created by nesting 58 multicentury chronologies located within our six climate regions into a grid composed of 32 multicentury chronologies from surrounding areas (Table 5.2; Fig. 5.1). These chronologies were extracted from the ITRDB (www.ngdc.noaa.gov/paleo) and from Girardin et al. (2005). All measurement series were processed as described in Section 5.3.2. The 1781-1980 period was chosen to maximize the length of the period of analysis and the number of chronologies in each region. Though tree species were unequally distributed in the area of study (this may have altered some of the physical dynamics), the approach was justified by the persistence of the relationship between radial growth and climate in the six regions.

Continuous Wavelet Transform (CWT) analyses were conducted to identify non-stationary signals in the first and second PCs of the six reconstructions. CWT was used to decompose signals into wavelets, small oscillations which are highly localized in time (Torrence and Compo 1998). CWT analyses were performed using a nonorthogonal Morlet wavelet basis with a wave number of 6. Other wavelet bases (the Paul basis for instance) with various adjustable parameters were also tested and results tended to be consistent (within the uncertainty of the wavelet basis' definition). CWT analyses were performed using the program AutoSignal version 1.5 (AISN Software 1999).

The atmosphere's physical dynamics were analyzed using May to July 500-hPa NCEP Reanalysis geopotential height (expressed in meters) and vector wind (m/s) composites. The NCEP Reanalysis 500-hPa grid has a global spatial coverage of 2.5° latitude by 2.5° longitude with 144x73 points and a temporal coverage from 1948 to present, with output every 6 hours (Kalnay et al. 1996). Daily data were averaged by months for each grid point. SST composites were also created using NOAA ERSST (from Smith and Reynolds 2003). The ERSST covers the period 1854 to present and was constructed using the most recently available Comprehensive Ocean-Atmosphere Data Set. All maps were created with the aid of the NOAA-CIRES Climate Diagnostics Center, Boulder, Colorado (www.cdc.noaa.gov).

5.4 Results

5.4.1 Tree-ring width and climate relationships

The RDA eigenvectors indicated that the majority of chronologies within their respective climate regions shared common environmental signals (Fig. 5.2). This was

particularly true for the APw and SL regions in which the first canonical axis alone explained at least 25% of the total variance (Table 5.3). The partitioning of the chronologies was particularly strong on the positive side of the first eigenvector with 60.8% of the chronologies having an eigenvector loading greater than 0.40. Only 5.8% of the chronologies had a similar loading on eigenvector 2 and a tendency for a distribution of *Betula papyrifera* Marsh. and *Quercus macrocarpa* Michx. along the second eigenvector was observed. Clustering of species within the reduced space was also observed, particularly with *Pinus resinosa* Ait. and *Pinus strobus* Lamb.. The species *P. banksiana* was often distributed on the edges of these clusters. This is an indication of strong common signals within species and genus. Clustering was also observed in the genus *Picea*; *T. occidentalis* had no specific locations within the reduced spaces.

The significant climate variables retained in each RDA indicated that the strongest climate influence was from the summer season (Fig. 5.2). Of the total 43 significant monthly variables, 24 were related to June, July, or August from either the year prior (t-1) or current (t) to ring formation. The July (t) CDC demonstrated strong association with radial growth in five of six regions. August (t-1) temperature was a dominant variable in all six regions, and July (t-1), November (t-1), and April (t) temperatures in respectively 3, 3 and 5 regions. Despite the absence of a relationship between the CDC and radial growth in the SL region, the combined effects of July (t-1) and August (t-1) mean temperatures suggested a negative effect of a temperature-induced stress on radial growth of the following year.

In general, the genus *Pinus* (particularly *P. resinosa* and *P. strobus*) presented the strongest correlation (negative) with the July-CDC (Fig. 5.2). August (t-1) temperature more often pointed in the direction opposite to *Picea mariana* (Mill) B.S.P. and *P. banksiana*, suggesting a negative influence of previous year warm late

summer temperature on their radial growth. The radial growth response to other climate variables was more ambiguous, with no consistent patterns emerging.

5.4.2 Reconstruction model performance

In all regions but SL, the mean July-CDC was reconstructed as a proxy for summer drought. Because of its daily weather cumulative scale, the mean July-CDC gathers information over a season approximating May to July (refer to Section 5.3.3 and to Girardin et al. 2004b). Despite the results of the RDA from the SL region, trials have indicated significant correlation ($p<0.10$) between July-CDC indices from meteorological stations Barrage Gouin, Mistassini Posts and Hemon (Table 5.1) and seven chronologies from surrounding areas. The low predictive skills of the calibration models however did not allow reconstruction of the CDC with confidence. Therefore, the mean July-August temperature was reconstructed as a proxy for mid-summer temperature in the SL region. Despite the absence of a drought signal, the SL reconstruction provides valuable information on past climate variability, notably on the occurrence of mid-summer warm spells and persistent ridging. Hereafter, the SL reconstruction is more often referred to as a "drought" reconstruction for consistency throughout the paper.

Figure 5.3 presents the regional model performance (RE) for the drought reconstructions plotted against the time period for which a multiple linear regression model was used. The best model obtained was the BP reconstruction with RE exceeding 0.30 for a reconstructed period reaching the early 1700s. The LS, LN and APw reconstructions also showed good reconstruction skills for their whole period. The LN and APw reconstructions, however, demonstrated lower model R^2. Finally, both APe and SL reconstructions showed a decline of the RE statistic with a decrease

in the number of predictors. The predictive skills of the sub-models covering the 19th and 20th centuries are high, and acceptable for sub-models covering the 18th century.

5.4.3 Multicentury drought variability

The regional drought reconstructions and their smoothed curves are shown in Figure 5.4. Plots of cumulative departures from the mean were also produced for each reconstruction and reconstruction sub-model (Fig. 5.5). The plots of cumulative departures indicated strong regional common signals among reconstruction sub-models (Fig. 5.5). Pearson correlation coefficients calculated between pairs of reconstruction sub-models confirmed that within any regions the sub-models were sharing very strong common variance (Table 5.4). 75% of all coefficients were greater than 0.70. Sub-models sharing low common variance were generally those built from a low number of predictors.

Observation of the smoothed reconstructions indicated the presence of three periods dominated by important decadal variations: the late 1700s to 1850 in most regions, the first half of the 20th century in eastern regions, and the later part of the 20th century in LS and BP regions (Fig. 5.4a-f). Based on standard deviations of smoothed reconstructions arbitrarily chosen as > 1.0 and for at least four consecutive years, persisting dry events marked the BP region during 1735-1743, 1838-1843, 1887-1892, 1936-1940, and 1958-1963. The plots in Figure 5.5a of cumulative departures from the long-term mean of drought severity revealed that in the BP, the mid-19th century was preceded by a century of frequent negative departures, as well as the mid 20th century. In contrast, the period ~1840-1940 was dominated by positive departures. In the LS region, dry events marked 1791-1795, 1838-1842, 1860-1867, 1908-1911, 1932-1937, and 1973-1983. A prolonged episode of negative departures marked the second half of the 20th century (Fig. 5.5b).

Dry events were recorded in the APe regions during the periods 1734-1738, 1748-1754, 1789-1792, 1819-1822, 1837-1849, and 1917-1922 (Fig. 5.4e). The period 1750-1850 was particularly intriguing, with succeeding episodes of prolonged and severe droughts. These droughts were also well highlighted by the cumulative departures (Fig. 5.5e), which also indicated a strong coherence with the BP region (Fig. 5.5a) from 1720s to 1850s. In the APw and LN regions, dry events were recorded during 1696-1700 (in LN), 1787-1796, 1736-1744 (in LN), 1806-1810, 1836-1841 (in APw), 1888-1892 (in APw), 1905-1911, 1918-1922, 1934-1938, and 1991-1995. Finally, warm spells during 1791-1796, 1876-1882, 1909-1916, and 1971-1978 occurred in the SL region (Fig. 5.4f).

5.4.4 Spatial and temporal patterns of drought variability

A non-rotated PCA of all six drought reconstructions was run on the period 1768-1984 and the resulting first and second component scores (PC1 and PC2) were projected on a time axis (Fig. 5.6). The relationship was extended to 1718 by running a second PCA on the BP, LN, and APe reconstructions on their common interval 1718 to 1984. The component scores from this last PCA were highly correlated with the former ones (r_{pc1}=0.88 and r_{pc2}=0.84 for n=217). The intent of this work was to focus on the west to east gradient and thus succeeding PCs were not accounted for.

PC1 shared common variability with all six reconstructions; its centre was located over the Lake Nipigon and the western Abitibi Plains (Fig. 5.6a). The component showed strong interdecadal drought variability in the 1770-1845 and 1905-1940 intervals with a period of strong interannual variations in the period 1770-1815. Spectral analyses (Fig. 5.7a) effectively indicated the presence of strong and quasi-stationary signals in the band 17-32-years/cycle over much of the reconstructed

period (accounts for 20.3% of the variance in PC1). The spectrum also showed 9-16-year signal peaks in the early 1800s and 1900s (Fig. 5.7a). Starting in 1940s, signals have weakened considerably, suggesting a change in the pattern of drought variability during recent decades. Over the past three centuries prolonged events of positive PC1 scores occurred from 1735-1743, 1789-1795, 1837-1842, 1862-1865, 1906-1910, 1919-1921, and 1933-1938. The year 1961 recorded the highest PC1 score, closely followed by 1735, 1741, 1794, 1910, 1921, 1886, and 1864 (Fig. 5.6).

The PCA orthogonality constraint in space generally dictates the second PC to be a domain-wide dipole (e.g., about half the data set being inversely correlated with the component loading). The second PC was effectively associated with a dipole between the western and eastern regions and thus was referred to a meridional component (Fig. 5.6b). Positive (+) PC2 scores indicated drier condition in the BP-LS regions and lower drought severity in the APe-SL regions, and vice versa. PC2 (Fig. 5.6b) suggested that the twentieth century was marked by a substantial increase in the magnitude of the meridional component, particularly of its decadal mode. We recognized that strong interdecadal variability has also occurred during the period 1718-1750 and ~1830-1870. Spectral analysis (Fig. 5.7b) further indicated an unprecedented 9-16-years/cycle oscillation during the late twentieth century. A rise in the spectral power of the 17-32-years/cycle signal was also observed. Prolonged events of +PC2 were observed from 1737-1745, 1782-1785, 1861-1865, 1887-1892, 1926-1932, and 1979-1984; events of negative (-) PC2 were 1718-1721, 1750-1753, 1846-1853, 1878-1881, 1915-1922, 1945-1953, and 1966-1973 (Fig. 5.6b). Historical years of +PC2 were 1746, 1800, 1842, 1865, and 1961; historical years of negative (-) PC2 were 1723, 1916, 1919, 1941, and 1947. The dynamics between PC1 and PC2 and the atmosphere are analyzed in the subsection that follows.

5.4.5 Tropospheric circulation

Prior to investigating the composites, tests were carried out to validate the use of the 500-hPa geopotential heights against PC1 and PC2. Correlation maps with 500-hPa geopotential heights (not shown) indicated that variability in PC1 was associated with a north and south dipole, with one cell at 57°N-95°W and another at 35°N-90°W. This configuration suggested that drought over the six regions was positively associated with anticyclonic shear vorticity in the mid-latitude and weak cyclonic shear vorticity at more southern latitudes (shear vorticity is the rate of change of wind speed normal to the direction of the flow). In contrast, the second PC was associated with an east and west dipole, with one cell at 50°N-115°W and the other at 50°N-50°W. This configuration suggested that drought in the BP region was positively associated with an intensified western ridge and eastern trough. In contrast, drought in the APe region was positively associated with a weakened western ridge and eastern trough. The zonal index (ZI) and the meridional index (MI) may be used to define these types of circulation over the six regions (after Bonsal et al. 1999):

[E1] ZI = Grad(55°N to 65°N) – Grad(35°N to 45°N)

[E2] MI = Z(45°N to 55°N, 115°W) – Z(45°N to 55°N, 80°W)

where Z = average 500-hPa value and Grad = average 500-hPa gradient from 70°W to 100°W (the approximate longitudinal extent of the study region). The ZI measures the characteristic of the west-east flow over the six regions where +ZI defines a state with weak westerlies and strong meridional flow. A –ZI is associated with strong westerlies and a weak meridional flow. The MI measures the meridionality of the flow. A +MI indicates an amplified western ridge and a deepened eastern trough; a –MI indicates the reverse relation.

Time series of ZI and MI were correlated with their respective PC component over the period 1948-1984 using the Pearson coefficient. Results indicated that PC1 depicted significant responses to the ZI (r=0.48, p<0.005). Thus it reflected variations in the strength of the westerly flow between the northern (55°-65°N) and southern (35°-45°N) regions. PC2 correlated well with the MI (r=0.47, p<0.005), indicating that it reflected variations in the western ridge and eastern trough. These results were comparable to calculations on PCs obtained from instrumental records over the interval 1948-1998 (ZI_{pc1}=0.41, MI_{pc2}=0.43).

Years of highest and lowest PC1 and PC2 scores during the period 1948 to 1984 were selected for the creation of 500-hPa geopotential height and vector wind anomaly composites. Non-parametric t-tests (Mann-Whitney U test statistic) indicated a significant difference in means among samples of ZI indices at the time of the 5 highest and the 5 lowest PC1 scores (p<0.028). Similarly, a significant difference in means was observed among MI samples of highest and lowest PC2 scores (p<0.009). These two tests validated the use of the composite maps for exploration of the mid-tropospheric circulation variability associated with PC1 and PC2.

The five years of +PC1 (dry years; Fig. 5.8a) were associated, in average, with intensified ridging over the western Hudson Bay, lower level divergence and subsidence of air over much of the boreal forest (giving rise to dryer conditions particularly in LN, APw and APe regions). A meridional component gave rise to northeasterly winds in eastern Canada and southerly winds in the Great Plains. The five years of –PC1 (Fig. 5.8b) were associated with lower heights over boreal Canada. As opposed to +PC1 scores, –PC1 scores were associated with stronger mid-tropospheric westerlies and an amplified jet stream at 45°N and 70°-110°W. During years of low drought severity, moisture-bearing systems from the North Pacific

Ocean were free to move across the continent. At 60°N the situation was essentially opposite, with the near absence of mid and high zonal tropospheric winds (in absolute chart reduced westerlies, not shown).

PC2 was in average associated with an oscillation in the position and direction of the jet stream and meridional flows from westward (+PC2) to eastward (-PC2). +PC2 scores (Figure 5.8c) were characterized by ridging over the Gulf of Alaska and Greenland and intensified troughing in eastern Canada. An anomalous anticyclonic flow over the Rocky Mountain combined with the cyclonic flow above Ontario gave rise to mid-tropospheric northwesterlies over central Canada and western Ontario. The persistence of the ridge induced subsidence of air over the eastern Boreal Plains, low precipitation, warming, and drying. In eastern Canada, the cyclonic activity drove mid-tropospheric southerlies along the east U.S.A. coast toward the Quebec interior. This flow allowed the advection into Quebec of warm, moist and unstable air from the subtropical North Atlantic basin. The five years of –PC2 (Fig. 5.8d) were associated with a weakening of the eastern trough and a downstream convergence and subsidence zone near 70°W. The circulation was associated with southerlies in the Boreal Plains and western Boreal Shield, which brought moisture rich air from the coastal subtropical North Pacific. In eastern Quebec the anticyclonic flow drove an outflow of dry arctic air.

The PCs are cumulative, so any pattern from PC1 (either Fig. 5.8a or 5.8b) can be superimposed on any pattern from PC2 (Fig. 5.8c or 5.8d). For instance, PC1 indicated that 1955 was generally dry over the LS, LN, and APw regions. PC2 indicated that it was drier in APe than in BP. Climatologically, this suggested that the circulation in 1955 featured a strong anticyclone (i.e. Fig. 5.8a), but with a centre located northeast of Ontario.

5.4.6 Sea surface temperatures

The connection between the west-east meridional component (PC2) and global ERSST is presented in Figure 5.9. Analyses conducted on PC1 have shown no significant correlation with the mean May-July SST and thus are not presented. A PC2 correlation chart (not shown) indicated significant positive correlation ($p<0.05$) with SST along the eastern North Pacific coast and into the tropics. A centre of significant negative correlation was also observed in the interior North Pacific, roughly at 160°W and 30°N. The spatial structure of the variability was very similar to that of the Southern Oscillation (Ropelewski and Jones 1987), but with greater amplitude at high-latitudes and a reduced tropical expression. The Pacific pattern is the one commonly referred to as the Pacific Decadal Oscillation (PDO; Mantua et al. 1997; Zhang et al. 1997) or North Pacific pattern (Latif and Barnett 1996). A significant Pearson correlation ($r=0.25$; $p<0.004$, $n=131$) between PC2 and the May-July ERSST PDO of Smith and Reynolds (2003; not shown) was obtained. Analysis between the PDO and PC2 10-30-years/cycle waveforms (not shown) further indicated a highly significant correlation of 0.72 in this bandwidth during the period 1854-1984, with a 95% confidence interval [0.64; 0.79] (computed using program PearsonT, Mudelsee 2003). The hypothesis of a correlation between two serially correlated time series is rejected when the confidence interval contains zero.

Non-parametric t-tests indicated a significant difference in means among samples of ERSST PDO indices at the time of the 10 highest and the 10 lowest PC2 scores ($p<0.004$). Figure 5.9a indicated that +PC2 were associated with SSTs higher by ~0.5°C along the western coast of North America. A centre of positive anomalies (by ~0.4°C) not dissimilar to the typical El Niño signature but with reduced expression was also observed in the tropical Pacific, roughly at 150°W. Two centres of lower than normal SSTs (by ~0.3°C) were observed in the interior North Pacific near 160°W-37°N and in the western North Pacific near 155°W-45°N (Fig. 5.9a). In

the South Pacific, a similar pattern was observed, with SSTs warmer by ~0.6°C along the American coast.

During average PC2 scores (not shown), the interior North Pacific anomaly shifted in sign, with SSTs higher than average by ~0.3°C. Lower SST occurred in the tropical (by ~0.6°C) and east subtropical North Pacific and along the western coast of North America (by ~0.3°C) and South America (by ~0.6°C). During –PC2 scores (Fig. 5.9b), the centre of anomalously positive SSTs in the interior North Pacific intensified and attained ~0.7°C. SSTs lowered to reach more than ~1.5°C below normal in the eastern tropical and subtropical North Pacific (the typical La Niña signature) and ~0.7°C below normal along the western coast of Alaska. In the South Pacific, a similar pattern was observed, with SSTs warmer by ~0.2°C in the interior and cooler by ~0.6°C along the South American coast.

5.4.7 Frequency of composites

Histograms showing the frequency per decades of + and – PC score departures were created (Fig. 5.10). The PC scores were classified as either part of the upper 33.3% percentiles (positive PC departures), lower 33.3% percentiles (negative PC departures), or in between (residual PC departures). The 33.3% percentile threshold was arbitrarily chosen; results were consistent with the 20.0% and 40.0% thresholds.

The temporal distribution of the PC2 scores suggested a period of less frequent +PC2 from 1751 to 1850, with the exception of the intervals 1781-1800 and 1821-1840. The 1751-1850 interval contrasted with periods of frequent +PC2 from 1721-1750 and 1851-1940 (Fig. 5.10d). From 1751 to 1850, +PC2 occurred at an average rate of 2.3 years per decade, whereas from 1851 to 1940 the average was 4.1 years per decade. This change in the frequency of occurrences of +PC2 was tested

significant at the 5% level using the Mann-Whitney U test statistic (p=0.010). A significant change toward a reduced frequency in the residuals of PC2 (Fig. 5.10f) from the former period to the later was also detected (p=0.024). No significant long-term change was detected in the frequency of PC1 and –PC2 departures.

Climatologically, this change in the frequency of PC2 scores suggested a period of greater zonality from 1751 to 1850 across the eastern Boreal Plains and Boreal Shield during summertime. It implied that less frequent ridging and air subsidence marked the 1751-1850 over the eastern Boreal Plains, while in the eastern Boreal Shield it meant a weaker trough and less frequent advection of humid air masses from the subtropical North Atlantic. The mid-tropospheric pattern associated with Figure 5.8c and the SST pattern associated with Figure 5.9a (cooler SST in the interior North Pacific and warmer ones along the American North Pacific coast and in the tropics) were likely less frequent from 1751 to 1850.

5.4.8 Reanalysis of spatiotemporal variability

The spatiotemporal structure of climate across the six regions was reanalyzed by studying the long-term stability of the shared variance between 90 tree-ring sites residual chronologies distributed across a rectangular grid covering 101°W to 61°W and 41°N to 61°N (Fig. 5.11). The shared variance was analyzed by constructing four sequential maps, each one representing the chronology loadings on a principal component for a given period of 100 years (PC1 and PC2 were analyzed). The following description relies on the connection between upper atmospheric circulation and surface climate over the area where the chronologies originated.

The analysis of the interval 1781-1880 (Fig. 5.11a) indicated that in the earliest period chronologies from all sectors shared common variance. After 1851, a

break-up of the common signal was observed with the weakening of the correlation coefficients between PC1 and chronologies from Northern Canada and Quebec. This transition from a domain-wide pattern to a dipole most likely reflects a shift in mid-tropospheric wind flow between the north and the south. The percentage of explained variance has not changed substantially from the first interval to the last. A similar analysis conducted on the six reconstructions (Fig. 5.11a) did not show major changes in the common variance over time.

In the earliest interval PC2 (Fig. 5.11b) was characterized by a north-south dipole with the axis (zero line) passing through approximately 55°N. The dipole was weak on its negative centre (average correlation >-0.20) and strong on its positive one (average correlation <0.45). In the interval post 1851, the orientation of the dipole shifted toward a west-east direction with the axis passing through approximately 90°W i.e., just west of Lac Seul. This is the current location of the average summer position of the axis dividing the western ridge from the eastern trough (refer to Figure 5.8c-d). The analysis conducted on the six reconstructions (Fig. 5.11b) reaffirmed the occurrence of a stronger dipole over time, especially between the LS and APe regions.

5.5 Discussion

5.5.1 Atmospheric circulation

The summer reconstructions produced constitute the first climate reconstructions ever made covering the southern limit of the central to eastern Canadian boreal forest. The analyses presented provide new information on the spatiotemporal variability of summer drought severity. Results suggest that the area covering the eastern Boreal Plains to the eastern Boreal Shield of Canada is under the influence of two

components of synoptic scale atmospheric circulation. The zonal component (PC1) is associated with a circulation of cool and moist westerlies over the central area of the Boreal Shield during years of low drought severity, and a circulation of dry and cold northerlies during years of high drought severity. The analysis of the component's spectra showed a quasi stationary 17-32-years/cycle signal over most of the reconstructed period. The analysis revealed no major changes in its magnitude at ~1850, and nor in its oscillation mode. Changes were, however, noted in other periods, with peaks of higher frequencies around 1800 and 1900, and a change toward a reduced signal in the late twentieth century. Despite the absence of changes in the component at ~1850, the analysis of the spatiotemporal variability in radial growth suggested that the expression of the zonal pattern has changed between the northern and the southern areas of the Boreal Shield. This shift may be concordant with the reported contraction of the Aleutian and Icelandic lows at 1850 (refer to Guiot 1985 and Gajewski and Atkinson 2003).

The meridional component reflects regional drought variability in the west-east dimension. This variability occurs as a response to blocking of moisture carrying systems upstream and advection of moisture air downstream the longwaves (refer to Flannigan and Harrington 1988; Weber 1990; Knox and Lawford 1990; Bonsal et al. 1999; Skinner et al. 1999; 2002). An amplified western ridge is associated with a northerly-displaced jet stream over western Canada and a southerly displacement in eastern Canada. This configuration favours northerly winds, air subsidence, and increasing drought severity in the eastern Boreal Plains. In the eastern Boreal Shield, this configuration favours cyclonic development, inflows of subtropical North Atlantic air, and lower drought severity. Spatiotemporal analyses conducted on the 90 tree-ring chronologies and on the six reconstructions suggested that the meridional component has gained in magnitude over the past 150 years and particularly in the decadal scale of variability. This suggested that more intense longwave oscillations

occurred during the past century over the Canadian boreal forest, contributing to a greater contrast in summer drought severity between the eastern Boreal Plains and Boreal Shield. Analyses indicated that from ~1751-1850, amplifications of the western ridge and eastern trough were infrequent relative to ~1851-1940 (Fig. 5.10c). This meant reduced frequency in the occurrence of air subsidence in the eastern Boreal Plains and air mass advection in the eastern Boreal Shield during the former interval.

Skinner et al. (1999) addressed the effect of atmospheric circulation shifts on area burned across Canada. The authors found that a transition toward a higher frequency of ridging (troughing) over western (eastern) Canada after 1974 contributed to significant increases in the area burned, especially in the northwest and central regions (1975-1995 versus 1953-1974). Preliminary analyses by Girardin et al. (2004b) effectively showed significant correlations between seasonal area burned across the six regions during the period 1959-1998 and the instrumental zonal PC1 and meridional PC2. However, despite the fact that the season covered by the reconstructions may be a good proxy for fire weather conditions at the time of greatest area burned, it may underestimate or omit variability and temporal changes in conditions leading to spring and late summer fire disturbances. In Canada, 78% of the area burned from 1959 to 1998 occurred in June and July, while 8% occurred during May and 13% during August (Stocks et al. 2003).

5.5.2 North Pacific air-sea interactions

It is now commonly accepted that the atmospheric response to SST anomalies in the equatorial Pacific determines ocean conditions over the remainder of the global ocean (Yang and Zhang 2003; Kumar and Hoerling 2003; Lau et al. 2004; Shabbar and Skinner 2004). Tropical SSTs, with the contribution of stochastic feedback from the

atmosphere, generate the North Pacific SST anomalies (Schneider et al. 2002; Newman et al. 2003; Wu and Liu 2003). Wu and Liu (2003) indicated that anomalies in the central North Pacific and eastern North Pacific Ocean, well simulated by global ocean-atmosphere models, could be obtained from anomalous Ekman transport and surface heat flux. Lau et al. (2004) suggested a mechanism in which air-sea interactions amplify North Pacific anomalies and sustain them through feedback processes, involving the interplay of surface fluxes, atmospheric mean circulation and transient eddies, and radiation effects of stratocumulus cloud decks.

Several paleoclimate studies suggested important changes in the North Pacific climate over the past three centuries (Luckman et al. 1997; Stahle et al. 1998; D'Arrigo et al. 2001; Evans et al. 2002; Finney et al. 2002; Wilson and Luckman 2003). The significant association observed between the meridional component and tropical and North Pacific SSTs indicated that spatiotemporal drought variability over the eastern half of Canada has been under the influence of this coupling for a period covering at least 150 years. Because of the relationship between Pacific SSTs and atmospheric circulation, the combined information from these studies could support the observation of a weakened western ridge and eastern trough from ~1760 to 1840. Investigation of prominent aquatic population declines in the Gulf of Alaska by Finney et al. (2002) suggested the prevalence of cooler water along the coast from approximately 1750 to 1850. A prolonged period of cooler Pacific and western coast air temperature during the pre-industrial period was also reported by Luckman et al. (1997), D'Arrigo et al. (2001), Evans et al. (2002), and Wilson and Luckman (2003). Reconstruction of the Southern Oscillation (SOI) by Stahle et al. (1998) showed a statistically significant increase in the SOI interannual variability during the mid-ninetieth century. Though there may be a teleconnection, the meridional component developed here is not optimized to capture the maximum atmospheric circulation

variability associated with the Pacific, and thus it should not be interpreted as a proxy for past SST variability.

This study may be complementary to recent work by Jacobeit et al. (2003) in which July dynamical modes of atmospheric circulation in Europe were reconstructed. The authors also observed a period dominated by a westerly flow from about 1750 toward the end of the 19th century. Thereafter followed a steady increase of a meridional component associated with increasing anticyclonic activity over the eastern North Atlantic and the European continent. While it is difficult to link European and Canadian climate variability, the combined information from this study and that of Jacobeit et al. (2003) suggests that the circulation transition at about 1850 from zonal to meridional flows could be part of a global scale phenomenon. In the context of global oceans teleconnections, it is suggested that North Pacific and North Atlantic SST patterns may be connected through an extratropical climate mode, linking SST variability in the North Pacific and the North Atlantic via an atmospheric bridge across North America (Lau et al. 2004).

5.5.3 Concluding remarks

This work constitutes an important step in the development of climate change adaptation strategies in the Canadian boreal forest sector. Paleoclimate information can improve our understanding of how the atmosphere-ocean and land climate systems have evolved over the past centuries, and provides a baseline to anticipate future vegetation response to climate variability and change across Canada. The results suggest that broad-scale atmospheric circulations are important in meteorological conditions like drought. Weather, and specifically drought, is related to fire so it is likely that uncovered atmospheric patterns have also influenced forest fires and vegetation dynamics over the past centuries. It the light of the present

findings, it is pertinent to believe that the decrease in the frequency of large areas burned at about 1850 on the Canadian Boreal Shield is due to more frequent advection of air masses from the subtropical North Atlantic. The meridional circulation is however highly variable in the decadal scale and this variability likely gave rise to several succeeding episodes of severe and prolonged mid-tropospheric circulation blocking during the past 80 years or so.

5.6 Acknowledgements

We acknowledge the Sustainable Forest Management Network (SFMN) for funding this research and supporting M.P. Girardin. The author was also supported by scholarships from the Fonds Québécois de la Recherche sur la Nature et les Technologies (FQRNT) and the Prairies Adaptation Research Collaborative (PARC). The field and lab work for the development of the Ontario chronologies could not have been without the incredible support of Elizabeth Penner and Daniel Card. We wish to thank Ontario Provincial Park for granting us permission to conduct this research in their parks. Many thanks to Stan Vasiliauskas, Ed Iskra, Don Armit, Charlotte Bourdignon, and Dave New from the Ontario Ministry of Natural Resources and Timothy Lynham from the Canadian Forest Service for making our search for sites of old trees in Ontario successful. We thank the National Oceanic and Atmospheric Administration (NOAA; NCEP/NCAR reanalysis project) and the Meteorological Service of Canada for their aid and contribution of climate data. We thank Kim Monson, Danny Blair, and Malcom Cleaveland for commenting and editing the manuscript.

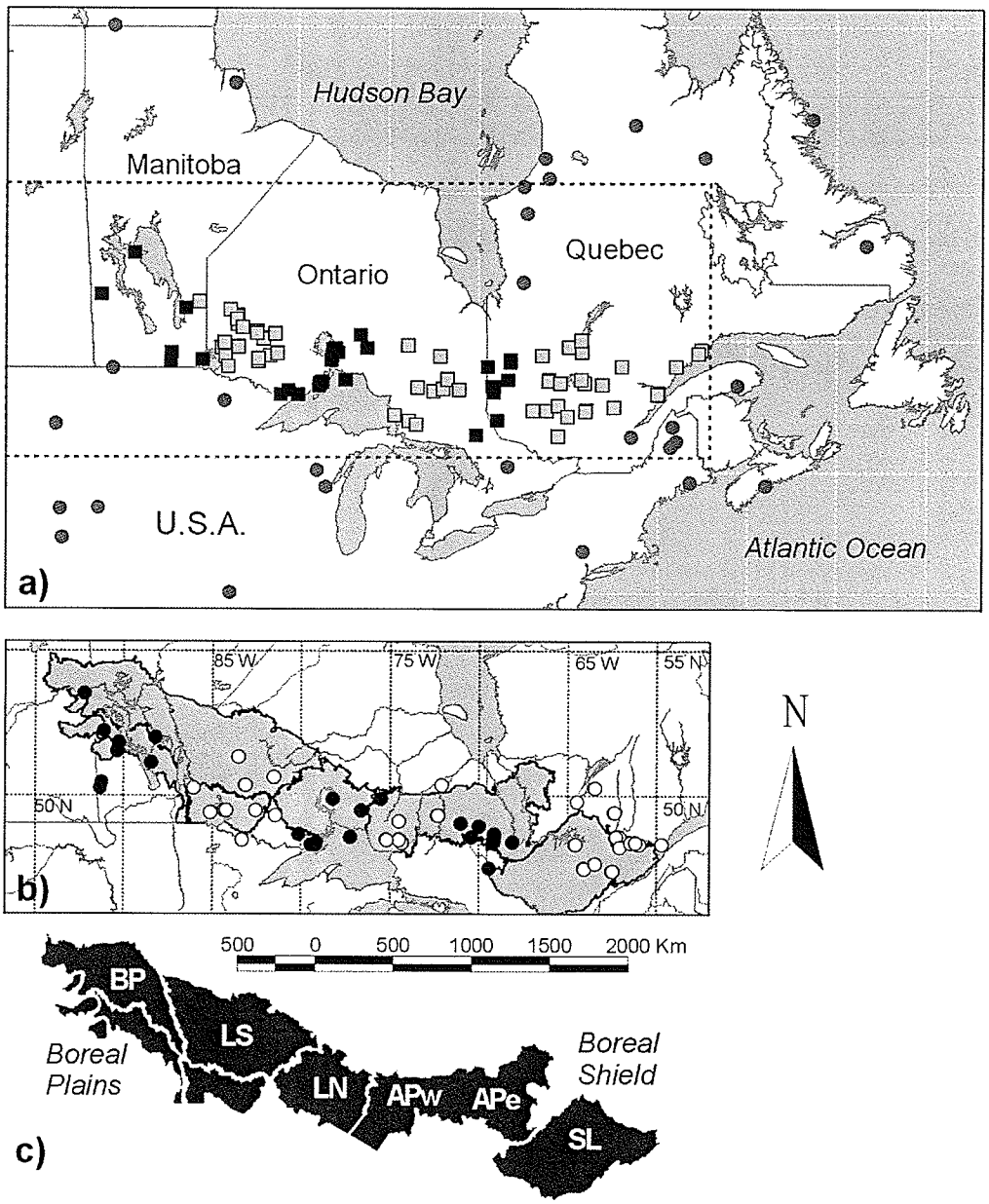

Figure 5.1 (a) Geographical distribution of the locations of the 120 residual tree-ring chronologies used for the climate reconstructions (squares). The color scheme delineated the six regions. Supplemental chronologies used in the spatiotemporal analysis are shown with circles. (b) Geographical distribution of the locations of the meteorological stations used in the calculation of the regional climate variables (refer to Table 5.1). (c) Domain of the area under study. Six regions enclosed by the shaded areas were selected for the climate reconstruction.

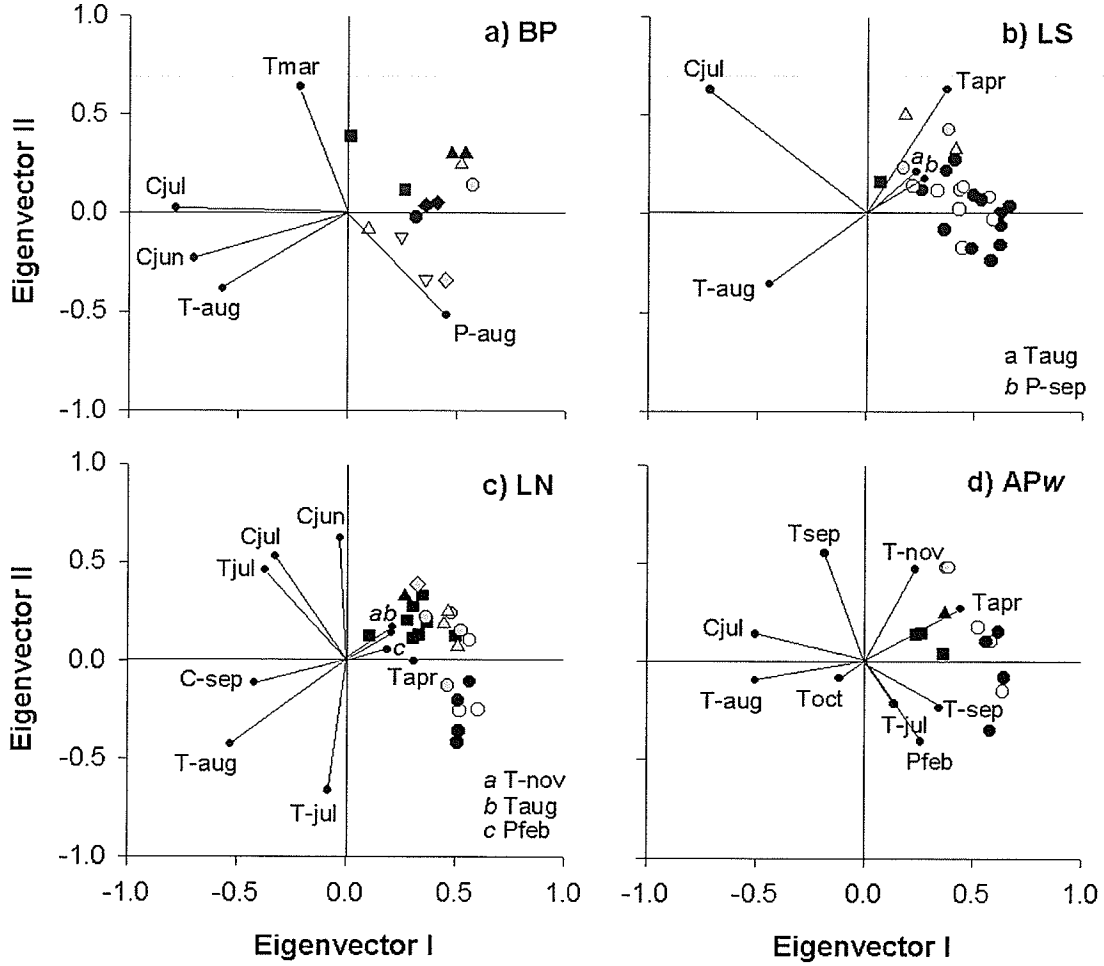

Figure 5.2 Eigenvectors of the redundancy analysis (RDA) conducted on the site residual chronologies for the six regions. For clarity, arrows pointing from the origin to the descriptors (species chronologies) were not drawn. The descriptors are positioned in the biplot based on their correlations with the canonical axes. In addition, the biplot also approximates the correlation coefficient among descriptors and climate variables (Legendre and Legendre 1998). Climate variables and residual chronologies with 'arrows' at sharp angles are positively correlated (cos $0^{\circ} = 1.0$, i.e. perfect correlation). Conversely, obtuse angles indicate negative correlation (cos $180^{\circ} = -1.0$, i.e. perfect correlation). Climate variable abbreviations are for temperature (T), precipitation (P), and CDC (C). Months range from July of the year prior (-jul) to September of the year current (sep) to ring formation. Statistics of the RDA are given in Table 5.3. The significance of all canonical axes is $p<0.001$.

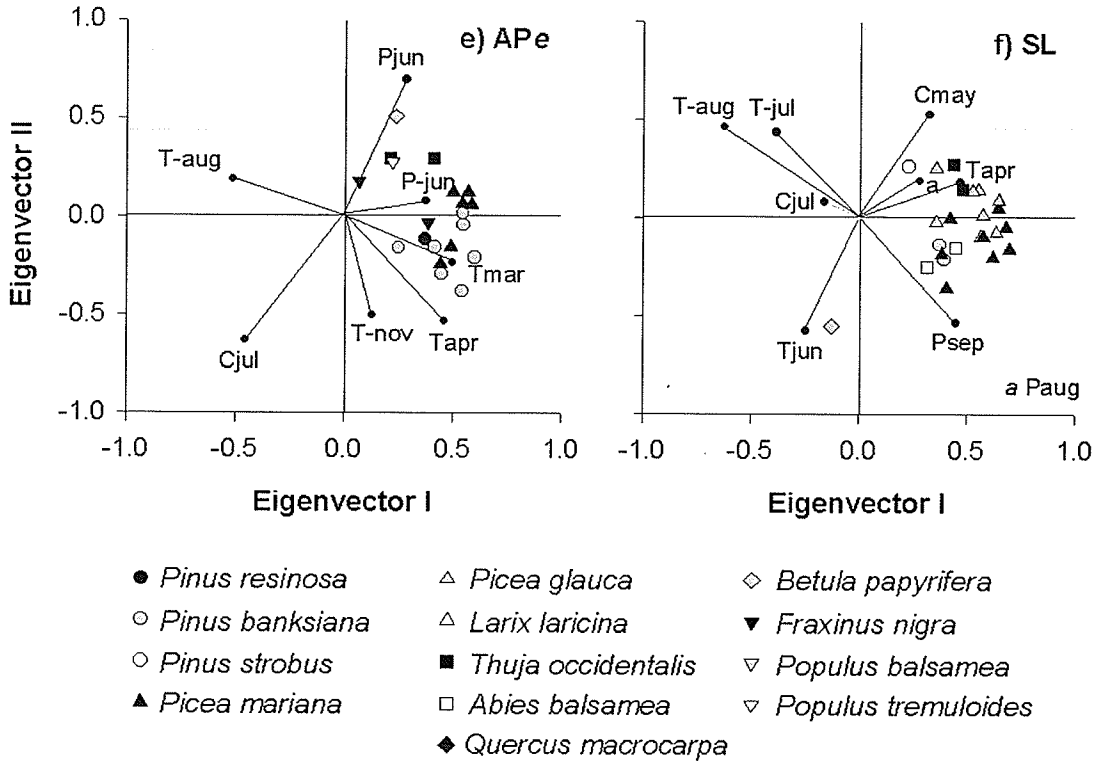

Figure 5.2 *Continues.*

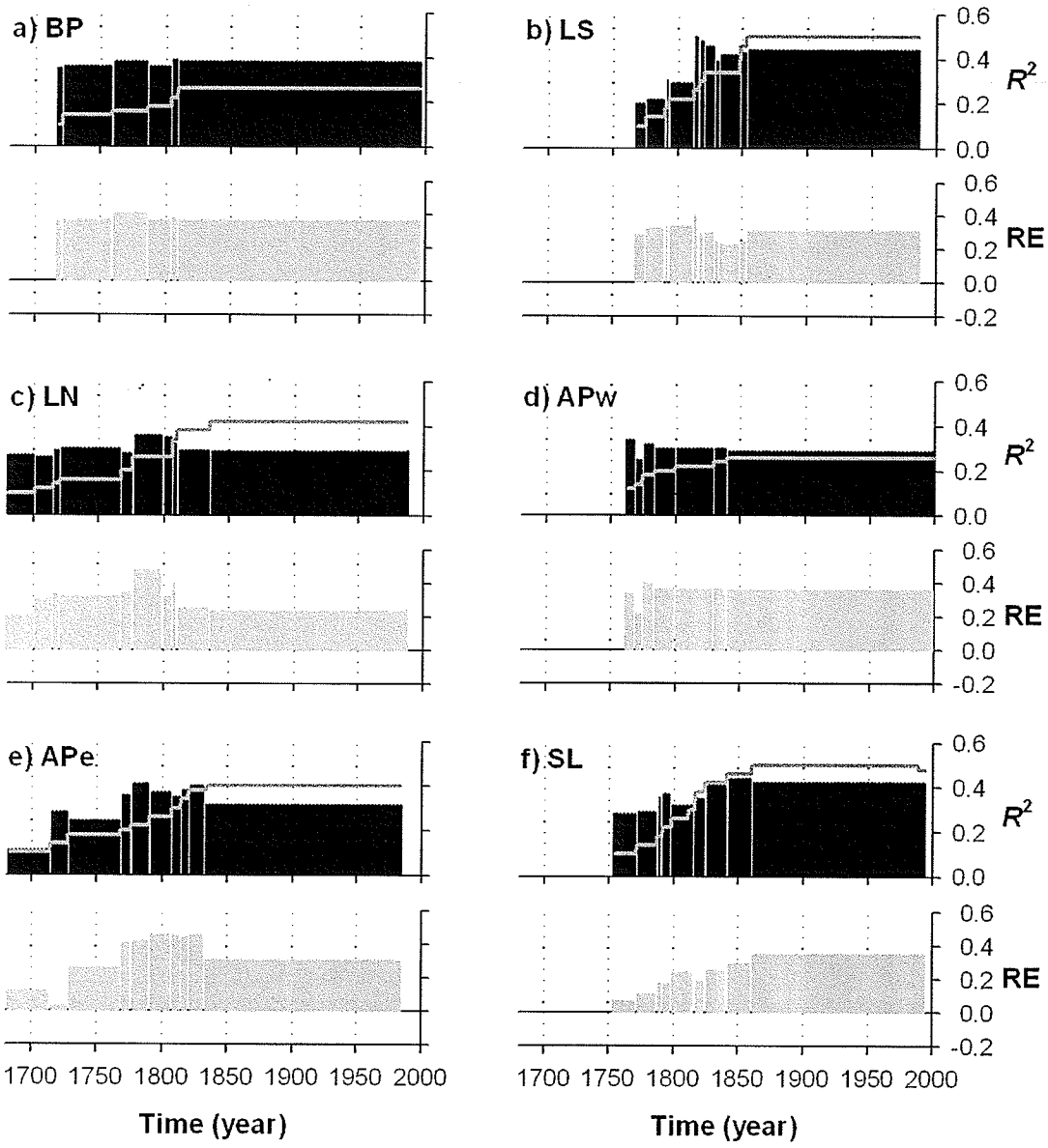

Figure 5.3 Transfer function model R^2 for the calibration period 1919-1984 (black bars) and the corresponding reduction of error (RE) statistics (gray bars) for the verification period 1919-1940, plotted against the time period for which a given calibration model was used (period 1941-1984). Any RE > 0 is considered to represent significant regression skill. Transitions from one sub-model to another are delineated with vertical lines. The gray lines show the temporal developments of the number of chronologies (multiply the y-scale by 50) used for the regional climate reconstructions.

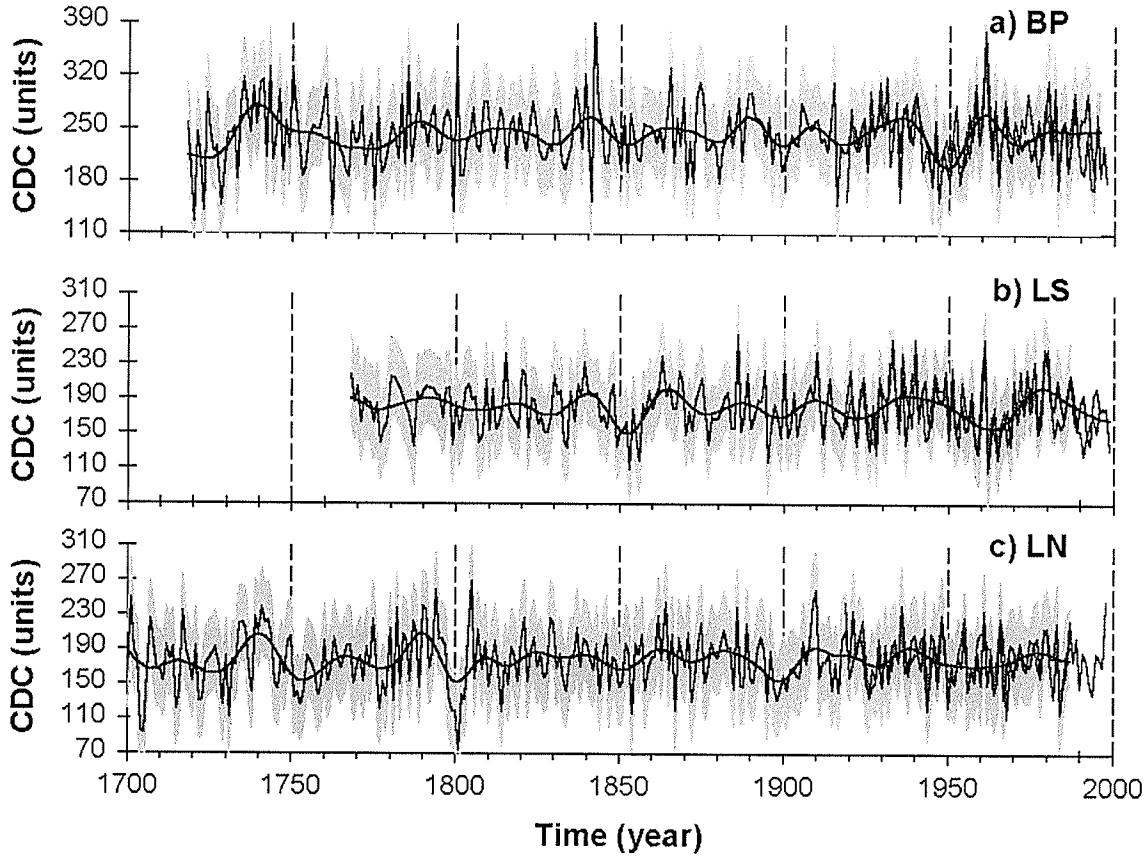

Figure 5.4 (a) to (e) Reconstructions of the mean July CDC (units) for the BP, LS, LN, APe, and APw regions. (f) Reconstruction of the SL mean July to August temperature (TEMP, °C). The CDC scale ranges from soil saturation (zero) to extreme drought (>300). Shaded areas represent errors bars plotted against the time period for which a given calibration model was used. Red lines show instrumental 1913-1998 records. Variance in the instrumental records was adjusted to correspond to reconstructions. Smoothed curves (black-lines) were obtained from a second degree least squares polynomial fitting across a moving 10-year window within the data. From a) to f) these curves accounted for 15.4%, 20.8%, 18.0%, 27.0%, 10.4%, and 5.6% of the variance in the reconstructions.

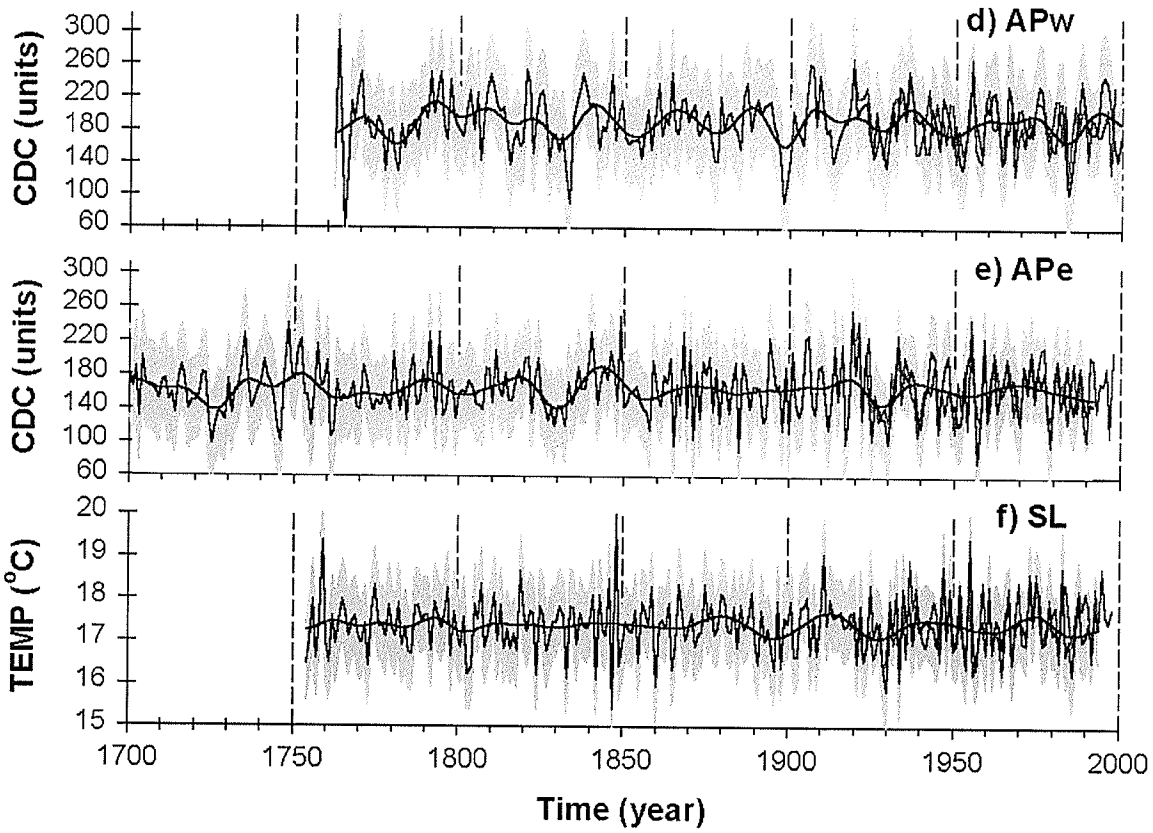

Figure 5.4 *Continues.*

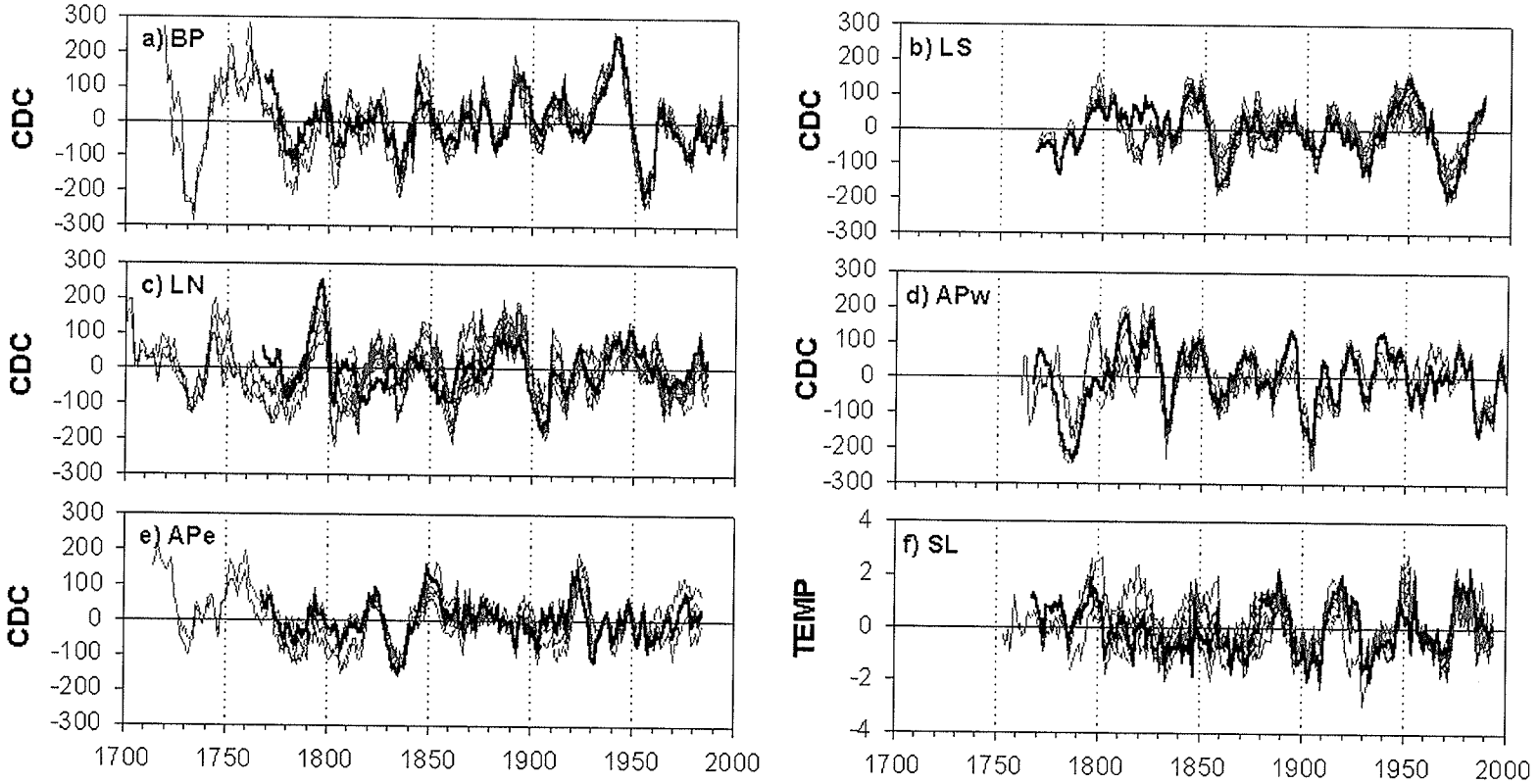

Figure 5.5 Cumulative departures of (a-e) CDC (units) and (f) temperature (°C). Bold lines show cumulative departures calculated from the final reconstructions over the common period 1768 to 1984; thin-lines show cumulative departures calculated from reconstruction sub-models. All reconstructions were transformed to zero mean prior to calculating the cumulative departures.

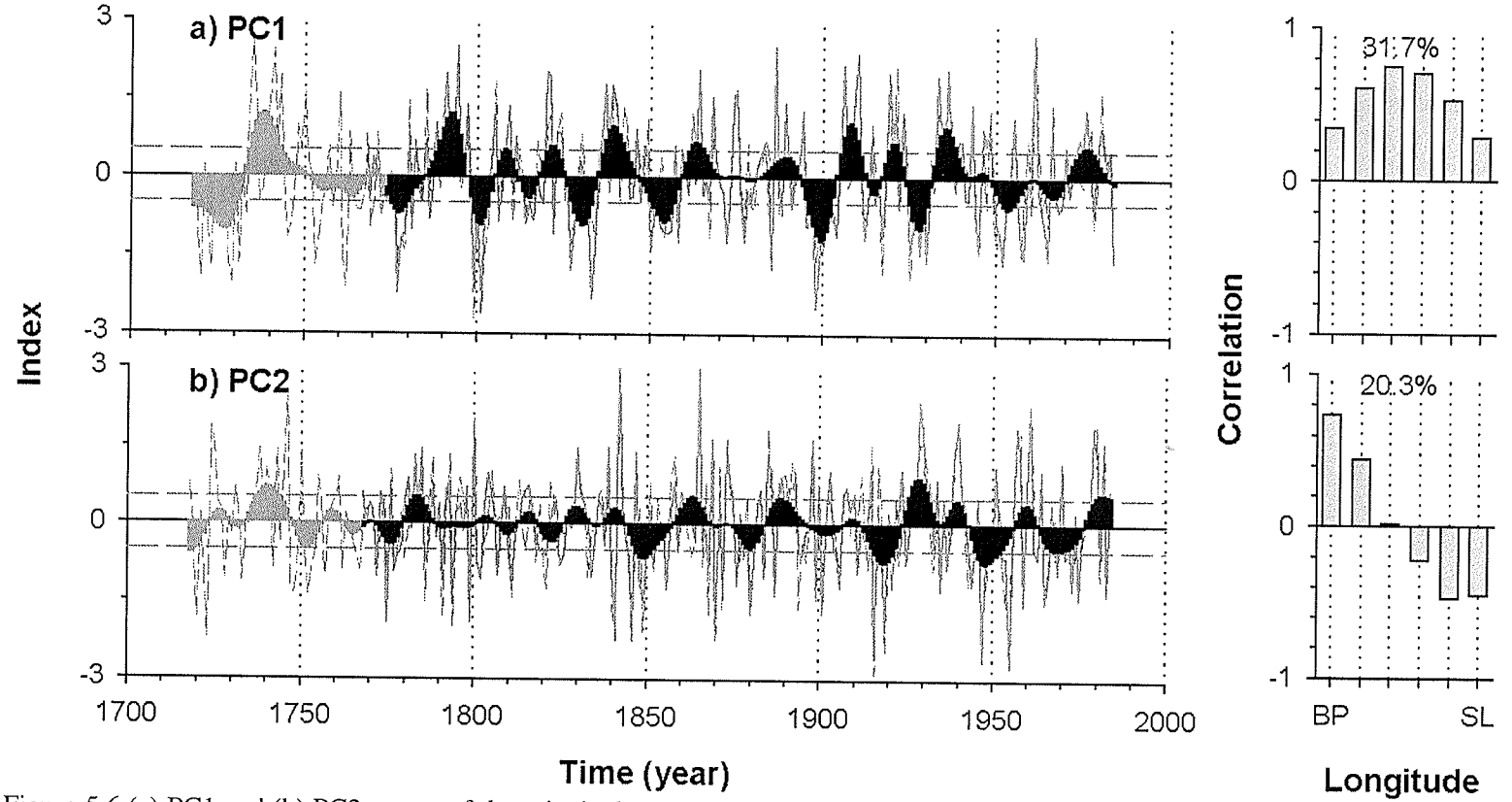

Figure 5.6 (a) PC1 and (b) PC2 scores of the principal component analysis (thin-solid lines) illustrating the relationship among the six climate reconstructions over their common interval 1768 to 1984. The vertical bar charts at right express the correlation coefficients between a PC score and a given climate reconstruction (BP for western and SL for eastern sectors); the percentage (%) of expressed variance by the PC scores is indicated. Also projected are the PC scores covering the interval 1718-1767 (thin-dashed lines) obtained from the BP, LN and APe reconstructions. Smoothed PC scores are overlaid in black.

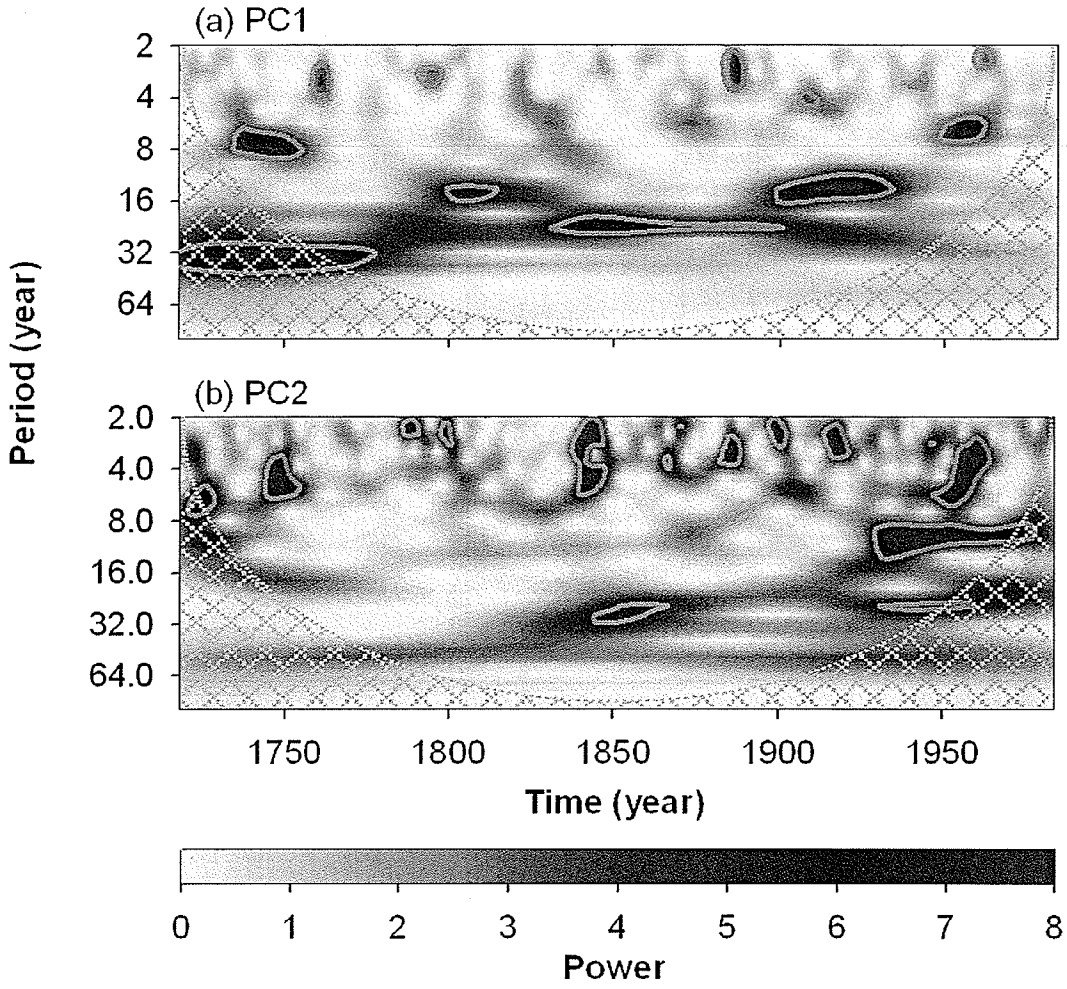

Figure 5.7 Continuous wavelet transformation power spectrums of (a) PC1 and (b) PC2. The dark blue color indicates areas of large power; thick-red contour is the 5% significance level for red noise (AR(1)=0.25 in (a) and AR(1)=0.00 in (b)). The crosshatched regions on either end delineate the cone of influence where zero padding has reduced the variance. Note that for the period 1718-1767 the PCs were computed from only three climate reconstructions (BP, LN and APe).

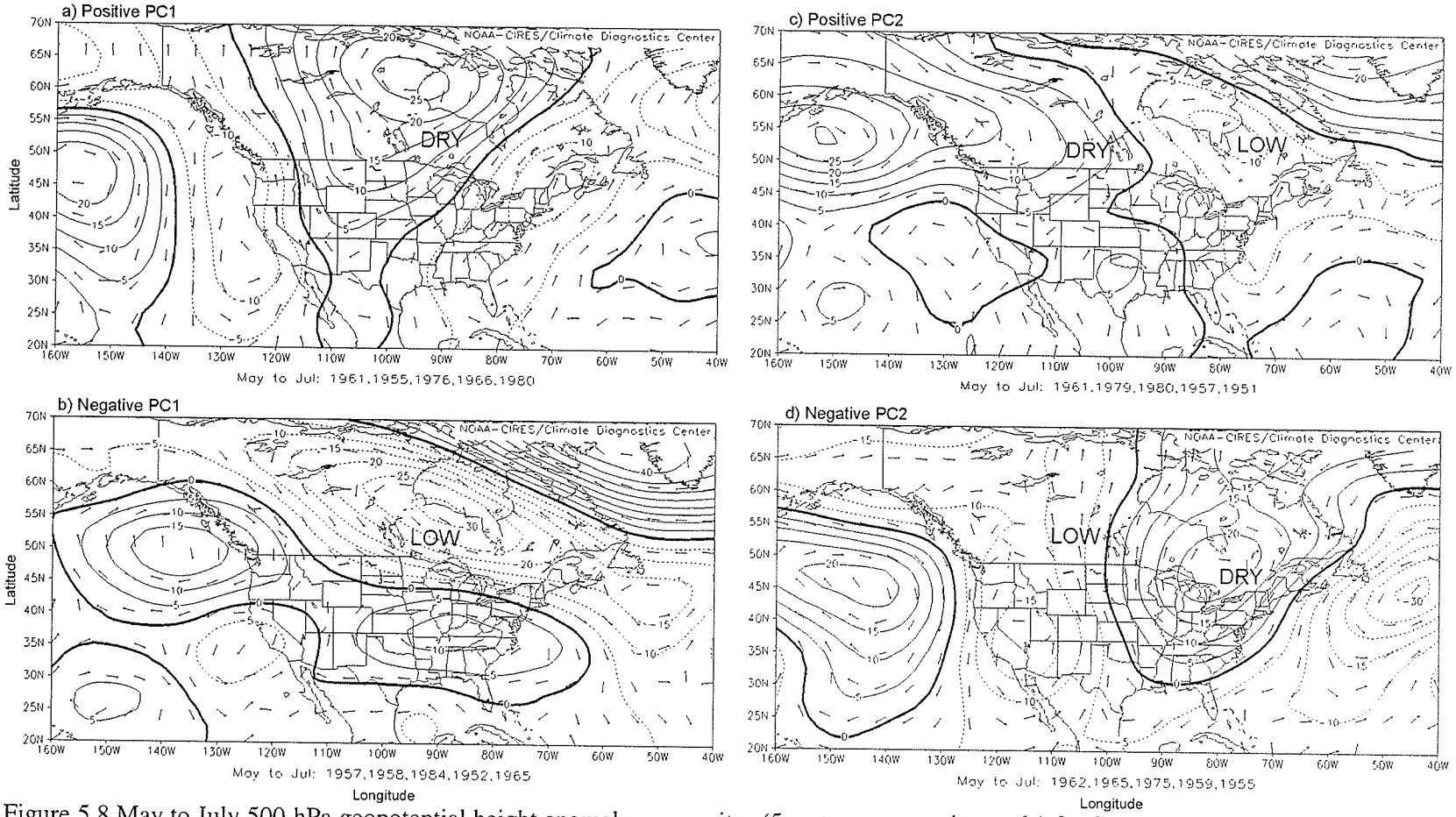

Figure 5.8 May to July 500-hPa geopotential height anomaly composites (5 meters contour intervals) for five years of (a) highest PC1 scores, (b) lowest PC1 scores, (c) highest PC2 scores, and (d) lowest PC2 scores. Regions of anomalously low (LOW) and high (DRY) drought severities are indicated. Solid contours indicate positive anomalies; dashed contours indicate negative anomalies (zero interval is bold). Directions of 500-hPa vector wind anomalies (arrows) are also shown. The anomalies were calculated from the mean of the reference period 1968-1996. Years used in the composites are listed below each map.

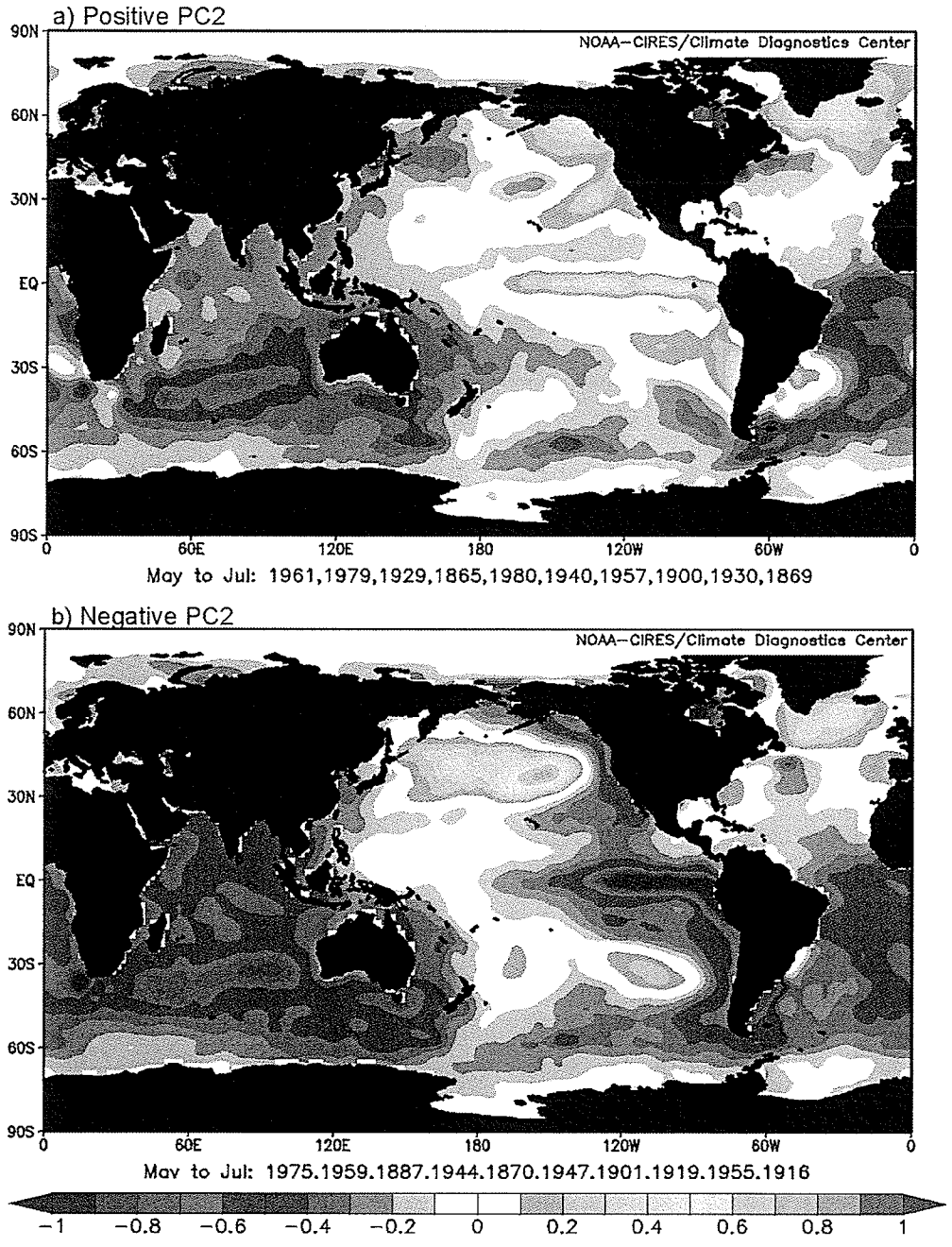

Figure 5.9 May to July SST anomaly composites for ten seasons of (a) highest PC2 scores and (B) lowest PC2 scores over the interval 1854-1984. The anomalies were calculated from the mean of the reference period 1971-2000. Years used in the composites are listed below each map.

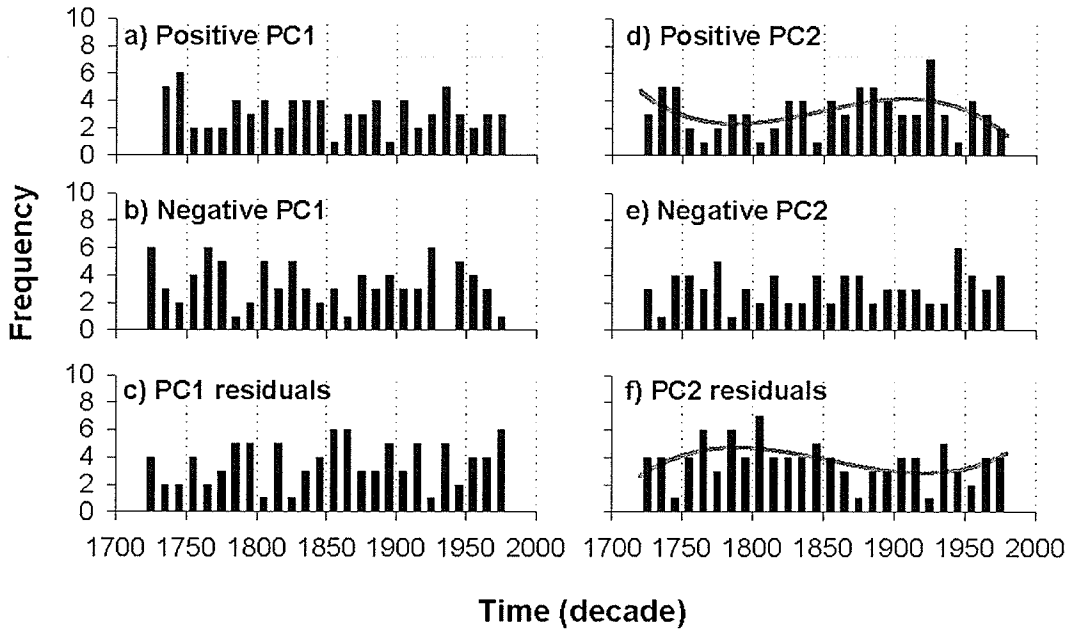

Figure 5.10 Histograms showing the frequency per decade of PC1 and PC2 positive and negative departures exceeding the higher and lower 33.3% percentiles from the long term mean of the reference period 1718-1984. The frequency per decade of non-departure years (PC residuals) is also shown. Third order polynomial regression lines accounting for 22.6% and 20.4% ($p<0.05$) are shown in d) and f). PCs were obtained from the analysis of the BP, LN and APe reconstructions.

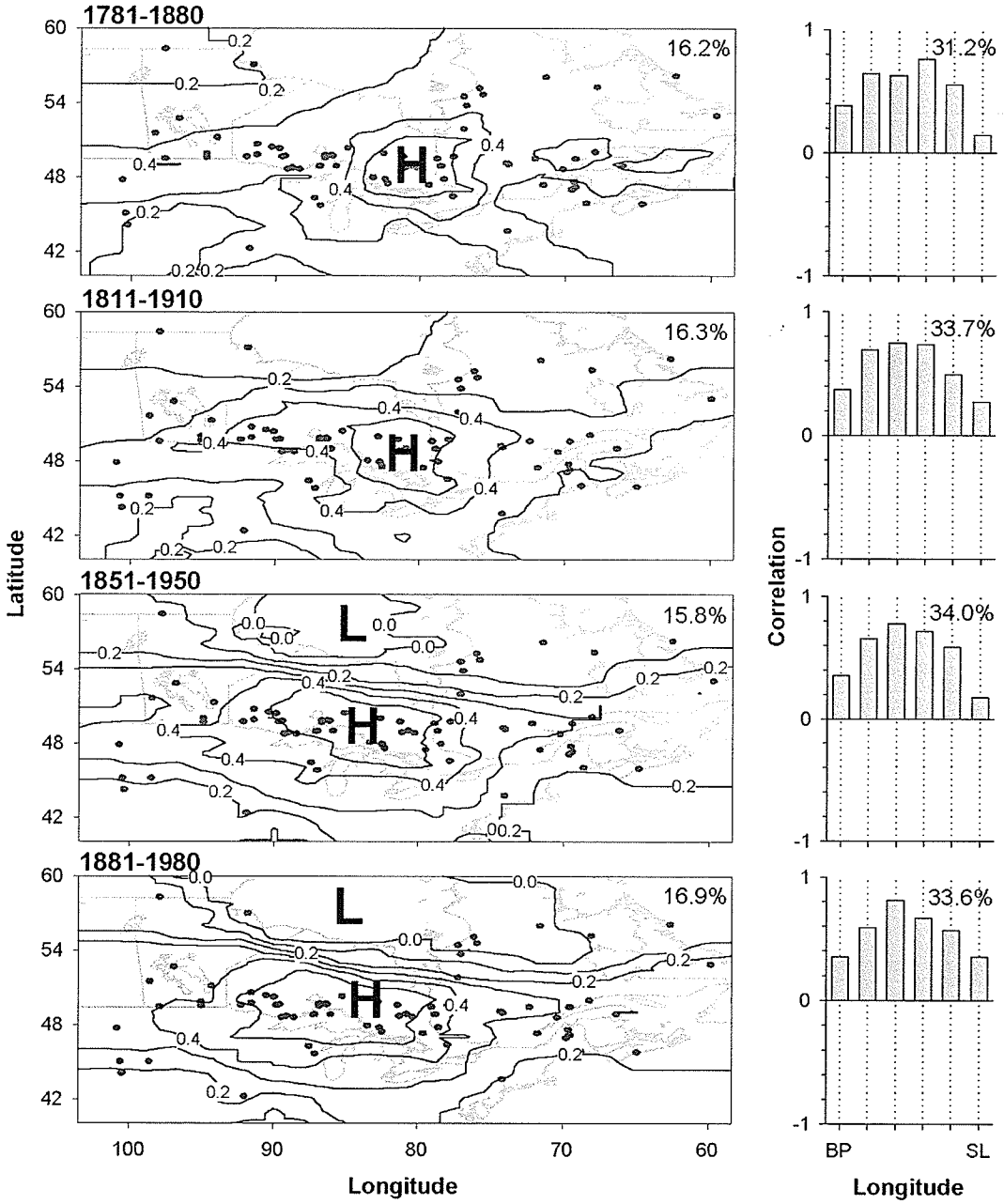

Figure 5.11a Spatial correlation fields of PC1 of the 90 tree-ring chronologies for different 100-year time periods. The respective eigenvalues are shown in %. Centers of positive (H) and negative (L) correlation are indicated. The total sum of the squares of the data matrix is respectively for each time period 262.1, 236.2, 209.6, and 218.6. The vertical bar plots show the eigenvectors from a similar analysis carried on the six drought reconstructions and for the same time intervals (a given bar expresses the correlation coefficient between the PC score and a given climate reconstruction; BP for western and SL for eastern regions).

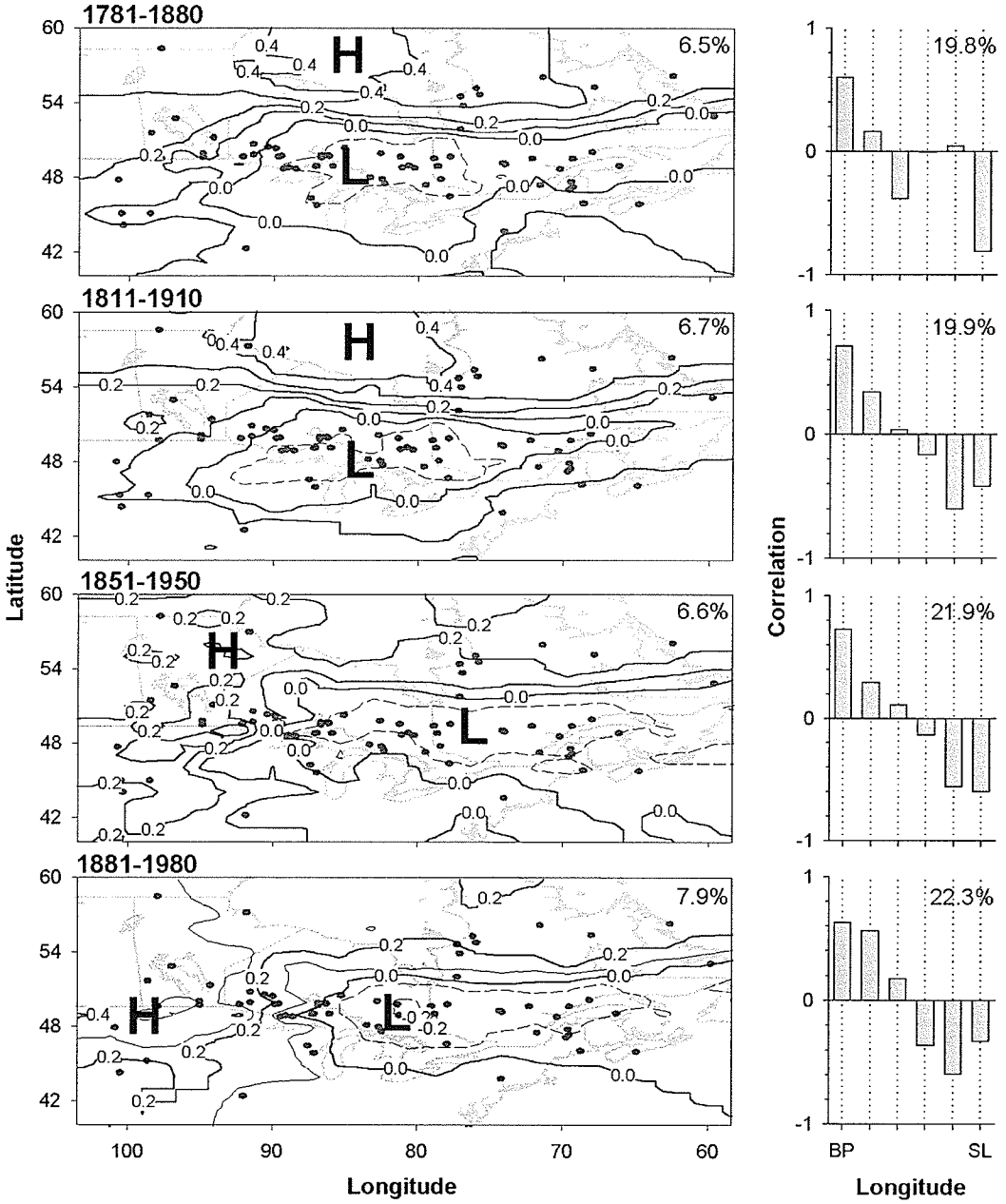

Figure 5.11b. Spatial correlation fields of PC2 of the 90 tree-ring chronologies for different 100-year time periods.

Table 5.1 Meteorological stations used in the calculation of the regional monthly Canadian Drought Code (CDC), temperature (T) and precipitation (P) variables. The period covered by each station and variable is indicated.

Stations	Code	Longitude	Latitude	Elevation	CDC	T	P
A-Boreal Plains							
Birtle	5010240	101.30W	50.26N	522	1917-1995	1904-1999	1918-1999
Ashern	5040120	98.22W	52.08N	263	1967-1989	-	-
Cumberland House	4071960	102.18W	53.58N	271	1937-1964	-	-
Dauphin	5040675	100.20W	51.90N	292	1890-1941	-	-
Dauphin A	5040680	100.30W	51.60N	305	1943-1998	1903-1999	1911-1999
Gilbert Plains	5040985	100.28W	51.60N	404	1959-1998	-	-
Moosehorn	5041800	98.37W	51.18N	250	1910-1963	-	-
Russell	5012520	101.17W	50.46N	567	1884-1990	1916-1990[a]	1916-1999
Swan River	5042800	101.13W	52.30N	347	1910-1998	-	-
B-Lac Seul Upland and Lake of the Woods							
Dryden	6032117	92.50W	49.47N	372	1914-1997	1914-1999	1914-1999
Earl Falls	6012198	93.13W	50.38N	361	1930-1996	-	-
Fort Frances	6022475	93.25W	48.37N	343	1892-1995	1912-1999	1912-1999
Great Falls	5031200	96.00W	50.28N	249	1923-1996	1922-1999	1923-1999
Ignace	6033690	91.39W	49.25N	447	1914-1970	-	-
Indian Bay	5031320	95.12W	49.37N	327	1915-1998	1914-1999	1916-1999
Kenora	6034070	94.32W	49.48N	336	1900-1938	-	-
Kenora A	6034075	94.22W	49.47N	410	1939-1998	1899-1999	1900-1999
Red Lake A	6016975	93.48W	51.40N	386	1939-1998	-	-
Sioux Lookout	6037775	91.54W	50.70N	390	1939-1998	-	1914-1999
C-Lake Nipigon							
Cameron Falls	6041109	88.21W	49.90N	229	1925-1997	1924-1998	1925-1999
Geraldton A	6042716	86.56W	49.47N	349	1981-1999	-	1950-1999
Kakabeka Falls	6043930	89.37W	48.24N	278	1910-1976	-	-
Manitouwadge	6044903	85.48W	49.90N	332	1956-1994	-	-
Port Arthur	6046588	89.13W	48.26N	195	1878-1941	-	-
Savanne	6047615	90.12W	48.58N	459	1892-1946	-	-
Schreiber	6047624	87.16W	48.49N	302	1910-1975	-	-
Thunder Bay A	6048261	89.20W	48.22N	199	1942-1993	1895-1993	1895-1999

Stations	Code	Longitude	Latitude	Elevation	CDC	T	P
D-Abitibi Plains west							
Smokey Falls	6077845	82.10W	50.40N	183	1934-1996	-	1934-1999
Franz	6052563	84.25W	48.28N	373	1918-1949	-	-
Hornepayne	6053570	84.46W	49.12N	329	1920-1989	-	-
Kapuskasing	6073975	82.26W	49.27N	218	1937-1998	-	-
Kapuskasing A	6073960	82.28W	49.25N	227	1919-1998	1918-1999	1918-1999
Steep Hill Falls	6058010	84.48W	48.40N	335	1920-1938	-	-
White River	6059475	85.17W	48.36N	379	1889-1975	-	-
E-Abitibi Plains east							
Abitibi Post	7090050	79.22W	48.43N	259	1898-1935	-	-
Amos	7090120	78.07W	48.34N	259	1915-1997	1913-1999	1914-1999
Cochrane	6071712	81.02W	49.04N	275	1912-1991	-	-
Duparquet	709BBDH	79.16W	48.31N	290	1982-1993	-	-
Haileysbury	6073138	79.38W	47.27N	189	1895-1922	-	-
Iroquois Falls	6073810	80.40W	48.45N	259	1913-1997	1913-1999	1916-1999
Kirkland Lake	6074209	80.00W	48.90N	324	1951-1996	-	-
La Sarre	7094120	79.12W	48.48N	244	1952-1998	-	-
Val St-Gilles	70986RN	79.07W	48.59N	290	1973-1998	-	-
F-Southern Laurentian							
Albanel	7060080	72.27W	48.53N	152	1923-1990	-	1923-1999
Bagotville	7060400	71.00W	48.20N	159	1942-1999	1895-1999	1943-1999
Barrage à Lac Kempt	7070448	74.11W	47.33N	421	1913-1963	-	-
Barrage Gouin	7070454	74.60W	48.21N	404	1914-1979	-	-
Chibougamau Chapais A	7091399	74.53W	49.77N	387	1963-1998	1914-2001	1963-1998[a]
Chicoutimi	7061441	71.50W	48.25N	175	1881-1979	-	-
Hemon	7063090	72.36W	49.40N	183	1966-1998	-	-
Kenogamie	7063400	71.15W	48.25N	116	1924-1964	-	-
La Tuque	7074240	72.47W	47.24N	152	1915-1998	1911-1999	1912-1999
Lac Bouchette	7063560	72.10W	48.13N	358	1951-1998	-	-
Manouan Sanmaur	7074600	73.48W	47.54N	357	1919-1972	-	-
Mistassini	7064998	72.12W	48.51N	122	1964-1994	-	-

Stations	Code	Longitude	Latitude	Elevation	CDC	T	P
Mistassini Post	7095000	73.53W	50.25N	380	1899-1980	-	-
Normandin	7065640	72.32W	48.51N	137	1936-1992	-	1937-1999
Roberval	7066688	72.14W	48.32N	102	1888-1965	-	1915 -1999
Roberval airport	7066685	72.16W	48.31N	179	1958-1998	-	-
Tadoussac	7048320	69.72W	48.15N	45	1914-1998	1914-1999[a]	1914-2001

Legend:
Elevation (meters) is above mean sea level.
[a] Temperature and precipitation data obtained from the Environment Canada (2000).

Table 5.2 Sources of the 152 tree-ring chronologies.

Species	Cont[a]	Location	Long (°W)	Lat (°N)	Period (Yr)	Mean[b] (Yrs)	N[c]	SSS[d] >0.85 (Yr)	Sens[e]
A-Boreal Plains									
1 *Quercus macrocarpa*	Ss	Red River Alluvial Logs	97.10	49.20	1448-1999	98	92	1523	0.19
2 *Quercus macrocarpa*	Ss	Kildonan Park	97.06	49.56	1720-1999	137	44	1851	0.24
3 *Thuja occidentalis*	Tj	Middlebro	95.23	49.27	1802-2003	130	20	1875	0.16
4 *Thuja occidentalis*	Tj	Cedar Lake	99.16	53.00	1713-1999	117	77	1811	0.14
5 *Pinus resinosa*	Tj	Black Island	96.30	51.10	1709-2001	102	148	1724	0.15
6 *Larix laricina*	Tj	Duck Mountain Prov. Forest	101.00	51.60	1676-2002	99	89	1729	0.21
7 *Picea mariana wet*	Tj	Duck Mountain Prov. Forest	101.00	51.60	1758-2001	177	64	1795	0.13
8 *Picea mariana dry*	Tj	Duck Mountain Prov. Forest	101.00	51.60	1724-2000	156	19	1895	0.16
9 *Pinus banksiana*	Tj	Duck Mountain Prov. Forest	101.00	51.60	1717-2001	87	521	1757	0.15
10 *Picea glauca*	Tj	Duck Mountain Prov. Forest	101.00	51.60	1776-2001	129	81	1829	0.18
11 *Populus balsamea*	Tj	Duck Mountain Prov. Forest	101.00	51.60	1808-2001	106	47	1890	0.28
12 *Populus tremuloides*	Tj	Duck Mountain Prov. Forest	101.00	51.60	1806-2001	94	264	1888	0.25
13 *Betula papyrifera*	Tj	Duck Mountain Prov. Forest	101.00	51.60	1785-2001	102	114	1893	0.24
B-Lac Seul Upland & Lake of the Woods									
14 *Picea glauca*	Sf	Bruno Lake	95.50	51.37	1822-1988	126	24	1846	0.19
15 *Picea glauca*	Sf	High Stone Lake	91.27	50.24	1813-1988	130	25	1827	0.18
16 *Pinus resinosa*	Gm	Caliper Lake Prov. Park	93.92	49.05	1851-2001	134	17	1857	0.20
17 *Pinus resinosa*	Gm	Kenora	94.12	49.92	1792-2001	129	41	1828	0.16
18 *Pinus resinosa*	Gm	Sioux Lookout Prov. Park	94.05	49.42	1772-2001	134	44	1808	0.23
19 *Pinus strobus*	Gm	Longbow Lake	94.28	49.72	1789-2002	123	41	1844	0.21
20 *Pinus resinosa*	Gm	Longbow Lake	94.28	49.72	1830-2001	157	43	1836	0.23
21 *Pinus banksiana*	Gm	Highway 105	93.12	50.45	1815-2001	130	44	1818	0.19
22 *Pinus banksiana*	Gm	Lake Packwash Prov. Park	93.43	50.77	1852-2001	86	12	1872	0.21
23 *Pinus resinosa*	Gm	Lake Packwash Prov. Park	93.43	50.75	1744-2002	168	38	1823	0.20
24 *Pinus strobus*	Gm	Camping Lake	93.37	50.58	1827-2002	112	37	1857	0.17
25 *Thuja occidentalis*	Gm	Lac Seul south	92.28	50.27	1762-2002	110	42	1875	0.17
26 *Pinus resinosa*	Gm	Lac Seul south	92.28	50.32	1837-2001	132	40	1855	0.12
27 *Pinus resinosa*	Gm	Red Lake	93.82	51.08	1818-2001	155	41	1823	0.18
28 *Pinus banksiana*	Gm	Snail Lake	93.38	50.87	1847-2002	91	24	1898	0.17
29 *Pinus resinosa*	Gm	Stormy Lake	92.23	49.35	1791-2001	112	37	1812	0.14
30 *Pinus strobus*	Gm	Eagle Lake	93.33	49.77	1712-2002	126	40	1765	0.22
31 *Pinus resinosa*	Gm	Eagle Lake	93.33	49.78	1808-2001	146	39	1825	0.18
32 *Pinus strobus*	Gm	Sioux Lookout	91.92	50.07	1784-2002	112	40	1848	0.17

Species	Cont[a]	Location	Long (°W)	Lat (°N)	Period (Yr)	Mean[b] (Yrs)	N[c]	SSS[d] >0.85	Sens[e]
33 *Pinus resinosa*	Gm	Sioux Lookout	91.92	50.07	1766-2002	116	29	1807	0.18
34 *Pînus resinosa*	Gm	Sowden Lake	91.17	49.53	1640-2001	216	40	1738	0.15
35 *Pînus strobus*	Gm	Sowden Lake	91.17	49.53	1816-2002	110	39	1836	0.18
36 *Pinus strobus*	Gm	Turtle River Prov. Park	92.22	49.25	1810-2001	104	34	1834	0.15
37 *Pinus resinosa*	Gm	Lake Sandbar Prov. Park	91.55	49.45	1828-2000	100	35	1899	0.19
38 *Pinus strobus*	Gm	Lake Sandbar Prov. Park	91.55	49.45	1773-2002	104	54	1889	0.18
C-Lake Nipigon									
39 *Pinus resinosa*	Gl	Saganaga Lake	90.00	48.00	1719-1988	188	43	1780	0.23
40 *Pinus resinosa*	Sc	Ed Shave Lake	91.00	48.00	1700-1982[f]	162	38	1797	0.24
41 *Pinus resinosa*	Gl	Saganaga Lake	90.54	48.13	1644-1988	201	51	1693	0.26
42 *Betula papyrifera*	Gm	Rainbow Fall Prov. Park	87.38	48.50	1766-2001	143	48	1783	0.33
43 *Picea glauca*	Gm	Rainbow Fall Prov. Park	87.38	48.50	1788-2001	122	58	1813	0.19
44 *Thuja occidentalis*	Gm	Rainbow Fall Prov. Park	87.38	48.50	1774-2001	141	42	1825	0.15
45 *Pinus strobus*	Gm	Nipigon	88.17	49.23	1833-2002	98	47	1861	0.17
46 *Pinus banksiana*	Gm	Lake Nipigon Prov. Park	88.12	49.45	1866-2001	101	30	1875	0.16
47 *Pinus banksiana*	Gm	Shakespeare Island	88.08	49.62	1864-2002	83	62	1871	0.14
48 *Thuja occidentalis*	Gm	Beardmore campground	87.82	49.53	1734-2001	141	56	1819	0.15
49 *Thuja occidentalis*	Gm	Beardmore marina	88.08	49.63	1677-2001	154	69	1814	0.12
50 *Picea glauca*	Gm	MacLeod Prov. Park	87.90	49.68	1804-2000	140	50	1835	0.15
51 *Thuja occidentalis*	Gm	MacLeod Prov. Park	87.90	49.68	1790-2001	116	43	1859	0.14
52 *Thuja occidentalis*	Gm	Upper Twin Lake	86.55	50.15	1772-2001	124	32	1842	0.17
53 *Picea mariana*	Gm	Upper Twin Lake	86.55	50.15	1797-2002	150	39	1812	0.13
54 *Pinus banksiana*	Gm	Longlac	86.22	49.67	1847-2001	105	34	1864	0.21
55 *Picea mariana*	Gm	Sleeping Giant Prov. Park	88.82	48.37	1676-2001	132	30	1785	0.16
56 *Pinus banksiana*	Gm	Sleeping Giant Prov. Park	88.73	48.47	1817-2001	101	35	1826	0.18
57 *Thuja occidentalis*	Gm	Sleeping Giant Prov. Park	88.73	48.45	1713-2001	140	33	1828	0.13
58 *Pinus resinosa*	Gm	Sleeping Giant Prov. Park	88.73	48.45	1805-2001	159	41	1817	0.19
59 *Pinus strobus*	Gm	Sleeping Giant Prov. Park	88.73	48.45	1805-2001	116	42	1840	0.16
60 *Pinus strobus*	Gm	Sleeping Giant Prov. Park	88.75	48.43	1807-2001	145	53	1814	0.17
61 *Thuja occidentalis*	Gm	Sleeping Giant Prov. Park	88.82	48.37	1662-2001	162	55	1746	0.12
62 *Thuja occidentalis*	Gm	Sleeping Giant Prov. Park	88.87	48.32	1665-2001	137	68	1824	0.14
D-Abitibi Plains west									
63 *Thuja occidentalis*	Gm	Fushimi Lake Prov. Park	83.92	49.83	1765-2002	154	34	1815	0.14
64 *Picea mariana*	Gm	René-Brunelle Prov. Park	82.13	49.42	1721-2002	148	50	1790	0.13
65 *Pinus strobus*	Gm	Geiki Lake	81.08	48.18	1709-2002	96	41	1876	0.17

	Species	Cont[a]	Location	Long (°W)	Lat (°N)	Period (Yr)	Mean[b] (Yrs)	N[c]	SSS[d] >0.85	Sens[e]
66	*Pinus resinosa*	Gm	Blue Lake	81.72	48.58	1606-2002	223	46	1772	0.19
67	*Pinus banksiana*	Gm	Blue Lake	81.72	48.58	1760-2002	156	55	1772	0.17
68	*Pinus banksiana*	Gm	Foliyet	82.00	48.23	1769-2002	113	30	1819	0.17
69	*Pinus resinosa*	Gm	Ivanhoe Lake Prov. Park	82.50	48.15	1828-2002	126	38	1848	0.17
70	*Thuja occidentalis*	Gm	Missinaibi Prov. Park	83.40	48.27	1798-2002	128	43	1842	0.17
71	*Pinus resinosa*	Gm	Highway 556	83.45	46.87	1837-2002	144	33	1848	0.14
72	*Thuja occidentalis*	Gm	Highway 556	83.43	46.88	1760-2002	130	44	1827	0.17
73	*Pinus strobus*	Gm	Ranger Lake	83.88	47.02	1760-2002	99	40	1823	0.22
74	*Pinus strobus*	Gm	Montreal River	84.63	47.22	1779-2002	117	33	1880	0.20
75	*Pinus resinosa*	Gm	Montreal River	84.65	47.22	1773-2003	158	37	1780	0.28
E-Abitibi Plains east										
76	*Pinus strobus*	Gr	Hobbs Lake	80.12	46.43	1547-1994	212	31	1714	0.16
77	*Pinus resinosa*	Ce	Lac Temagami	79.00	47.00	1644-1983[f]	266	36	1666	0.18
78	*Populus tremuloides*	Cd	Lac Duparquet	79.19	48.28	1831-1996	146	30	1840	0.24
79	*Betula papyrifera*	Cd	Lac Duparquet	79.19	48.28	1766-1998	138	74	1804	0.25
80	*Picea mariana*	Gm	Lac Duparquet	79.19	48.28	1800-1999	126	61	1849	0.14
81	*Fraxinus nigra*	Tj	Lac Duparquet	79.19	48.28	1790-1991	100	36	1834	0.20
82	*Fraxinus nigra*	Tj	Lac Duparquet	79.19	48.28	1682-1991	134	253	1716	0.20
83	*Thuja occidentalis*	As	Lac Duparquet	79.19	48.28	1186-1987	507	46	1569	0.14
84	*Thuja occidentalis*	Tj	Lac Duparquet	79.19	48.28	1417-1987	302	43	1262	0.16
85	*Picea mariana*	Ha	Joutel	78.27	49.26	1778-1994	NA	57	NA	0.18
86	*Picea mariana*	Ha	Hedge Hills	78.24	49.16	1816-1992	NA	67	NA	0.17
87	*Picea mariana*	Ha	Chicobi Hills	78.38	48.51	1820-1994	NA	61	NA	0.16
88	*Picea mariana*	Ha	Lac Opasatica	79.18	48.06	1703-1994	NA	61	NA	0.17
89	*Picea mariana*	Ha	Lac Hébécourt	79.27	48.29	1790-1993	NA	59	NA	0.17
90	*Pinus banksiana*	By	Abitibi Lake	79.50	49.00	1713-1987	103	75	1732	0.17
91	*Pinus banksiana*	By	Lac Duparquet	79.19	48.28	1726-1985	97	94	1775	0.16
92	*Pinus banksiana*	Ha	Joutel	78.27	49.26	1714-1994	NA	51	NA	0.19
93	*Pinus banksiana*	Ha	Hedge Hills	78.24	49.16	1811-1992	NA	67	NA	0.22
94	*Pinus banksiana*	Ha	Chicobi Hills	78.38	48.51	1814-1994	NA	57	NA	0.19
95	*Pinus banksiana*	Ha	Lac Hébécourt	79.27	48.29	1776-1993	NA	49	NA	0.22
F-Southern Laurentian										
96	*Picea mariana*	GsDl	Lac Dionne	67.76	49.52	1809-1999	166	40	1824	0.13
97	*Picea mariana*	GsDl	Lac Dionne	67.58	49.66	1743-1999	181	48	1803	0.16
98	*Pinus banksiana*	GsDl	Lac Dionne	67.76	49.52	1811-1998	133	21	1817	0.16

	Species	Cont[a]	Location	Long (°W)	Lat (°N)	Period (Yr)	Mean[b] (Yrs)	N[c]	SSS[d] >0.85	Sens[e]
99	*Abies balsamea*	KcMh	Mont Valin	70.04	48.05	1789-1994	NA	NA	NA	NA
100	*Picea mariana*	KcMh	Cote-Nord 30	69.03	49.05	1713-1996	NA	NA	NA	NA
101	*Pinus strobus*	KcGf	St-Marguerite	70.00	48.02	1768-1995	133	12	1850	0.17
102	*Picea mariana*	Sf	Lac Chevrillon	74.27	50.01	1797-1988	87	37	1813	0.14
103	*Abies balsamea*	KcMh	Lac Liberal	72.06	49.04	1751-1995	NA	NA	NA	NA
104	*Picea mariana*	Ld	Réservoir Gouin	74.30	48.56	1775-1997	116	81	1828	0.15
105	*Pinus banksiana*	Ld	Réservoir Gouin	74.30	48.56	1767-1998	74	91	1806	0.16
106	*Betula papyrifera*	Cf	Réservoir Gouin	74.30	48.56	1740-1997	147	80	1778	0.19
107	*Picea glauca*	JyMh	Lac Waswanipi	76.50	49.45	1821-1996	134	30	1848	0.16
108	*Thuja occidentalis*	JyMh	Lac des Iles	75.62	46.44	1814-1996	126	29	1863	0.15
109	*Thuja occidentalis*	JyMh	Lac Wedge	75.09	47.20	1786-1996	135	30	1845	0.19
110	*Picea glauca*	JyMh	Chibougameau	74.26	49.58	1793-1996	152	37	1829	0.20
111	*Picea glauca*	JyMh	Lac Cavan	74.97	49.75	1798-1996	161	33	1823	0.18
112	*Picea glauca*	JyMh	Lac Indiana	73.14	48.39	1749-1996	117	37	1846	0.16
113	*Picea mariana*	JyMh	Baie du Vison	74.11	48.42	1830-1996	130	29	1852	16.00
114	*Picea mariana*	JyMh	Le Canal	75.47	48.43	1811-1996	166	20	1819	0.19
115	*Picea glauca*	JyMh	Lac Bertthelot	76.13	48.54	1814-1996	127	28	1864	0.19
116	*Picea glauca*	JyMh	Lac Edouard	72.44	47.54	1846-1996	119	24	1866	0.18
117	*Picea glauca*	JyMh	Lac Kempt	74.03	47.38	1859-1996	93	35	1884	0.22
118	*Picea mariana*	JyMh	Lac du Coucou	75.58	47.58	1789-1996	144	45	1820	0.19
119	*Picea glauca*	JyMh	Rivière Cabonga	76.24	47.41	1839-1996	117	32	1880	0.19
120	*Picea glauca*	JyMh	Réservoir Dozois	77.00	47.40	1823-1996	131	25	1861	0.19
Supplementary chronologies										
121	*Picea glauca*	Sf	Mountain Lake	58.40	53.29	1709-1988	142	28	1747	0.21
122	*Picea glauca*	Sf	Churchill	93.50	58.40	1695-1988	197	26	1721	0.14
123	*Picea mariana*	Sf	Charlie Lake	100.26	60.02	1768-1988	122	26	1843	0.18
124	*Pinus strobus*	GrCb	Dividing Lake	78.36	45.24	950-1993	182	50	1508	0.14
125	*Picea glauca*	Dr	Nutak	61.45	57.30	1700-1996	190	10	1748	0.19
126	*Thuja occidentalis*	Ce	Sag Pond	69.20	46.80	1674-1986	246	23	1702	0.15
127	*Pinus resinosa*	KdGm	Hartwick Pines State Park	88.45	44.40	1770-1987	202	52	1778	0.18
128	*Quercus macrocapa*	MdSc	Masonic Island / Bear Island	100.30	49.00	1676-1990	167	17	1803	0.23
129	*Juniperus scopulorum*	MdSc	T. Roosevelt National Park	103.50	46.90	1597-1991	180	42	1685	0.32
130	*Larix laricina*	Mk	Churchill	93.50	58.40	1721-2000	125	71	1780	0.25
131	*Tsuga canadensis*	Ce	Bowater-Mersey	64.00	44.49	1572-1982	262	28	1637	0.22
132	*Tsuga canadensis*	Ce	Rivière Du Moulin	71.53	46.38	1524-1982	255	50	1627	0.27
133	*Thuja occidentalis*	Ce	St. Anne River	65.55	48.35	1404-1982	412	29	1475	0.13

	Species	Cont[a]	Location	Long (°W)	Lat (°N)	Period (Yr)	Mean[b] (Yrs)	N[c]	SSS[d] >0.85	Sens[e]
134	*Picea mariana*	Sf	Lac Romanel	67.43	56.14	1659-1988	330	29	1743	0.12
135	*Picea mariana*	Sf	No Name Lake	77.34	54.35	1748-1988	100	31	1781	0.12
136	*Picea mariana*	Sf	No Name Lake	77.34	54.35	1743-1988	119	32	1758	0.12
137	*Picea mariana*	Sf	Lac Natuak	71.30	57.13	1743-1988	141	23	1823	0.17
138	*Picea mariana*	Sf	Eastmain River	77.51	52.02	1739-1988	164	27	1810	0.16
139	*Picea mariana*	Sf	Coats River	76.09	55.44	1777-1988	153	26	1806	0.14
140	*Picea glauca*	Jg	Castle Peninsula	76.33	56.10	1663-1982	261	35	1689	0.17
141	*Picea mariana*	Sf	Bonif, Quebec	77.50	55.20	1352-1989	116	84	1369	0.17
142	*Picea glauca*	Mk	Churchill	93.50	58.40	1646-2000	158	28	1782	0.13
143	*Picea mariana*	Mk	Churchill	93.50	58.40	1527-2000	171	69	1683	0.12
144	*Quercus alba*	Dd	Nine Eagles State Park	93.80	40.06	1672-1982	134	27	1861	0.25
145	*Tsuga canadensis*	Ce	Reed Pond	69.00	46.20	1639-1986	217	34	1729	0.26
146	*Pinus strobus*	Ce	Soper Brook West Branch	69.30	46.00	1692-1982	236	32	1711	0.15
147	*Picea rubens*	Ce	Wizard Pond	68.20	44.60	1692-1982	262	38	1709	0.14
148	*Pinus ponderosa*	WcBp	Ash Canyon	103.15	42.38	1642-1997	183	31	1738	0.33
149	*Tsuga canadensis*	Ce	Spruce Glen	74.20	41.80	1511-1984	281	31	1645	0.21
150	*Pinus ponderosa*	MdSc	Cedar Butte	101.10	43.60	1646-1991	222	16	1671	0.44
151	*Pinus ponderosa*	MdSc	Reno Gulch Pipo	103.26	43.54	1281-1991	282	32	1595	0.24
152	*Tsuga canadensis*	Ce	Bass Lake Peninsula	88.90	45.10	1595-1983	308	45	1619	0.25

[a] Cont (data contributors): Archambault, S. (As), Bergeron, Y. (By), Charron, D. (Cd), Conciatori, F. (Cf), Cook, E.R. (Ce), D'Arrigo, R. et al. (Dr), Duvick, D.N. (Dd), Gauthier, S. and Degranpré, L., (GsDl), Girardin, M.P. (Gm), Graumlich, L.J. (Gl), Guyette, R.P. (Gr), Guyette, R.P. and Cole, B. (GrCb), Hofgaard, A. (Ha), Jacoby, G. et al. (Jg), Jardon, Y. and Morin, H. (JyMh), Koop, D.L. and Grissino-Mayer, H.D. (KdGm), Krause, C and Morin, H. (KcMh), Krause, C. and Gionest, F. (KcGf), Lesieur, D. (Ld), Meko, D. and Sieg, C.H. (MdSc), Monson, K. (Mk), Schweingruber, F. (Sf), St-Gorge, S. (Ss), Stockton, C.W. (Sc), Tardif, J. (Tj), Woodhouse, C.A. and Brown, P.M. (WcBp).

[b] Mean is mean length of measurement series

[c] N is sample depth of tree-ring series

[d] SSS is subsample signal strength and is used to define the portion of the residual chronology (year *y* to present) with a strong common signal (Wigley et al. 1984).

[e] Sens is mean sensitivity of the residual chronology

NA information not available.

[f] These two residual chronologies were increased in length by inserting the value of 1.0 (average of the residual chronology) from their latest year to present to optimize the degree-of-freedom (PCA rectangular matrix constraint).

Table 5.3 Redundancy analyses statistics per climate region.

	canonical axis 1	canonical axis 2
A-Boreal Plains		
Eigenvalues[a]	0.15	0.05
Species-environment correlations [b]	0.68	0.55
Cumulative percentage variance (%) of species-environment relation [c]	63.20	85.10
B-Lac Seul and Lake of the Woods		
Eigenvalues [a]	0.23	0.03
Species-environment correlations [b]	0.70	0.58
Cumulative percentage variance (%) of species-environment relation [c]	81.00	92.10
C-Lake Nipigon		
Eigenvalues [a]	0.21	0.07
Species-environment correlations [b]	0.82	0.71
Cumulative percentage variance (%) of species-environment relation [c]	56.70	75.50
D-Abitibi Plains west		
Eigenvalues [a]	0.28	0.07
Species-environment correlations [b]	0.78	0.69
Cumulative percentage variance (%) of species-environment relation [c]	68.40	86.00
E-Abitibi Plains east		
Eigenvalues [a]	0.18	0.07
Species-environment correlations [b]	0.76	0.68
Cumulative percentage variance (%) of species-environment relation [c]	58.40	79.80
F-Southern Laurentian		
Eigenvalues [a]	0.25	0.04
Species-environment correlations [b]	0.77	0.69
Cumulative percentage variance (%) of species-environment relation [c]	75.20	87.80

Legend:
a Variance in a set of variables explained by a canonical axis.
b Amount of the variation in species composition that may be 'explained' by the environmental variables.
c Amount of variance explained by the canonical axes as a fraction of the total explainable variance.

Table 5.4 Inter reconstruction sub-models Pearson correlation coefficients for the six climate regions. All coefficients were calculated using the interval 1870-1984. The labels in italic refer to the number of chronologies used by each sub-model. Refer to Figure 5.3 for the identification of the interval covered by each sub-model.

BP	*5*	*6*	*8*	*10*	*11*	*13*
5	1.00					
6	0.95	1.00				
8	0.92	0.97	1.00			
10	0.84	0.84	0.84	1.00		
11	0.86	0.86	0.85	0.98	1.00	
13	0.90	0.87	0.88	0.91	0.95	1.00

LN	*5*	*6*	*7*	*8*	*10*	*13*	*15*	*17*	*19*	*21*	*24*
5	1.00										
6	0.96	1.00									
7	0.88	0.92	1.00								
8	0.84	0.83	0.96	1.00							
10	0.85	0.91	0.87	0.84	1.00						
13	0.83	0.83	0.75	0.74	0.87	1.00					
15	0.82	0.79	0.79	0.82	0.80	0.93	1.00				
17	0.82	0.81	0.85	0.89	0.84	0.87	0.96	1.00			
19	0.84	0.80	0.76	0.78	0.83	0.80	0.78	0.80	1.00		
21	0.79	0.77	0.72	0.73	0.81	0.80	0.77	0.78	0.99	1.00	
24[a]	0.78	0.75	0.69	0.70	0.80	0.79	0.75	0.77	0.98	0.99	1.00

APe	*5*	*7*	*9*	*10*	*11*	*13*	*15*	17	19	20
5	1.00									
7	0.62	1.00								
9	0.66	0.84	1.00							
10	0.44	0.49	0.53	1.00						
11	0.53	0.56	0.61	0.96	1.00					
13	0.50	0.46	0.56	0.97	0.95	1.00				
15	0.51	0.48	0.57	0.97	0.95	1.00	1.00			
17	0.50	0.56	0.65	0.94	0.91	0.96	0.97	1.00		
19	0.49	0.56	0.66	0.93	0.91	0.95	0.96	1.00	1.00	
20	0.53	0.62	0.75	0.76	0.81	0.79	0.81	0.88	0.90	1.00

LS	*5*	*7*	*9*	*11*	*13*	*15*	*17*	*19*	*21*	*23*	*25*
5	1.00										
7	0.98	1.00									
9	0.78	0.82	1.00								
11	0.85	0.90	0.91	1.00							
13	0.83	0.86	0.79	0.94	1.00						
15	0.88	0.91	0.88	0.97	0.94	1.00					
17	0.91	0.94	0.88	0.93	0.87	0.97	1.00				
19	0.78	0.82	0.84	0.78	0.71	0.79	0.87	1.00			
21	0.75	0.78	0.69	0.85	0.96	0.85	0.78	0.63	1.00		
23	0.66	0.70	0.64	0.79	0.92	0.76	0.69	0.62	0.97	1.00	
25	0.64	0.68	0.64	0.75	0.86	0.70	0.64	0.65	0.90	0.96	1.00

APw	*6*	*7*	*9*	*10*	*11*	*12*	*13*
6	1.00						
7	0.69	1.00					
9	0.66	0.73	1.00				
10	0.64	0.72	0.98	1.00			
11	0.64	0.71	0.97	1.00	1.00		
12	0.65	0.72	0.98	1.00	1.00	1.00	
13	0.64	0.71	0.98	0.99	0.99	1.00	1.00

SL	*5*	*7*	*9*	*11*	*13*	*19*	*21*	*23*	*25*
5	1.00								
7	0.93	1.00							
9	0.80	0.80	1.00						
11	0.85	0.79	0.87	1.00					
13	0.84	0.79	0.83	0.94	1.00				
19	0.85	0.89	0.79	0.87	0.89	1.00			
21	0.82	0.80	0.78	0.93	0.88	0.90	1.00		
23	0.81	0.83	0.77	0.85	0.82	0.90	0.94	1.00	
25	0.83	0.87	0.81	0.85	0.85	0.91	0.89	0.89	1.00

a This LN sub-model covering 1869-1987 was not included in the final reconstruction (RE = 0.17); its statistics were omitted from Figure 3.

CHAPTER 6

GENERAL DISCUSSION AND CONCLUSION

6.1 Drought variability during the instrumental period

Results of this thesis suggest that there was no detectable linear trend in the estimated moisture content of deep duff layers during the instrumental period that could be related to climate change, neither for the eastern Boreal Plains nor the eastern Boreal Shield. These results contradicted those from studies of the Canadian boreal forest suggesting a reduction in fire frequency since ca. 1850 and, therefore, the presence of a trend toward a moister climate (Master 1990; Johnson and Larsen 1991; Larsen 1997; Bergeron et al. 2001; Bergeron et al. 2004b). In addition, our results also contradicted recent fire statistics showing an increase in fire frequency and area burned over boreal Canada since 1960s (Stocks et al. 2003; Amiro et al. 2004). It was however found that decadal variation was a dominant feature in drought severity during the 20th century, particularly in the eastern Boreal Plains and western Boreal Shield.

The failure to identify a linear trend in drought severity during the recent decades leads to the development of two alternative hypotheses. First, the absence of trends in the Canadian Drought Code (CDC) may reflect the fact that an increase in precipitation compensated for the increasing temperature. This hypothesis was suggested by Bergeron and Archambault (1993) and Bergeron et al. (2001) in an attempt to explain the discrepancy between the observed Northern Hemisphere warming trend since ca. 1850 and the decrease in fire frequency in the southeastern Canadian boreal forest. Second, the absence of trends in the CDC may be due to the omission in the CDC computation procedure of daily precipitation events less than to 2.80 mm and thus of any trends associated with these events. The frequency of small

rainfall events is important in the determination of fuel moisture for the finer fuels (Van Wagner 1987). Flannigan and Harrington (1988) reported that among the most important predictors for area burnt are the long sequences of days with less than 1.5 mm of rain. The frequency of these events determines the ease of ignition and the flammability of fine fuels. In contrast, rainfall of greater magnitude determines fuel consumption in loosely compacted organic layers of moderate depth and, in the long term, the amount of smouldering in deep duff layers and large logs (Van Wagner 1987). If temporal changes were to occur in moisture content of any of these layers, changes may occur in fire behaviour, such as the spread rate of fire and the amount of fuel available for the fire.

From an ecological point of view, a validation of the second hypothesis could yield meaningful information. Zhang et al. (2001), in their analysis of temporal characteristics of heavy precipitation events for the country as a whole, found no trends in extreme precipitation during the last century, but significant increases in the number of small to moderate precipitation events. Temporal variations of regional heavy precipitation display strong interdecadal variability with limited evidence of long-term trends (Zhang et al. 2001). Recent analyses of trends in seasonal FWI parameters from across Canada and covering the period 1959-1999, however, indicated that temporal changes in fire weather components associated with large fires could not yet be detected (Amiro et al. 2004). The short period of analysis and the strong interannual variations in the fire weather data sets however created difficulties in the detection of trends. Amiro et al. (2004) stressed the importance of creating longer data sets for the evaluation of climate change impacts on fire weather conditions. Trend analysis on the FWI component covering the period 1916-1998 did identify a significant but weak trend in extreme fire weather conditions over the eastern Abitibi Plains region (Lefort et al. 2003), not shown in our data. The improvement of daily meteorological data covering the 20th century through rehabilitation and homogenization procedures (Mekis and Hogg 1999; Vincent and

Zhang 2002) will enable studies of trends in FWI System components over longer time periods.

6.2 Drought variability during the past three centuries

The development of a network of tree-ring chronologies across the southern Canadian boreal forest is an important contribution. Many of the chronologies span several centuries and, in the absence of long instrumental data, can be used as natural archives to infer past climate variability (Sheppard and Cook 1988). The summer drought reconstructions presented in this work constituted the first network of climate reconstructions ever made within the portion of the boreal forest studied. Despite the absence of a dominant drought signal in tree-ring chronologies of the Southern Laurentian (SL region), the reconstruction provides valuable information on past climate variability, notably on the occurrence of warm spells and persistent ridging. Therefore, the network of reconstructions represents an important advance toward understanding decadal scale summer climate variability. But, importantly, this data set may also be used for other ecological and environmental benefits such as for insect outbreak reconstructions (e.g. Girardin et al. 2001; Jardon et al. 2003) and prediction of climate change impacts on forest productivity (e.g. Laroque et al. 2003).

While the analysis of the instrumental CDC indices failed in the detection of trends in drought severity, the development and intercomparison of the regional summer drought reconstructions allowed the identification of significant changes in spatiotemporal variability at ca. 1850. First, the spectrum analyses conducted on the CDC reconstruction of the Abitibi Plains *east* showed that periodicities in drought severity have evolved during the past 400-years, particularly toward greater interannual variations. Droughts sustained for several years were particularly recurrent during the interval 1750 to 1850. In contrast to the Abitibi Plains *east*, in the

eastern Boreal Plains these events were recurrent features of the interval 1750 to 1850 and through most of the 20th century. Second, the analyses of spatiotemporal variability indicated that ca. 1850 marked a transition toward more regional drought variability. Large-scale droughts across the portion of the boreal forest under study were apparently more commons in the period prior to ca. 1850 than during the second half of the 20th century.

Little attention was given to the reconstruction of low frequency variations in drought, other than the attempt using the *Thuja occidentalis* L. measurement series. In the past year or so discussions have taken place regarding various methods applied to standardize tree-ring data (Esper et al. 2004). The debate is focussed on differencing the long-term climate signal from the long-term tree growth signal (decreasing radial growth with age). For instance, the different approaches of tree-ring data standardization appear to most substantially account for the differing low-frequency trends in the reconstructed Northern Hemisphere temperature (Esper et al. 2004). The use of non-conservative detrending may however be increasingly important in tree-ring data showing noise due to stand disturbances (herbivory and post forest fire growth releases). But most importantly, the age of most samples collected in the boreal forest (mean age of approximately 137 years, Table 5.2) is insufficiently long to cover a period that would allow robust reconstruction of low frequency variations. The contribution of other types of proxies could be valuable in attempting to reconstruct long-term trends in fire weather conditions across the Canadian boreal forest.

Work is currently under way to extract information contained in the reconstructions and translate it in terms of annual burn rates over large regions, such as on the Boreal Shield. Over 36% of the variance in the Boreal Shield annual area burned (period 1959-1998, data from Stocks et al. 2003) could be accounted for by the atmospheric circulation components defined in this work (first and second

principal components of the six reconstructions; Girardin et al. unpublished). In Wood Buffalo National Park, Northern Alberta, Larsen (1996) found that 56% of the variance in area burned could be accounted for by variance in radial growth. The authors suggested that tree-rings could be used as proxy of the regional fire activity. In east European Russia, Drobyshev and Niklasson (2004) found that 40% of area burned variance in the Komi Republic during 1950-1990 could be accounted for by tree-ring chronologies. They suggested that it was possible to define an indirect relationship between variance in tree-rings and records of fire activity. Preliminary results from the Boreal Shield (Girardin et al. unpublished) indicated that an indirect relationship between variance in the CDC reconstructions and the records of fire activity could be used to estimate past fire activity for the whole region.

6.3 Connection with the global climate

The synoptic analyses presented in this work have been valuable tools in the identification of relationships among tree-ring indices, regional drought variability, and patterns of atmospheric circulation. It is often tempting to link regional climate variability with dominant Northern Hemisphere patterns of atmospheric circulation variability like the North Atlantic Oscillation (NAO), Pacific Decadal Oscillation (PDO) and Southern Oscillation (SO) (Section 1.3.2). Often this is done to improve regional long-range weather forecasts (Shabbar and Khandekar 1996; Flannigan and Wotton 2001). As shown in this work, these patterns can share significant amounts of variance in summertime drought variability. Both instrumental and reconstructed CDC indices from the Abitibi Plains region, for instance, shared significant variance with the NAO-like dipole structure during the instrumental period. Most of this common variance was in the decadal scale of variability. On an interannual scale, regional drought variability may be more influenced by local forcing related to soil moisture and insolation distribution.

Patterns such as the NAO and SO describe average circulation variability and should not necessarily be considered as drivers of climate variability. The connection between regional drought variability and the circulation indices is however useful for detecting linkage between weather changes occurring in widely separated areas of the globe (American Meteorological Society 2000). Significant correlations between regional drought variability and circulation indices suggest that information is propagating between distant areas through the atmosphere via the longwaves. However, spatiotemporal analyses conducted in this work indicated that relations between regional drought variability and atmospheric circulation are non-stationary. It therefore cannot be assumed that information is always propagating between the distant areas in the same way.

This work showed empirical evidence of an increase in the frequency and amplitude of mid-troposphere high-pressure systems over western Canada from ca. 1851 to 1940. An observed deepening of the eastern trough was also reported downstream of the longwave. This change in the frequency and magnitude of the longwaves during summertime may help to explain the reported decrease of fire frequency in many areas of the Canadian boreal forest. An amplified continental ridge implies an anomalously displaced storm track over western boreal Canada and intensified advection of humid air masses from the subtropical Atlantic onto the eastern portion of the Boreal Shield. The net result is an apparent decrease of fire prone weather conditions for these regions.

It is apparent that underlying processes responsible for the atmospheric circulation shift over the boreal forest involved ocean and atmosphere couplings. Remarkable advances in the understanding of atmospheric and oceanic dynamics marked the period during which this work was conducted. This is notable by the changes in opinion from Chapter 3 toward Chapter 5 regarding the relationship

between stochastic feedback in the atmosphere, tropical SSTs, and North Pacific SSTs. It has now become much clearer that tropical SSTs, with the contribution of stochastic atmospheric forcing, influences North Pacific SSTs (Schneider et al. 2002; Kumar and Hoerling 2003; Newman et al. 2003; Wu and Liu 2003; Yang and Zhang 2003; Lau et al. 2004). The correlation field between the meridional flow component and the North Pacific SST field suggests that the summertime meridional circulation over Canada is intimately related to the North Pacific oceanic and atmospheric coupling, and thus also under the influence of tropical and stochastic atmospheric feedback. Despite the advance toward better understanding of the meridional circulation, little information was gained on the global scale drivers of the zonal component (the leading principal component of all six regions under study). This is critical since the variability over the Canadian Shield is to a large extent dependent on this circulation. This aspect of atmospheric circulation should be subject to further study.

6.4 Tree growth and climate relationship

In general, the quality of the summer drought reconstructions is comparable with summer climate reconstructions conducted in northeastern and central Canada (Guiot 1985; Jacoby et al. 1988; Jacoby and D'Arrigo 1989; D'Arrigo and Jacoby 1989; D'Arrigo and Jacoby 1993; Briffa et al. 1994; Sauchyn et al. 2003). Reconstructions that are based on tree-ring density measurements however tended to demonstrate slightly better predictive skills than the drought reconstructions presented in this study. It is generally recognized that the climate response of maximum latewood density is more consistent with year-to-year climate variation than ring-width and also covers a longer portion of the growing season (Jacoby et al. 1988; D'Arrigo et al. 1992; Briffa et al. 1994). Nevertheless, the six reconstructions provide meaningful information on historical weather at a time when fire conditions are most critical, that is, during the months of June and July (Skinner et al. 2002; Stock et al. 2003).

Calibration of the CDC with tree-ring chronologies from the boreal forest was successful in five of six attempts. The dendroclimatic analyses indicated that the summer temperature-moisture budget was among the strongest factor influencing tree radial growth in the boreal forest. A proper moisture budget allows optimal radial growth and assimilation of carbohydrates for the next year's growth if soil moisture is sufficient to maintain foliage water potential and minimise vapour pressure deficits (Dang et al. 1998; Bonan 2002). Analysis of the relationship between tree growth and the atmospheric vertical profile suggested that mid-tropospheric circulation was the delivery system of surface moisture condition regulating tree radial growth.

It is not clear as to why a reduced expression of the correlation between the CDC and tree growth was encountered in the Southern Laurentian (SL region). Perhaps it reflects the possibility that summer precipitation is not a limiting factor for tree growth in this region. However, the observed negative response to previous year summertime temperature is potentially an indicator that summer warm spells do induce a closure of stomata, reducing net photosynthesis (Bonan 2002) and next year's radial growth. But the absence of a relationship with the July CDC could also reflect the occurrence of strong heterogeneity in precipitation over the area. Significant correlation at the 10% level with the July CDC from single meteorological stations was effectively obtained in the analyses of several chronologies. A sampling campaign in which the effort would be targeted on the collection of samples from *Pinus spp.* and from dry prone environments could lead to an extension of the CDC network into eastern Quebec. The significant predictive skill of the calibration procedures in five regions further suggests a strong possibility for extending the network of CDC reconstructions into other regions of the boreal forest.

The distortion created by insect herbivory on the expression of tree radial growth and climate relationships may be problematic in some situations. The reduced

expression of the climate signals on *Larix laricina* (Du Roi) K. Koch tree-ring chronologies originating from the boreal forest by the larch sawfly (*Pristiphora erichsonii* (Hartig)), for instance, is now well-documented. In boreal studies, past growth suppressions presumably caused by severe larch sawfly outbreaks occurred in more than 50% and up to 100% of the host trees (Girardin et al., 2001; Case and MacDonald, 2003). Other examples of defoliation are those of the forest tent caterpillar (*Malacosoma disstria* Hubner) on *Betula papyrifera* Marsh., *Populus tremuloides* Michx. and *Populus balsamifera* L., and of the spruce budworm (*Choristoneura fumiferana* (Clemens)) on *Abies balsamea* L. Mill. and *Picea glauca* (Moench) Voss. Important defoliation by the forest tent caterpillar can lead to significant growth reductions of *Populus tremuloides*. In northern Alberta, Hogg et al. (2002) reported that forest tent caterpillar defoliation in the current year growth accounts for more temporal variation in stem-area increment of *Populus tremuloides* than any of the variables describing climate variation.

The implication of distortion effects caused by insect defoliation on climate reconstructions was recently quantified in the southern United States using *Pinus edulis* Engelm. (Trotter III et al. 2002). This species is chronically attacked by *Matsucoccus acalyptus* Herbert (Margarodidae, Homoptera). Trotter III et al. (2002) reported that climate reconstruction conducted from trees susceptible to insect herbivory might lead to erroneous estimations, particularly of extreme events. The authors however recognised that pooling samples across stands, populations, and regions should reduce the bias. The combination of several species and the filtering of the climate signal as done in the present work can also contribute to a minigation of this distortion.

6.5 Conclusion

Results from this work demonstrated the linkage among the global scale climate, tree growth, and fire weather conditions along the portion of the boreal forest covering the eastern Boreal Plains to the eastern Boreal Shield. Variability in drought severity, defined here by the Canadian Drought Code of the Fire Weather Index System, shares significant relationship in several time scales with well-known patterns of climate variability originating in the North Pacific and North Atlantic sectors. Similar correspondence was made with tree radial growth.

There is a generalized recognition that global-scale atmospheric circulation patterns have their most pronounced impacts on regional climate during wintertime (e.g. Barnston and Livezey 1987; Hurrell 1995; Shabbar and Khandekar 1996; Wanner et al. 2001). The results from this work suggested that they are also strong enough during summertime to affect ecosystem processes, namely tree radial growth and fire activity. The findings of this work corroborated previous studies reporting the influence of synoptic and global scale climate systems on ecosystem processes (Hirschboeck et al. 1996; Garfin 1998; Skinner et al. 1999; 2002; Gillett et al. 2004). The evolution of global atmospheric circulation, by affecting the regional climate, has likely influenced vegetation structure and composition over the past centuries in the Canadian boreal forest. The potential effect of anthropogenic climatic change, which could alter variations in low-frequency oscillations of the natural atmospheric and oceanic circulation patterns (e.g. Hurrell 1995; Wanner et al. 2001; Bigg et al. 2003), could be significant for the Canadian boreal forest.

LIST OF REFERENCES

Agee, J.K. 1997. The severe weather wildfire - too hot to handle? Northwest Science 71: 153-156.

Ahrens, C.D. 2003. Meteorology today: an introduction to weather, climate, and the environment, Seventh edition. Brooks/Cole – Thomson Learning, Pacific Grove, California, 544 pages.

AISN Software 1999. AutoSignal, version 1.5 for Windows. SPSS Inc. Chicago, IL, USA.

Alexander, M.E. 1982. Calculating spring Drought Code starting values in the Prairie Provinces and Northwest Territories. Environment Canada. Canadian Forest Service, Northern Forestry Centre, Edmonton, Alberta. Forest Management Note 12.

American Meteorological Society, 2000. Glossary of Meteorology, 2nd ed. Allen Press. 855 pp. http://amsglossary.allenpress.com/glossary

Amiro, B.D., Logan, K.A., Wotton, B.M., Flannigan, D.M., Todd, J.B., Stocks, B.J., and Martell, D.L., 2004. Fire weather index system components for large fires in the Canadian boreal forest. International Journal of Wildland Fire 13: 391-400.

Archambault, S., and Bergeron, Y. 1992. An 802-year tree-ring chronology from the Quebec boreal forest. Canadian Journal of Forest Research 22: 674–682.

Baldwin, M.P., and Dunkerton, T.J. 1999. Propagation of the Arctic Oscillation from the stratosphere to the troposphere. Journal of Geophysical Research 104: 30 937-30 946.

Baldwin, M.P., and Dunkerton, T.J. 2001. Stratospheric harbingers of anomalous weather regimes. Science (Washington D.C.) 294: 581-584.

Baldwin, M.P., Thompson, D.W.J., Shuckburgh, E.F., Norton, W.A., and Gillett, N.P. 2003. Weather from the stratosphere? Science (Washington D.C.) 301: 317-318.

Barlow, M., Nigam, S., and Berbery, E.H. 2001. ENSO, Pacific decadal variability, and U.S. summertime precipitation, drought, and stream flow. Journal of Climate 14: 2105–2128.

Barnston, A.G., and Livezey, R.E. 1987. Classification, seasonality and persistence of low-frequency atmospheric circulation patterns. Monthly Weather Review 115: 1083-1126.

Barry, R.G., and Carleton, A.M. 2001. Synoptic and dynamic climatology. Routledge, New York. 620 pages

Bégin, Y. 2000. Ice-push disturbances in high-Boreal and Subarctic lakeshore ecosystems since AD 1830, northern Québec, Canada. The Holocene 10: 173–183.

Bégin, Y., and Payette, S. 1988. Dendroecological evidence of lake-level changes during the last three century in subarctic Québec. Quaternary Research 30: 210–220.

Bégin, Y., Bérubé, D., and Grégoire, M. 1993. Downward migration of coastal conifers as a response to recent land emergence in Hudson Bay, Québec. Quaternary Research 40: 81–88.

Benestad, R.E. 1999. Solar activity and global sea-surface temperature. Astronomy and Geophysics 40: 14-17.

Bergeron, Y. 1991. The influence of island and mainland lakeshore landscapes on boreal forest fire regimes. Ecology 6: 1980–1992.

Bergeron, Y. 1998. Les conséquences des changements climatiques sur la fréquence des feux et la composition forestière au sud-ouest de la for êt boréale québécoise. Géographie Physique et Quaternaire 52: 167–173.

Bergeron, Y. 2000. Species and stand dynamics in the mixed woods of Quebec's southern boreal forest. Ecology 81: 1500-1516.

Bergeron, Y. 2004. Is regulated even-aged management the right strategy for the Canadian boreal forest? Forestry Chronicle 80: 458-462.

Bergeron, Y., and Dubuc, M. 1989. Succession in the southern part of the Canadian boreal forest. Vegetatio 79: 51–63.

Bergeron, Y., and Archambault, S. 1993. Decreasing frequency of forest fires in the southern boreal zone of Quebec and its relation to global warming since the end of the 'Little Ice Age'. The Holocene 3: 255-259.

Bergeron, Y., and Flannigan, M.D. 1995. Predicting the effects of climate change on fire frequency in the southeastern Canadian boreal forest. Water, Air, and Soil Pollution 82: 437–444.

Bergeron, Y., and Harvey, B. 1997. Basing silviculture on natural ecosystem dynamics: An approach applied to the southern boreal mixedwood forest of Quebec. Forest Ecology and Management 92: 235-242.

Bergeron, Y., Gauthier, S., Kafka, V., Lefort, P., and Lesieur, D. 2001. Natural fire frequency for the eastern Canadian boreal forest: consequences for sustainable forestry. Canadian Journal of Forest Research 31: 384-391.

Bergeron, Y., Leduc, A., Harvey, B., and Gauthier, S. 2002a. Natural fire regime: A guide for sustainable forest management in the Canadian boreal forest. Silva Fennica 36: 81-95.

Bergeron, Y., Denneler, B., Charron, D., and Girardin, M.P. 2002b. Using dendrochronology to reconstruct disturbance and forest dynamics around Lake Duparquet, northwestern Quebec. Dendrochronologia 20: 175–189.

Bergeron, Y., Flannigan, M., Gauthier, S., Leduc, A., and Lefort, P. 2004a. Past, current and future fire frequency in the Canadian boreal forest: implications for sustainable forest management. Ambio 33: 356-360.

Bergeron, Y., Gauthier, S., Flannigan, M., and Kafka, V. 2004b. Fire regimes at the transition between mixedwoods and coniferous boreal forest in northwestern Quebec. Ecology 85: 1916-1932.

Bessie, W.C., and E.A. Johnson. 1995. The relative importance of fuels and weather on fire behavior in subalpine forests in the southern Canadian Rockies. Ecology 26: 747-762.

Bigg, G.R., Jickells, T.D., Liss, P.S., and Osborn, T.J. 2003. The role of the ocean in climate. International Journal of Climatology 23: 1127-1159.

Biondi, F., Gershunov, A., and Cayan, D.R. 2001. North Pacific decadal climate variability since AD 1661. Journal of Climate 14: 5–10.

Boer, G.J., Flato, G., and Ramsden, D. 2000. A transient climate change simulation with greenhouse gas and aerosol forcing: projected climate to the twenty-first century. Climate Dynamics 16: 427-450.

Bonan, G. 2002. Ecological climatology. Cambridge University Press, New York. 678 pages.

Bonsal, B.R., and Lawford, R.G. 1999. Teleconnections between El Niño and La Niña events and summer extended dry spells on the Canadian Prairies. International Journal of Climatology 19: 1445–1458.

Bonsal, B.R., Chakravarti, A.K., and Lawford, R.G. 1993. Teleconnections between North Pacific SST anomalies and growing season extended dry spells on the Canadian Prairies. International Journal of Climatology 13: 865–878.

Bonsal, B.R., Zhang, X., and Hogg, W.D. 1999. Canadian Prairies growing season precipitation variability and associated atmospheric circulation. Climate Research 11: 191–208.

Bonsal, B.R., Shabbar, A., and Higuchi, K. 2001. Impacts of low frequency variability modes on Canadian winter temperature. International Journal of Climatology 21: 95–108.

Bourgeau-Chavez, L.L., Alexander, M.E., Stocks, B.J., and Kasischke, E.S. 2000. Distribution of forest ecosystems and the role of fire in the North American boreal region. *In* Fire, Climate Change, and Carbon Cycling in the Boreal Forest. Springer, New York, pp. 111-131.

Bradley, R.S. 1999. Paleoclimatology: reconstructing climates of the Quaternary. Academic Press, Toronto, Canada. 610 pages

Briffa, K.R. 2000. Annual climate variability in the Holocene: Interpreting the message of ancient trees. Quaternary Science Review 19: 87-105.

Briffa, K., and Cook, E.R. 1990. Methods of response function analysis. *In* Methods of dendrochronology. *Edited by* E.R. Cook and L.A. Kairiuktsis. Kluwer Academic, Dordrecht. Pages 240-247.

Briffa, K.R., Bartholin, T.S., Eckstein, D., Jones, P.D., Karlén, W., Scheingruber, F.H., and Zetterberg, P. 1990. A 1,400-year tree-ring record of summer temperatures in Fennoscandia. Nature 346: 434-446.

Briffa, K.R., Jones, P.D., and Schweingruber, F.H. 1994. Summer temperatures across northern north america: Regional reconstructions from 1760 using tree-ring densities. Journal of Geophysical Research 99: 25 835-25 844.

Burns, R.M., and Honkala, B.H. 1990. Silvics of North America, Vol. 1, Conifers. Washington DC: U.S.D.A. Forest Service Agriculture Handbook 654.

Carcaillet, C., Bergeron, Y., Richard, P., Fréchette, B., Gauthier, S., and Prairie, Y. 2001. Change of fire frequency in the eastern Canadian boreal forests: Does vegetation composition or climate trigger the fire regime? Journal of Ecology 89: 930–946.

Case, R.A., and MacDonald, G.M. 2003. Dendrochronological analysis of the response of tamarack (*Larix laricina*) to climate and larch sawfly (*Pristiphora erichsonii*) infestations in central Saskatchewan. Ecoscience 10: 380-288.

Charron, D., and Bergeron, Y. 2000. Paper birch and trembling aspen chronologies from the Québec boreal forest. Int. Conf. dendrochronology for the third millennium, Mendoza, Argentina, 2-7 April 2000, pp 10.

Chhin, S., Wang, G.G., and Tardif, J. 2004. Dendroclimatic analysis of white spruce at its southern limit of distribution in the Spruce Woods Provincial Park, Manitoba, Canada. Tree-Ring Research 60: 31-44.

Clark, J.S., and Richard, P.J.H. 1996. The role of paleofire in boreal and other cool-coniferous forests in the boreal forest in J.G. Goldammer and V.V. Furyaev, eds. Fire in Ecosystem of Boreal Eurasia. Kluwer Academic Publishers, Dordrecht, The Netherlands. pp 65-89.

Cook, E.R., and Peters, K., 1981. The smoothing spline: a new approach to standardizing forest interior tree-ring width series for dendroclimatic studies. Tree-Ring Bulletin 41: 45-53.

Cook, E.R., and Holmes, R. 1986. Guide for computer program ARSTAN. Laboratory of Tree-Ring Research, University of Arizona, Tucson, Arizona. 51 pages.

Cook, E.R., and Kairiukstis, L.A. 1990. Methods of dendrochronology. Applications in the environmental sciences. Kluwer Academic Publishers, Boston, pp 408.

Cook, E.R., and D'Arrigo, R.D. 2002. A well-verified, multiproxy reconstruction of the winter North Atlantic Oscillation index since A.D. 1400. Journal of Climate 15: 1752-1764.

Cook, E.R., Briffa, K.R., and Jones, P.D. 1994. Spatial regression methods in dendroclimatology: a review and comparison of two techniques. International Journal of Climatology 14: 379–402.

Cook, E.R., D'Arrigo, R., and Briffa, K.R. 1998. A reconstruction of the North Atlantic Oscillation using tree-ring chronologies from North America and Europe. The Holocene 8: 9–17.

Cook, E.R., D'Arrigo, R.D., and Mann, M.E. 2002. A well-verified, multiproxy reconstruction of the winter North Atlantic Oscillation index since A.D. 1400. Journal of Climate 15: 1752-1764.

Cook, E.R., Esper, J., D'Arrigo, R. 2004. Extra-tropical Northern Hemisphere temperature variability over the past 1000 years. Quaternary Science Reviews 23: 2063-2074.

D'Arrigo, R.D., and Jacoby, G.C. 1993. Secular trends in high northern latitude temperature reconstructions based on tree rings. Climatic Change 25: 163-177.

D'Arrigo, R.D., Jacoby, G.C., and Free, R.M. 1992. Tree-ring width and maximum latewood density at the North American tree line: parameters of climatic change. Canadian Journal of Forest Research 22: 1290-1296.

D'Arrigo, R., Villalba, R., and Wiles, G. 2001. Tree-ring estimates of Pacific decadal climate variability. Climate Dynamics 18: 219–224.

D'Arrigo, R., Buckley, B., Kaplan, S., and Woollett, J. 2002. Interannual to multidecadal modes of Labrador climate variability inferred from tree rings. Climate Dynamics 20: 219–228.

D'Arrigo, R.D., Cook, E.R., Mann, M.E., Jacoby, G.C. 2003. Tree-ring reconstruction of temperature and sea-level pressure variability associated with the warm-season Arctic Oscillation since AD 1650. Geophysical Research Letters 30, 1549, 10.1029/2003GL017250.

Dang, Q.L., Margolis, H.A., and Collatz, G.J. 1998. Parameterization and testing of a coupled photosynthesis-stomatal conductance model for boreal trees. Tree Physiology 18: 141-153.

Dommenget, D., and Latif, M. 2002. A cautionary note on the interpretation of EOFs. Journal of Climate 15: 216-225.

Drobyshev, I., and Niklasson, M. 2004. Linking tree-rings, summer aridity, and regional fire data: an example from the boreal forests of the Komi Republic, east European Russia. Canadian Journal of Forest Research 34: 2327-2339.

Ecological Stratification Working Group 1996. A national ecological framework for Canada, Agriculture and Agri-Food Canada and Environment Canada, Ottawa. 125 pages.

Environment Canada 2000. Canadian daily climate data: temperature and precipitation. Meteorological Service of Canada. Climate Monitoring and Data Interpretation Division of the Climate Research Branch. Downsview, Ontario, Canada.

Environment Canada 2002. Canadian Climate Normals 1971-2000. Canadian Climate Program. Environment Canada. Atmospheric Environment Service, Downsview, Ontario.

Esper, J., Cook, E.R., and Schweingruber, F.H. 2002. Low-frequency signals in long tree-ring chronologies for reconstructing past temperature variability. Science (Washington, D.C.) 295: 2250-2253.

Esper J, Frank, D.C., Wilson, R.J.S. 2004. Climate reconstructions - low frequency ambition and high frequency ratification. EOS, American Geophysical Union, 85, 113, 120.

Evans, M.N., Kaplan, A., and Cane, A. 2002. Pacific sea surface temperature field reconstruction from coral $\delta^{18}O$ data using reduced space objective analysis. Paleoceanography 17: 7-1-713.

Finney, B., Gregory-Eaves, I., Sweetman, J., Douglas, M., and Smol, J.P. 2000. Impacts of climatic change and fishing on Pacific salmon abundance over the past 300 years. Science (Washington, D.C.) 290: 795–799.

Fire Ecology Research Group 2005. Experimental Climate Prediction Center - Fire Weather Index Forecast. The Global Fire Monitoring Center (GFMC), Freiburg University, Freiburg.

Flannigan, M.D., and Harrington, J.B. 1988. A study of the relation of meteorological variables to monthly provincial area burned by wildfire in Canada (1953-80). Journal of Applied Meteorology 27: 441-452.

Flannigan, M. D., and Van Wagner, C. E. 1991. Climate change and wildfire in Canada. Canadian Journal of Forest Research 21: 66-72.

Flannigan M.D., and Wotton, B.M. 2001. Climate, weather, and area burned. *In* Forest fires: behavior and ecological effects. E.A. Johnson and K. Miyanishi, Eds., Academic Press, New York, pp. 351-373.

Flannigan, M.D., Bergeron, Y., Englemark, O., and Wotton, B.M. 1998. Future wildfire in circumboreal forests in relation to global warming. Journal of Vegetation Science 9: 469–476.

Flannigan, M.D., Cambell, I., Wotton, M., Carcaillet, C., Richard, P., and Bergeron, Y. 2001. Future fire in Canada's boreal forest: paleoecology results and general circulation model – regional climate model simulations. Canadian Journal of Forest Research 31: 854–864.

Forsters, P.M. de F., and Shine, K.P. 1999. Stratospheric water vapour changes as a possible contributor to stratospheric cooling. Geophysical Research Letters 26: 3309-3312.

Fritts, H.C. 1991. Reconstructing large-scale climatic patterns from tree-ring data - a diagnostic analysis. The University of Arizona Press, Tucson, Arizona USA. 286 pages.

Fritts, H.C. 1998. Factors preconditioning growth with Kalman filter: an empirical model of the tree ring response to monthly variations in climate. Laboratory of Tree-Ring Research, University of Arizona, Tucson, Arzona.

Fritts, H.C. 2001. Tree-Ring and climate. Blackburn Press, Caldwell, N.J. USA. 567 pages.

Fritts, H.C., Vaganov, E.A., Sviderskaya, I.V., and Shashkin, A.V. 1991. Climatic variation and tree-ring structure in conifers: Empirical and mechanistic models of tree-ring width, number of cells, cell-size, cell-wall thickness and wood density. Climate Research 01: 97-116.

Gajewski, K., and Atkinson, D.A. 2003. Climatic change in northern Canada. Environmental Reviews 11: 69-102.

Garfin, G.M. 1998. Relationships between winter atmospheric circulation patterns and extreme tree growth anomalies in the Sierra Nevada. International Journal of Climatology 18: 725-740.

Gill, C.B. 1930. Cyclic forest phenomena. Forestry Chronicle 6: 42-56.

Gillett, N.P., Allen, M.R., McDonald, R.E., Senior, C.A., Shindell, D.T., and Schmidt, G.A. 2002. How linear is the Arctic Oscillation response to greenhouse gases? Journal of Geophysical Research 107, ACL 1-1-1-7, 10.1029/2001JD000589.

Gillett, N.P., Weaver, A.J., Zwiers, F.W., Flannigan, M.D. 2004. Detecting the effect of climate change on Canadian forest fires. Geophysical Research Letters 31, L18211, 10.1029/2004GL020876.

Girardin, M. P., and Tardif, J. 2005. Sensitivity of tree growth to the atmospheric vertical profile in the Boreal Plains of Manitoba. Canadian Journal of Forest Research 35: 48-64.

Girardin, M.P., Tardif, J., and Bergeron, Y. 2001. Radial growth analysis of *Larix Laricina* from the Lake Duparquet area, Quebec, in relation to climate and larch sawfly outbreaks. Ecoscience 8: 127-138.

Girardin, M.P., Tardif, J., and Bergeron, Y. 2002a. Dynamics of eastern larch stands and its relationships with larch sawfly outbreaks in the Northern Clay Belt of Quebec. Canadian Journal of Forest Research 32: 206–216.

Girardin, M.P., Tardif, J., Flannigan, M.D., and Bergeron, Y. 2002b. Reconstructing atmospheric circulation history using tree rings: one more step toward understanding temporal changes in forest dynamics. *In* Proceedings of the 3rd Sustainable Forest Management Network Conference, Advances in forest management: from knowledge to practice. *Edited by* Veeman TS, Duinker PN, Macnab BJ, Coyne AG, Veeman kM, and Korber D.. Shaw Conference Centre, Edmonton, Alberta, November 13–15. Edmonton Alberta, Canada, pp 105–110.

Girardin, M.P., Tardif, J., Flannigan, M.D., and Bergeron, Y. 2004a. Multicentury reconstruction of the Canadian Drought Code from eastern Canada and its relationship with paleoclimatic indices of atmospheric circulation. Climate Dynamics 23: 99-115.

Girardin, M.P., Tardif, J. Flannigan, M.D., Wotton, B.M., and Bergeron, Y. 2004b. Trends and periodicities in the Canadian Drought Code and their relationships

with atmospheric circulation for the southern Canadian boreal forest. Canadian Journal of Forest Research 34: 103-119.

Girardin, M.P., Berglund, E. Tardif, J. and Monson, K. 2005. Radial growth of tamarack (*Larix laricina*) in the Churchill area (Manitoba) in relation to climate and larch sawfly (*Pristiphora erichsonii*) herbivory. Arctic, Antarctic and Alpine Research 37: 206-217.

Glueck, M.F., and Stockton, C.W. 2001. Reconstruction of the North Atlantic Oscillation. International Journal of Climatology 21: 1453–1465.

Graumlich, L. 1993. Response of tree growth to climatic variation in the mixed conifer and deciduous forests of the upper Great Lakes region. Canadian Journal of Forest Research 23: 133-143.

Guiot, J. 1985. Reconstruction of seasonal temperatures and sea-level pressures in the Hudson Bay area back to 1700. Climatological Bulletin 19: 11-59.

Guiot J. 1991. The bootstrapped response function. Tree-Ring Bulletin 51: 39-41.

Hare, S.R., and Mantua, N.J. 2000. Empirical evidence for North Pacific regime shifts in 1977 and 1989. Progress in Oceanography 47: 103–145.

Harrington, J., Kimmins, J., Lavender, D., Zoltai, S., and Payette, S. 1991. The effect of climate change on forest ecology in Canada. *In* Proceeding of the 10th World Forestry Congress, 17-26 Sept 1991, Paris. École nationale du génie rural, des eaux et des forêts, Nancy, France. Revue Forestière Française (Numéro Spécial) 2: 49-58.

Harrison, J.D.B. 1934. The forests of Manitoba. Department of the Interior, Ottawa, Ontario. Forest Service Bulletin 85.

Hartmann, D.L., Wallace, J.M., Limpasuvan, V., Thompson, W.J., and Holton, J.R. 2000. Can ozone depletion and global warming interact to produce rapid climate change? Proceedings of the Natural Academy of Sciences U.S.A. 97: 1412-1417.

Harvey, B.D., Leduc, A., Gauthier, S., and Bergeron, Y. 2002. Stand-landscape intergration in natural disturbance-based mangement of the southern boreal forest. Forest Ecology and Management 155: 369-385.

Harvey, B.D., Nguyen-Xuan, N., Bergeron, Y., Gauthier, S., and Leduc, A. 2003. Forest management planning based on natural disturbance and forest dynamics. *In* Toward Sustainable Management of the Boreal Forest. *Edited by* P.J. Burton, C. Messier, D.W. Smith, and W.L. Adamowicz. NRC Research Press, Ottawa, Ontario. pp 395-432.

Hély, C., Bergeron, Y., and Flannigan, M.D. 2000. Effects of stand composition on fire hazard in the mixedwood Canadian boreal forest. Journal of Vegetration Science 11: 813–824.

Hirschboeck, K.K., Ni, F., Wood, M.L., and Woodhouse, C. 1996. Synoptic dendroclimatology: overview and outlook. *In* Dean, J.S., Meko, D.M. and Swetnam, T.W., eds., Tree rings, environment, and humanity: Radiocarbon, Tucson, Arizona, pp. 205-223.

Hofgaard, A., Tardif, J., Bergeron, Y. 1999. Dendroclimatic response of *Picea mariana* and *Pinus banksiana* along a latitudinal gradient in the eastern Canadian boreal forest. Canadian Journal of Forest Research 29: 1333–1346.

Hogg, E.H. 1994. Climate and the southern limit of the western Canadian boreal forest. Canadian Journal of Forest Research 24: 1835-1845.

Hogg, E.H., Brandt, J.P., and Kochtubajda, B. 2002. Growth and dieback of aspen forests in northwestern Alberta, Canada, in relation to climate and insects. Canadian Journal of Forest Research 32: 823-832.

Holmes, R.L. 1983. Computer-assisted quality control in tree-ring dating and measurement. Tree-Ring Bulletin 43: 69-78.

Holmes, R.L. 1999. Dendrochronology program library and the dendroecology program library. Laboratory of Tree-Ring Research, University of Arizona, Tucson, Arizona, USA.

Holmes, R.L., Adams, R.K., and Fritts, H.C. 1986. Tree-ring chronologies of western North America: California, eastern Oregon and northern Great Basin with procedures used in chronology development work including users manuals for computer programs COFECHA and ARSTAN. Laboratory of Tree-Ring Research, University of Arizona, Tucson, Arizona, pp 182.

Houghton, J.T., Ding, Y., Griggs, D.J., Noguer, M. , van der Linden, P.J., Xiaosu, D., Maskell, K., and Johnson, C.A. Houghton, J. T., Ding, Y., Griggs, D. J., Noguer, M., van der Linden, P. J., Xiaosu, D., Maskell, K., and Johnson, C. A. Climate change 2001: The scientific basis. Contribution of Working Group I to the third assessment report of the Intergovernmental Panel on Climate Change (IPCC). 2001. Cambridge University Press, Cambridge.

Hunter, M.L. 1999. Maintaining biodiversity in forest ecosystems. Cambridge University Press, Cambridge, England. 698 pages.

Hurrell, J.W. 1995. Decadal trends in the North Atlantic Oscillation regional temperatures and precipitation. Science (Washington, D.C.) 269: 676–679.

Hurrell, J.W. 1996. Influence of variations in extratropical wintertime teleconnections on Northern Hemisphere temperatures. Geophysical Research Letters 23: 665–668.

Hurrell, J.W. 2000. The North Atlantic Oscillation. Prepared for the National Academy of Sciences, 12th Annual Symposium on Frontiers of Science, Irvine, CA. http://www.cgd.ucar.edu/~jhurrell/

Hurrell J,W., and Van Loon, H. 1997. Decadal variations in climate associated with the North Atlantic Oscillation. Climatic Change 36: 301–326.

Jacobeit, J., Wanner, H., Luterbacher, J., Beck, C., Philipp, A., and Sturm, K. 2003. Atmospheric circulation variability in the North-Atlantic-European area since the mid-seventeenth century. Climate Dynamics 20: 341-352.

Jacoby, G.C., and D'Arrigo, R. 1989. Reconstructed northern hemisphere annual temperature since 1671 based on high-latitude tree-ring data from North-America. Climatic Change 14: 39-59.

Jacoby, G.C., Ivanciu, I.S., and Ulan, L.D. 1988. A 263-year record of summer temperature for northern Québec reconstructed from tree-ring data and evidence of a major climatic shift in the early 1800's. Palaeogeography, Palaeoclimatology, Palaeoecology 64: 69-78.

Jardon, Y., Filion L., and Cloutier, C. 1994. Tree-ring evidence for endemicity of the larch sawfly in North America. Canadian Journal of Forest Research 24: 742-747.

Jardon, Y., Morin, H., and Dutilleul, P. 2003. Périodicité et synchronisme des épidémies de la tordeuse des bourgeons de l'épinette au Québec. Canadian Journal of Forest Research 33: 1947-1961.

Johnson, E.A. 1992. Fire and Vegetation Dynamics: Studies from the North American Boreal Forest. Cambridge University Press, United Kingdom.

Johnson, E.A., and Larsen, C.P.S. 1991. Climatically induced change in fire frequency in the southern Canadian Rockies. Ecology 72: 194-201.

Johnson, E.A., and Wowchuck, D.R. 1993. Wildfires in the southern Canadian Rockies and their relationship to mid-tropospheric anomalies. Canadian Journal of Forest Research 23: 1213-1222.

Johnson, E.A., Fryer, G.I., and Heathcott, M.J. 1990. The influence of man and climate on the fire frequency in the Interior Wet Belt Forest, British Columbia. J. Ecol. 78: 403-412.

Kalnay, E., Kanamitsu, M., Kistler, R., Collins, W., Deaven, D., Gandin, L., Iredell, M., Saha, S., White, G., Woollen, J., Zhu, Y., Chelliah, M., Ebisuzaki, W., Higgins, W., Janowiak, J., Mo, K.C., Ropelewski, C., Wang, J., Leetmaa, A., Reynolds, R., Jenne, R., and Joseph, D. 1996. The NCEP/NCAR reanalysis 40-year project. Bulletin of the American Meteorological Society **77**: 437-471.

Kaennel, M. and Schweingruber, F.H. 1995. Multilingual Glossary of Dendrochronology. Swiss Federal Institute for Forest, Snow and Landscape Research, Birmensdorf / Paul Haupt Publishers, Berne. 467 pages.

Kenkel, N., and Hamel, C. 2000. Structure and dynamics of boreal forest stands in the Duck Mountains, Manitoba. Sustainable Forest Management Network. Project Reports 2000 series. University of Alberta, Edmonton, Alberta. 54 pages.

Kiladis, G.N., and Diaz, H.F. 1989. Global climate anomalies associated with extremes in the Southern Oscillation. Journal of Climate 2: 1069–1090.

Knox, J.L., and Lawford, R.G. 1990. The relationship between Canadian Prairie dry and wet months and circulation anomalies in the mid-troposhere. Atmosphere and Ocean 28: 189-215.

Kumar, A., and Hoerling, M.P. 2003. The nature and causes for the delayed atmospheric response of to El Niño. Journal of Climate 16: 1391-1403.

Laprise, R., Caya, D., Frigon, A., and Paquin, D. 2003. Current and perturbed climate as simulated by the second-generation Canadian Regional Climate Model (CRCM-II) over northwestern North America. Climate Dynamics 21: 405-421.

Laroque, C.P., and Smith, D.J. 2003. Radial-growth forecasts for five high-elevation conifer species on Vancouver Island, British Columbia. Forest Ecology and Management 183: 313-325.

Larsen, C.P.S. 1996. Fire and climate dynamics in the boreal forest of northern Alberta, Canada, from AD 1850 to 1989. The Holocene 6: 449-456.

Larsen, C.P.S. 1997. Spatial and temporal variations in boreal forest fire frequency in northern Alberta. Journal of Biogeography 24: 663-673.

Latif, M., and Barnett, T.P. 1996. Decadal climate variability over the North Pacific and North America: dynamics and predictability. Journal of Climate 9: 2407-2423.

Latif, M., Arpe, K., and Roeckner, E. 2000. Oceanic control of decadal North Atlantic sea level pressure variability in winter. Geophysical Research Letters 27: 727–730.

Lau, K.M., and Weng, H.Y. 1995. Climate signal detection using wavelet transform: how to make a time series sing. Bulletin of the American Meteorological Society 76: 2391–2402.

Lau, K.-M., Lee, J.-Y., Kim, K.-M., and Kang, L.-S. 2004. The North Pacific as a regulator of summertime climate over Eurasia and North America. Journal of Climate 17: 819-833.

Lavoie, L., and Sirois, L. 1998. Vegetation changes caused by recent fires in the northern boreal forest of eastern Canada. Journal of Vegetation Science 9: 483-492.

Lees, J., and Park, J. 1995. Multiple taper spectral analysis. Computer Geoscience 21: 199.

Lefort, P., Gauthier, S., and Bergeron, Y. 2003. The influence of fire weather and land use on the fire activity of the Lake Abitibi area, eastern Canada. Forest Science 49: 509-521.

Legendre, P., and Legendre, L. 1998. Numerical ecology. Elsevier. New York. 853 pages.

Linkosalo, T. 2000. Mutual regularity of spring phenology of some boreal tree species: predicting with other species and phenological models. Canadian Journal of Forest Research 30: 667-673.

Loehle, C., and LeBlanc, D. 1996. Model-based assessments of climate change effects on forests: a critical review. Ecological Modelling 90: 1-31.

Luckman, B.H., Briffa, K.R., Jones, P.D., and Schweingruber, F.H. 1997. Tree-ring based reconstruction of summer temperature at the Columbia Icefield, Alberta, Canada, AD 1073-1983. The Holocene 7: 375-389.

Luterbacher, J., Schmutz, C., Gyalistras, D., Xoplaki, E., and Wanner, H. 1999. Reconstruction of monthly NAO and EU indices back to AD 1675. Geophyscal Research Letters 26: 2745–2748.

Luterbacher, J., Xoplaki, E., Dietrich, D., Rickli, R., Jacobeit, J., Beck, C., Gyalistras, D., Schmutz, C., and Wanner, H. 2002. Reconstruction of sea level pressure fields over the Eastern North Atlantic and Europe back to 1500. Climate Dynamics 18: 545–561.

Manitoba Conservation, 2004. Duck Mountain Provincial Park. Park information and maps. Parks and Natural Areas Branch, Winnipeg, Manitoba [online]. (www.gov.mb.ca/conservation/parks/popular_parks/duck_mtn/info.html) (Cited February 2004).

Manitoba Provincial Parks Branch. 1973. Outdoor recreation master plan: Duck Mountain Provincial Park. Manitoba Department of Tourism, Recreation and Cultural Affairs, Winnipeg, Manitoba.

Mann, M.E., and Jones, P.D. 2003. Global Surface Temperatures over the Past Two Millennia, Geophysical Research Letters 30, 1820, 10.1029/2003GL017814.

Mann, M.E., Bradley, R.S., and Hughes, M.K. 1998. Global-scale temperature patterns and climate forcing over the past six centuries. Nature 392: 779-787.

Mantua, N.J., Hare, S.R., Zhang, Y., Wallace, J.M., and Francis, R.C. 1997. A Pacific decadal climate oscillation with impacts on salmon. Bulletin of the American Meteorological Society 78: 1069-1079.

Masters, A.M. 1990. Changes in forest fire frequency in Kooteney National Park (British Columbia, Canada), Canadian Rockies. Canadian Journal of Botany 68: 1763-1767.

McAlpine, R.S. 1990. Seasonal trends in the Drought Code component of the Canadian Forest Fire Weather Index System. Forestry Canada, Petawawa National Forestry Institute, Chalk River, Ontario Information Report PI-X-97 E/F.

McIntyre, S., and McKitrick, R. 2005. Hockey sticks, principal components, and spurious significance. Geophysical Research Letters 32: Art. No. L03710.

Meehl, G.A., Washington, W.M., Wigley, T.M.L., Arblaster, J.M., and Dai, A. 2003. Solar and greenhouse gas forcing and climate response in the twentieth century. Journal of Climate 16: 426-444.

Meehl, G. A., and C. Tebaldi, 2004: More intense, more frequent, and longer lasting heat waves in the 21st century. Journal of Climate, 305, 994-997.

Mehta, V.M., Suarez, M.J., Mangenello, J., and Delwoth, T.L. 2000. Oceanic influence on the North Atlantic Oscillation and associated Northern Hemisphere climate variations. Geophysical Research Letters 27: 121–124.

Mekis, E., and Hogg, W.D. 1999. Rehabilitated and analysis of Canadian daily precipitation time series. Atmosphere and Ocean 37: 53-85.

Minobe, S. 1997. A 50–70 year climatic oscillation over the North Pacific and North America. Geophysical Research Letters 24: 683–686.

Moberg, A., Sonechkin, D.M., Holmgren, K., Datsenko, N.M., and Karlen, W. 2005. Highly variable Northern Hemisphere temperatures reconstructed from low- and high-resolution proxy data. Nature 433: 613-617.

Morin, A., and Payette, S. 1984. Expansion récente du mélèze à la limite des forêts (Québec nordique). Canadian Journal of Botany 62: 1404-1408.

Mudelsee, M. 2003. Estimating Pearson's correlation coefficient with bootstrap confidence interval from serially dependent time series. Mathematical Geology 35: 651–665.

Murphy, P.J., Mudd, J.P., Stocks, B.J., Kasischke, E.S., Barry, D., Alexander, M.E., and French, N.H.F. 2000. Historical fire records in the North American boreal forest. *In* Fire, climate change, and carbon cycling in the boreal forest. *Edited by* E.S. Kasischke and B.J. Stocks. Springer Publishing Company, New York. pp. 274–288.

Myking, T., and Heide, O.M. 1995. Dormancy release and chilling requirement of buds of latitudinal ecotypes of *Betula pendula* and *B. pubescens*. Tree Physiology 15: 697-704.

Nairn, L.D., Reeks, W.A., Webb, F.E., and Hildahl, V. 1962. History of larch sawfly outbreaks and their effect on tamarack stands in Manitoba and Saskatchewan. Canadian Entomologist 94: 242-255.

Nash, C.H., and Johnson, E.A. 1996. Synaptic climatology of lightning-caused forest fires in subalpine and boreal forests. Canadian Journal of Forest Research 26: 1859-1874.

National Wildfire Coordination Group 1996. Glossary of Wildland Fire Terminology. National Interagency Fire Center. Boise, Idaho. 141 pages.

Newark, M.J. 1975. The relationship between forest fire occurrence and 500 mb longwave ridging. Atmosphere 13: 26-33.

Newman, M., Compo, G.P., and Alexander, M.A. 2003. ENSO-forced variability of the Pacific Decadal Oscillation. Journal of Climate 16: 3853-3857.

Nigam, S., Barlow, M., and Berbery, E.H. 1999. Analysis Links Pacific Decadal Variability to Drought and Streamflow in the United States. EOS, American Geophysical Union 80: 621-625.

Palmer, W.C. 1965. Meteorological drought. Research Paper No. 45, U.S. Department of Commerce Weather Bureau, Washington, D.C..

Palmer, W.C. 1968. Keeping track of crop moisture conditions, nationwide: the new Crop Moisture Index. Weatherwise 21: 156-161.

Podur, J. Martell, D.L., and Knight, K. 2002. Statistical quality control analysis of forest fire activity in Canada. Canadian Journal of Forest Research 32: 195-205.

Robertson, B.W., Mechoso, C.R., and Kim, Y.-J. 2000. The influence of Atlantic sea surface temperature anomalies on the North Atlantic Oscillation. Journal of Climate 13: 122–138.

Rogers, J.C. 1984. The association between the North Atlantic Oscillation and the Southern Oscillation in the Northern Hemisphere. Monthly Weather Reviews 112: 1999-2015.

Ropelewski, C.F., and Jones, P.D. 1987. An extension of the Tahiti-Darwin Southern Oscillation Index. Monthly Weather Reviews 115: 2161–2165.

Rowe, J.S. 1983. Concepts of fire effects on plant individuals and species. *In* The Role of Fire in Northern Circumpolar Ecosystems. *Edited by* R.W. Wein and D.A. MacLean. John Wiley and Sons, New York, pp 135-151.

Sauchyn, D.J., Barrow, E., Hopkinson, R.F., and Leavitt, P. 2002. Aridity on the Canadian Plains. Geographie Physique et Quaternaire 56: 247-259.

Sauchyn, D., Stroich, J., and Beriault, A. 2003. A paleoclimatic context for the drought of 1999-2001 in the northern Great Plains of North America. The Geographical Journal 169: 158-167.

Schneider, U., and Schönwiese, C.D. 1989. Some statistical characteristics of El Niño/Southern Oscillation and North Atlantic Oscillation indices. Atmosfera 2: 167-180.

Schneider, N., Miller, A.J., and Pierce, D.W. 2002. Anatomy of North Pacific Decadal Variability. Journal of Climate 15: 586-605.

Seager, R., Kushnir, Y., Visbeck, M., Naik, N., Miller, J.A., Krahmann, G., and Cullen, H.M. 2000. Causes of Atlantic Ocean climate variability between 1958 and 1998. Journal of Climate 13: 2845–2862.

Shabbar, A., and Khandekar, M. 1996. The impact of El Nino-Southern Oscillation on temperature field over Canada. Atmosphere and Ocean 34: 401-416.

Shabbar, A., and Skinner, W. 2004. Summer drought patterns in Canada and the relationship to global sea surface temperature. Journal of Climate 17: 2866-2880.

Shabbar, A., Bonsal, B., and Khandekar, M. 1997a. Canadian precipitation patterns associated with the Southern Oscillation. Journal of Climate 10: 3016–3027.

Shabbar, A., Higuchi, K., Skinner, W., and Knox, J.L. 1997b. The association between the BWA index and winter surface temperature variability over eastern Canada and west Greenland. International Journal of Climatology 17: 1195–1210.

Sheppard, P.R., and Cook, E.R. 1988. Scientific value of trees in old-growth natural areas. Natural Areas Journal 8: 7-12.

Shindell, D.T., Schmidt, G.A., Mann, M.E., Rind, D., and Waple, A. 2001a. Solar forcing of regional climate change during the Maunder Minimum. Science (Washington, D.C.) 294: 2149–2152.

Shindell, D.T., Schmidt, G.A., Miller, R.L., and Rind, D. 2001b. Northern Hemisphere winter climate response to greenhouse gas, ozone, solar, and volcanic forcing. Journal of Geophysical Research 106: 7193-7210.

Skinner, W.R., Stocks, B.J., Martell, D.L., Bonsal, B., and Shabbar, A. 1999. The association between circulation anomalies in the mid-troposphere and the area burned by wildland fire in Canada. Theoretical and Applied Climatology 63: 89-105.

Skinner, W.R., Flannigan, M.D., Stocks, B.J., Martell, D.L., Wotton, B.W., Todd, J.B., Mason, J.A., Logan, K.A., and Bosch, E.M. 2002. A 500-hPa synoptic wildland fire climatology for large Canadian forest fires, 1959-1996. Theoretical and Applied Climatology 71: 157-169.

Smith, T.M., and Reynolds, R.W. 2003. Extended Reconstruction of Global Sea Surface Temperatures Based on COADS Data (1854-1997). Journal of Climate 16: 1495-1510.

Spittlehouse, D.L., and Stewart, R.B. 2003. Adaptation to climate change in forest management. Journal of Environmental Management 4: 1-11.

Stahle, D.W., D'Arrigo, R., Krusic, P.J, Cleaveland, M.K., Cook, E.R., Allan, R.J., Cole, J.E., Dunbar, R.B., Therrell, M.D., Gay, D.A., Moore, M.D., Stokes, M.A., Burns, B.T., Villanueva-Diaz, J., and Thompson, L.G. 1998. Experimental dendroclimatic reconstruction of the Southern Oscillation. Bulletin of the American Meteorological Society 79: 2137–2152.

Stilwell, W.J. 1988. The Baldy Mountain cabin: the history and role of forest rangers and game wardens in the Baldy Mountain area. Regional Services Branch, Manitoba Department of Natural Resources, Winnipeg, Manitoba.

Stocks, B.J., Mason, J.A., Todd, J.B., Bosch, E.M., Wotton, B.M., Amiro, B.D., Flannigan, M.D., Hirsch, K.G., Logan, K.A., Martell, D.L., and Skinner, W.R. 2003. Large forest fires in Canada, 1959–1997. Journal of Geophysical Research 108, 8149, 10.1029/2001JD000484.

Stokes, M.A., and Smiley, T.L. 1996. An introduction to tree-ring dating. University of Arizona Press, Tucson, Arizona. 73 pages.

Systat 1998. SYSTAT Version 9.1 software. SPSS Inc. Chicago.

Swetnam, T. 1993. Fire history and climate change in giant sequoia groves. Science (Washington, D.C.) 262: 885-889

Tardif, J. 2004. Fire history in the Duck Mountain Provincial Forest, western Manitoba Sustainable Forest Management Network. Project Reports 2003/2004 series. University of Alberta, Edmonton, Alberta. 30 pages.

Tardif, J., and Bergeron, Y. 1997a. Ice-flood history reconstructed with tree-rings from the southern boreal forest limit, western Québec. The Holocene 7: 291–300.

Tardif, J., and Bergeron, Y. 1997b. Comparative dendroclimatological analysis of two black ash and two white cedar populations from contrasting sites in the Lake Duparquet region, northwestern Québec. Canadian Journal of Forest Research 27: 108–116.

Tardif, J., and Bergeron, Y. 1999. Population dynamics of *Fraxinus nigra* in response to flood-level variations, in northwestern Québec. Ecological Monograph 69: 107-125.

Tardif, J., Brisson, J., and Bergeron, Y. 2001. Dendroclimatic analysis of *Acer saccharum*, *Fagus grandifolia*, and *Tsuga canadensis* from an old-growth forest, southwestern Quebec. Canadian Journal of Forest Research 31: 1491-1501.

Tardif, J., Conciatori, F., and Bergeron, Y. 2002. Comparative analysis of the climatic response of seven boreal tree species from northwestern Québec, Canada. Tree-Ring Research 57: 25-37.

Tardif, J., Camarero, J.J., Ribas, M., and Gutiérrez, E. 2003. Spatiotemporal variability in tree growth in the Central Pyrenees: climatic and site influences. Ecological Monograph 73: 241–257.

Ter Braak, C.J.F., and Prentice, I.C. 1988. A theory of gradient analysis. Advance Ecology Research 18: 271–317.

Ter Braak, C.J.F. 1994. Canonical community ordination. Part I: basic theory and linear methods. Écoscience 1: 127–140.

Ter Braak, C.J.F., and Smilauer, P. 1998. Canoco reference manual and users guide to Canoco for windows: software for canonical community ordination version 4.. Microcomputer power, Ithaca, NY, USA. 325 pages.

Thompson, D.W.J., and Wallace, J.M. 1998. The Arctic Oscillation signature in the wintertime geopotential height and temperature fields. Geophysical Research Letters 25: 1297–1300.

Thompson, D.W.J., and Wallace, J.M. 2001. Regional climate impacts of the Northern Hemisphere annular mode. Science (Washington, D.C.) 293: 85–89.

Thompson, D.W.J., Baldwin, M.P., and Wallace, J.M. 2002. Stratospheric connection to Northern Hemisphere wintertime weather: implications for prediction. Journal of Climate 15: 1421-1428.

Thornthwaite, C.W., and Mather, J.R. 1955. The water balance. Publications in Climatology 8: 1–86.

Timm, O., Ruprecht, E., and Kleppek, S. 2004. Scale-dependant reconstruction of the NAO index. Journal of Climate 17: 2157-2169.

Torrence, C., and Compo, G.P. 1998. A practical guide to wavelet analysis. Bulletin of the American Meteorological Society 79: 61–78.

Torrence, T., and Webster, P.J. 1999. Interdecadal changes in the ENSO-Monsoon System. Journal of Climate 12: 2679–2690.

Trenberth, K.E. 1990. Recent observed interdecadal climate changes in the northern hemisphere. Bulletin of the American Meteorological Society 71: 988-993.

Trenberth, K.E., and Hurrell, J.W. 1994. Decadal atmosphere-ocean variations in the Pacific. Climate Dynamics 9: 303-319.

Trotter III, R.T., Cobb, N.S., and Whithman, T.G. 2002. Herbivory, plant resistance, and climate in the tree ring record: Interactions distort climatic reconstructions. PNAS 99: 10197-10202.

Turner, J.A. 1972. The drought code component of the Canadian Forest Fire Behaviour System. Canadian Forest Service Publication 1316.

Turner, J.A., and Lawson, B.D. 1978. Weather in the Canadian Forest Fire Danger Rating system: a user guide to national standards and practices. Canadian Forest Service Publication 1316.

Turnock, W.J. 1972. Geographical and historical variability in population patterns and life systems of the larch sawfly (Hymenoptera: Tenthredinidae). Canadian Entomologist 104: 1883-1900.

Van Loon, H., and Rogers, J.C. 1978. The seasaw in winter temperature between Greenland and northern Europe. Part 1: general description. Monthly Weather Reviews 106: 296-310.

Van Wagner, C.E. 1970. New development in forest fire danger rating. Canada Department of Fisheries Forestry Canadian Forest Service Information Report PS-X-19.

Van Wagner, C.E. 1974. Effect of duff weight on drying rate. Canadian Forest Service Bi-Monthly Research Notes 30: 11–12.

Van Wagner, C.E. 1978. Age-class distribution and the forest fire cycle. Canadian Journal of Forest Research 8: 220-227.

Van Wagner, C.E. 1987. Development and structure of the Canadian Forest Fire Weather Index System. Cannadian Forest Service, Ottawa, Ontario, Forestry Technical Report 35. 37 pages.

Varem-Sanders, T. 2000. ITRVIEW 2.0 program. Canadian Forest Service, Edmonton, Alberta, Canada.

Vincent, J.S., and Hardy, L. 1977. L'évolution et l'extinction des lacs glaciaires Barlow et Ojibway en territoire québécois. Géographie Physique et Quaternaire 31: 357–372.

Vincent, L.A. 1998. A technique for the identification of inhomogeneities in Canadian temperature series. Journal of Climate 11: 1094–1104.

Vincent, L.A., and Gullett, D.W. 1999. Canadian historical and homogeneous temperature datasets for climate change analyses. International Journal of Climatology 19: 1375–1388.

Vincent, L.A., Zhang, X., Bonsal, B.R., and Hogg, W.D. 2002. Homogenization of daily temperature over Canada. Journal of Climate 15: 1322-1334.

Wanner, H., Brönnimann, S., Casty, C., Gyalistras, D., Luterbacher, J., Schmutz, C., Stephenson, D.B., and Xoplaki, F. 2001. North Atlantic Oscillation – concepts and studies. Surveys in Geophysics 22: 321–382.

Weber, G.R., 1990. North Pacific circulation anomalies, El Nino and anomalous warmth over the North American continent in 1986-1988: possible causes of the 1988 North American Drought. International Journal of Climatology 10: 279-289.

Weber, M.G., and Flannigan, M.D. 1997. Canadian boreal forest ecosystem structure and function in a changing climate: impact on fire regime. Environmental Reviews 5: 145-166.

Weir, J.M.H., Johnson, E.A., and Miyanishi, K. 2000. Fire frequency and the spatial age mosaic of the mixed-wood boreal forest in western Canada. Ecological Application 10: 1162-1177.

Wigley, T.M.L., Briffa, K.R., and Jones, P.D. 1984. On the average of correlated time series, with application in dendroclimatology and hydrometeorology. Journal of Climate and Applied Meteorology 23: 201-213.

Wilson, R.J.S., and Luckman, B.H. 2003. Dendroclimatic reconstruction of maximum summer temperature from upper tree-line sites in Interior British Columbia. The Holocene 13: 851-861.

Wu, L., and Liu, Z. 2003. Decadal Variability in the North Pacific: the Eastern North Pacific mode. Journal of Climate 16: 3111-3131.

Yamaguchi, D.K. 1991. A simple method for cross-dating increment cores from living trees. Canadian Journal of Forest Research 21: 414-416.

Yang, H., and Zhang, Q. 2003. On the decadal and interdecadal variability in the Pacific Ocean. Advances in Atmospheric Sciences 20: 173-184.

Yarnal, B. 1993. Synoptic climatology in environmental analysis: a primer. Belhaven Press, London, U.K. 195 pages.

Yarnal, B., Comrie, A.C., Frakes, B., and Brown, D.P. 2001. Development and prospects in synoptic climatology. International Journal of Climatology 21: 1923–1950.

Zhang, Y., Wallace, J.M., and Battisti, D.S. 1997. ENSO-like interdecadal variability: 1900–93. Journal of Climate 10: 1004–1020.

Zhang, X., Vincent, L., Hogg, W.D., and Niitsoo, A. 2000. Temperature and precipitation trends in Canada during the 20th century. Atmosphere and Ocean 38: 395–429.

Zhang, X., Hogg, W.D., and Mekis, É. 2001. Spatial and temporal characteristics of heavy precipitation events over Canada. Journal of Climate 14: 1923–1936.

Zheng, D., Chao, B.F., Zhou, Y., and Yu, N. 2000. Improvement of edge effect of the wavelet time-frequency spectrum: application to the length-of-day series. Journal of Geodesy 74: 249–254.

GLOSSARY

Sources: modified from Cook and Holmes (1986), Kaennel and Schweingruber (1995), the National Wildfire Coordination Group (1996), Legendre and Legendre (1998) and the American Meteorological Society (2000).

Advection: the horizontal transport of an atmospheric property (e.g., moisture) by the wind.

Air subsidence: A descending motion of air in the atmosphere, usually with the implication that the condition extends over a rather broad area.

Anticyclone: an area of high pressure around which the wind blows clockwise in the Northern Hemisphere. With respect to the relative direction of its rotation, it is the opposite of a cyclone.

Atmospheric bridge: connection between ocean basins via the contribution of surface heat fluxes.

Autoregression: a regression in which one value in a time series is regressed upon, or related to, one or more values which precede it in time.

Baroclinic instability: A type of instability arising from a meridional (north to south) temperature gradient, a strong vertical wind speed shear, temperature advection, and divergence in the flow aloft. Many mid-latitude cyclones develop as a result of this instability.

Biweight mean: removes effects of endogenous stand disturbances and enhances the common signal contained in the tree ring data.

Bootstrap: a statistical technique that estimates the error of a data set by repeated random sampling of the data so as to increase the sample size artificially. The scheme involves generating subsets of the data on the basis of random sampling with replacements as the data are sampled.

Bulk density: The dry weight of combustible materials per unit volume. Numerically, it is equal to fuel load divided by the depth of the particular fuel layer.

Cloud deck: a broad cloud formation.

Composite charts: a map constructed by overlaying critical values of atmospheric parameters analyzed to assess severe weather potential.

Convective activity: general term for manifestations of convection in the atmosphere, alluding particularly to the development of convective clouds and resulting weather phenomena, such as showers, thunderstorms, squalls, hail, tornadoes, etc.

Convergence: an atmospheric condition that exists when the winds cause a horizontal net inflow of air into a region; the opposite of divergence

Cumulative percentage variance of species-environment relation: in canonical ordination, expresses the amount of variance explained by the canonical axes as a fraction of the total explainable variance.

Cyclone: an area of low pressure around which the wind blows counter clockwise in the Northern Hemisphere. With respect to the relative direction of its rotation, it is the opposite of an anticyclone.

Divergence: an atmospheric condition that exists when the winds cause a horizontal net outflow of air from a region, the opposite of convergence

Durbin–Watson test: statistic designed for detecting errors that follow a first-order correlation in the residuals of a time series regression. The last assumption is that of independence, which means that the error terms are not correlated with each other.

Eigenvalue: in ordination, the variance in a set of variables explained by an axis or component.

Ekman transport: net surface water transport due to the Ekman spiral. The Ekman spiral is an idealised description of the way the wind-driven ocean currents vary with depth. In the Northern Hemisphere, the transport of surface water is at right

angles to the prevailing winds. At the very surface the water moves at an angle of 45° from the wind direction; in successively deeper layers the movement will be deflected farther and farther from the wind direction, and the speed will decrease.

Extra tropical: in meteorology, typical of occurrences poleward of the belt of tropical easterlies. The tropical easterlies occupy the poleward margin of the Tropics in summer and can cover most of the tropical belt in winter.

F-ratio: a statistical index relating systematic variation in the data (caused by treatment effects plus random error) to unsystematic variability in the data (caused by random error alone). The effect of treatments plus error is the numerator and the effect of error (chance) is the denominator of the F-ratio.

Geopotential height: approximates the actual height of a pressure surface above mean sea-level (in meters). Numerically, it equals the height of a given point in the atmosphere, in units proportional to the work that would be done in lifting a unit mass from sea level to the height at which the mass is located. The amount of work done will be a function of the initial and final states of the atmosphere (e.g. density).

Global scale: A specific scale of atmospheric motion with a typical range of ~5000km, including such phenomena as longwaves in the westerlies. *Compare synoptic scale.*

Goodness-of-fit: in general terms, a quantitative measure of the ability of an assumed functional form to fit a given set of data.

Longwaves: also called Planetary and Rossby waves. With regard to atmospheric circulation, a wave in the major belt of westerlies that is characterized by long length (thousands of kilometres) and significant amplitude.

Meridionality: a flow in a direction that is parallel to a line of longitude, that is, northerly or southerly; as opposed to zonal.

Momentum: a measure of the amount of spin or motion an object has.

Normalisation: a statistical method that rescales values by substracting their mean and dividing them by their standard deviation

Orthogonal: at right angles to, or completely uncorrelated with. Usually in ordination, axes (or principal components) are orthogonal to each other.

Permutation: the process of generating alternative arrangements of given data which would be consistent with the experimental design. The Monte Carlo procedure is in contrast to the bootstrap procedure in that the sampling of the subsets is without replacement.

Potential evapotranspiration: generally, the amount of moisture that, if available, would be removed from a given land area by evapotranspiration.

Predictand: in a statistical system, actual data (e.g. climatic measurements) to which the statistical estimates from the calibration are compared.

Predictor: the input variable or variables of a system (e.g. tree-ring chronologies), values of which are used to obtain prediction (estimates, reconstructions) of the predictands.

Principal components: Principal Components Analysis (PCA) is an ordination technique that involves an eigenanalysis of the correlation matrix or the covariance matrix of descriptors. The first Principal Component will, ideally, represent the dominant gradient. The second Component will be orthogonal to the first, and will explain some of the residual variation. The third will be orthogonal to the first and second components, and so on.

Ridge: an elongated area of relatively high atmospheric pressure, almost always associated with and most clearly identified as an area of maximum anticyclonic curvature of wind flow; the opposite of a trough.

Shear vorticity: shear developed along the airflow due to the differing velocities of the moving particles.

Smouldering: A fire burning without flame and barely spreading.

Species-environment correlations: in canonical ordination, indicates how much of the variation in species composition may be 'explained' by the environmental variables.

Spline function: method that fits a succession of cubic polynomial curves to a time series. The "frequency response" of the spline function describes the effect that detrending has on the original series. The amount of variance to be removed at a particular frequency can be precisely specified; it will remove variance of lower frequencies (longer wavelengths) with a transition to little or no removal of variance of higher frequencies (shorter wavelengths).

Standardisation: removing long-term variations from a tree-ring measurement series by dividing the measurements by a standardising smoothing function, and their conversion to a time series of ring-width indices. The standardising smoothing function is the mathematical representation of physiological growth (caused by bio-ecological factors such as tree age and stand dynamics), expressed as a function of time and fitted to measurements of a tree-ring parameter such as ring width.

Stratosphere: The region of the atmosphere extending from the top of the troposphere at heights of roughly 10–17 km, to the base of the mesosphere at a height of roughly 50 km.

Subsidence: a descending motion of air in the atmosphere, usually with the implication that the condition extends over a rather broad area.

Sub-tropics: the indefinite belts in each hemisphere between the regions of tropical and temperate climates. The polar boundaries are considered to be roughly 35°N and 35°S latitudes, but vary greatly according to continental influence.

Succession: the natural replacement, in time, of one plant community with another. Conditions of the prior plant community (or successional stage) create conditions that are favorable for the establishment of the next stage.

Synoptic scale: a specific scale of atmospheric motion with a typical range of ~2000 km, including such phenomena as cyclones. Compare global scale.

Synoptic: in meteorology, this term has become somewhat specialised in referring to the use of meteorological data obtained simultaneously over a wide area for the purpose of presenting a comprehensive and nearly instantaneous picture of the state of the atmosphere.

Thermocline: a vertical temperature gradient, in some layer of a body of water, that is appreciably greater than the gradients above and below it.

Trade winds: The wind system that blows from the subtropical highs toward the equatorial trough; a major component of the general circulation of the atmosphere.

Transient eddies: in contrast to stationary or standing eddies, the component of the eddy field that varies with time. In this context "eddy" refers to departures from the zonal mean, such as the migratory cyclones and anticyclones in the extra tropics.

Tropics: any portion of the earth characterized by a tropical climate, that is, one with continually high temperatures and with considerable precipitation, at least during part of the year.

Troposphere: that portion of the atmosphere from the earth's surface to the tropopause; that is, the lowest 10–20 km of the atmosphere.

Trough: an elongated area of relatively low atmospheric pressure; the opposite of a ridge.

Zonality: a latitudinal flow, that is, easterly or westerly; as opposed to meridional.